UNIVERSITY OF SUSSEX

Actinide Complexes for Small Molecule Activation Featuring a Bis(phenoxide) Ligand with a Chelating Arene

by

Christopher J. Inman

Submitted for the degree of Doctor of Philosophy

July 2018

The work detailed in this thesis was carried out at the University of Sussex from September 2014 to July 2018, under the supervision of Professor F. G. N. Cloke. All the work is my own, unless stated to the contrary and has not been previously submitted for any degree at this or any other university.

Christopher J. Inman

July 2018

ACKNOWLEDGMENTS

With thanks to:

Prof. F. G. N. Cloke FRS

Dr. N. Tsoureas

Mr. M. K. Molloy

Mr. R. K. Brown

Dr A. F. R. Kilpatrick

Dr. S. Furfari

Members of lab 14 past and present

Dr. I. R. Crossley

Dr. Abdul-Sada

Dr. S. M. Roe

Dr. I. J. Day

Prof. J. C. Green

Dr. F. Tuna

Dr. F Ortu

Dr. D. P. Mills

Prof. G. Wildgoose

Dr. L. Natrajan

EPSRC EPR Facility, University of Manchester

UK National Crystallography Service

Special thanks go to my parents for their patience, constant support and encouragement.

ABSTRACT

Actinide Complexes for Small Molecule Activation Featuring a Bis(phenoxide) Ligand with a Chelating Arene

Christopher J. Inman

Ph.D Thesis

This thesis focuses on the use of Tp^{Me2} (Tp^{Me2} = [$HB(C_3N_2HMe_2)_3$]-) or pMe_2O_2 (pMe_2O_2 = C_6H_4{p-C-$(CH_3)_2C_6H_2Me_2O$-}$_2$) as alternatives to Cp* and COT^{TIPS2} (Cp* = C_5Me_5 and COT^{TIPS2} C_8H_6{1,4-Si^iPr_3}$_2$) respectively, in the synthesis of U(III) complexes for small molecule activation studies. The pMe_2O_2 ligand scaffold has also been incorporated into heteroleptic Th(IV) complexes and a formally Th(III) complex.

The synthesis and reactivity studies of the half-sandwich complexes ($U(\eta^8\text{-}C_8H_6\{1,4\text{-}SiMe_3\}_2)(\kappa^3\text{-}Tp^{Me2})$, $U(\eta^8\text{-}C_8H_4\{1,4\text{-}Si^iPr_3\}_2)(\kappa^3\text{-}Tp^{Me2})$ and $U(\eta^8\text{-}C_8H_6\{1,4\text{-}Si^iPr_3\}_2)(\kappa^3\text{-}Tp^{Me2})$ ($C_8H_4\{1,4\text{-}Si^iPr_3\}_2$ = $Pent^{TIPS2}$)) are documented and the observation of the uranium-carbonyl complex, $U(\eta^8\text{-}C_8H_4\{1,4\text{-}Si^iPr_3\}_2)(\kappa^3\text{-}Tp^{Me2})CO$, at low-temperatures is reported. Electrochemical studies were carried out on these compounds to determine the U^{III}/U^{IV} redox couple and compare the electron-donating ability of the Tp^{Me2} complexes with their Cp* analogues.

The bis(phenoxide) ligand, pMe_2O_2, featuring a central chelating arene is synthesised and incorporated into the new mixed-ligand U(III) complex, UCp*(pMe_2O_2). Cyclic voltammetry studies indicate this complex is highly reducing and suitable to activate small molecules. Reactivity studies have shown UCp*(pMe_2O_2) is able to activate CO_2, CS_2, C_3O_2 (carbon suboxide) and PhNNPh. One of these products, [{UCp*(pMe_2O_2)}$_2${μ-η^2(C,S):η^2(S,S)-CS_2], was also found to activate CO_2 and CO.

A homoleptic thorium complex (Th(pMe_2O_2)$_2$) was synthesised and subsequently reduced to [K(2.2.2-cryptand)][Th(pMe_2O_2)$_2$] using K/Hg and 2.2.2-Cryptand in THF. This reduced complex features a δ-bonding thorium-arene SOMO with electron density that resides mostly on the arene. Also synthesised are several heteroleptic thorium-pMe_2O_2 complexes for the investigation of thorium-arene interactions and efforts towards ThCp*(pMe_2O_2).

LIST OF ABBREVIATIONS USED IN THE TEXT

General Abbreviations

μ_B	Bohr magneton
Å	Angstrom
acac	acetylacetonate
Ad	adamantyl
ADF	Amsterdam Density Functional
An	actinide
Ar	aryl group
ArO	aryl oxide
BDE	bond dissociation energy
Bz	benzyl, CH_2Ph
Ca	*circa*, about
cm^{-1}	wavenumbers
COD	1,5-cyclooctadiene
COT	1,3,5,7-cyclooctatetraene
COT^{TMS2}	$C_8H_6\{1,4\text{-}SiMe_3\}_2$
COT^{TIPS2}	$C_8H_6\{1,4\text{-}Si^iPr_3\}_2$
Cp	cyclopentadienyl
Cp*	pentamethylcyclopentadienyl, C_5Me_5
Cp^{Me4H}	C_5Me_4H
Cp^{TMS2}	$1,3\text{-}\{SiMe_3\}_2C_5H_3$
Cp^{TMS}	$\{SiMe_3\}C_5H_4$
Ct	centroid
Cyclam	1,4,8,11-tetraazacyclotetradecane
Cyclen	1,4,7,10-tetraazacyclododecane
°	degree
°C	degree celsius
DFT	density functional theory
DME	dimethoxyethane
E1/2	half-wave potential

EA	elemental analysis
EI-MS	electron ionisation mass-spectrometry
EPR	electron paramagnetic resonance
esd	estimated standard deviance
FTIR	Fourier transform infrared
FVP	flash vacuum pyrolysis
HOMO	highest occupied molecular orbital
Ipa	oxidation peak current value
Ipc	reduction peak current value
ITMe	1,3,4,5-tetramethylimidazol-2-ylidene
LUMO	lowest unoccupied molecular orbital
m	meta
Me	methyl
Mes	mesityl (2,4,6-$Me_3C_6H_2$)
Naph	Napthalene
nP	Neopentane
NHC	N-heterocyclic carbene
NIR	near-infrared
o	ortho
p	para
PDI	pyridine(Diimime)
PMe_2O_2	$C_6H_4\{p\text{-}C\text{-}(CH_3)_2C_6H_2Me_2O\text{-}\}_2$
Pent	pentalene, $[C_8H_6]^{2-}$, also referred to as Pn
$Pent^{TIPS2}$	$C_8H_4\{1,4\text{-}Si^iPr_3\}_2$
Ph	phenyl
Pn*	permethylated pentalene, $C_{14}H_{18}$
ppm	parts per million
Py	pyridine
SOMO	singly occupied molecular orbital
Tacn	1,4,7-Triazacyclononane
TBDMS	*tert*-butyl dimethyl silyl
TBME	*tert*-butyl methyl ether

TIPS	triisopropylsilyl
TMS	trimethylsilyl
^{t}Bu	*tert*-butyl
THF	tetrahydrofuran
TMEDA	Tetramethylethylenediamine
Tp^{Me2}	tris(3,5-dimethyl-1-pyrazolyl)borate, $[HB(C_3N_2HMe_2)_3]$-
V *vs* $FeCp_2^{+/-}$	ferrocenium/ferrocene reference potential
XANES	X-ray absorption near edge structure
XRD	X-ray diffraction

Nuclear Magnetic Resonance Abbreviations

$\{^1H\}$	proton decoupled
δ	chemical shift
Br	broad
d	doublet
^{x}J	coupling constant over x bonds
NMR	nuclear magnetic resonance
S	singlet
t	triplet
VT	variable temperature

TABLE OF CONTENTS

1 Chapter One: Introduction

1.1 Foreword

Organometallic chemistry has had a profound impact on society, ranging from the development of catalysts that are able to facilitate novel and innovative chemical transformations for the production of fine chemicals such as polymers and pharmaceuticals, to cutting edge research that pushes the boundaries of our current knowledge and understanding on the behaviour of metal complexes and challenges scientific assumptions through new and unprecedented discoveries. A fundamental aspect of organometallic chemistry is the transformation and subsequent upgrading of small molecules such as CO, CO_2, H_2 and ethylene and others into more reactive and higher value chemicals.[1] Although the bulk of industrial catalytic processes use heterogeneous catalysts, organometallic chemistry has provided the fundamental knowledge and mechanistic understanding for certain processes such as the enantioselective synthesis of menthol.[2] The organometallic chemistry of the transition metals has played a pivotal role in such advances, for example, the polymerisation of alkenes using Ziegler-Natta catalysts. The production of polyethylene and polypropylene is one of the world's largest scale applications of organometallic chemistry with an estimated production of about 100-150 million tons of polymers per annum worldwide.[1]

Even though uranium was a very competent catalyst in the original Haber-Bosch patent for ammonia synthesis,[3] its use and our understanding of the actinides lags far behind that of the transition metals. Although it is extremely unlikely that the actinides will replace transition metals for most of their current applications, from a fundamental point of view it is important to further our knowledge and deepen our understanding of these elements as they have unique properties that undoubtedly will lead to novel chemical transformations and a host of different applications.

This thesis will explore the use of several ancillary ligands including a novel bis(phenoxide) ligand which features a central chelating arene ring that can support novel and reactive uranium(III) complexes. Furthermore, their reactivity towards small molecules – CO, CO_2 and CS_2 – and the

characterisation of the resulting products, using a range of techniques including electrochemistry is discussed. The chemistry of thorium has also been investigated using the bis(phenoxide) ligand, enabling the examination of thorium-arene interactions in both the +3 and +4 oxidation states.

1.2 An Overview of Organometallic Uranium and Thorium Chemistry

Uranium is one of the most divisive elements in society due to its applications in nuclear weapons and nuclear power. Uranium was first discovered in 1789 as the naturally occurring mineral U_3O_8, also known as pitchblende.[4] Naturally occurring uranium consists of three isotopes: U^{238} (99.3%), U^{235} (*ca* 0.7%) and trace amounts of U^{234}.[5] U^{238} is a weak α emitter and has a half-life of 4.5 billion years while U^{235} is fissile; the only naturally occurring fissile isotope on earth, and hence is of great interest for nuclear applications. Interest in organouranium compounds originates from the time of the Manhattan Project with the aim of creating volatile uranium compounds for isotope separation and enrichment.

Thorium was first discovered in 1828 by Berzelius in the phosphate ore, monazite, which constitutes by mass approximately 10% Th alongside several other lanthanides.[6] Thorium is found in a much higher abundance in the earth's crust than uranium (9.6 ppm and 2.7 ppm, respectively) with the major isotope being Th^{232} (99.98%).[5] Thorium-based nuclear reactors have been proposed as alternatives to uranium-based reactors due to thorium's nature of being a self-sustaining fuel that does not require fast neutron reactors, resulting in potentially safer operating conditions.[7–9]

The chemistry of the early actinides is markedly different to that of the lanthanides and transition metals. This is due to the more diffuse nature of the 5f orbitals in comparison to the 4f orbitals of the lanthanides which are more contracted, through a much higher degree of shielding by the 5s and 5p electrons. The bonding regime of these elements are classed as mainly ionic, although the diffuse nature of the 5f orbitals allows for some degree of covalent bonding unlike that observed for the lanthanides.[10] Thorium and uranium are classified as hard Lewis acids that are oxophilic and highly reducing in the +3 oxidation state, and exhibit redox couples approaching the strength of the alkali metals (*ca* -2.2 V *vs* $FeCp_2^{+/0}$, Na: -3.04 V *vs* $FeCp_2^{+/0}$).[11,12] Moreover, their ionic radii are larger than those of the transition metals.[13] The

combination of these properties results in a rich and diverse chemistry,[14] but also inherently leads to difficulties in the preparation and characterisation of novel, low-valent and mid-valent species.

1.3 Ligand Environments for Uranium Complexes

The ligands that surround a metal centre are key to discovering new reactivity and accessing difficult oxidation states. For example, to isolate low-valent species, it is often necessary to use ligands that provide steric bulk to protect the highly reactive low valent metal centre. Electronic properties are also important as ligands can alter the redox couple of metal centres by hundreds of millivolts. Other important properties include crystallinity, and solubility properties, both of which are affected by ligands. The correct choice of ligand for the chosen application is vital. Below is a survey of ligands that have been used in this thesis.

1.3.1 Cyclopentadienyl Uranium Complexes

One of one the most common ligand systems used in organometallic chemistry is the anionic, aromatic, carbocyclic cyclopentadienyl ligand. Its use in organouranium chemistry was first reported in 1956 by Wilkinson *et al*. and since then it has featured heavily in uranium organometallic chemistry.[15] The hybridised orbitals are able to form σ- and π-bonds with the 5f and 6d orbitals of uranium. The electronic and steric properties of the Cp ligand can be tuned using a variety of substituents; some characteristic examples are shown below in **Figure 1.1**.

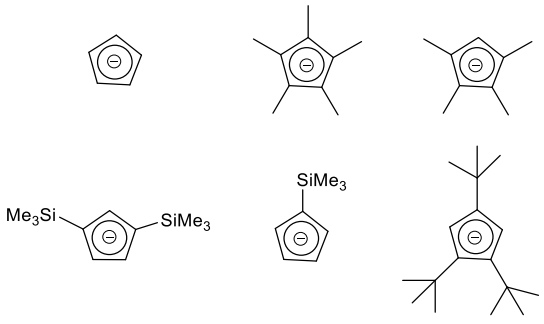

Figure 1.1 Examples of cyclopentadienyl ligands featured in uranium complexes, left to right, top to bottom: C_5H_5, [15] C_5Me_5,[16] C_5Me_4H,[17] 1,3-{$SiMe_3$}$_2C_5H_3$,[18] $C_5H_4(SiMe_3)$,[19] 1,2,4-{^{t}Bu}$_3C_5H_2$.[20]

Pentamethylcyclopentadienyl (Cp*) is one of the most common cyclopentadienyl derivatives in uranium chemistry due to the crystallinity, steric bulk and strong electron donating ability the methyl groups provide to the ligand and in turn to the metal centre. The Cp* ligand has provided an excellent platform for organometallic uranium chemistry to flourish with applications including small molecule activation, U–L multiple bond studies and catalysis.[21] Although, the Cp* ligand has enabled a wide variety of uranium chemistry, it is not well-suited for isolating highly reducing low-valent species such as U(II). Cp^{TMS} and Cp^{TMS2} are inherently less electron-donating to the metal centre and are more kinetically stabilising compared to Cp* and have featured in rare U(II) compounds (**Scheme 1.1**).[19,22]

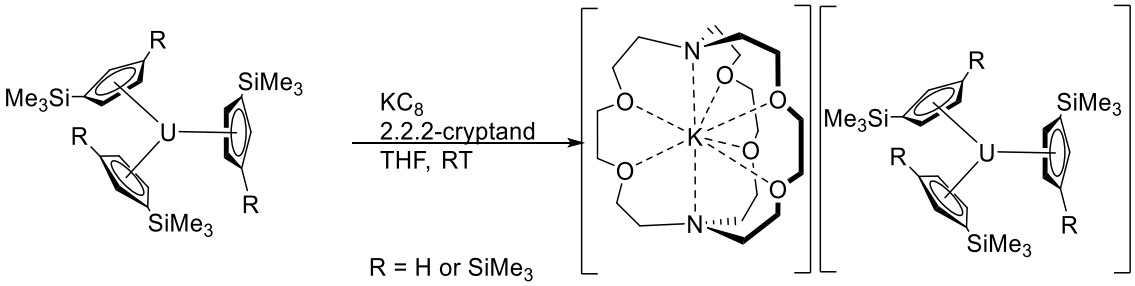

Scheme 1.1 Synthesis of [K(2.2.2-cryptand)][$UCp^{SiMe3R}{}_3$].

1.3.2 COT Uranium Complexes

Another prominent metallocene ligand in organometallic uranium chemistry is COT^{2-}. COT^{2-} is an eight-membered, dianionic, 10π-aromatic carbocyclic ligand featuring a HOMO that is of the correct symmetry to interact with the 5f orbitals of uranium in a δ-bond fashion. Combined with the potential for two of these ligands to saturate the coordination sphere of uranium, it was anticipated that it may be possible to prepare a bis(COT) uranium metallocene complex analogous to the transition metal analogues. Streitwieser *et al*. outlined the synthesis and characterisation of such a complex, $UCOT_2$ (**Figure 1.2**) (referred to as uranocene), in 1968.[23] Uranocene was the first sandwich complex of uranium and its structure resembles a dumbbell with D_{8h} symmetry as confirmed by X-ray crystallography.

Further studies involving COT focused on the functionalisation of the ligand to provide additional steric bulk and increase solubility to aid spectroscopic characterisation. Examples of functionalisation include

work by Streitwieser and Dempf, who synthesised derivatives of $UCOT^{R}_2$ (R = OMe, NMe_2, Et, ^{t}Bu and Mes) (**Figure 1.2**),[24,25] and the tetra-substituted derivatives $U(COT^{4R})_2$ (R = Me, Ph).[26,27] Curiously $U(COT^{4Ph})_2$ is stable in air over several weeks. Silyl functionalisation has also been successfully carried out with examples including (1,4-{$SiMe_3$}C_8H_6),[28] (1,4-{Si^iPr_3}C_8H_6) (**Figure 1.2**),[29] (1,4-{Si^tBuMe_2}C_8H_6),[30] (1,3,5-{$SiMe_3$}C_8H_6)[31] and (1,4-{$SiPh_3$}C_8H_6).[32] The silylated ligands are cheaper, easier to synthesise and higher yielding in comparison to the alkylated congeners.

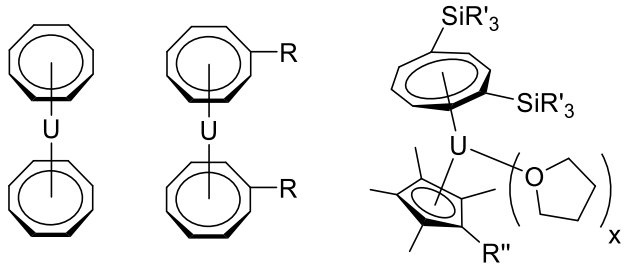

Figure 1.2 Organouranium complexes featuring COT ligands: $UCOT_2$, $UCOT^{R2}_2$, $UCp^{Me4R''}COT^{SiR'}(THF)_x$ where R = OMe, NMe_2, Et, ^{t}Bu and Mes, R' = TIPS or TMS groups and R''= H or Me and x = 0 or 1.

Uranocenes are excellent for probing the interactions between the highly symmetric 5f orbitals and ligand orbitals though they offer very little in terms of reactivity due to saturation of the metal centre. Closely related to uranocenes are mono-COT compounds, these offer the steric protection of a single COT ligand and in combination with other ligands show a wider variety of reactivity. Streitwiser *et al*. reported the synthesis of $UCOTCl_2(Py)_2$, $UCOTCl_2(THF)_2$ (**Figure 1.3**) and $UCOT(acac)_2$ though were unsuccessful in functionalising the dichloride complexes with alkylmetal reagents. [33] Employing the bulkier COT^{TMS2} ligand Cloke *et al*. demonstrated that the increased steric encumbrance and solubilising nature of the TMS ligand results in the isolation of $UCOT^{TMS2}(BH_4)_2$ (**Figure 1.3**), free of coordinating solvent. Ephritikhine *et al*. were able to crystallographically characterise $UCOT(BH_4)_2(OPPh_3)$, the structure of which shows a three-legged piano stool configuration.[34] In the same publication, the synthesis of the first uranium mixed-sandwich complex, $UCOT(Cp)(BH_4)OPPh_3$, was outlined. Soon after this, Clark *et al*. reported the synthesis of the U(III) mixed-ring complex, UCOTCp*(THF). [35] Though no crystal structure was obtained, ^{1}H NMR, IR and elemental analysis supported this formulation. Interestingly, UCOTCp*(THF) reacts with Me_2bpy to form UCOTCp*(Me_2bpy), an early

indication that U(III) mixed-sandwich compounds have a suitable 'pocket' which substrates may bind to. Several years later, Ephritikhine *et al*. reported the synthesis of $UCOTI_2(THF)_2$, which they used as a precursor to a range of mixed-sandwich systems, for example UCOTCp*I(THF).[36] In terms of the reactivity of these complexes, Cloke *et al*. demonstrated how the mixed-sandwich complex, $UCOT^{TIPS2}Cp^*(THF)$ (**Figure 1.2**),[29] is able to reductively cyclotrimerize CO to give a binuclear deltate-bridged structure.

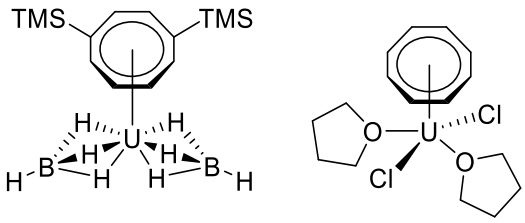

Figure 1.3 Examples of organouranium 'half-sandwich' complexes, $UCOT^{TMS2}(BH_4)_2$ and $UCOTCl_2(THF)_2$.

1.3.3 Pentalene Uranium Complexes

Pentalene, $[C_8H_6]^{2-}$ is an alternative 8-membered dianionic carbocyclic ligand to COT. It features two fused-five-membered rings with a 1,5-transannular bond and can participate in a wide variety of bonding modes. Due to challenging syntheses required, pentalene has received much less attention than COT but has been increasingly studied over the past two decades as the number of reliable synthetic procedures has increased. Jones and Schwab first demonstrated the synthesis of $PentH_2$, a precursor to $[C_8H_6]^{2-}$, as a mixture of four isomers from COT using flash vacuum pyrolysis (FVP). Cloke *et al*. later optimised the reaction conditions by carefully controlling the COT addition rate, pressure, flow rate and temperature to produce the isomers of $PentH_2$. These isomers are then deprotonated with ^{n}BuLi to give $[Li(DME)_x]_2Pent$ in 90% yield. In 1999 Cloke *et al*. reported the synthesis of $U(Pent^{TIPS2})_2$.[37] The complex features two silylated pentalene ligands for increased crystallinity and solubility in hydrocarbon solvents.

Several years later the U(III) complex, $UPent^{TIPS2}Cp^*$, was shown to mediate the reduction of N_2 to N_2^{2-} under an over pressure of N_2 (**Figure 1.4**). Crystallographic analysis of the reduced dinitrogen moeity, $[(U\{\eta^5\text{-}Cp^*\}\{\eta^8\text{-}Pent^{TIPS2}\})_2(\mu\text{-}\eta^2\text{:}\,\eta^2\text{-}N_2)]$, revealed an N–N bond length of 1.232(10) Å, significantly

longer than that of free N_2 (1.098 Å), consistent with an N–N double bond.[38] Using the same mixed-sandwich compound, Cloke *et al*. later showed how ^{t}BuCP could be doubly reduced to give the bimetallic complex, [(U{η^5-Cp*}{η^8-Pent^{TIPS2}})$_2$(μ-η^2:η^1-^{t}BuCP)], with the reduced ^{t}BuCP fragment coordinating to one of the uranium centres in an η^2 fashion.[39]

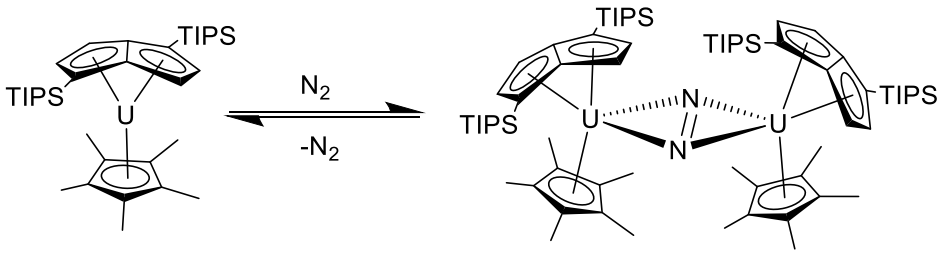

Figure 1.4 Dinitrogen activation using UCp*Pent^{TIPS2}.

Using permethylated pentalene, Pn*, O'Hare *et al*. synthesised several uranium sandwich and half-sandwich complexes, including: [Pn*U(μ-Cl)$_4$][Li(TMEDA)]$_2$,[40] UPn*,[41] [Pn*UCp*(μ-Cl)$_2$][Li(TMEDA)][40] and Pn*UCp$_2$*.[40] UPn*$_2$ was shown to have complicated electrochemical behaviour. The authors suggested a U^{IV}/U^{III} redox couple of -1.13 V *vs* $FeCp_2^{+/0}$ though this is not in agreement with similar uranium compounds measured in our laboratory; it seems more likely given our findings that the reduction event observed at *ca* -2.2 V *vs* $FeCp_2^{+/0}$ is the U^{IV}/U^{III} redox couple.

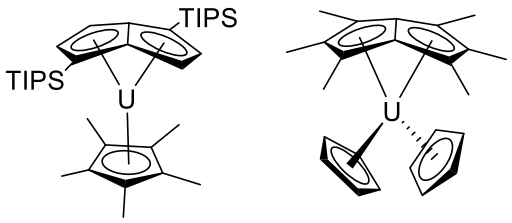

Figure 1.5 Examples of pentalene containing uranium complexes, UCp*Pent^{TIPS2} and UPn*$_2$.

1.3.4 Arene Uranium Complexes

Metal-arene interactions for uranium are a cornerstone of modern organometallic chemistry. The first report of such an interaction was published in 1971 and described the synthesis of U(AlCl$_4$)$_3$(C$_6$H$_6$) under reducing conditions.[42] The neutral π-basic arene ligand is coordinated to a highly Lewis acidic U(III) centre in a dative bonding interaction. Almost two decades later, Ephritikhine *et al*. published

work on a compound featuring a similar interaction, the synthesis of $U(BH_4)_3Mes$ involved heating $U(BH_4)_4$ in mesitylene at 150 °C for 20 minutes to give the desired compound in 80% yield.[43]

In 2000, Cummins *et al*. reported the synthesis of $(\mu\text{-}\eta^6\,\eta^6\text{-}C_7H_8)[U(N[R]Ar)_2]_2$ (R = $C(CH_3)_3$ and Ar = 3,5-C_6H_3-Me_2) by the reduction of $U(I)(N[R]Ar)_2$ with KC_8 in toluene to form the bimetallic inverted sandwich complex (**Figure 1.6**).[44] Structural analysis revealed a shortening of the C–C bonds in the central toluene moiety (with respect to free toluene) and a 'puckering' of one of the carbon atoms above the mean plane, indicating a strong uranium arene interaction. Most interestingly, DFT evidence suggests the uranium arene interaction features a considerable δ-backbonding interaction. Reactivity studies with PhSSPh indicate uranium is acting as a U(II) synthon, however, contrasting evidence from XANES studies suggest the uranium centres are in the +3 oxidation state.[45]

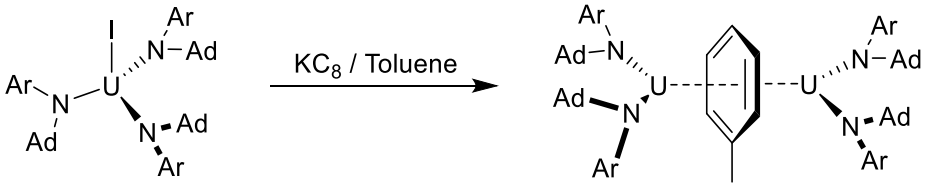

Figure 1.6 Formation of uranium arene complex.

The work by Cummins *et al*. on uranium δ-backbonding interactions sparked interest in uranium arene interactions and the following years saw an increase in publications on this subject, encompassing a wider range of uranium oxidation states, ligands, arene substrates and experimental techniques to probe the bonding interaction. Using a tri-anionic tripodal ligand system, Liddle *et al*. synthesized, $[\{U(Ts^{Xy})\}_2(\mu\text{-}\eta^6\eta^6\text{-}C_6H_5Me)]$ (Ts^{Xy} = HC-$(SiMe_2NAr)_3$; Ar = 3,5-$Me_2C_6H_3$) (**Figure 1.7**),[46] with experimental evidence suggesting the uranium centres are in the +5 oxidation state where the toluene bears a formal 4- charge.

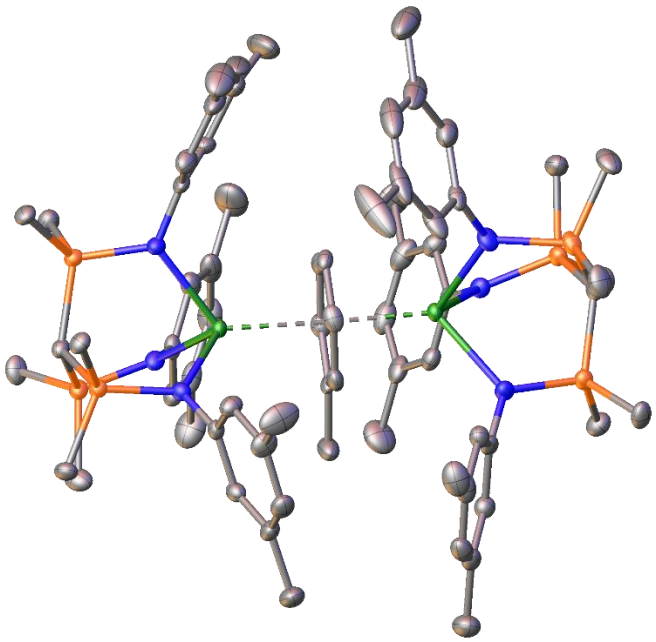

Figure 1.7 Molecular structure of [{U(Ts^{Xy})}$_2$(μ-η^{6}η^6-C_6H_5Me)]. Uranium, green; nitrogen, blue; silicon, orange; carbon, grey. Hydrogen atoms omitted for clarity. Displacement ellipsoids set to 30%. From ref[46].

Another method of investigating uranium arene interactions is to incorporate arene rings into preorganised ligands, effectively forcing such an interaction. Meyer *et al*. achieved this in the [((^{tBu}ArO)$_3$mes)U] (**Figure 1.8**) complex which features a covalent δ-backbonding uranium-mesitylene interaction as shown by theoretical studies.[47] This change in ligand framework results in significantly different electronic properties compared to the tacn-based ligand system as shown by differences in the magnetic moment and electronic absorption spectra, due to the U(5f)-mesityl(π*) δ-interaction.

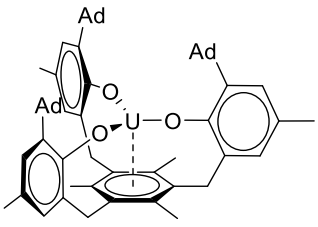

Figure 1.8 Structure of [((^{Ad,Me}ArO)$_3$mes)U].

Several years later, using an extremely bulky monoanionic aryloxide,[48] Meyer *et al*. synthesised two U(III) compounds featuring a terminal U-arene interaction with a pendant phenyl ring from the bulky

aryloxide ligand, $[(Ar^*O)_3U(THF)]$ (Ar^*O = 2,6-Ph_2-C_6H_4-Me, 2,6-bis(diphenylmethyl)-4-methylphenyl) (**Figure 1.9**).

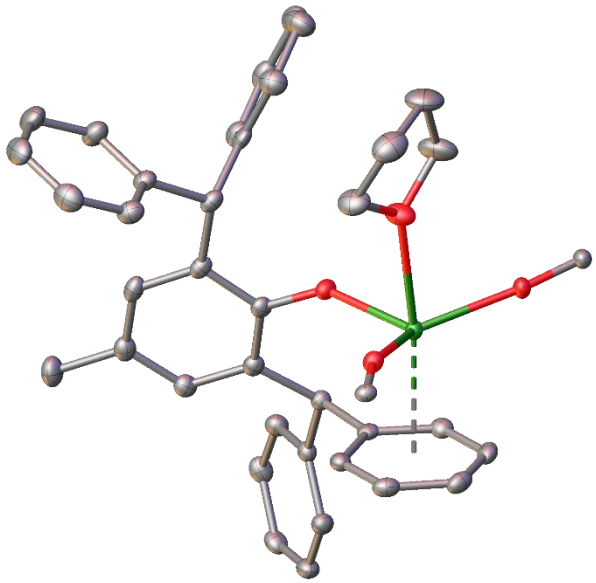

Figure 1.9 Molecular structure of $[(Ar^*O)_3U(THF)]$. U, green; oxygen, red; carbon, grey. Hydrogen atoms and parts of phenyl groups omitted for clarity. Displacement ellipsoids set to 50%.

A recent publication from Fortier *et al*. outlined the synthesis of $L^{Ar}U(I)(DME)$ (L = *p*-terphenyl bis(anilide)) (**Figure 1.10**) which features a uranium arene interaction that is mostly electrostatic in nature and lacking in δ-backbonding, according to DFT studies.[49]

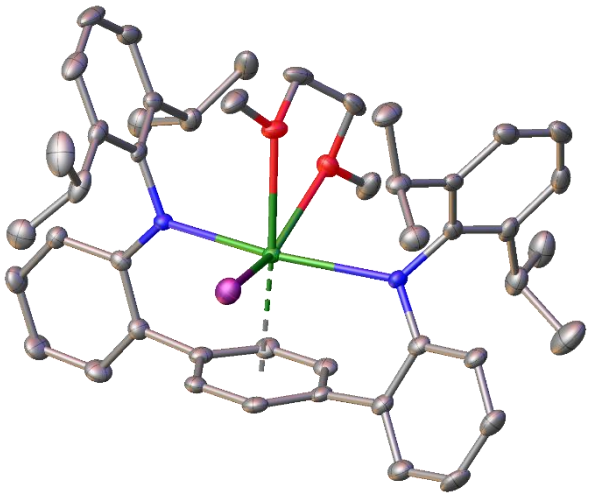

Figure 1.10 Molecular structure of $L^{Ar}U(I)(DME)$. Uranium, green; nitrogen, blue; iodine, purple; carbon, grey. Hydrogen atoms and co-crystallised solvent omitted for clarity. Displacement ellipsoids set to 50%.

1.3.5 Aryloxide Uranium Complexes

In comparison to cyclopentadienyl uranium complexes, complexes featuring aryloxides are far less common. Aryloxide ligands offer alternative steric and electronic properties to metallocene ligands. Firstly, they tend to have lower coordination numbers due to their mono-haptic coordination *via* the hard oxygen donor atom. Secondly, the steric profile of the ligand is more flexible as the phenyl ring that provides steric protection is not coordinated to the metal, thus enabling movement. These differences result in remarkably different reactivity in comparison to homoleptic cyclopentadienyl uranium complexes, especially towards small molecules. Aryloxides can be ligated onto metal centres *via* either salt metathesis or protonolysis methodologies, thus providing a greater synthetic scope.

In 1983 Lappert *et al*. published a report which contained several uranium aryloxide complexes including $UCl_2O(O\text{-}2,6\text{-}^tBu_2C_6H_3)_2$ and $U(NEt_2)(OPh)$.[50] The first homoleptic U(III) aryloxide complex was synthesised by Sattelberger *et al*. in 1988,[51] $U(O\text{-}2,6\text{-}R_2C_6H_3)_3$ (R = ^{i}Pr, ^{t}Bu) *via* protonolysis of the free phenol with $U(N(SiMe_3)_2)_3$ to give the resultant compounds in 50% yield. The crystal structure of $U(O\text{-}2,6\text{-}^iPr_2C_6H_3)_3$ revealed a three legged piano stool structure with a weak uranium-phenyl ring π-interaction resulting in a dimeric structure. Sattelberger *et al*. later published two examples of homoleptic uranium aryloxide complexes, $U(O\text{-}2,6\text{-}R_2C_6H_3)_4$ (R = ^{i}Pr, ^{t}Bu).[52,53]

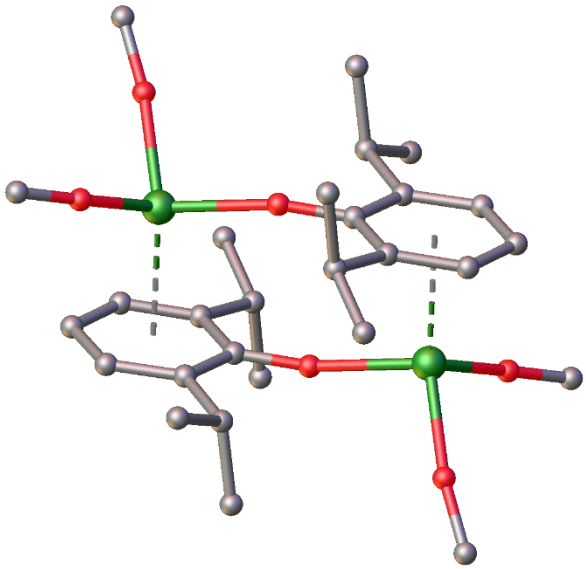

Figure 1.11 Molecular structure of U(O-2,6-^{i}Pr$_2$C$_6$H$_3$)$_3$ featuring the π-arene bridging interaction. Uranium, green; oxygen, red; carbon, grey. Hydrogen atoms have been omitted and only ipso carbons of the terminal phenoxides are shown for clarity.

Nearly 30 years later Arnold *et al*. used some of the aforementioned U(III) aryloxide complexes to activate N_2, CO and CO_2.[54] The U(III) complexes, U(O-2,6-^{t}Bu$_2$C$_6$H$_3$)$_3$ and U(O-2,4,6-^{t}Bu$_3$C$_6$H$_2$)$_3$, activate N_2 to give, [U(OAr)$_3$]$_2$(μ-η^2:η^2-N_2) (OAr = O-2,6-^{t}Bu$_2$C$_6$H$_3$ and O-2,4,6-^{t}Bu$_3$C$_6$H$_2$) (**Scheme 1.2**), which is consistent with a N_2^{2-} moiety as indicated by X-ray crystallography. [U(O-2,4,6-^{t}Bu$_3$C$_6$H$_2$)$_3$]$_2$(μ-η^2:η^2-N_2) is able to activate CO_2 unlike U(O-2,6-^{t}Bu$_2$C$_6$H$_3$)$_3$, which undergoes ligand rearrangement upon reaction with CO_2 to form U(O-2,6-^{t}Bu$_2$C$_6$H$_3$)$_4$ (**Scheme 1.2**).

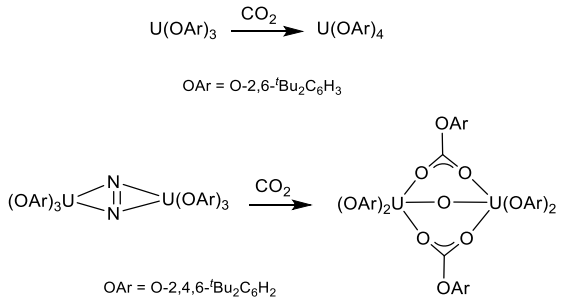

Scheme 1.2 Reactivity of U(OAr)$_3$ and [U(OAr)$_3$]$_2$(μ-η^2:η^2-N_2) towards CO_2.

Meyer *et al*. have been very successful in incorporating aryloxide ligands in various anchor motifs (**Figure 1.8** and **Figure 1.12**).[47,55,56] The steric bulk of the aryloxide arms can be readily modified with derivatives including tert-butyl, adamantyl and even diamantanyl, thus enabling a range of

environments around the 'reaction pocket' above the metal and between the ortho-substituents on the three aryoxide arms.[57] The mesitylene anchored trisaryloxide ligand has been used to isolate a U(II) complex,[58] [K(2.2.2-crypt)][((^{Ad,Me}ArO)$_3$mes)U], from the low-temperature potassium reduction of [((^{Ad,Me}ArO)$_3$mes)U] in the presence of 2.2.2-cryptand, with the mesitylene anchor key to stabilising uranium in the +2 oxidation state *via* a δ-backbonding interaction.

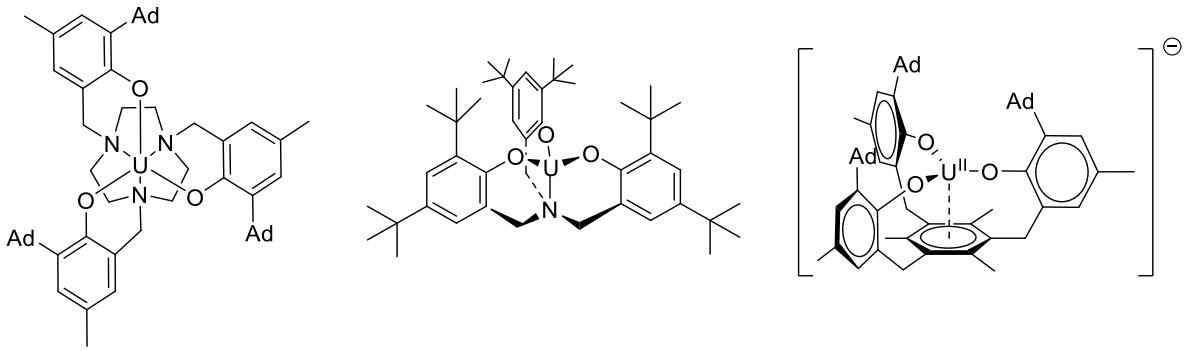

Figure 1.12 Structures of [((^{Ad,Me}ArO)$_3$tacn)U] (left), [((^{tBu}ArO)$_3$N)U] (centre) and [K(2.2.2-crypt)][((^{Ad,Me}ArO)$_3$mes)U] (right, [K(2.2.2-crypt)] not shown for clarity).

A monoiodide U(III) cyclam complex, [U(κ^6-{(^{tBu2}ArO)$_2$Me$_2$-cyclam})I] (**Figure 1.13**), featuring two phenolate arms was synthesised in 2015.[59] Two equivalents of this complex are able to effect the four-electron reduction of azobenzene to give the U(VI) bis(imido) complex [U(κ^4-{(^{t}Bu$_2$ArO)$_2$Me$_2$-cyclam})(NPh)$_2$] and the U(IV) species [U(κ^6 -{(tBu$_2$ArO)$_2$Me$_2$-cyclam})I][I].

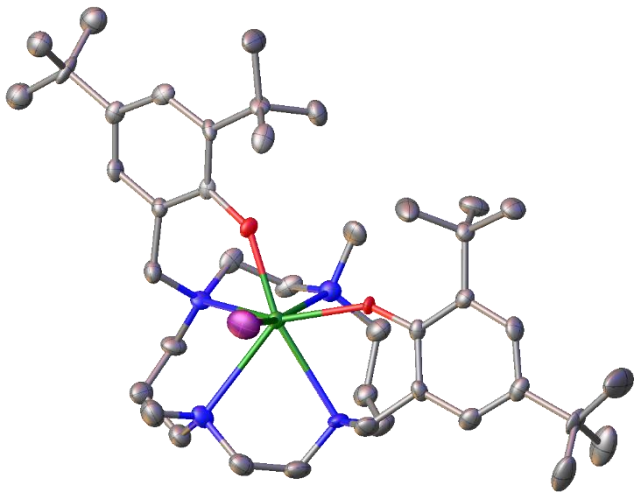

Figure 1.13 Molecular structure of [U(κ^6-{(^{tBu2}ArO)$_2$Me$_2$-cyclam})I]. Uranium, green; oxygen, red; nitrogen, blue; iodine, purple; carbon, grey. Hydrogen atoms and co-crystallised solvent omitted for clarity. Displacement ellipsoids set to 50%.

Recent years have seen the synthesis of tetra(aryloxide) uranium complexes. Arnold *et al*. synthesised the dinuclear uranium complex, ($U_2I_4(THF)_6LP^*$) (**Figure 1.14** , left), as part of a family of compounds that provide a flexible,[60] robust and modular platform for the two uranium centres suitable to mediate transformations. Using a cyclen anchor, Meyer *et al*. synthesised an air-stable tetra(aryloxide) complex,[61] [((^{tBu,tBu}ArO)$_4$cyclen)U] (**Figure 1.14**, right), with the uranium centre in an eight-coordinate tetragonal environment.

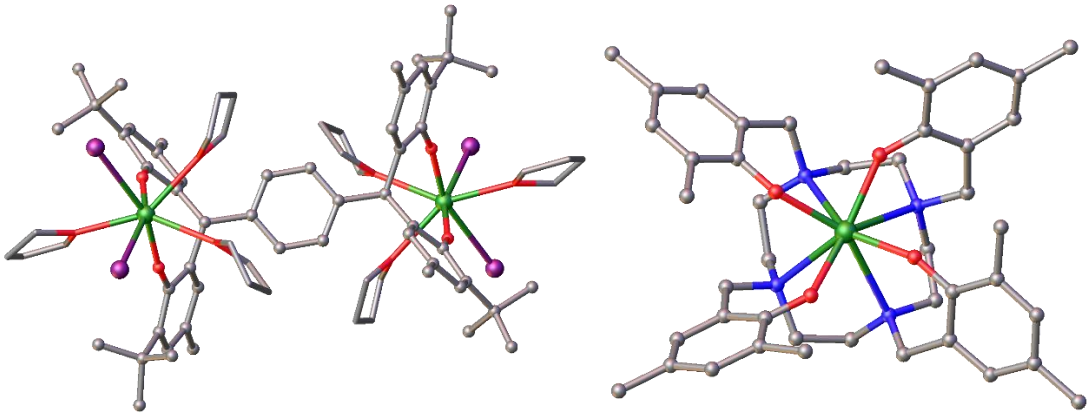

Figure 1.14 Molecular structures of ($U_2I_4(THF)_6LP^*$) (left) and [((^{tBu,tBu}ArO)$_4$cyclen)U] (right). Uranium, green; oxygen, red; nitrogen, blue; iodine, purple; carbon, grey. Hydrogen atoms and co-crystallised solvent omitted for clarity.

1.3.6 Tris(pyrazolyl)borate Uranium Complexes

Since their initial synthesis by Trofimenko, tris(pyrazolyl)borate (Tp) ligands have featured prominently in d-bock chemistry,[62] whereas their application to f-block chemistry has been less prevalent. Tp ligands have proven to be extremely versatile due to the simplicity of their synthesis and the ease at which the electronic and steric properties can be tuned. Tp ligands are analogous to cyclopentadienyl (Cp) in that they are both anionic 6-electron donors, however, they differ in that Tp ligands are hard σ-donors while Cp ligands are softer π-donors.

The first uranium-Tp^{Me2} complex was reported by Bagnall *et al*. in 1975, synthesised by the reaction of UCl_4 and KTp^{Me2} to give UCl_3Tp^{Me2}.[63] Takats *et al*. (and other laboratories), have published many reports investigating the structure of f-element complexes bearing scorpionate ligands, many of which have featured uranium with chloride and alkyl ligands.[64,65] Using $UI_3(THF)_4$, Takats synthesised [U(κ^3-

$Tp^{Me2}I_2(THF)_2$] and [U(κ^3-Tp^{Me2})(κ^2-N,N-η^2-(*N*=*N*)-Tp^{Me2})I], the latter displaying an unexpected side-on interaction between U and N=N of one of the pyrazolyl rings (**Figure 1.15**).[66] The bulky nature of the Tp^{Me2} ligand has enabled the exploration of rare U(III) alkyl insertion chemistry as part of a closed synthetic cycle with CO_2.[67] The use of Tp^{Me2} has also enabled the synthesis of terminal-oxo complexes,[68] compounds containing redox active bpy ligands and low-valent uranium fluoride complexes that activate C–F bonds. [69,70]

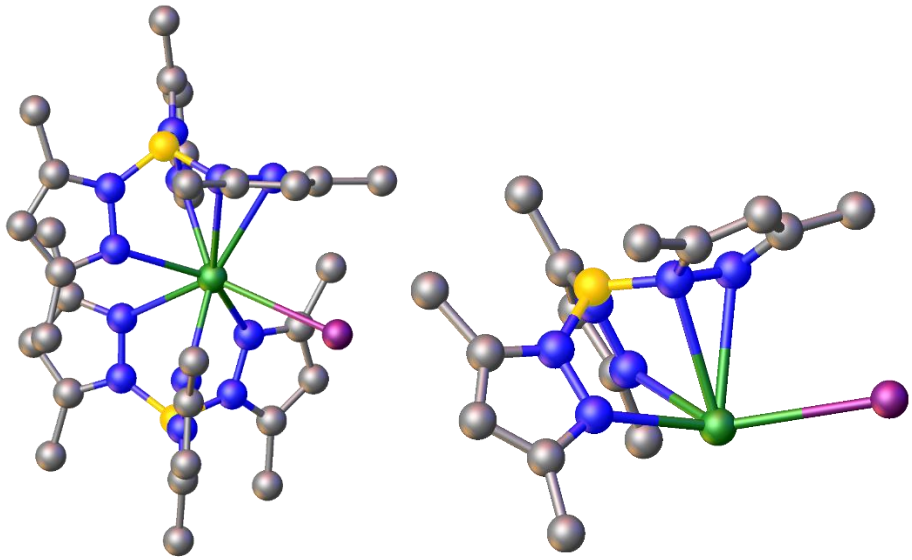

Figure 1.15 Molecular structure of [U(κ^3-Tp^{Me2})(κ^2-N,N-η^2-(*N*=*N*)-Tp^{Me2})I]. Uranium, green; nitrogen, blue; boron, yellow; carbon, grey. Hydrogen atoms omitted for clarity. Displacement ellipsoids not shown. A Tp^{Me2} ligand has been removed from the right-hand image for clarity.

This literature review has covered organometallic uranium complexes containing ligands relevant to this thesis. The next section will focus on small molecule activation using U(III) complexes, some of which have already been mentioned.

1.4 Uranium Small Molecule Activation

Judicious choice in ligands around the U(III) centre is key to enabling the activation of small molecules. Tuning of the steric and electron properties of the supporting ligands can result in exceptional differences in reactivity. Uranium in the +3 oxidation state is well placed to mediate transformations of

substrates such as CO and CO_2 by virtue of its large ionic radii,[13] oxophilic nature and easily accessible, yet large U^{III}/U^{IV} redox couple.[11] A summary of transformations mediated by U(III) complexes is given below.

1.4.1 Carbon Monoxide

Carbon monoxide is an important carbon feedstock and is used alongside H_2 in the Fischer-Tropsch process in the production of hydrocarbons and oxygenates. This process is extremely energy intensive, due to the high temperatures and pressures typically used. Transition metal-CO interactions are extremely common due to the favourable σ bonding and π* back-bonding interactions with d-orbitals, while such interactions with the actinides are much less favourable due to the contracted and highly symmetric nature of the f-orbitals.

Interest in uranium carbonyl complexes originated in the Manhattan Project as it was hoped that, like transition metal carbonyl complexes, a $U(CO)_6$ complex would be more volatile and safer than UF_6. $U(CO)_6$ was synthesised in 1971 by condensing uranium metal vapour into a carbon monoxide-argon matrix at 4 K. The observation of a band at 1961 cm^{-1} implies that the uranium metal centre is acting as a π-donor to CO as indicated by the decreased CO stretch value.[71]

The first organometallic uranium carbonyl complex was reported in 1986 by Andersen and co-workers.[72] Upon exposure to 1 atm of CO, a solution of $UCp^{TMS2}{}_3$ immediately changed colour to give $UCp^{TMS2}{}_3CO$, however, upon exposure to vacuum or purging with argon, CO was removed, indicating CO is only weakly bound. DFT studies calculated a U–CO bond strength of 14 Kcal mol^{-1} for $UCp^{TMS2}{}_3CO$, substantially less than for the transition metal complex $ZrCp^*{}_2CO_2$, which has a BDE value of 40 Kcal mol^{-1}.[73]

The first crystallographically characterised uranium carbonyl complex was synthesised in 1995 by Carmona *et al*..[74] A solution of $UCp^{Me4H}{}_3$ was exposed to an atmosphere of CO to give an end-on bound uranium carbonyl complex, $UCp^{Me4H}{}_3CO$. As with $UCp^{TMS2}{}_3CO$, the binding of CO to $UCp^{Me4H}{}_3CO$ (**Figure 1.16**) is reversible and the starting material can be reformed upon exposure to vacuum. X-ray diffraction studies revealed that the CO molecule is C bound with an elongated C–O bond length of

1.42(7) Å (free CO, 1.28 Å). Due to the value being within 3 σ of the value for free CO caution should be taken. Further CO activation studies were carried out on other tris cyclopentadienyl uranium complexes, including [UCp^{TMS2}_3CO] and [$(Cp^{tBu})_3UCO$].[75] In 2003, Evans *et al.,* reported the synthesis and characterisation of UCp^*_3CO, which has a linear U–C–O unit like the aforementioned complexes.[76] In comparison to other uranium carbonyl complexes, the higher stretching frequency found in UCp^*_3CO is due to the steric crowding from the Cp* ligands. Donation of electron density to CO *via* π-symmetry back bonding from UCp^R_3 originate from ligand based orbitals as shown by DFT studies of such uranium complexes and, more recently a cationic Th(IV) carbonyl complex.[77]

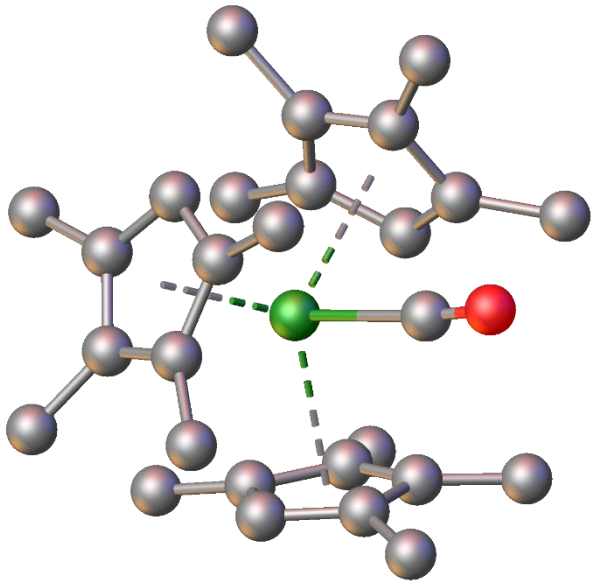

Figure 1.16 Molecular structure of $U(Cp^{Me4H})_3CO$. Uranium, green; oxygen, red; carbon, grey. Hydrogens omitted for clary. Displacment ellipsoids not shown.

The first report of stoichiometric reduction of CO by a uranium(III) complex was published by Meyer *et al*. in 2004.[78] A solution of [$(({}^{tBu}ArO)_3tacn)U$] was placed under 1 atm of CO to give [$\{(({}^{tBu}ArO)_3tacn)U\}_2(\mu{:}\eta^1,\eta^1\text{-}CO]$(**Figure 1.17**). The product was characterised as a mixed valence bimetallic U(III)/U(IV) system with CO sitting on an inversion centre. The proposed mechanism involves the capping of a charge-separated species, [$\{(({}^{tBu}ArO)_3tacn)U\}_2(\mu{:}\eta^1,\eta^1\text{-}CO)$] by an equivalent of the uranium(III) reactant.

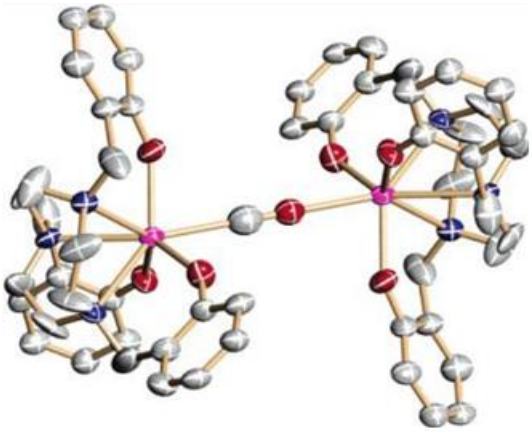

Figure 1.17: Crystal structure of [{((^{tBu}ArO)$_3$tacn)U}$_2$(μ:η^1,η^1-CO]. Colours: U, pink; O, red; N, blue; C, grey. Hydrogen atoms and tert-butyl groups omitted for clarity. Displacement ellipsoids shown at 50% probability level. Image from.[78]

Cloke *et al*. reported the reductive homologation of CO by UCOT^{TIPS2}Cp^{Me4R} to give the deltate dianion (R = Me) ($C_3O_3^{2-}$) or squarate dianion ($C_4O_4^{2-}$) (R = H) (**Figure 1.18**).[17,29] Up until these publications the homologation of carbon monoxide was limited to extremely harsh conditions involving molten alkali metals and high pressures. Addition of 0.95 equivalents of CO to UCOT^{TIPS2}Cp* resulted in the selective formation of a uranium ynediolate complex, though addition of further equivalents of CO to this ynediolate complex did not yield higher oxocarbons. Subsequent theoretical studies suggested the formation of oxocarbons occurred through a zig-zag intermediate (**Figure 1.18**, top left).[79,80] Discovery of this intermediate encouraged experiments involving CO and H_2, leading to the reductive coupling of CO and H_2 mediated by UCOT^{TIPS2}Cp* to yield UCOT^{TIPS2}Cp*(OMe).[81]

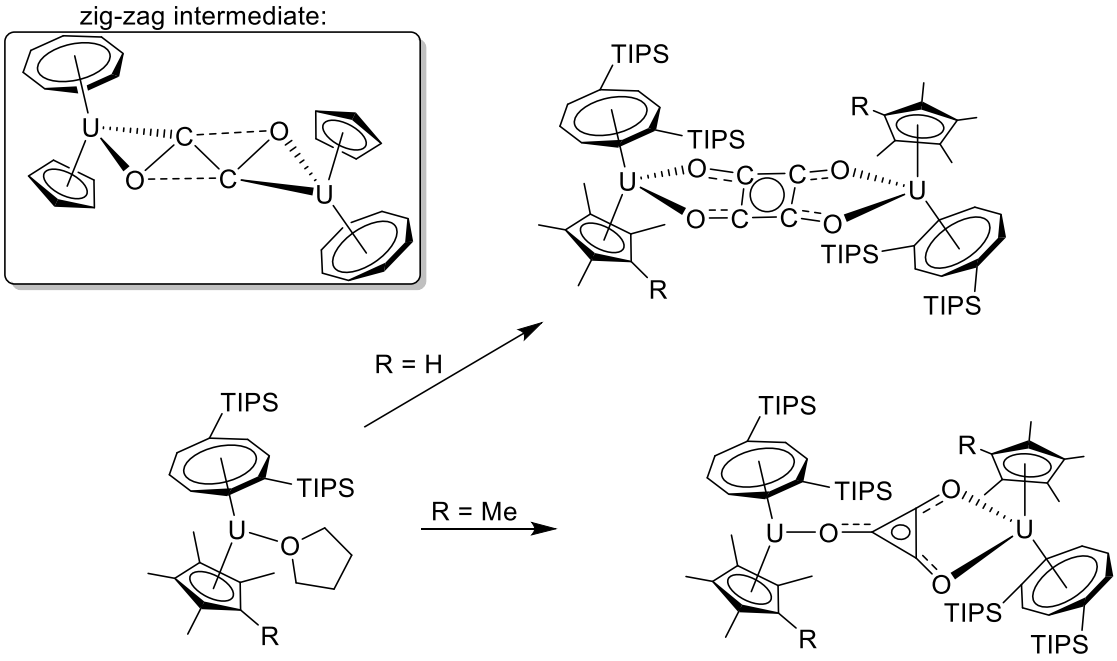

Figure 1.18 Reaction between $UCOT^{TIPS2}Cp^{Me4R}THF$ (where R = H or Me) and CO. The proposed zig-zag intermediate calculated using DFT is also shown in the top left corner.

Other examples of uranium ynediolate complex formation have been achieved using $UCOT^{TMS2}Cp^{Me4R}$ (R = Et and $SiMe_3$),[82] $UN^{TMS2}{}_3$,[83] $UOAr_3$ (OAr = O-2,6-$tBuC_6H_3$ and O-2,4,6-$^tBuC_6H_2$) and $U(TREN^{TBDMS})$ (**Figure 1.19**).[54,84] Upon heating $U(TREN^{TBDMS})_2(\mu\text{-}\eta^1\text{: }\eta^1\text{-}C_2O_2)$ or $(UN^{TMS2}{}_3)_2(\mu\text{-}\eta^1\text{: }\eta^1\text{-}C_2O_2)$ ligand activation occurs, indicating functionalisation of the ynediolate moiety is possible. A closed synthetic cycle involving $U(TREN^{TBDMS})_2(\mu\text{-}\eta^1\text{: }\eta^1\text{-}C_2O_2)$ was also shown to be possible with the use of RMe_2SiI (R = Me or Ph) and potassium as electrophiles and strong reducing agents, respectively.

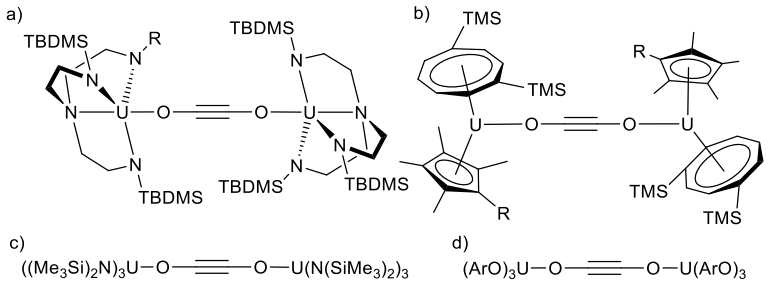

Figure 1.19 Uranium ynediolate products. a) $U(TREN^{TBDMS})_2(\mu\text{-}\eta^1\text{: }\eta^1\text{-}C_2O_2)$, b) $(UCOT^{TMS2}Cp^{Me4R})_2(\mu\text{-}\eta^1\text{: }\eta^1\text{-}C_2O_2)$ (R = Et and $SiMe_3$), c) $U(N(SiMe_3)_2)_3)_2$ $(\mu\text{-}\eta^1\text{: }\eta^1\text{-}C_2O_2)$ and d) $U((OAr)_3)_2(\mu\text{-}\eta^1\text{: }\text{-}C_2O_2)$ (OAr = O-2,6-$tBuC_6H_3$ and O-2,4,6-$tBuC_6H_2$).

1.4.2 Carbon Dioxide

CO_2 is a potent greenhouse gas and is produced and released into the atmosphere from anthropogenic sources in large quantities. It is therefore highly desirable to find technologies that utilise CO_2 from the atmosphere as a C_1 feedstock. One way of utilising CO_2 is to use organometallic complexes to mediate its transformation into higher value chemicals such as methanol, as Millstein has shown.[85] The first step in the transformation of CO_2 is coordination to a metal centre, which is possible in several coordination modes, some of which are shown below (**Figure 1.20**).

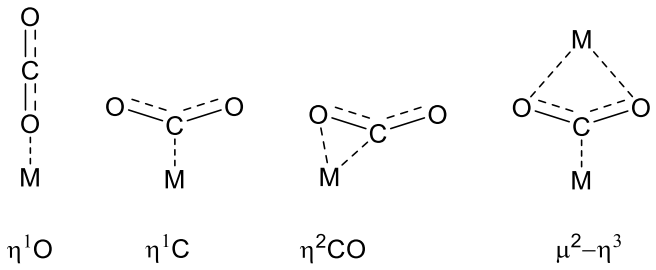

Figure 1.20 Coordination modes of CO_2 in mono- and dinuclear complexes.

Uranium is well placed to activate the strong (532 kJ mol^{-1}) polar bonds of CO_2 due to the oxophilic and highly reducing nature in the +3 oxidation state. Uranium reacts with CO_2 in one of two main modes, one being the insertion of CO_2 into a U–E bond that typically gives a product that coordinates in a bidentate fashion due to the large coordination sphere of the metal. As this reaction pathway has not been studied in this thesis, it will not be mentioned in further detail.

More relevant to this thesis is the second mode of reactivity, the reduction of CO_2. Early reports of CO_2 reduction involved the U(III) complex, $UCp^{TMS2}{}_3$.[86] Upon reaction with 1 atm of CO_2, $UCp^{TMS2}{}_3$ formed a μ-oxo bridging moiety, $[\{(UCp^{TMS2}{}_3\}_2(\mu\text{-}O)]$, with concomitant release of CO. The authors suggested that the mechanism involves a bimetallic μ-CO_2 complex, based on the analogous CS_2 complex, $\{ UCp^{TMS2}{}_3\}_2(\mu\text{-}\eta^1\text{:}\eta^2\text{-}CS_2)$, isolated from CS_2. Meyer *et al*. carried out similar work with U(III) in the $[((^{tBu}ArO)_3tacn)U]$ system.[87] Upon exposure to CO_2 a μ-O adduct was formed along with concomitant release of CO. In the report, a colourless intermediate was observed, proposed to be an unstable bimetallic bridged CO_2 species.

In 2004, it was demonstrated that a change in the sterics of the ligand from [((^{tBu}ArO)$_3$tacn)U] to the adamantyl derivative [((^{Ad}ArO)$_3$tacn)U] can bring about a drastic change in reactivity.[88] An η^1-O-CO_2 capped monometallic species was formed when [((^{Ad}ArO)$_3$tacn)U] was reacted with excess CO_2 at room temperature (**Figure 1.21**). This coordination mode is rare and can be attributed to the reactivity pocket created by the bulky adamantyl groups. The resonance structure for the product is shown below (**Figure 1.22**) and is consistent with magnetic data and electronic/vibrational spectroscopic data.

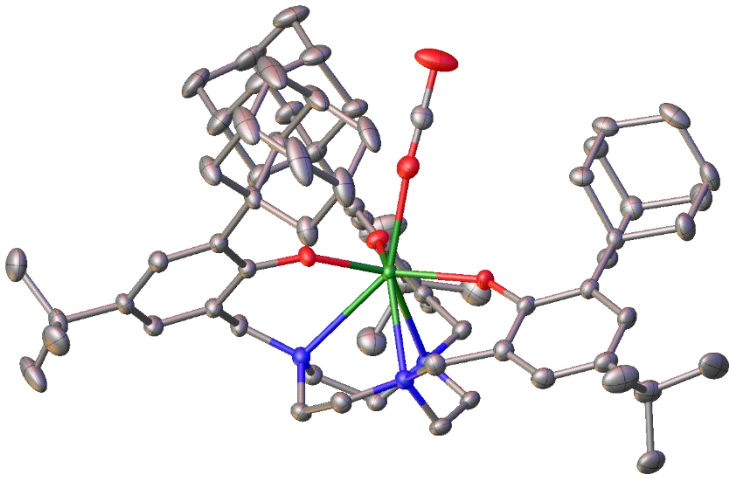

Figure 1.21: Crystal structure of [((^{Ad}ArO)$_3$tacn)U(CO_2^S)]. Colours: U, green; N, blue; C, grey; O, red. Hydrogens omitted for clarity.

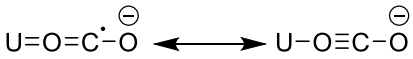

Figure 1.22 Resonance structures for the uranium CO_2 reduction product.

[((^{tBu}ArO)$_3$tacn)U_2(μ-O)] reacts with CO_2 to give [((^{tBu}ArO)$_3$N)U)$_2$(μ-O)], no carbonate formation is observed due to the lack of accessibility of the bridging O^{2-} ligand.[87] Modifying the chelating anchor of these trisaryloxides systems to N- or mesitylene- in the following compounds, [((^{Ad}ArO)$_3$N)U] and [((^{tBu}ArO)$_3$mes)U], results in different reactivity towards CO_2.[56] These complexes form the carbonate species, [{((^{Ad}ArO)$_3$N)U}$_2$(μ-η^1:η^2-CO_3)] and [{((^{tBu}ArO)$_3$mes)U}$_2$(μ-η^2:η^2-CO_3)] respectfully, as the central anchors of these two complexes increase how much of the central oxygen is exposed in the bridging μ-O intermediates, therefore opening up the pathway to carbonate formation from CO_2 insertion into the U–O bond. Similar bridged carbonate systems have been observed with

$UCOT^{TIPS2}Cp^{Me4H}$ and [{$U(OSi(O^tBu)_3)_2(\mu\text{-}OSi(O^tBu)_3\}_2$].[89,90] Upon exposure to an excess of CO_2 both of these U(III) complexes form bimetallic U(IV) carbonate complexes.

1.4.3 Reductive coupling of CO_2

Formation of oxalate, $(C_2O_4)^{2-}$, from the reductive coupling of CO_2 has been accomplished with many well-defined organometallic complexes across the periodic table including Mg(I),[91,92] Ti(III),[93] Fe(I),[94] Cu(I),[95] Ln(II) complexes and more recently $ThCp^{TMS2}{}_3$.[96]

Recently, it has been shown uranium(III) complexes can mediate such transformations. Several years ago it was reported that $UCOT^{TMS2}Cp^{Me4R}$ (R = Me, Et and iPr) was able to reductively couple CO_2 to give bimetallic $\eta^2{:}\eta^2\text{-}C_2O_4$ bridged complexes (**Scheme 1.3**), among other products, depending on the steric bulk of the Cp ligand.[11] When $UCOT^{TMS2}Cp^{Me4tBu}$ was used, oxalate formation was not observed, presumably due to increased steric bulk. Electrochemical and theoretical studies indicated the difference in reactivity is due to the increasingly bulky ligands and not due to differing electronic properties of the marginally different ligand systems. Meyer *et al*. published a similar study outlining how [($(^{n\text{P}}ArO)_3$tacn)U] is also able to reductively couple CO_2 to form oxalate.[97]

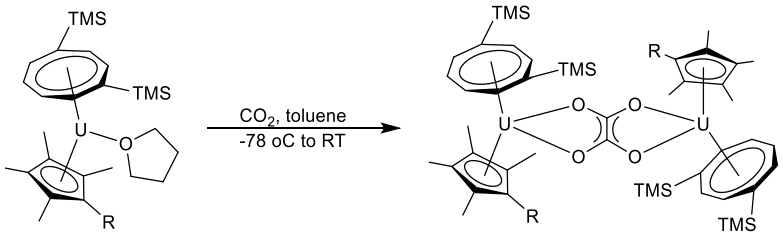

Scheme 1.3 Synthesis of $\{UCOT^{TMS2}Cp^{Me4R}\}_2(\mu\text{-}\eta^2{:}\eta^2\text{-}C_2O_4)$ (R = Me, Et and iPr).

1.4.4 Carbon Disulphide

Activation and functionalisation of CS_2 is of interest due to it being a CO_2 analogue so it may augment our current understanding of CO_2 and enable the isolation of otherwise unstable species.

The first example of U(III) reduction of CS_2 was reported by Andersen *et al*. who showed that two equivalents of $U(Cp^{Me})_3(THF)$ doubly reduce CS_2 to CS_2^{2-} to form the complex, $\{U(Cp^{Me})_3\}_2(\mu\text{-}\eta^1{:}\eta^2\text{-}CS_2)$ (**Scheme 1.1**), which features two inequivalent uranium centres as shown by ^{1}H NMR and X-ray

crystallography.[98] The bonding in this complex is very different to that of typical transition-metal CS_2 complexes as π-donation from U(IV) to the LUMO of CS_2 is not possible due to the symmetry of the metal orbitals.

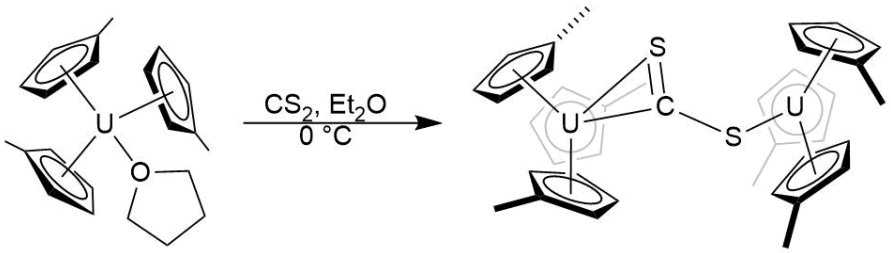

Scheme 1.4: Formation of $\{U(Cp^{Me})_3\}_2(\mu\text{-}\eta^1\text{:}\eta^2\text{-}CS_2)$ from $U(Cp^{Me})_3(THF)$ and CS_2.

Meyer *et al*. showed how $[((^{Ad}ArO)_3N)U(DME)]$ reacts with CS_2 to form $[\{((^{Ad}ArO)_3N)U\}_2(\mu\text{-}\eta^2\text{:}\eta^2\text{-}C_2S_4)]$ as the major product (80%) and $[\{((^{Ad}ArO)_3N)U\}_2(\mu\text{-}\eta^2\text{:}\eta^2\text{-}CS_3)]$ as the minor product (20%) (**Scheme 1.5**).[99,100] The formation of tetrathiooxalate is likely due to dimerization of a reactive $[((^{Ad}ArO)_3N)U(CS_2^{\cdot-})]$ species, while the formation of thiocarbonate mirrors CO_2 chemistry with the loss of 'CS' and insertion of CS_2 into $[((^{Ad}ArO)_3N)U_2(\mu\text{-}S)]$. Reduction of $[\{((^{Ad}ArO)_3N)U\}_2(\mu\text{-}\eta^2\text{:}\eta^2\text{-}C_2S_4)]$ with Na/Hg led to the formation of the ethylenetetrathiolate complex, $[Na(DME)_3]_2[\{((^{Ad}ArO)_3N)U\}_2(\mu\text{-}C_2S_4)]$.

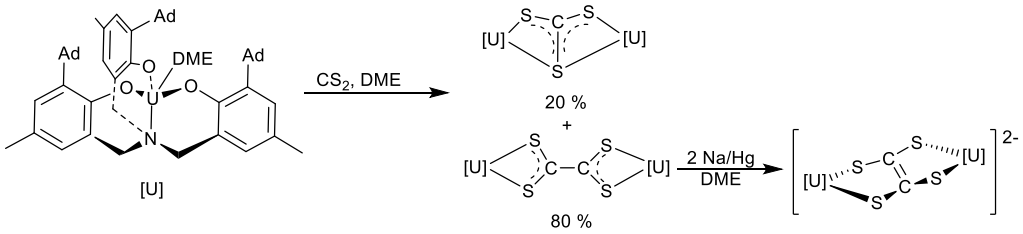

Scheme 1.5: Reaction of $[((AdArO)_3N)U(DME)]$ with CS_2 to form $[\{((^{Ad}ArO)_3N)U\}_2(\mu\text{-}\eta^2\text{:}\eta^2\text{-}CS_3)]$ (20% yield) and $[\{((^{Ad}ArO)_3N)U\}_2(\mu\text{-}\eta^2\text{:}\eta^2\text{-}C_2S_4)]$ (80% yield). Also shown is the reduction of $[\{((^{Ad}ArO)_3N)U\}_2(\mu\text{-}\eta^2\text{:}\eta^2\text{-}C_2S_4)]$ with Na/Hg in DME to give $[Na(DME)_3]_2[\{((^{Ad}ArO)_3N)U\}_2(\mu\text{-}C_2S_4)]$.

Mazzanti *et al*. have reported the reaction of $[\{U(OSi(O^tBu)_3)_2(\mu\text{-}OSi(O^tBu)_3)\}_2]$ with CS_2 to form the dinuclear bridged species, $[\{U(OSi(OtBu)_3)_3\}_2\text{-}\{\mu\text{-}\eta^2(C,S)\text{:}\eta^2(S,S)\text{-}CS_2\}]$ (**Scheme 1.6**).[90]

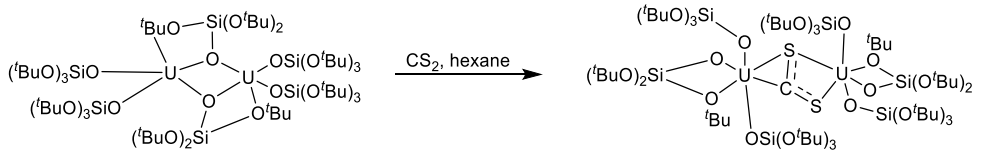

Scheme 1.6: Synthesis of [{U(OSi(OtBu)$_3$)$_3$}$_2$-{μ-η^2(C,S):η^2(S,S)-CS$_2$}] from [{U(OSi(O^{t}Bu)$_3$)$_2$(μ-OSi(O^{t}Bu)$_3$)}$_2$] and CS$_2$.

The same group has also shown that CS_2 is activated by [K(18C6)][U(OSi(O^{t}Bu)$_3$)$_4$] to give rise to trithiocarbonate *via* a disproportionation reaction alongside other products (**Scheme 1.7**).[101]

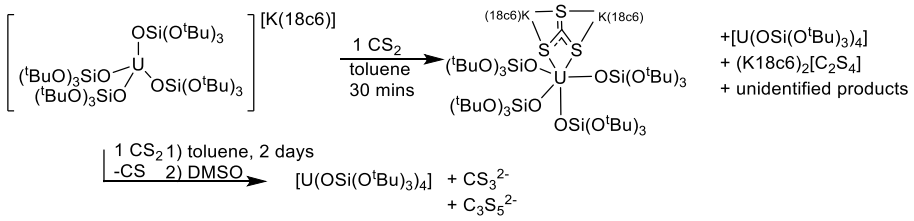

Scheme 1.7: [K(18c6)][U(OSi(O^{t}Bu)$_3$)$_4$] and its reactivity towards CS$_2$.

Mazzanti *et al*. carried out CS_2 reactivity studies with [U(OSi(O^{t}Bu)$_3$)$_4$K]. Upon reaction with CS_2 several products were formed (**Scheme 1.8**). These products are readily displaced by the supporting siloxide ligands due to the tendency of uranium to preferentially bond to harder atoms such as oxygen as opposed to sulphur. It has been observed with these systems that the K^+ cation is necessary to promote the reductive coupling of CS_2.

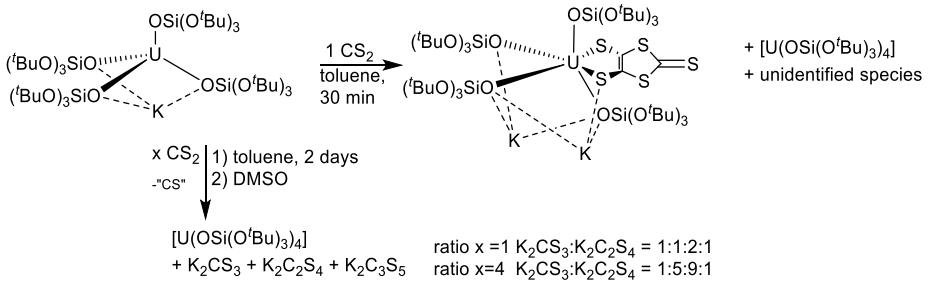

Scheme 1.8: [U(OSi(O^{t}Bu)$_3$)$_4$K] and its reactivity towards CS$_2$.

Employing the exceptional dinuclear uranium(III) nitride complex, Cs$_3$[{U(OSi(O^{t}Bu)$_3$)$_3$}$_2$(μ-N)], Mazzanti *et al*. were able to demonstrate that upon reaction with CS_2, the nucleophilic nitride group is transferred to the electrophilic CS_2 resulting in the extrusion of SCN^- and formation of a bridging disulphide complex (**Scheme 1.9**).[102]

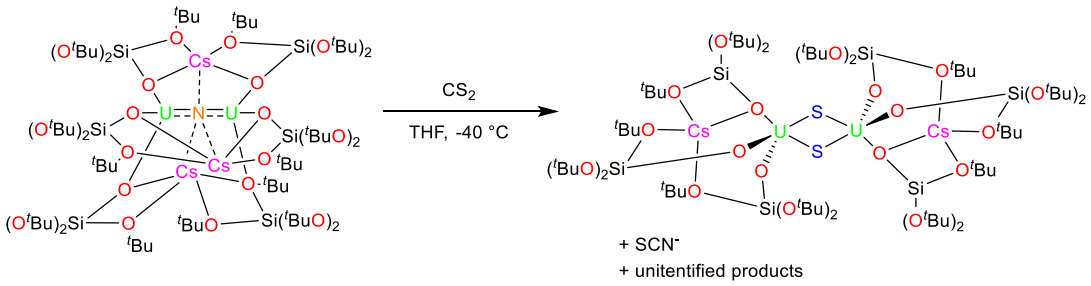

Scheme 1.9 Reactivity of $Cs_3[\{U(OSi(O^tBu)_3)_3\}_2(\mu\text{-}N)]$ towards CS_2. Atoms coloured for clairity.

Dinuclear U^{III} complexes containing anthracene-hinged 'Pacman' Schiff-base pyrrole ligand, $[Na(THF)_4][\{U(BH_4)\}_2(BH_4)(L^A)(THF)_2]$ and $[\{U(OAr)\}_2(KBH_4)(L^A)(THF)_2]$, have also been used to activate CS_2.[103] $[Na(THF)_4][\{U(BH_4)\}_2(BH_4)(L^A)(THF)_2]$ formally undergoes a four-electron process in which three CS_2^{2-} moieties and two U(V) centres are formed in a "triple-decker" fashion with the uranium centres sandwiched between the thiocarbonates (**Scheme 1.10**, left). Upon reaction with excess CS_2, $[\{U(OAr)\}_2(KBH_4)(L^A)(THF)_2]$ forms a μ-S compound from a presumed μ-CS_2 intermediate (**Scheme 1.10**, right). These compounds are remarkable as they are the first examples of pre-organised multinuclear U(III) complexes activating small molecules.

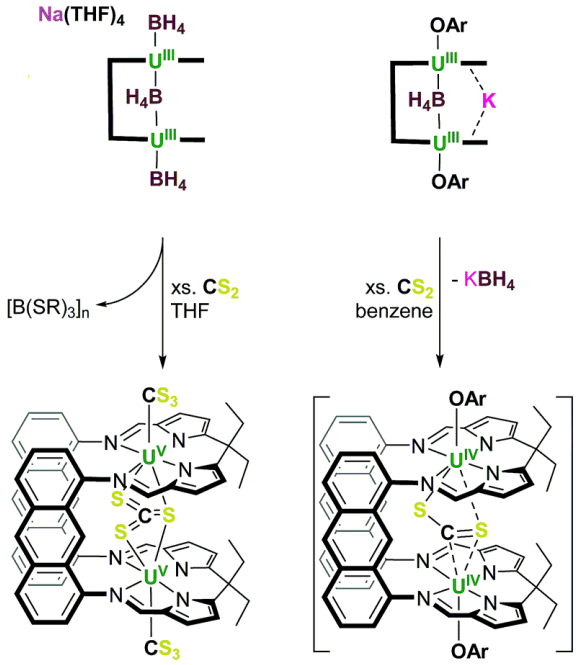

Scheme 1.10 Reactions of $[Na(THF)_4][\{U(BH_4)\}_2(BH_4)(L^A)(THF)_2]$ and $[\{U(OAr)\}_2(KBH_4)(L^A)(THF)_2]$ with CS_2. Scheme from reference [103].

1.5 Ligand Environments for Thorium Complexes

1.5.1 Cyclopentadienyl Thorium Complexes

Over the past few decades, cyclopentadienyl ligands have been ubiquitous in thorium as well as uranium chemistry,[104] due to the steric saturation and crystallinity that cyclopentadienyl-derived ligands impart. The Cp^*_2Th moiety is common, and certain complexes containing it have been shown to have high catalytic activity in olefin polymerisation reactions and dimethylamine borane dehydrogenation.[105,106] The Cp^*_2Th fragment also enabled the isolation of metal-ligand multiple bonds in thorium-phosphorus and thorium-arsenic complexes.[107] Tris-cyclopentadienyl thorium complexes date back to the 1970s with a report from Baumgärtner *et al*., who outlined the synthesis of $ThCp_3$. Similar complexes will be highlighted below in the 'Thorium in the +3 Oxidation State' section.

1.5.2 Arene Thorium Complexes

Reports of thorium arene interactions in the literature are scarce. The first example of a thorium arene interaction was reported by Gambarotta in 2003, in a publication which outlined the synthesis of $[\{Et_8\text{-calix[4]tetrapyrrole})Th\}\{K(dme)\}(\mu\text{-}\eta^4\text{:}\eta^6\text{-}C_{10}H_8)(\mu\text{-}K)]_n$ and $[\{Et_8\text{-calix[4]tetrapyrrole})Th\}\{K(dme)\}(\mu\text{-}\eta^4 : \eta^6\text{-}C_{10}H_8)][Li(DME)_3]$.[108] Both of these compounds were synthesised from $[\{Et_8\text{-calix[4]tetrapyrrole})Th(\mu\text{-}Cl)_2][K(DME)]_2$ and two equivalents of M(naphthalene) (M = K, Li) in DME. Both compounds contain η^4 interactions with a bent naphthalene fragment.

Research carried out by Britten *et al*. showed how a series of thorium cations and a rare thorium dication, involve π-coordination of benzyl ligands from the counter anions.[109,110] In the dicationic complex, $[(XA_2)Th][B(C_6F_5)_3(CH_2Ph)]_2$ [XA_2 = 4,5-bis(2,6-diisopropylanilido)-2,7-di-tert-butyl-9,9-dimethylxanthene] (**Figure 1.23**), thorium is ligated to two benzyl ligands from the $[B(CH_2Ph)(C_6F_5)_3]$ anions, through π-interactions as part of ion contact interactions. These complexes were tested as catalysts for ethylene polymerisation, however, polymer formation was not observed, most likely due to π-arene interactions blocking the metal centre.

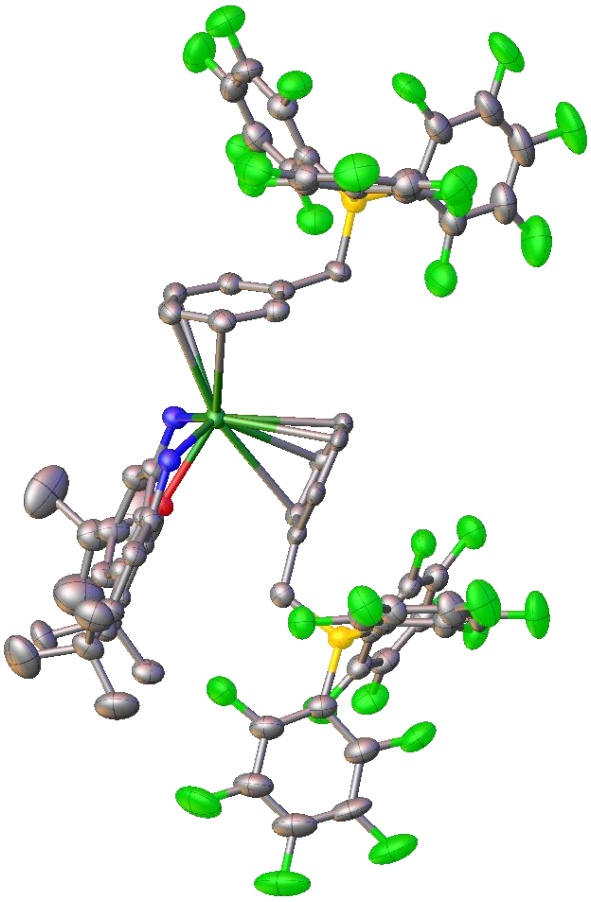

Figure 1.23 Molecular structure of $[(XA_2)Th][B(C_6F_5)_3(CH_2Ph)]_2$. Th, green; O, red; N, blue; C, grey; B, yellow; F, bright green. Hydrogens omitted for clarity. Thermal ellipsoids set to 50%.

Gambarotta *et al*. later synthesised a thorium complex with a dianionic bis-pyrrolide ligand system containing a central chelating C_6 ring, which coordinates to the metal centre due to steric constraint.[111] The aforementioned complex, η^6-{1,3-[(2-C_4H_3N)$(CH_3)_2C]_2C_6H_4$}$ThCl_3$][Li$(DME)_3$], features an η^6-bonding interaction between the Th atom and phenyl ring with a Th-centroid distance of 2.701(8) Å. Reduction with potassium metal resulted in the formation of a paramagnetic complex containing a phenyl-based radical, as indicated by a non-planar phenyl ring (**Figure 1.24**) and a singlet with a G_{av} value of 2.0012 in the EPR spectrum.

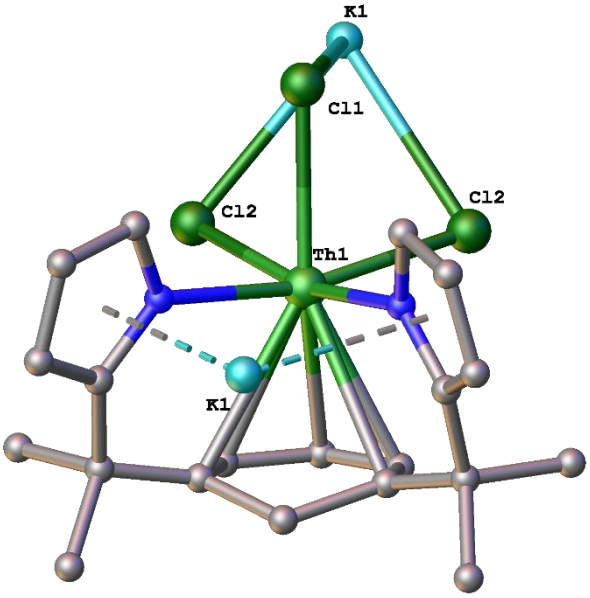

Figure 1.24 Molecular structure of [{η^5-1,3-[η^5-2-C_4H_3N)$(CH_3)_2C]_2C_6H_4$}ThK-(μ-Cl)$_3$][Li(DME)$_3$] . Thorium, light green; chloride, dark green; nitrogen, blue; carbon, grey. Hydrogens and [Li(DME)$_3$] omitted for clarity.

A thorium terphenolate complex featuring a thorium bis(arene) sandwich motif was published in 2014.[112] The thorium complex, Th(OTer^{Mes})$_2$(μ^3-BH_4)$_2$ (**Figure 1.25**, left), contains two terphenolate ligands, one of which forms an interaction with thorium (Th-Ct(arene) distance: 4.05(1) and 2.815(3) Å). Arnold *et al*. published an additional thorium complex containing a thorium bis(arene) motif,[113] in this instance the complex was [(*trans*-calix[2]benzene[2]pyrrolide)Th(N(SiMe$_3$)$_2$)][BPh$_4$] (**Figure 1.25**, right) and the average Th-Ct(arene) distance is 2.690 Å, indicative of a strong interaction.

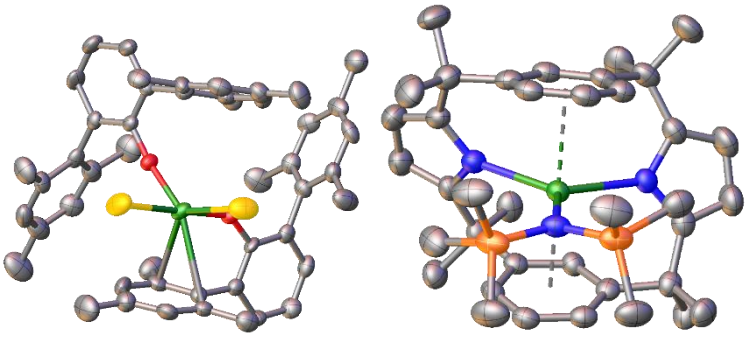

Figure 1.25 Molecular structures of Th(OTer^{Mes})$_2$(μ^3-BH_4)$_2$ (left) and [(*trans*-calix[2]benzene[2]pyrrolide)Th(N(SiMe$_3$)$_2$)][BPh$_4$] (right, BPh$_4$ counterion removed for clarity). Thorium, green; oxygen, red; boron, yellow; silicon, orange. Hydrogen atoms omitted for clarity.

1.5.3 Aryloxide Thorium Complexes

Thorium aryloxide complexes have been a synthetic goal for chemists for a substantial time with the chemistry advancing at a similar rate to that of uranium aryloxide chemistry. This interest originates from research studies often including both thorium and uranium, that demonstrate the similar behaviour of both elements in the +4 oxidation state. In 1987 Lappert *et al*. published a report outlining the synthesis of several thorium complexes including: [Li(THF)][Th(O-2,6^{i}Pr $_2$C$_6$H$_3$)$_5$], ThCl(O-2,6^{i}Pr $_2$C$_6$H$_3$)$_3$, ThCl$_2$(O-2,6^{i}Pr $_2$C$_6$H$_3$)$_2$ and Th(O-2,6^{i}Pr $_2$C$_6$H$_3$)$_4$,[114] all in good yields. Over a decade later Clark *et al*. published several aryloxide/Cp* thorium compounds of the formula ThCp*X(OAr)$_2$ (where X = Br, Me, CH$_2$SiMe$_3$ and OAr = O-2,6^{i}Pr $_2$C$_6$H$_3$) for use as ethylene polymerisation catalysts.[115]

Using the bis(phenolate) complex shown in **Figure 1.26**,[116] Gambarotta *et al*. were able to cleave and hydrogenate dinitrogen. The authors propose the reaction proceeds *via* a transient zero-valent thorium species.

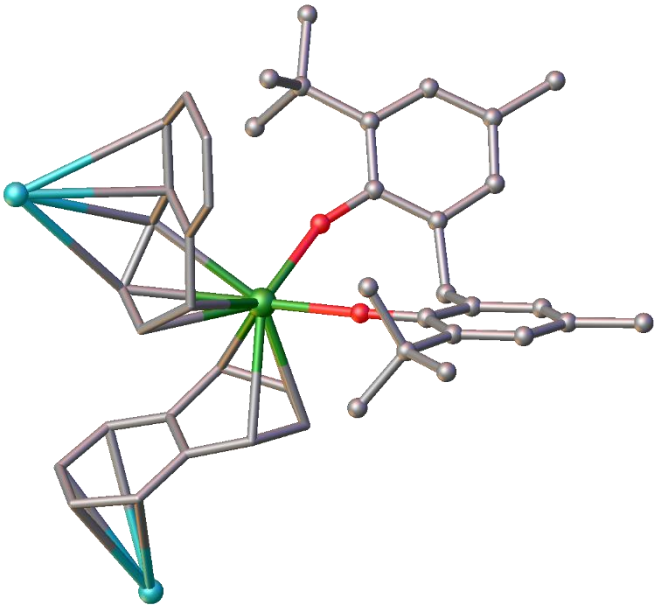

Figure 1.26 Molecular structure of a thorium bis(phenolate) complex. Thorium, green; oxygen, red; potassium, cyan; carbon, grey. Hydrogens and 18-crown-6 groups removed, and naphthalene molecules drawn as ‘tubes’ for clarity.

A year later Gambarotta *et al*. synthesised the bulky homoleptic complex,[117] Th(O-2,6-$Ph_2C_6H_3$)$_4$ as part of studies attempting to prepare low-valent species *via* potassium reduction. Solvent deoxygenation and cyclometallation were the result of these reactions, as opposed to the desired metal-based processes.

In 2017 Arnold *et al*. synthesised a macrocyclic thorium complex containing two aryloxide ligands as part of studies exploring the coordination chemistry of the macrocyclic ligand TMTAA (TMTAA = Tetramethyl-tetra-aza-annulene),[118] in uranium and thorium complexes. Th(O-2,6^{i}Pr $_2C_6H_3$)$_2$TMTAA was synthesised from [Th(TMTAA)Cl_2(THF)$_2$] and two equivalents of KO-2,6^{i}Pr $_2C_6H_3$ in THF to give the desired product in 64% yield. A tetradentate Schiff base ligand containing two aryloxide arms was used to synthesise several Th(IV) complexes, (L)ThCl_2Py$_2$ (L = (±)-trans-6,6′-diethoxy-2,2′-[cyclohexane-1,2-diylbis(nitrilomethanylylidene)]diphenoxide) is shown below (**Figure 1.27**, right).[119]

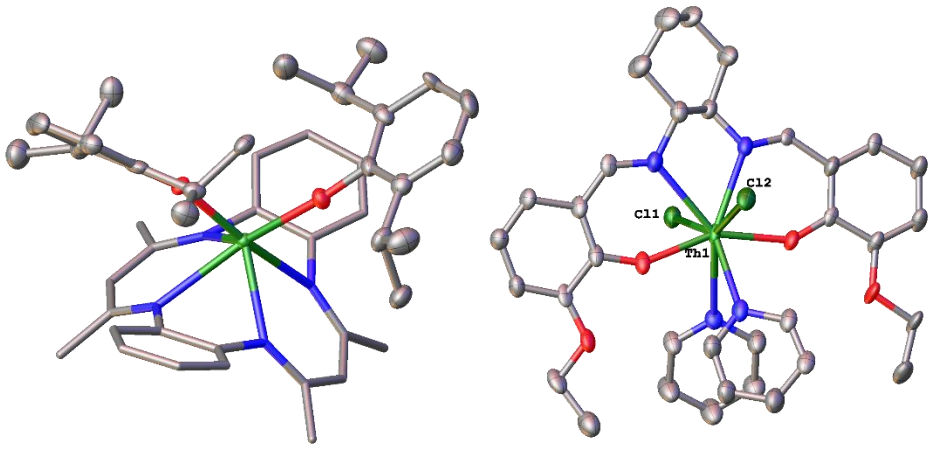

Figure 1.27 Molecular structures of Th(O-2,6^{i}Pr $_2C_6H_3$)$_2$TMTAA (left) and (L)ThCl_2Py$_2$ (right). Thorium, light green; chloride, dark green; nitrogen, blue; carbon, grey. Hydrogen atoms omitted and TMTAA ligand is shown as 'tubes' for clarity. Displacement ellipsoids set to 50% where shown.

1.6 Thorium in the +3 Oxidation State

Thorium primarily exists in the +4 oxidation state with only eight crystallographically authenticated examples of thorium in the +3 oxidation state reported to date.[30,77,120–125] This is due to the highly reducing nature of the lower oxidation states and the lack of easily accessible starting materials in the +3 oxidation state. The possibility that thorium could exist in lower oxidation states was suggested by reports of "Th(III)" and "Th(II)" subhalides in the 1950s and 1960s.[126,127] Subsequent reports of Th(II)

complexes using the tris-cyclopentadienyl framework have recently been reported,[128] exemplifying how the ligand environment is key to isolating low-valent complexes.

In 1974 the first attempts at preparing a molecular Th(III) species was reported; Baumgartner disclosed the preparation of $ThCp_3$ from the Na/Naphalene reduction of $ThCp_3Cl$.[129] The authors characterised this species using elemental analysis, and infrared spectroscopy, but low solubility hindered obtaining single crystals of suitable quality for X-ray diffraction studies, possibly due to the formation of a polymeric ionic species as has been observed in Ln chemistry.[130,131] Circumventing the use of chemical reduction agents Marks explored the use of photolytic synthetic routes to Th(III) species. Experiments involving UV photolysis of $ThCp^R_3{}^i Pr$ (R = H or Me) gave the Th(III) complexes, $ThCp^R_3$, with concomitant formation of $^i Pr$ and propylene in equal amounts.[132] These complexes were characterised by mass spectrometry, elemental analysis, FTIR, Raman and electronic spectroscopy. Attempts were made to obtain magnetic data, however, results varied across several batches of the sample, possibly due to diamagnetic impurities.

Marks also reported the synthesis of $Th(C_9H_7)_3$, prepared *via* the photolysis of the Th(IV) alkyl precursor.[133] Again, structural characterisation was not possible, though ^1H NMR, elemental analysis, and IR analysis agree with the formulation.

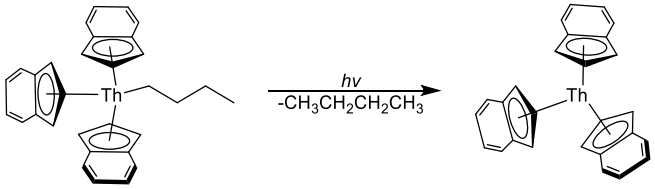

Scheme 1.11 Synthesis of $Th(C_9H_7)_3$ using photolysis.

It was not until 1986 that the first crystal structure of an authenticated Th(III) sample was published. Lappert described the preparation of $ThCp^{TMS2}_3$ *via* the reduction of $ThCp^{TMS2}_2Cl_2$ with NaK in toluene to provide the compound in 85% yield.[120] The electronic configuration was originally reported as $5f^1$ though in a later publication this was corrected to a $6d^1$ configuration based on EPR studies.[134]

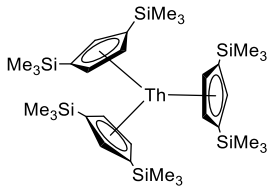

Figure 1.28 Structure of $ThCp^{TMS2}{}_3$.

Over 15 years later Cloke *et al*. reported the synthesis of the trivalent sandwich complex, $[ThCOT^{TBDMS2}{}_2][K(DME_3)]$ (**Figure 1.29**),[30] by the reduction of $ThCOT^{TBDMS2}{}_2$ with a potassium mirror in DME. To this day this remains the only example in the literature of a Th(III) complex that does not contain a cyclopentadienyl ligand. Evans magnetic moment measurements gave a value of 1.20 μ_B, which is low in comparison to the expected value for a complex containing a single unpaired electron (1.73 μ_B); the authors propose this is due to diamagnetic impurities and low-lying magnetic states, whereby the observation of higher values for μ_B at higher temperatures agree with this hypothesis.

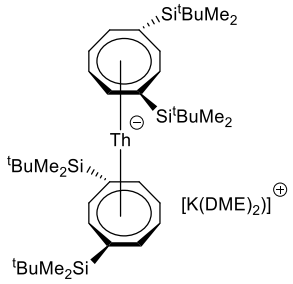

Figure 1.29 Structure of $[ThCOT^{TBDMS2}{}_2][K(DME_3)]$.

The heteroleptic Th(III) species, $ThCp_2^*(^i PrNC(Me)N^i Pr)$, was prepared by the reduction of $[ThCp_2^*(^i PrNC(Me)N^i Pr)][BPh_3Me]$ with KC_8. EPR and electronic spectroscopic data are consistent with the formation of a Th(III) species containing a $6d^1$ configuration.

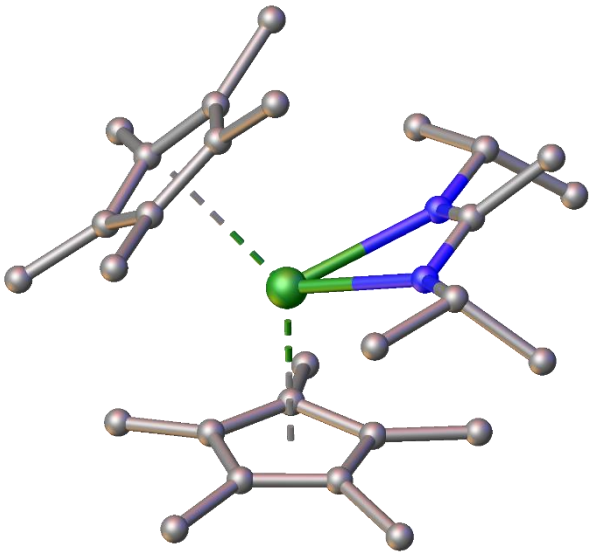

Figure 1.30 Molecular structure of $ThCp^*_2(^iPrNC(Me)N^iPr)$. Thorium, green; nitrogen, blue; carbon, grey. Hydrogens omitted for clarity.

Several derivatives of $ThCp^R_3$ (R = Me_4H, Me_5 and 1,3-^{t}Bu) have also been synthesised and structurally authenticated with the $6d^1$ configuration confirmed using EPR and electronic spectroscopy.[77,123,124] Using pulsed EPR methods Mills *et al*. were able to obtain experimental evidence to quantify the electron-spin density at the ligand-nuclei and thus infer the extent of covalency in $AnCp^{tBu2}_3$ (An = Th and U). Their studies suggest that there is considerably more total spin density on the ligands in the uranium complex compared to that of thorium in $AnCp^{tBu2}_3$, which is due to the angular lobe of the $6d_{z2}$ orbital being the only part of the orbital that has the correct orientation to overlap with ligand orbitals, while the 5f orbitals on uranium are more able to transfer spin density onto the ligands due to greater in-plane character.

$ThCp^{TMS2}_3$ has also been shown to activate CO_2 and CS_2 (**Scheme 1.12**).[96] Two equivalents of $ThCp^{TMS2}_3$ reduce CS_2 to give $\{ThCp^{TMS2}_3\}_2(\mu\text{-}\eta^1\text{:}\eta^2\text{-}CS_2)$, reactivity analogous to similar U(III) complexes (**Scheme 1.4**). More interestingly, $ThCp^{TMS2}_3$ was found to react with CO_2 to form an oxalate-bridged product as well as a carboxylate, resulting from the insertion reaction of CO_2 into the Th-Cp^{TMS2}_3 moiety followed by silyl migration.

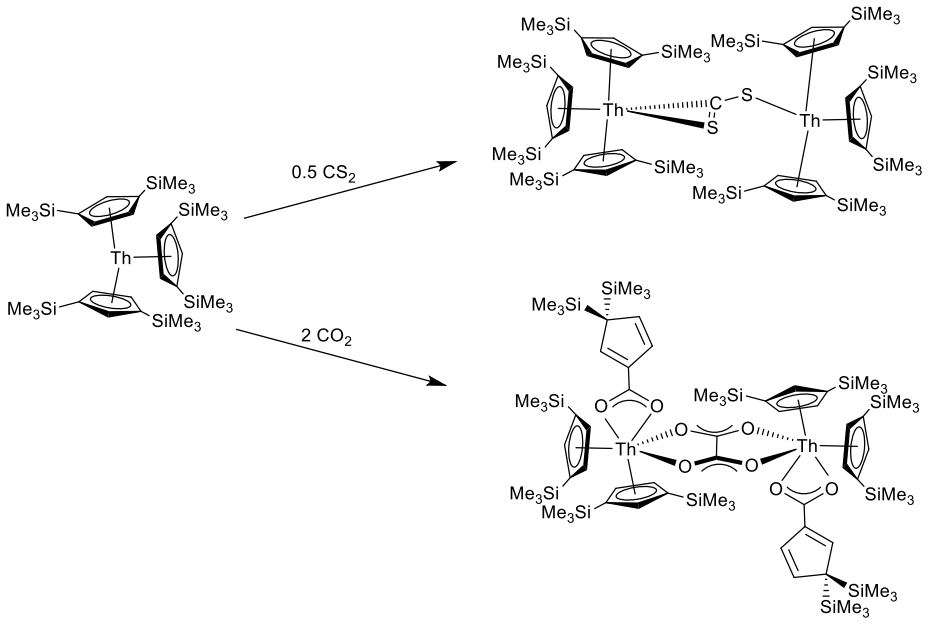

Scheme 1.12 Reactivity of $ThCp^{TMS2}{}_3$ towards CS_2 and CO_2.

As illustrated, over the past 50 years there has been many exciting discoveries that highlight the unique nature of actinide chemistry. Many of these discoveries have been facilitated using carbocyclic ligands such as Cp and COT, and more recently with aryloxide and arene ligands. The last decade has seen an increase in the number of actinide reactivity studies. This is an exciting area of research as the unique properties of the actinide elements will no doubt lead to fascinating reactivity modes. However, there are still many areas that could be developed. For example, reports of thorium electrochemistry are scarce, yet would provide valuable data on fundamental properties of this element which would help develop, still nascent, low-valent thorium chemistry. Another area of interest is that of actinide-arene interactions which hold much promise for stabilising highly reactive, low-valent species that may display exceptional reactivity. This thesis aims to address these deficits by exploring the use of mixed-ligand systems, some of which feature arene ligands, with the aim of altering steric and electronic properties to furnish complexes that feature novel bonding interactions and unique reactivity towards small molecules.

1.7 References for Chapter One

1 M. Bochmann, *Organometallics and Catalysis: An Introduction*, OUP Oxford, Oxford, United Kingdom, UK ed. edition., 2014.
2 R. Eccles, *J. Pharm. Pharmacol.*, 1994, **46**, 618–630.
3 Fritz Haber - Nobel Lecture: The Synthesis of Ammonia from Its Elements, https://www.nobelprize.org/nobel_prizes/chemistry/laureates/1918/haber-lecture.html, (accessed 26 February 2018).
4 L. L. Huill, *Chem. Rev.*, 1938, **23**, 87–155.
5 D. R. Lide, Ed., *CRC Handbook of Chemistry and Physics: 86th Edition*, Taylor & Francis, 86th edn., 2005.
6 S. A. Cotton, *Lanthanide and Actinide Chemistry*, John Wiley & Sons, Ltd, Chichester, First Edit., 2006.
7 P. Bagla, *Science*, 2015, **350**, 726–727.
8 D. Heuer, E. Merle-Lucotte, M. Allibert, M. Brovchenko, V. Ghetta and P. Rubiolo, *Ann. Nucl. Energy*, 2014, **64**, 421–429.
9 M. B. Schaffer, *Energy Policy*, 2013, **60**, 4–12.
10 N. Kaltsoyannis, *Chem. Soc. Rev.*, 2003, **32**, 9–16.
11 N. Tsoureas, L. Castro, A. F. R. Kilpatrick, F. G. N. Cloke and L. Maron, *Chem. Sci.*, 2014, **5**, 3777–3788.
12 N. G. Connelly and W. E. Geiger, *Chem. Rev.*, 1996, **96**, 877–910.
13 M. Rahm, R. Hoffmann and N. W. Ashcroft, *Chem. – Eur. J.*, 2016, **22**, 14625–14632.
14 H. S. La Pierre and K. Meyer, in *Progress in Inorganic Chemistry, vol. 58*, ed. K. D. Karlin, Wiley, 2014, vol. 58, pp. 301–413.
15 L. T. Reynolds and G. Wilkinson, *J. Inorg. Nucl. Chem.*, 1956, **2**, 246–253.
16 J. M. Manriquez, P. J. Fagan and T. J. Marks, *J. Am. Chem. Soc.*, 1978, **100**, 3939–3941.
17 O. T. Summerscales, F. G. N. Cloke, P. B. Hitchcock, J. C. Green and N. Hazari, *J. Am. Chem. Soc.*, 2006, **128**, 9602–9603.
18 P. C. Blake, M. F. Lappert, R. G. Taylor, J. L. Atwood, W. E. Hunter and H. Zhang, *J. Chem. Soc. Chem. Commun.*, 1986, 1394–1395.
19 M. R. MacDonald, M. E. Fieser, J. E. Bates, J. W. Ziller, F. Furche and W. J. Evans, *J. Am. Chem. Soc.*, 2013, **135**, 13310–13313.
20 G. Zi, L. Jia, E. L. Werkema, M. D. Walter, J. P. Gottfriedsen and R. A. Andersen, *Organometallics*, 2005, **24**, 4251–4264.
21 M. Ephritikhine, *Organometallics*, 2013, **32**, 2464–2488.
22 C. J. Windorff, M. R. MacDonald, K. R. Meihaus, J. W. Ziller, J. R. Long and W. J. Evans, *Chem. – Eur. J.*, 2016, **22**, 772–782.
23 A. Streitwieser and U. Mueller-Westerhoff, *J. Am. Chem. Soc.*, 1968, **90**, 7364–7364.
24 C. A. Harmon, D. P. Bauer, S. R. Berryhill, K. Hagiwara and A. Streitwieser Jr, *Inorg. Chem.*, 1977, **16**, 2143–2147.
25 A. Streitwieser, M. H. Lyttle, H. Wang, T. Boussie, A. Weinländer and J. P. Solar, *J. Organomet. Chem.*, 1995, **501**, 245–249.
26 A. Streitwieser Jr, D. Dempf, G. N. La Mar, D. G. Karraker and N. M. Edelstein, *J. Am. Chem. Soc.*, 1971, **93**, 7343–7344.
27 A. Streitwieser Jr and R. Walker, *J. Organomet. Chem.*, 1975, **97**, C41–C42.
28 N. C. Burton, F. G. N. Cloke, P. B. Hitchcock, H. C. de Lemos and A. A. Sameh, *J. Chem. Soc. Chem. Commun.*, 1989, 1462–1464.
29 O. T. Summerscales, F. G. N. Cloke, P. B. Hitchcock, J. C. Green and N. Hazari, *Science*, 2006, **311**, 829–831.
30 J. S. Parry, Cloke, S. J. Coles and M. B. Hursthouse, *J. Am. Chem. Soc.*, 1999, **121**, 6867–6871.

31 U. Kilimann, R. Herbst-Irmer, D. Stalke and F. T. Edelmann, *Angew. Chem. Int. Ed. Engl.*, 1994, **33**, 1618–1621.

32 V. Lorenz, B. M. Schmiege, C. G. Hrib, J. W. Ziller, A. Edelmann, S. Blaurock, W. J. Evans and F. T. Edelmann, *J. Am. Chem. Soc.*, 2011, **133**, 1257–1259.

33 T. R. Boussie, R. M. Moore, A. Streitwieser Jr, A. Zalkin, J. G. Brennan and K. A. Smith, *Organometallics*, 1990, **9**, 2010–2016.

34 D. Baudry, E. Bulot, M. Ephritikhine, M. Nierlich, M. Lance and J. Vigner, *J. Organomet. Chem.*, 1990, **388**, 279–287.

35 A. R. Schake, L. R. Avens, C. J. Burns, D. L. Clark, A. P. Sattelberger and W. H. Smith, *Organometallics*, 1993, **12**, 1497–1498.

36 J.-C. Berthet, J.-F. Le Maréchal and M. Ephritikhine, *J. Organomet. Chem.*, 1994, **480**, 155–161.

37 F. G. N. Cloke, J. C. Green and C. N. Jardine, *Organometallics*, 1999, **18**, 1080–1086.

38 F. G. N. Cloke and P. B. Hitchcock, *J. Am. Chem. Soc.*, 2002, **124**, 9352–9353.

39 N. Tsoureas, A. F. R. Kilpatrick, O. T. Summerscales, J. F. Nixon, F. G. N. Cloke and P. B. Hitchcock, *Eur. J. Inorg. Chem.*, 2013, **2013**, 4085–4089.

40 F. M. Chadwick and D. M. O'Hare, *Organometallics*, 2014, **33**, 3768–3774.

41 F. M. Chadwick, A. Ashley, G. Wildgoose, J. M. Goicoechea, S. Randall and D. O'Hare, *Dalton Trans.*, 2010, **39**, 6789–6793.

42 M. Cesari, U. Pedretti, A. Zauetta, G. Lugli and W. Marconi, *Inorg. Chim. Acta*, 1971, **5**, 439–444.

43 D. Baudry, E. Bulot and M. Ephritikhine, *J. Chem. Soc. Chem. Commun.*, 1988, 1369–1370.

44 P. L. Diaconescu, P. L. Arnold, T. A. Baker, D. J. Mindiola and C. C. Cummins, *J. Am. Chem. Soc.*, 2000, **122**, 6108–6109.

45 B. Vlaisavljevich, P. L. Diaconescu, W. L. Lukens Jr., L. Gagliardi and C. C. Cummins, *Organometallics*, 2013, **32**, 1341–1352.

46 D. Patel, F. Moro, J. McMaster, W. Lewis, A. J. Blake and S. T. Liddle, *Angew. Chem. Int. Ed.*, 2011, **50**, 10388–10392.

47 S. C. Bart, F. W. Heinemann, C. Anthon, C. Hauser and K. Meyer, *Inorg. Chem.*, 2009, **48**, 9419–9426.

48 S. M. Franke, B. L. Tran, F. W. Heinemann, W. Hieringer, D. J. Mindiola and K. Meyer, *Inorg. Chem.*, 2013, **52**, 10552–10558.

49 S. Fortier, J. R. Aguilar-Calderón, B. Vlaisavljevich, A. J. Metta-Magaña, A. G. Goos and C. E. Botez, *Organometallics*, 2017, **36**, 4591–4599.

50 P. B. Hitchcock, M. F. Lappert, A. Singh, R. G. Taylor and D. Brown, *J. Chem. Soc. Chem. Commun.*, 1983, 561–563.

51 W. G. Van der Sluys, C. J. Burns, J. C. Huffman and A. P. Sattelberger, *J. Am. Chem. Soc.*, 1988, **110**, 5924–5925.

52 J. M. Berg, D. L. Clark, J. C. Huffman, D. E. Morris, A. P. Sattelberger, W. E. Streib, W. G. V. D. Sluys and J. G. Watkin, *J. Am. Chem. Soc.*, 1992, **114**, 10811–10821.

53 W. G. Van Der Sluys, A. P. Sattelberger, W. E. Streib and J. C. Huffman, *Polyhedron*, 1989, **8**, 1247–1249.

54 S. M. Mansell, N. Kaltsoyannis and P. L. Arnold, *J. Am. Chem. Soc.*, 2011, **133**, 9036–9051.

55 I. Castro-Rodriguez, K. Olsen, P. Gantzel and K. Meyer, *Chem. Commun.*, 2002, 2764–2765.

56 O. P. Lam, S. C. Bart, H. Kameo, F. W. Heinemann and K. Meyer, *Chem. Commun.*, 2010, **46**, 3137–3139.

57 I. Castro-Rodriguez, H. Nakai, P. Gantzel, L. N. Zakharov, A. L. Rheingold and K. Meyer, *J. Am. Chem. Soc.*, 2003, **125**, 15734–15735.

58 H. S. La Pierre, A. Scheurer, F. W. Heinemann, W. Hieringer and K. Meyer, *Angew. Chem. Int. Ed Engl.*, 2014, **53**, 7158–62.

59 L. Maria, I. C. Santos, V. R. Sousa and J. Marçalo, *Inorg. Chem.*, 2015, **54**, 9115–9126.

60 J. A. L. Wells, M. L. Seymour, M. Suvova and P. L. Arnold, *Dalton Trans.*, 2016, **45**, 16026–16032.

61 J. Hümmer, F. W. Heinemann and K. Meyer, *Inorg. Chem.*, 2017, **56**, 3201–3206.

62 S. Trofimenko, *J. Am. Chem. Soc.*, 1966, **88**, 1842–1844.

63 K. W. Bagnall, J. Edwards, J. G. H. du Preez and R. F. Warren, *J. Chem. Soc. Dalton Trans.*, 1975, 140–143.

64 M. A. Antunes, Â. Domingos, I. C. Santos, N. Marques and J. Takats, *Polyhedron*, 2005, **24**, 3038–3045.

65 M. A. Antunes, G. M. Ferrence, Â. Domingos, R. McDonald, C. J. Burns, J. Takats and N. Marques, *Inorg. Chem.*, 2004, **43**, 6640–6643.

66 Y. Sun, R. McDonald, J. Takats, V. W. Day and T. A. Eberspacher, *Inorg. Chem.*, 1994, **33**, 4433–4434.

67 E. M. Matson, W. P. Forrest, P. E. Fanwick and S. C. Bart, *J. Am. Chem. Soc.*, 2011, **133**, 4948–4954.

68 S. J. Kraft, J. Walensky, P. E. Fanwick, M. B. Hall and S. C. Bart, *Inorg. Chem.*, 2010, **49**, 7620–7622.

69 S. J. Kraft, P. E. Fanwick and S. C. Bart, *Inorg. Chem.*, 2010, **49**, 1103–10.

70 C. L. Clark, J. J. Lockhart, P. E. Fanwick and S. C. Bart, *Chem. Commun.*, DOI:10.1039/C5CC05049A.

71 J. L. Slater, R. K. Sheline, K. C. Lin and W. Weltner Jr, *J. Chem. Phys.*, 1971, **55**, 5129–5130.

72 J. G. Brennan, R. A. Andersen and J. L. Robbins, *J. Am. Chem. Soc.*, 1986, **108**, 335–336.

73 L. E. Schock and T. J. Marks, *J. Am. Chem. Soc.*, 1988, **110**, 7701–7715.

74 J. Parry, E. Carmona, S. Coles and M. Hursthouse, *J. Am. Chem. Soc.*, 1995, **117**, 2649–2650.

75 M. del Mar Conejo, J. S. Parry, E. Carmona, M. Schultz, J. G. Brennan, S. M. Beshouri, R. A. Andersen, R. D. Rogers, S. Coles and M. B. Hursthouse, *Chem. - Eur. J.*, 1999, **5**, 3000–3009.

76 W. J. Evans, S. A. Kozimor, G. W. Nyce and J. W. Ziller, *J. Am. Chem. Soc.*, 2003, **125**, 13831–13835.

77 R. R. Langeslay, G. P. Chen, C. J. Windorff, A. K. Chan, J. W. Ziller, F. Furche and W. J. Evans, *J. Am. Chem. Soc.*, 2017, **139**, 3387–3398.

78 I. Castro-Rodriguez, H. Nakai, L. N. Zakharov, A. L. Rheingold and K. Meyer, *Science*, 2004, **305**, 1757–1759.

79 A. S. Frey, F. G. N. Cloke, P. B. Hitchcock, I. J. Day, J. C. Green and G. Aitken, *J. Am. Chem. Soc.*, 2008, **130**, 13816–13817.

80 D. McKay, A. S. P. Frey, J. C. Green, F. G. N. Cloke and L. Maron, *Chem. Commun.*, 2012, **48**, 4118–4120.

81 A. S. P. Frey, F. G. N. Cloke, M. P. Coles, L. Maron and T. Davin, *Angew. Chem. Int. Ed.*, 2011, **50**, 6881–6883.

82 N. Tsoureas, O. T. Summerscales, F. G. N. Cloke and S. M. Roe, *Organometallics*, 2013, **32**, 1353–1362.

83 P. L. Arnold, Z. R. Turner, R. M. Bellabarba and R. P. Tooze, *Chem. Sci.*, 2011, **2**, 77–79.

84 B. M. Gardner, J. C. Stewart, A. L. Davis, J. McMaster, W. Lewis, A. J. Blake and S. T. Liddle, *Proc. Natl. Acad. Sci.*, 2012, **109**, 9265–9270.

85 J. R. Khusnutdinova, J. A. Garg and D. Milstein, *ACS Catal.*, 2015, **5**, 2416–2422.

86 J.-C. Berthet, J.-F. Le Maréchal, M. Nierlich, M. Lance, J. Vigner and M. Ephritikhine, *J. Organomet. Chem.*, 1991, **408**, 335–341.

87 I. Castro-Rodriguez and K. Meyer, *J. Am. Chem. Soc.*, 2005, **127**, 11242–11243.

88 I. Castro-Rodriguez, H. Nakai, L. N. Zakharov, A. L. Rheingold and K. Meyer, *Science*, 2004, **305**, 1757–1759.

89 O. T. Summerscales, A. S. P. Frey, F. G. N. Cloke and P. B. Hitchcock, *Chem. Commun.*, 2009, 198–200.

90 V. Mougel, C. Camp, J. Pécaut, C. Copéret, L. Maron, C. E. Kefalidis and M. Mazzanti, *Angew. Chem. Int. Ed.*, 2012, **51**, 12280–12284.

91 R. Lalrempuia, A. Stasch and C. Jones, *Chem. Sci.*, 2013, **4**, 4383–4388.

92 A. J. Boutland, I. Pernik, A. Stasch and C. Jones, *Chem. – Eur. J.*, 2015, **21**, 15749–15758.

93 H.-O. Fröhlich and H. Schreer, *Z. Für Chem.*, 1983, **23**, 348–349.

94 C. C. Lu, C. T. Saouma, M. W. Day and J. C. Peters, *J. Am. Chem. Soc.*, 2007, **129**, 4–5.

95 U. R. Pokharel, F. R. Fronczek and A. W. Maverick, *Nat. Commun.*, 2014, **5**, 5883.

96 A. Formanuik, F. Ortu, C. J. Inman, A. Kerridge, L. Castro, L. Maron and D. P. Mills, *Chem. – Eur. J.*, 2016, **22**, 17976–17979.

97 A.-C. Schmidt, F. W. Heinemann, C. E. Kefalidis, L. Maron, P. W. Roesky and K. Meyer, *Chem. – Eur. J.*, 2014, **20**, 13501–13506.
98 J. G. Brennan, R. A. Andersen and A. Zalkin, *Inorg. Chem.*, 1986, **25**, 1756–1760.
99 O. P. Lam, F. W. Heinemann and K. Meyer, *Angew. Chem. Int. Ed.*, 2011, **50**, 5965–5968.
100 O. P. Lam, L. Castro, B. Kosog, F. W. Heinemann, L. Maron and K. Meyer, *Inorg. Chem.*, 2012, **51**, 781–783.
101 C. Camp, O. Cooper, J. Andrez, J. Pécaut and M. Mazzanti, *Dalton Trans.*, 2015, **44**, 2650–2656.
102 L. Chatelain, R. Scopelliti and M. Mazzanti, *J. Am. Chem. Soc.*, 2016, **138**, 1784–1787.
103 P. L. Arnold, C. J. Stevens, N. L. Bell, R. M. Lord, J. M. Goldberg, G. S. Nichol and J. B. Love, *Chem. Sci.*, DOI:10.1039/C7SC00382J.
104 M. Sharma and M. S. Eisen, in *Organometallic and Coordination Chemistry of the Actinides*, ed. T. E. Albrecht-Schmitt, Springer Berlin Heidelberg, 2008, pp. 1–85.
105 L. Jia, X. Yang, C. Stern and T. J. Marks, *Organometallics*, 1994, **13**, 3755–3757.
106 K. A. Erickson and J. L. Kiplinger, *ACS Catal.*, 2017, **7**, 4276–4280.
107 S. P. Vilanova, P. Alayoglu, M. Heidarian, P. Huang and J. R. Walensky, *Chem. – Eur. J.*, 2017, **23**, 16748–16752.
108 I. Korobkov, S. Gambarotta and G. P. A. Yap, *Angew. Chem. Int. Ed.*, 2003, **42**, 814–818.
109 C. A. Cruz, D. J. H. Emslie, L. E. Harrington, J. F. Britten and C. M. Robertson, *Organometallics*, 2007, **26**, 692–701.
110 C. A. Cruz, D. J. H. Emslie, C. M. Robertson, L. E. Harrington, H. A. Jenkins and J. F. Britten, *Organometallics*, 2009, **28**, 1891–1899.
111 I. Korobkov, B. Vidjayacoumar, S. I. Gorelsky, P. Billone and S. Gambarotta, *Organometallics*, 2010, **29**, 692–702.
112 J. McKinven, G. S. Nichol and P. L. Arnold, *Dalton Trans.*, 2014, **43**, 17416–17421.
113 M. Suvova, K. T. P. O'Brien, J. H. Farnaby, J. B. Love, N. Kaltsoyannis and P. L. Arnold, *Organometallics*, 2017, **36**, 4669–4681.
114 P. C. Blake, M. F. Lappert, R. G. Taylor, J. L. Atwood and H. Zhang, *Inorg. Chim. Acta*, 1987, **139**, 13–20.
115 R. J. Butcher, D. L. Clark, S. K. Grumbine, B. L. Scott and J. G. Watkin, *Organometallics*, 1996, **15**, 1488–1496.
116 I. Korobkov, S. Gambarotta and G. P. A. Yap, *Angew. Chem. Int. Ed.*, 2003, **42**, 4958–4961.
117 I. Korobkov, A. Arunachalampillai and S. Gambarotta, *Organometallics*, 2004, **23**, 6248–6252.
118 S. Hohloch, M. E. Garner, B. F. Parker and J. Arnold, *Dalton Trans.*, 2017, **46**, 13768–13782.
119 B. C. Stobbe, D. R. Powell and R. K. Thomson, *Dalton Trans.*, 2017, **46**, 4888–4892.
120 P. C. Blake, M. F. Lappert, J. L. Atwood and H. Zhang, *J. Chem. Soc. Chem. Commun.*, 1986, 1148–1149.
121 P. C. Blake, N. M. Edelstein, P. B. Hitchcock, W. K. Kot, M. F. Lappert, G. V. Shalimoff and S. Tian, *J. Organomet. Chem.*, 2001, **636**, 124–129.
122 J. R. Walensky, R. L. Martin, J. W. Ziller and W. J. Evans, *Inorg. Chem.*, 2010, **49**, 10007–10012.
123 N. A. Siladke, C. L. Webster, J. R. Walensky, M. K. Takase, J. W. Ziller, D. J. Grant, L. Gagliardi and W. J. Evans, *Organometallics*, 2013, **32**, 6522–6531.
124 A. Formanuik, A.-M. Ariciu, F. Ortu, R. Beekmeyer, A. Kerridge, F. Tuna, E. J. L. McInnes and D. P. Mills, *Nat. Chem.*, 2017, **9**, 578.
125 R. R. Langeslay, M. E. Fieser, J. W. Ziller, F. Furche and W. J. Evans, *J. Am. Chem. Soc.*, 2016, **138**, 4036–4045.
126 G. W. Watt, D. M. Sowards and S. C. Malhotra, *J. Am. Chem. Soc.*, 1957, **79**, 4908–4910.
127 R. J. Clark and J. D. Corbett, *Inorg. Chem.*, 1963, **2**, 460–463.
128 R. R. Langeslay, M. E. Fieser, J. W. Ziller, F. Furche and W. J. Evans, *Chem. Sci.*, 2014, **6**, 517–521.
129 B. Kanellakopulos, E. Dornberger and F. Baumgärtner, *Inorg. Nucl. Chem. Lett.*, 1974, **10**, 155–160.
130 C.-H. Wong, T.-Y. Lee and Y.-T. Lee, *Acta Crystallogr. B*, 1969, **25**, 2580–2587.
131 J. H. Burns, W. H. Baldwin and F. H. Fink, *Inorg. Chem.*, 1974, **13**, 1916–1920.

132 D. G. Kalina, T. J. Marks and W. A. Wachter, *J. Am. Chem. Soc.*, 1977, **99**, 3877–3879.
133 J. W. Bruno, D. G. Kalina, E. A. Mintz and T. J. Marks, *J. Am. Chem. Soc.*, 1982, **104**, 1860–1869.
134 W. K. Kot, G. V. Shalimoff, N. M. Edelstein, M. A. Edelman and M. F. Lappert, *J. Am. Chem. Soc.*, 1988, **110**, 986–987.

2 Chapter Two: Uranium(III) Tp^{Me2} Half-sandwich Complexes

2.1 Introduction

In stark contrast to cyclopentadienyl ligands, the use of the tris(pyrazolyl)borate (Tp) ligand in uranium chemistry has been far less investigated. The first organouranium complexes synthesised in the 1950s contained cyclopentadienyl ligands, and since then this ligand has been widely used to support uranium complexes in a range of oxidation states in tandem with other ligands.[1] Tp-based ligands are, however, not without their merits; they are easily synthesised and modular, meaning steric and electronic properties can be easily modified.

Parallels have been drawn between the cyclopentadienyl and tris(pyrazolyl)borate ligands because they are both anionic 6-electron donors that coordinate facially. Nevertheless, significant differences can be found both in their steric properties as well as the orbitals involved in the metal ligand bonding situation. One such difference that is widely accepted is that Tp and Tp^{Me2} occupy substantially more space in the coordination sphere of metals compared to Cp and Cp*, respectively.[2,3] This increase in steric bulk has enabled the isolation of the rare U(III) alkyl complex, $UTp^{Me2}{}_2Bz$, which was used to functionalise CO_2 in a closed synthetic cycle.[4] Less clear is how these ligands affect the electronics of the metals they coordinate to. A report comparing the electron donating properties of group 3 to group 9 Tp and Cp metal complexes found that the electron donor ability of both ligands varies across multiple factors such as the identity of the metal, its oxidation state and other ligands present in the complex.[5] To date, no such study has been repeated for complexes of uranium. Furthering our understanding of ligand properties is of great importance, especially in the context of small molecule activation mediated by U(III) complexes, which has been the focus of research from our laboratory over the past decade. Our research has investigated the use of mixed-sandwich complexes containing the Cp* ligand with other carbocyclic ligands, specifically, silyl substituted COT and pentalene ligands discussed in the previous chapter.

This chapter focuses on the U(III) half-sandwich systems, U(η^8-C_8H_6{1,4-$SiMe_3$}$_2$)(κ^3-Tp^{Me2}) **2.1**, U(η^8-C_8H_4{1,4-Si^iPr_3}$_2$)(κ^3-Tp^{Me2}) **2.2** and U(η^8-C_8H_6{1,4-Si^iPr_3}$_2$)(κ^3-Tp^{Me2}) **2.3** and investigations to understand their reactivity and highlight differences with analogous Cp* systems.

2.2 Synthesis and Characterisation of 2.1- 2.5

Previous studies by Dr Joy Farnaby focused the synthesis and characterisation of **2.2** and **2.3**.[6,7] These investigations form the basis of the syntheses in this chapter, with an important alteration to the synthetic procedure as follows. A 2013 publication from our laboratory outlined the optimised procedure for the synthesis of $UCp^*COT^{TMS2}(THF)_x$ (x = 0 or 1) which required the addition of K_2COT^{TMS2} to $UI_2Cp^*(THF)_n$ (n = 0 – 3) to be carried out at a lower temperature than $UCp^*COT^{TIPS2}(THF)_x$ and with a shorter work-up procedure.[8] As a result, there was a significant decrease in the yield of the undesired thermodynamic side-product, $U(COT^{TMS2})_2$, and an increase in the yield of the desired product $UCp^*COT^{TMS2}(THF)_x$. It was therefore anticipated that this optimisation may result in improved yields of **2.2**, **2.3** and the synthesis of $UTp^{Me2}COT^{TMS2}$, especially since previous attempts to synthesise the latter compound were unsuccessful.[7]

The synthesis of **2.1**-**2.3** involves the addition of 0.8 equivalents of either the COT or pentalene dipotassium salt to $UI_2Tp^{Me2}(THF)_x$ at -45 °C over 90 minutes, followed by Celite® filtration and recrystallisation to give the desired compounds in modest yields (13 - 25%) (**Scheme 2.1**).

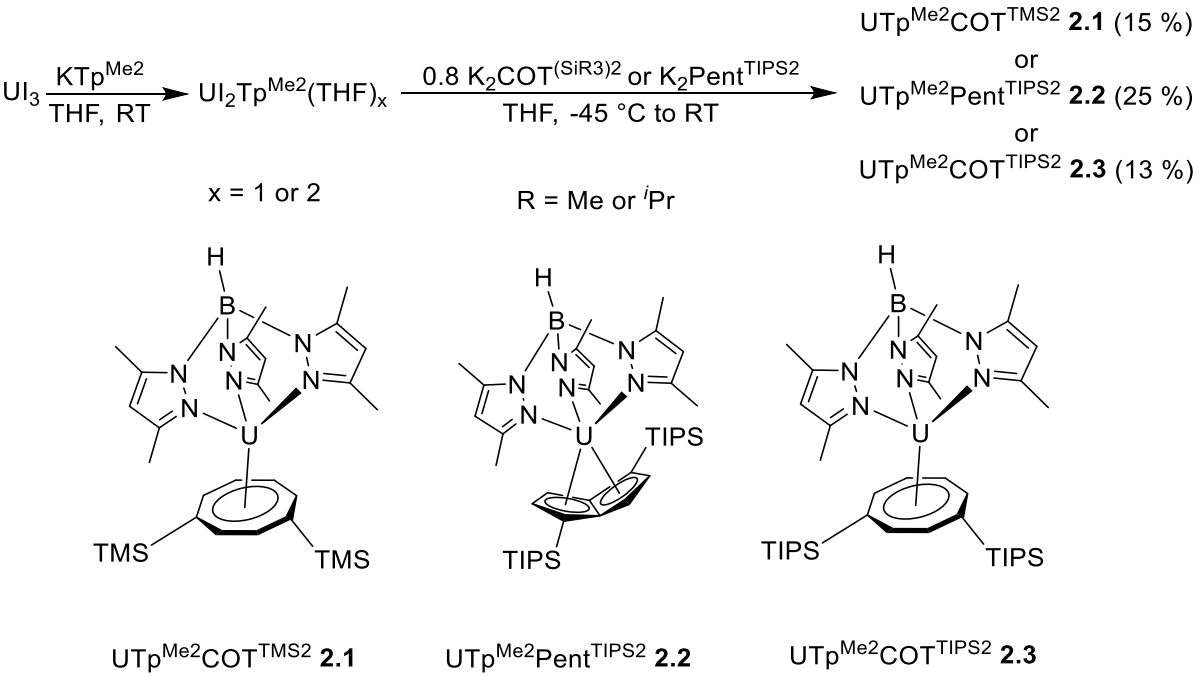

Scheme 2.1 Synthesis of **2.1**, **2.2** and **2.3**.

^{1}H NMR spectroscopic data for **2.1** show that the proton resonances for the three pyrazolyl arms of Tp^{Me2} are in a 9:9:3 ratio while the COT ring proton resonances exist in three distinct environments. This is similar to **2.2** in which the three pyrazolyl rings are also equivalent. In contrast to this, **2.3** features two equivalent pyrazolyl arms as indicated by the 3:3:1:6:6:2 ratio of the protons in the Tp^{Me2} environment. The ^{29}Si{^{1}H} NMR chemical shift of silicon-containing ligands in uranium complexes has been shown to correlate well with the oxidation state at uranium.[9] ^{29}Si{^{1}H} NMR data (**2.1**: -138.48, **2.2**: -159.3 and **2.3**: -115.6 ppm) are consistent with other U(III) complexes.[9] The ^{29}Si{^{1}H}NMR chemical shift for **2.1** is similar to $UCOT^{TMS2}Cp^{*}$ (-145 ppm) while **2.2** has a lower value in comparison to $UCp^{*}Pent^{TIPS2}$ (-173 ppm).[10,11] Less variation is observed in the ^{11}B{^{1}H} NMR spectra (**2.1**: 32.8, **2.2**: 37.7 and **2.3**: 31.8 ppm). Due to the silylated ligands, the three complexes are amenable to EI-MS experiments and the molecular ion peak is observed for all species and is consistent with the expected isotope pattern. IR spectroscopy of **2.1** exhibits a band at *ca* 2400 cm^{-1} corresponding to a B–H stretch.[12] Hydrogen and nitrogen values were within a low margin of error in combustion analysis for **2.1**, although percentage carbon values were found to be lower than expected. A possible reason for the observed values is incomplete combustion. Single crystals of **2.1** suitable for X-ray diffraction studies

were grown from a concentrated pentane solution at -35 °C, with the molecular structure given below (**Figure 2.1**).

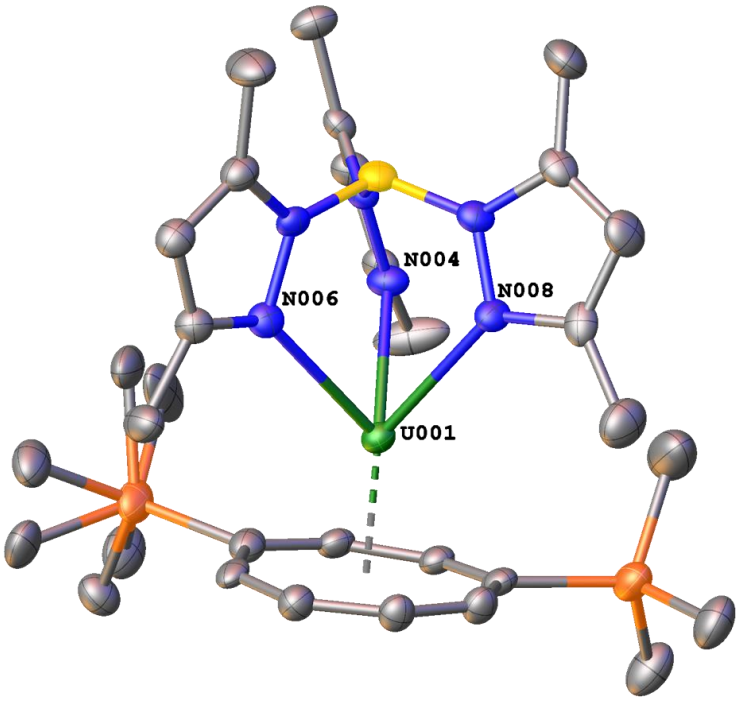

Figure 2.1 Molecular structure of **2.1**. Uranium, green; nitrogen, blue; carbon, grey; boron, yellow; silicon, orange. Hydrogen atoms omitted for clarity. The disordered TMS groups on COT^{TMS2} are shown. Selected structural parameters (Å): U1–Ct(COT) = 1.9868(5), average U–N = 2.615.

Unsurprisingly, the molecular structure of **2.1** is similar to the analogous COT^{TIPS2} complex **2.3**.[6] The U–COT centroid distance of 1.9868(5) Å is slightly shorter than in **2.3** (2.000(5) Å)[6] due to the reduced steric bulk of the TMS groups. This value is the same as in UCp^*COT^{TMS2} (1.971(15) Å) within esds.[8] The $U–N_{av}$ value of 2.630 Å is similar to that in **2.2** (2.596 Å), **2.3** (2.615 Å) and $UTp^{Me2}I_2(THF)_2$ (2.53(3) Å).[13]

As we were planning to study compounds **2.1** – **2.3** electrochemically, it would be advantageous to also prepare analogous U(IV) complexes, *e.g.* $UTp^{Me2}Pent^{TIPS2}Cl$, to verify whether electrochemical processes are indeed related to a U^{IV}/U^{III} redox couple while enabling comparisons with Cp* congeners. Unfortunately, attempts towards the synthesis of the U(IV) chloride derivatives of **2.1** and **2.2** were unsuccessful. Initially, the synthesis of the chloride analogues of **2.1** and **2.2** were attempted by reacting

with one equivalent of ^{t}BuCl as a chloride transfer agent, which has been successfully used previously by us and others.[14,15] Unfortunately, resulting reactions yielded intractable mixtures with significant amounts of ligand decomposition observed in the ^{1}H NMR spectra. Due to the decomposition observed, a different oxidising agent was tested. Compound **2.3** was reacted with $[FeCp^{*}_{2}][B(C_6F_5)_4]$ in an attempt to synthesise the U(IV) cation, $[\mathbf{2.3}][B(C_6F_5)_4]$. Analysis of the ^{1}H NMR data (C_6D_6) showed the consumption of **2.3** and the formation of $FeCp^{*}_{2}$, indicating a reaction had taken place. Unfortunately, all attempts at crystallisation were unsuccessful.

This having failed, we then turned our attention to an alternative synthesis. Unpublished work from our laboratory has involved the synthesis of $\{U(Pent^{tips2})(\mu\text{-}Cl_2\}_4$ (**2.4**), an ideal precursor to $UTp^{Me2}Pent^{tips2}Cl$, whereas COT analogues were not synthetically accessible.[16] Compound **2.4** was synthesised through a ligand rearrangement reaction between $U(Pent^{TIPS2})_2$ and an excess of UCl_4 in a concentrated solution of THF at 90 °C (**Scheme 2.2**).[16] A concentration of *ca* 0.050 M $U(Pent^{TIPS2})_2$ is optimal for the reaction to reach completion overnight. ^{1}H NMR spectroscopy of **2.4** is relatively simple and contains five environments with the expected integral values. Due to low solubility, a peak for **2.4** was not observed in the $^{29}Si\{^{1}H\}$ NMR spectrum. Instead, d_8-THF was used to break up the tetrameric structure of **2.4** and form the more soluble, monomeric THF-adduct of **2.4**. ^{1}H NMR spectroscopic data are consistent with this formulation and one environment is observed in the $^{29}Si\{^{1}H\}$ NMR spectrum (-111.58 ppm) which is also consistent with other U(IV) $^{29}Si\{^{1}H\}$ chemical shift values.[9] Elemental analysis results are consistent with the proposed formulation. Compound **2.4** is tetrameric in the solid state, as evidenced *via* a single crystal X-ray diffraction study.[16]

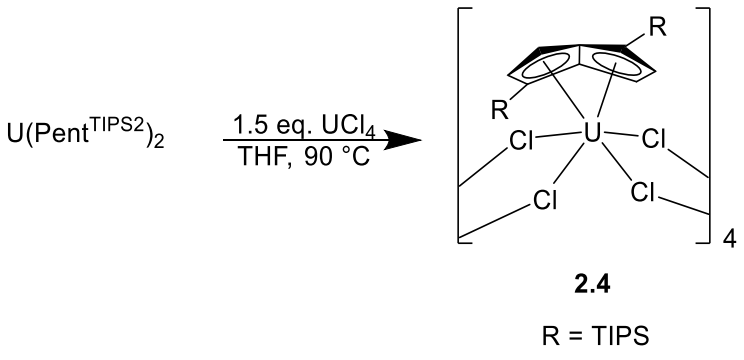

2.4

R = TIPS

Scheme 2.2 Synthesis of **2.4**. Simplified representation of tetrameric **2.4** is drawn.

To synthesise the desired $UTp^{Me2}Pent^{TIPS2}Cl$ complex, compound **2.4** was then reacted with four equivalents of KTp^{Me2} to give **2.5** as a dark green crystalline solid. Analysis by ^{1}H NMR revealed peaks across a range between 55 and -63 ppm which could not be assigned.

$^{11}B\{^{1}H\}$ NMR spectroscopy revealed one resonance at -5.21 ppm as anticipated, however, no peaks were observed in the $^{29}Si\{^{1}H\}$ NMR spectrum despite long experiment times (10,000 scans) and the use of concentrated samples. EI-MS showed the desired peak at m/z = 985. Carbon values were low in the elemental analysis, a result that has been previously observed with other uranium-pentalene-containing compounds.[17]

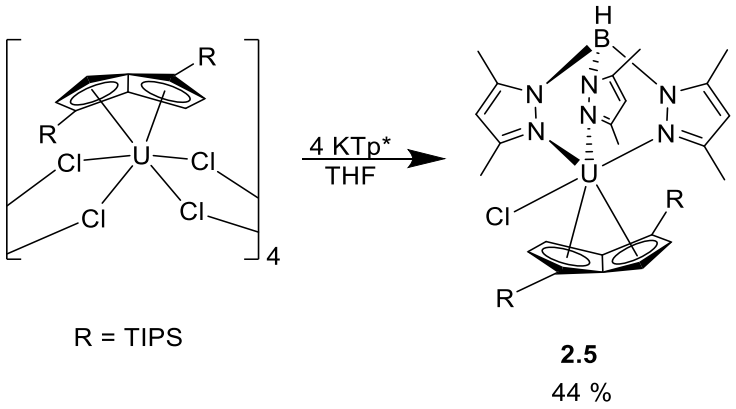

Scheme 2.3 Synthesis of $UTp^{Me2}Pent^{tips2}Cl$ (**2.5**).

Single crystals of **2.5** were obtained from a saturated pentane solution (-35 °C), which enabled X-ray diffraction studies to be carried out and confirm the molecular structure of **2.5** (**Figure 2.2** and **Table 2.1**). The Pent–U–Tp^{Me2} angle in **2.5** is 15° smaller than that observed in **2.2**, due to the extra chloride ligand in the coordination sphere of the uranium to minimise steric interaction between Tp^{Me2} and pentalene ligands. The U–Cl bond length of 2.6575(12) Å is comparable to that found in $UCp^{*}COT^{tips2}Cl$ (2.6496(12) Å)[18]. The average U–N bond distance in **2.5** is 2.5593 Å, shorter than in **2.2** (2.596 Å). This is, however, expected due to **2.5** containing a smaller U(IV) centre; this is also the reasoning for the shorter pentalene centroid distance. A similar trend has previously been observed with $UCp^{*}COT^{TIPS2}Cl$.[18]

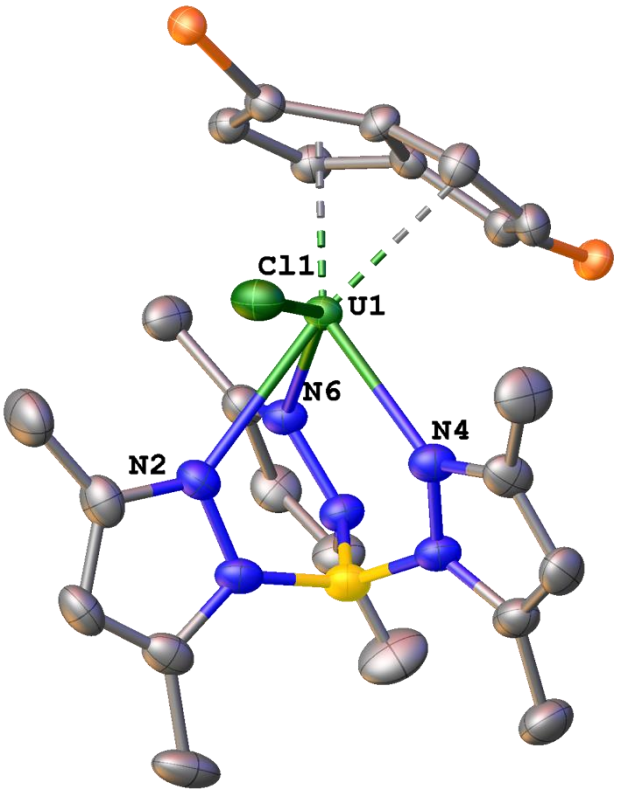

Figure 2.2 The molecular structure of **2.5**. Uranium, green; nitrogen, blue; boron, yellow; chlorine, green; carbon, grey; silicon, orange. H atoms and ^{i}Pr groups are omitted for clarity. Structure shown with 50% thermal ellipsoids.

Table 2.1 Bond lengths (Å) and angles (°) for **2.2** and **2.5**.

Parameter	**2.2**	**2.5**
Pentalene Centroid 1 to U distance	2.395(3)	2.3585(2)
Pentalene Centroid 2 to U distance	2.416(3)	2.3613(2)
Fold angle of pentalene	136.4(7)	135.7(5)
U1–C18–C19–C23 torsion angle	75.4(8)	73.0(6)
Centroid1–U1–Centroid 2 angle	65.04(14)	47.735(4)
Pent–U–Tp^{Me2} Angle	166.60(2)	151.630(7)
U1–N2	2.604(6)	2.615(5)
U1–N4	2.572(8)	2.486(5)
U1–N6	2.612(8)	2.577(4)
Average U–N	2.596(12)	2.5593(4)
U1– Cl1	n/a	2.6575(12)

2.4 Cyclic voltammetry of 2.1, 2.2, 2.3 and 2.5

With the U(III) complexes (**2.1** – **2.3**) and U(IV) complex (**2.5**) in hand, electrochemical studies were carried out to gauge how the Tp^{Me2} ligand affects the U^{IV}/U^{III} redox couple compared to their Cp* analogues. The cyclic voltammograms of **2.1**, **2.2**, **2.3** and **2.5** are shown below.

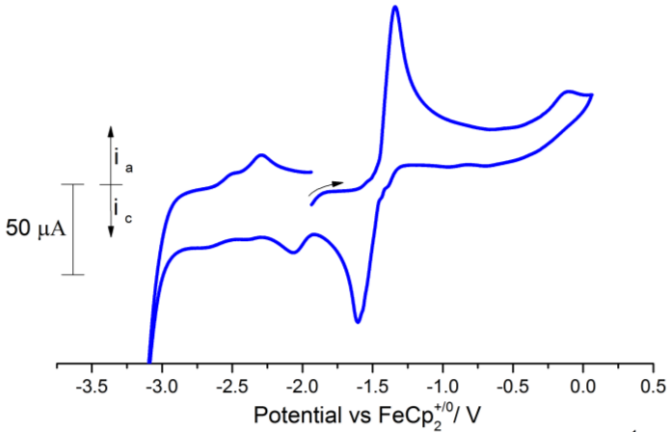

Figure 2.3: Cyclic voltammogram of a 5 mM solution of **2.1** in 0.1 M [^{n}Bu$_4$N][B(C$_6$F$_5$)$_4$] / THF. Scan rate 100 mV s^{-1}.

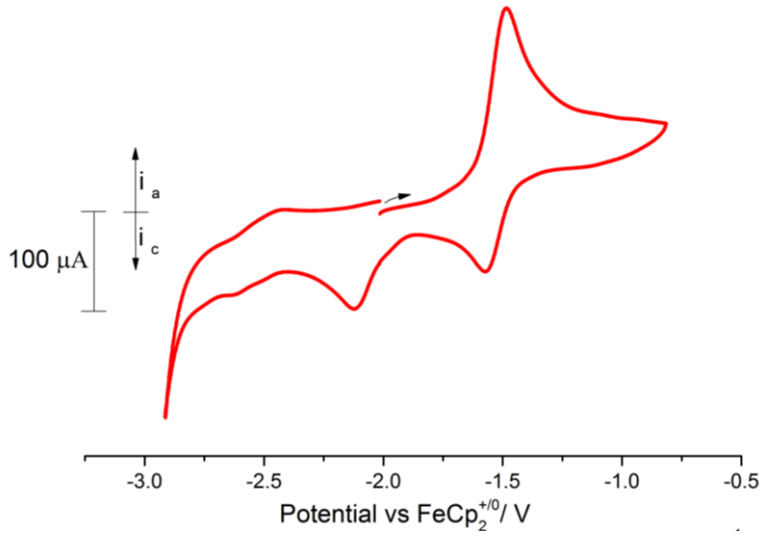

Figure 2.4: Cyclic voltammogram of a 5 mM solution of **2.2** in 0.1 M [^{n}Bu$_4$N][B(C$_6$F$_5$)$_4$] / THF. Scan rate 100 mV s^{-1}.

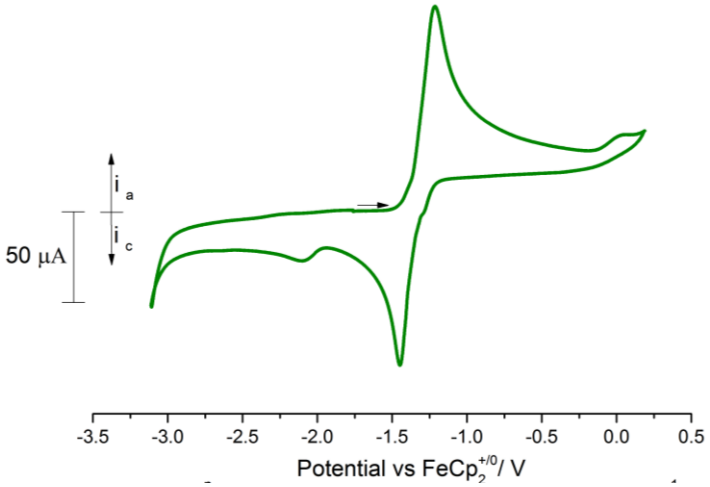

Figure 2.5: Cyclic voltammogram of a 5 mM solution of **2.3** in 0.1 M [^{n}Bu$_4$N][B(C$_6$F$_5$)$_4$] / THF. Scan rate 100 mV s^{-1}.

Scanning in the anodic direction revealed quasi-reversible processes at -1.40, -1.55 and -1.33 V *vs* $FeCp_2^{+/0}$ for **2.1** (**Figure 2.3**), **2.2** (**Figure 2.4**) and **2.3** (**Figure 2.5**) respectively and are tentatively assigned to a ligand-based process. Irreversible processes were observed for **2.1**, **2.2** and **2.3** at -2.10, -2.16 and -2.10 V *vs* $FeCp_2^{+/0}$ respectively. The Cp* analogues of **2.1** (UCp*COT^{TMS2}(THF)) and **2.3** (UCp*COT^{TIPS2}(THF)) show reduction potentials of *ca* -2.10 V *vs* $FeCp_2^{+/0}$,[19] while the Cp* analogue of **2.2** (UCp*Pent^{TIPS2}(THF)) has a reduction potential of *ca* -2.20 V *vs* $FeCp_2^{+/0}$,[20] 0.10 V more reducing than its COT^{TIPS2} congeners. The nature of these processes are unclear, therefore they remain unassigned. An oxidative half wave process seen at -2.30 V *vs* $FeCp_2^{+/0}$ in the voltammogram of **2.1** is unassignable.

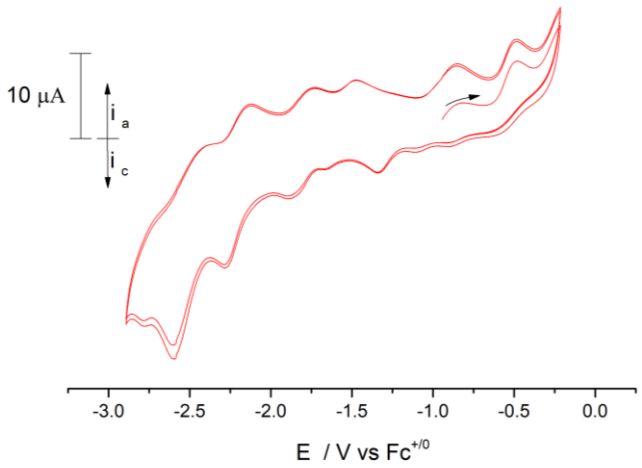

Figure 2.6 Cyclic voltammogram (2 cycles) of a 5 mM solution of **2.5** in 0.1 M [^{n}Bu$_4$N][B(C$_6$F$_5$)$_4$] / THF. Scan rate 100 mV s^{-1}

The voltammogram of **2.5** (**Figure 2.6**) is complex and displays several more processes in comparison to **2.2** where only three processes can be assigned with some confidence. The process at -2.52 V *vs* $FeCp_2^{+/0}$ is assigned to a pentalene-based process.[20] The processes that are unable to be assigned may originate from electrochemically-generated species, contaminants or decomposition products due to the solvent and/or electrolyte.

These cyclic voltammogram studies show that the U(III) complexes **2.1**, **2.2** and **2.3** contain complex electrochemistry that cannot be easily explained. Therefore, comparisons cannot be made with their Cp* congeners which are more reactive to small molecues. One possible reason for this lack of reactivity in the case of **2.1**, **2.2**, and **2.3** is the steric hindrance imposed by the Tp^{Me2} ligand that prevents small molecules approaching the metal centre. The bent COT^{R2}–U–Cp* (R = TIPS or TMS) arrangement in the mixed-sandwich compounds (UCp*COT^{R2}(THF)$_n$ (R = TIPS or TMS) and n = 0 or 1) allows small molecules to approach the metal centre more easily.

2.3 Reactivity of 2.1 and 2.2 Towards Small Molecules

The ability of the mixed-sandwich systems, UCp*COT^{R2} (R = TIPS or TMS) and UCp*Pent^{TIPS2}, to activate small molecules (CO, CO_2 and N_2 among others) was discussed in the previous chapter. Electrochemistry studies indicate these systems have similar reduction potentials to their Tp^{Me2} congeners, **2.1**-**2.3**, yet they show divergent reactivity towards the aforementioned small molecules. Previous studies by Dr Joy Farnaby demonstrated that **2.3** was unreactive towards CO and CO_2 under mild conditions. With this in mind it was envisaged that the reduced steric bulk of **2.1** compared to **2.3** would increase reactivity.

Unfortunately, **2.1** was unreactive towards CO and CO_2 under similar reaction procedures which is surprising given the wealth of U(III) compounds that activate CO_2.[22] Therefore, the more reactive NO molecule was reacted with **2.1**. Upon addition of one equivalent of NO at -78 °C, **2.1** undergoes a reaction, however, ^{1}H NMR spectroscopy on the resulting intractable mixture shows significant ligand decomposition products.

N_2O is a potent greenhouse gas that U(III) complexes are well placed to activate due to their oxophilic and reducing nature. There are numerous examples of U(III) complexes that cleanly react with N_2O to form μ-oxo or terminal-oxo species.[23,24] One equivalent of N_2O was added to a -78 °C solution of **2.1** and again NMR spectroscopic data indicated formation of ligand decomposition by-products. The decomposition of tris(pyrazolyl)borate ligands has previously been observed in low-valent lanthanide and uranium complexes.[25]

As outlined previously, UCp*COT^{TIPS2}(THF) reductively trimerizes CO to form a bimetallic deltate complex.[26] At the time of publication it was clear that **2.2** did not react with CO in the same way as observed for UCp*COT^{TIPS2}(THF), however, it was unclear how **2.2** did react with CO. Studies in this prior publication involved the reaction of **2.2** under an overpressure of CO at ambient conditions which was subsequently probed using NMR spectroscopy (^{1}H, ^{11}B{^{1}H}, ^{13}C{^{1}H} and ^{29}Si{^{1}H}) and EI-MS only.[6] There was no evidence for the formation of any new species using these methods at ambient temperature. It was proposed that exchange between free and bound CO was taking place at such a rate

that was too fast to be observed during NMR experiments at room temperature.[6] Therefore, VT-NMR and low-temperature *in situ* IR spectroscopy were targeted to probe this reaction further. It was hoped that NMR experiments at lower temperatures may enable the observation of new species. Also, *in situ* IR spectroscopy is well-suited to observe metal-carbonyl compounds due to the prominent nature of the metal-carbonyl stretches.

Upon addition of an excess of ^{13}CO to a solution of **2.2** at -78 ºC, a colour change from dark maroon to dark brown was observed, which persisted upon gradual warming to -25 °C. However, above this temperature the solution changed back to dark maroon indicating loss of CO in the proposed uranium carbonyl complex. This colour change was observed over several cycles of cooling and warming the solution, indicating that this process is reversible. Variable temperature NMR (^{1}H, ^{11}B{^{1}H}, ^{13}C{^{1}H} and ^{29}Si{^{1}H}) studies of a d_8-toluene solution of **2.2** containing an excess of ^{13}CO were carried out from -50 °C to 30 °C, but no new species were observed by NMR spectroscopy.

Next, IR spectroscopy on **2.2** was carried out. A solution of **2.2** in methylcyclohexane was degassed and then pressurised with an excess of ^{12}CO at -78 °C. After 30 minutes at -78 °C, an IR stretch was observed at 1941 cm^{-1} (**Figure 2.7**) which persisted up to -25 °C. Above this temperature this signal began to decrease in intensity. To verify whether this observed stretch is indeed related to a uranium carbonyl complex, the reaction was repeated using ^{13}CO, which led to the observation of a band at 1906 cm^{-1} as expected (**Figure 2.7**).[27] These observations are strong evidence for the formation and decay of a uranium carbonyl complex that is unstable above -25 °C. We hypothesise that the carbonyl complex is kinetically unstable and readily dissociates above -25 °C to reform **2.2.**

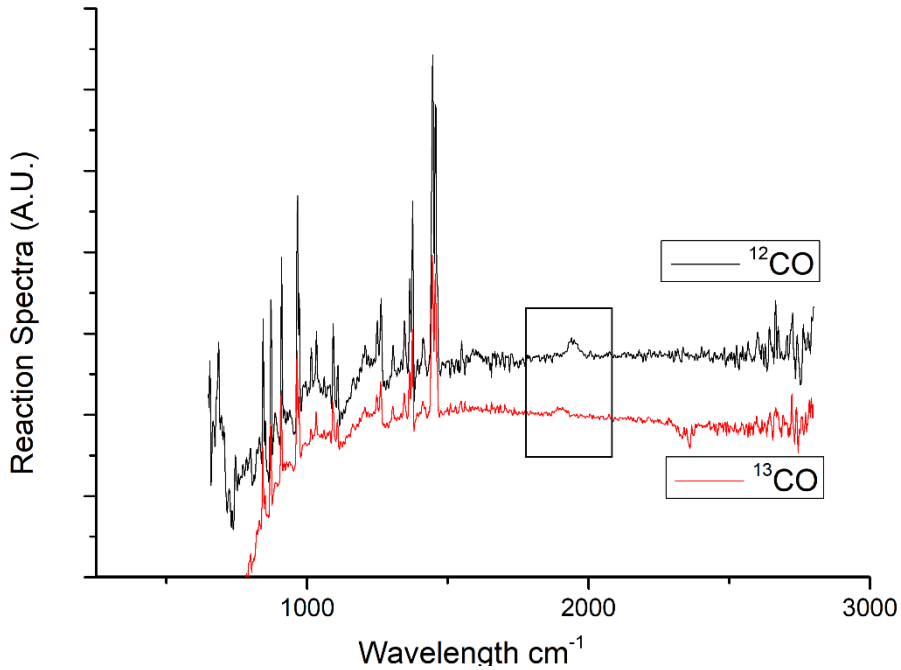

Figure 2.7 IR spectrum of **2.2** plus ^{12}CO (black) or ^{13}CO (red) at -78 °C. Carbonyl stretches are highlighted.

Reported solution ν_{12CO} values for uranium carbonyl complexes range from 1900 to 1976 cm^{-1} (**Table 2.2**). The ν_{12CO} of 1941 cm^{-1} for **2.2** indicates that the uranium complex is back-donating electron density into a π^* orbital of CO (ν_{CO} of free CO = 2145 cm^{-1}) and reducing it to a significant degree. Of the other reported uranium carbonyl complexes, $U(Cp^*)_3CO$ and $U(Cp^{Me4})_3CO$ can be isolated as a crystalline material, whereas complexes featuring ν_{12CO} values greater than 1925 cm^{-1} have not been isolated to date. DFT studies of actinide cyclopentadienyl (U, Th) systems have indicated donation to CO originates from cyclopentadienyl-based orbitals.[28,29] Owing to the similarities between pentalene and cyclopentadienyl, it is postulated this may also be the case in the carbonyl complex of **2.2** though computational studies would be required to evidence this.

Table 2.2 Uranium carbonyl complexes and their reported solution νCO.

Uranium carbonyl complex	Solution ν_{12CO} / cm^{-1}
$U(Cp^{TMS2}{}_3)CO$	1988[30]
$U(Cp^{TMS2})_3CO$	1976[31]
$U(Cp^{tBu})_3CO$	1960[30]
$UTp^{Me2}Pent^{TIPS2}CO$	**1941**
$U(Cp^*)_3$	1925[32]
$UCp^*COT^{TIPS2}CO$	1920[33]
$U(Cp^{Me4})_3CO$	1900[34]

2.4 Conclusions

The synthesis of three U(III) complexes **2.1**, **2.2** and **2.3** are described (**Scheme 2.1**). Unfortunately, compound **2.1** either decomposes or does not react with the small molecules surveyed. In contrast, complex **2.2** forms a uranium-carbonyl complex that is stable up to -25 °C as evidenced by *in-situ* IR studies with ^{12}CO and ^{13}CO. Furthermore, the synthesis of the potentially useful U(IV) complex **2.4** and its use as a synthon to access the U(IV) complex **2.5** has been achieved (**Scheme 2.3**).

Electrochemical studies were carried out to determine the U^{III}/U^{IV} redox couple of **2.1**, **2.2**, **2.3** and **2.5**, and these are comparable to their Cp* analogues, although their electrochemical behaviour is more complex than their Cp* analogoues therefore comparisons were made.

With these conclusions in mind, our attention was focused towards other U(III) complexes that are stable yet reactive towards small molecules, such as $UCp^*(pMe_2O_2)$, which will be explored in the next chapter.

2.5 Experimental Details for Chapter Two

Synthesis of $UTp^{Me2}COT^{TMS2}$ 2.1

An ampoule was charged with UI_3 (0.620 g, 1 mmol) and THF (40 ml) added. To this a suspension of KTp^{Me2} (0.337 g, 1 mmol) in THF (20 ml) was added dropwise over 30 minutes at room temperature and stirred for 24 h. The mixture was stripped to dryness, toluene (40 ml) was added, the suspension filtered and dried *in vacuo*. THF (30 ml) was added to the resulting solid and the solution cooled to -45 °C. To this, a solution of K_2COT^{TMS2} (0.263 g, 0.8 mmol) in THF (20 ml) was added over 90 minutes. The mixture was left to warm to room temperature over 30 minutes and then evacuated to dryness. The residue was dissolved in pentane (40 ml), filtered through Celite®, reduced by half and left overnight at -45 °C to yield dark maroon crystals of **2.1**. Yield: 114 mg, 14.5% based on UI_3.

Analysis calculated (found) for $C_{29}H_{46}BN_6Si_2U$: % C 44.443 (41.307), % H 5.916 (5.882), % N 10.723 (10.406). Low carbon values have also been seen with UCp^*COT^{TMS2} complexes, we propose this is due to incomplete combustion.

^{1}H NMR (399.5 MHz, d_8-toluene, 303 K): δ_H 19.0 (br, d, 1H, B-H), 8.4 (br, s, 3H, Tp^{Me2}-CH), 2.1 (br, s, 9H, Tp^{Me2}-CH_3), -6.6 (s, 18H, Si-CH_3), -17.9 (s, 9H, Tp^{Me2}-CH_3), -28.5 (s, 2H, COT ring CH), -47.1 (s, 2H, COT ring CH), -50.6 (s, 2H, COT ring CH).

^{11}B{^{1}H} NMR (128.2 MHz, d_8-toluene, 303 K): δ_B 32.8

^{29}Si{^{1}H} NMR (79.4 MHz, d_8-toluene, 303 K): δ_{Si} -138.48

MS (EI): m/z = 783 $(M)^+$

Synthesis of $UTp^{Me2}Pent^{TIPS2}$ 2.2

Compound **2.2** was synthesised following a similar procedure to that of **2.1** except that K_2Pent^{TIPS2} (0.390 g, 0.8 mmol) was used instead of K_2COT^{TMS2}. Yield: 248 mg, 25% based on UI_3.

^{1}H NMR (399.5 MHz, d_8-toluene, 303 K): δ_H 17.9 (br, S, 1H, B-H), 7.7 (s, 3H, Tp^{Me2}-CH), 7.3 (br, s, 1H, pentalene ring C-H), 2.5 (s, 9H, Tp^{Me2}-CH$_3$), -5.3 (s, 18H, iPr-CH$_3$), -9.9 (s, 18H, iPr-CH$_3$), -11.6 (s, 6H, iPr-CH), -17.0 (s, 9H, Tp-CH), -23.2 (s, 2H, pentalene ring CH).

^{11}B{^{1}H} NMR (128.2 MHz, d_8-toluene, 303 K): δ_B 37.7

MS (EI): m/z = 949 $(M)^+$

Synthesis of UTp^{Me2}COT^{TIPS2} 2.3

Compound **2.2** was synthesised following a similar procedure to that of **2.1** except that K_2Pent^{TIPS2} (0.375 g, 0.8 mmol) was used instead of K_2COT^{TIPS2}. Yield: 120 mg, 12.6% based on UI_3.

^{1}H NMR (399.5 MHz, d_8-toluene, 303 K): δ_H 19.2 (br, s, 1H, B-H), 10.9 (s, 2H, Tp^{Me2}-CH), 4.3 (s, 1H, Tp^{Me2}-CH), 3.4 (s, 6H, Tp^{Me2}-CH$_3$), -0.08 (s, 3H, Tp^{Me2}-CH$_3$), -1.8 (s, 18H, iPr-CH$_3$), -2.2 (s, 18H, iPr-CH$_3$), -2.7 (s, 6H, iPr-CH), -15.5 (s, 3H, Tp^{Me2}-CH), -17.7 (s, 6H, Tp^{Me2}-CH$_3$), -22.0 (s, 2H, COT ring CH), -50.2 (s, 2H, COT ring CH), -54.5 (s, 2H, COT ring CH).

^{11}B{^{1}H} NMR (128.2 MHz, d_8-toluene, 303 K): δ_B 31.8

MS (EI): m/z = 951 $(M)^+$

Synthesis of {UPent^{TIPS2}Cl$_2$}$_4$ 2.4

To a high pressure ampoule U(Pent^{TIPS2})$_2$ (0.260 g, 0.243 mmol), UCl_4 (0.143 g, 0.376 mmol), and THF (5 mL). The ampoule's headspace was evacuated and the vessel heated at 90 °C for 24 h. The crude reaction mixture was filtered and evacuated to dryness. The residues were extracted in hexane (15 mL), filtered, reduced to 8 mL and stored at -35 °C to yield **2.4** as a dark green crystalline solid.

^{1}H NMR (399.5 MHz, d_8-toluene, 303 K): δ_H 27.49 (s, 2H, Pn-H), -3.42 (s, 18H, ^{i}Pr-CH$_3$), -6.03 (s, 18H, iPr-CH$_3$), -15.35 (s, 6H, ^{i}Pr-CH), -46.59 (s, 2H, Pn-H).

^{29}Si{^{1}H} NMR (79.4 MHz, d_8-THF, 303 K): δ_{Si} -111.58

Analysis calculated (found) for $C_{26}H_{46}Cl_2Si_2U$: % C 43.147 (43.499), % H 6.406 (6.415).

Synthesis of UTp^{Me2}Pent^{Tips2}Cl 2.5

A 20 mL scintillation vial was charged with $\{UPent^{tips2}Cl_2\}_4$ (0.198 g, 0.067 mmol) and a stirrer bar. To this, pre-chilled THF (2 mL) was added and the vial stored at -35 °C for 10 minutes. A suspension of KTp^{Me2} (0.092 g, 0.273 mmol) in THF (2 mL) was added to a stirred solution of $\{UPent^{tips2}Cl_2\}_4$ over 2 minutes using a pipette. The solution was left to stir at room temperature for an hour and the solvent removed under reduced pressure. The green residues were extracted in pentane (10 mL) and filtered through Celite® on a frit. The solvent was reduced to *ca* 1.5 mL and the sample was stored at -35 °C. After 3 d the mother liquor was carefully removed and the crystalline material washed with cold $SiMe_4$ (0.5 mL) and pentane (2 x 1 mL) to give the title compound as a dark green crystalline solid. A second recrystallization using pentane was required to remove trace impurities observed in the $^{11}B\{^1H\}$ NMR.

Yield 0.120 g (44%)

Analysis calculated (found) for $C_{41}H_{68}BClN_6Si_2U$: % C 49.969 (48.989), % H 6.955 (6.980), % N 8.528 (7.840).

^1H NMR (399.5 MHz, d_6-benzene, 303 K): δ_H 32.02 (br, s, 0.60H, unknown), 28.03 (br, s, 0.52H, unknown), 17.24 (br, s, 0.29H, unknown), 15.60 (br, s, 0.43H, unknown), 8.94 (br, s, 2.32H ,unknown) 4.62 (br, s, 4.07H, unkown), 2.66 (br, s, 2.81H, unknown), 1.25 (m, pentane), 0.87 (t, pentane), 0.32 (br, s, 8.71H, unknown), -1.34 (br, s, 2.77H, unknown), -2.93 (br, s, 2.55H, unknown), -4.19 (br, d, ^{i}Pr-CH_3), -5.41 (br, several overlapping singlets, 12.46H, unknown), -6.58 (br, s, 1.05H, unknown), -7.22 (br, s, 1.29H, unknown), -10.26 (br, two overlapping singlets, 2.78H, unknown), -11.18 (br, s, 4.75H, unknown), -15.26 (br, s, 1.84H, unknown), -62.6 (br, s, 0.96H, unknown). Total H = 65.87, expected total is 68H. Spectrum cannot be assigned with confidence due to asymmetric nature of the complex.

$^{11}B\{^1H\}$ NMR (128.2 MHz, d_6-benzene, 303 K): δ_B -5.21

$^{29}Si\{^1H\}$ NMR (79.4 MHz, d_6-benzene, 303 K): δ_{Si} No signal observed after a 10,000 scan experiment.

EI-MS: m/z = 985 $(M)^+$

2.6 References for Chapter Two

1 L. T. Reynolds and G. Wilkinson, *J. Inorg. Nucl. Chem.*, 1956, **2**, 246–253.
2 N. Kitajima and W. B. Tolman, in *Progress in Inorganic Chemistry*, Wiley-Blackwell, 2007, pp. 419–531.
3 S. Trofimenko, *Scorpionates: The Coordination Chemistry of Polypyrazolylborate Ligands*, Imperial College Press, 1999.
4 E. M. Matson, W. P. Forrest, P. E. Fanwick and S. C. Bart, *J. Am. Chem. Soc.*, 2011, **133**, 4948–4954.
5 D. M. Tellers, S. J. Skoog, R. G. Bergman, T. B. Gunnoe and W. D. Harman, *Organometallics*, 2000, **19**, 2428–2432.
6 J. H. Farnaby, F. G. N. Cloke, M. P. Coles, J. C. Green and G. Aitken, *Comptes Rendus Chim.*, 2010, **13**, 812–820.
7 J. H. Farnaby, PhD thesis, University of Sussex, 2011.
8 N. Tsoureas, O. T. Summerscales, F. G. N. Cloke and S. M. Roe, *Organometallics*, 2013, **32**, 1353–1362.
9 C. J. Windorff and W. J. Evans, *Organometallics*, 2014, **33**, 3786–3791.
10 F. G. N. Cloke and P. B. Hitchcock, *J. Am. Chem. Soc.*, 2002, **124**, 9352–9353.
11 N. Tsoureas, O. T. Summerscales, F. G. N. Cloke and S. M. Roe, *Organometallics*, 2012, **32**, 1353–1362.
12 J. D. Carpenter and B. S. Ault, *J. Phys. Chem.*, 1991, **95**, 3502–3506.
13 Y. Sun, R. McDonald, J. Takats, V. W. Day and T. A. Eberspacher, *Inorg. Chem.*, 1994, **33**, 4433–4434.
14 J. A. Higgins, F. G. N. Cloke and S. M. Roe, *Organometallics*, 2013, **32**, 5244–5252.
15 R. G. Finke, S. R. Keenan, D. A. Schiraldi and P. L. Watson, *Organometallics*, 1986, **5**, 598–601.
16 N. Tsoureas and F. G. N. Cloke, *Private communication*, .
17 N. Tsoureas, *Unpublished results*, 2013.
18 J. Higgins, PhD thesis, University of Sussex, 2014.
19 N. Tsoureas, L. Castro, A. F. R. Kilpatrick, F. G. N. Cloke and L. Maron, *Chem. Sci.*, 2014, **5**, 3777–3788.
20 A. Kilpatrick, N. Tsoureas and F. G. N. Cloke, *Unpublished results*.
21 A. F. R. Kilpatrick, PhD thesis, University of Sussex, 2014.
22 H. S. La Pierre and K. Meyer, in *Progress in Inorganic Chemistry, vol. 58*, ed. K. D. Karlin, Wiley, 2014, vol. 58, pp. 301–413.
23 N. Tsoureas, A. F. R. Kilpatrick, C. J. Inman and F. G. N. Cloke, *Chem. Sci.*, 2016, **7**, 4624–4632.
24 S. M. Franke, B. L. Tran, F. W. Heinemann, W. Hieringer, D. J. Mindiola and K. Meyer, *Inorg. Chem.*, 2013, **52**, 10552–10558.
25 M. Ephritikhine, *Angew. Chem. Int. Ed.*, 2009, **48**, 4898–4899.
26 O. T. Summerscales, F. G. N. Cloke, P. B. Hitchcock, J. C. Green and N. Hazari, *Science*, 2006, **311**, 829–831.
27 J. A. Timney, in *Encyclopedia of Inorganic and Bioinorganic Chemistry*, American Cancer Society, 2011.
28 L. Maron, O. Eisenstein and R. A. Andersen, *Organometallics*, 2009, **28**, 3629–3635.
29 R. R. Langeslay, G. P. Chen, C. J. Windorff, A. K. Chan, J. W. Ziller, F. Furche and W. J. Evans, *J. Am. Chem. Soc.*, 2017, **139**, 3387–3398.
30 J. Parry, E. Carmona, S. Coles and M. Hursthouse, *J. Am. Chem. Soc.*, 1995, **117**, 2649–2650.
31 J. G. Brennan, R. A. Andersen and J. L. Robbins, *J. Am. Chem. Soc.*, 1986, **108**, 335–336.
32 W. J. Evans, S. A. Kozimor, G. W. Nyce and J. W. Ziller, *J. Am. Chem. Soc.*, 2003, **125**, 13831–13835.
33 A. S. Frey, F. G. N. Cloke, P. B. Hitchcock, I. J. Day, J. C. Green and G. Aitken, *J. Am. Chem. Soc.*, 2008, **130**, 13816–13817.

34 M. del Mar Conejo, J. S. Parry, E. Carmona, M. Schultz, J. G. Brennan, S. M. Beshouri, R. A. Andersen, R. D. Rogers, S. Coles and M. B. Hursthouse, *Chem. - Eur. J.*, 1999, **5**, 3000–3009.

3 Chapter Three: Synthesis of [U(Cp*)(*p*Me$_2$O$_2$)] and its Reactivity Towards CO_2

3.1 Introduction

Cyclopentadienyl and aryloxide ligands have played a pivotal role in the coordination chemistry of uranium complexes by influencing their reactivity towards small molecules. Both ligand classes have significantly different effects on the uranium centre due to their inherently different electronic and steric attributes. This point is emphasised by the difference in reactivity between $U(Cp^{Me4H})_3$ (**3A**) and $U(O(2,6\text{-}^tBuC_6H_3)_3$ (**3B**) towards CO.[1,2] Complex **3A** reacts to form the uranium-carbonyl complex, (**3A**)CO, while **3B** reductively homologates CO to give the enediolate complex, $(\mathbf{3B})_2(\mu\text{-}\eta^1\text{: }\eta^1\text{-}C_2O_2)$. With this observation in mind, we pursued a related aryloxide ligand that could be installed around a uranium metal centre in tandem with a Cp* ligand as an alternative to dianionic cyclooctatetraenyl or pentalene ligands, in the hopes of unveiling new reactivity. The new dianionic bis(aryloxide) *p*Me$_2$O$_2$ ligand containing a central arene ring was recently developed in our laboratory (**Figure 3.1**) and this chapter will discuss its synthesis, the synthesis of its Cp^*U^{III} derivative and reactivity towards CO_2. This chapter will also discuss the electrochemistry of these uranium complexes.

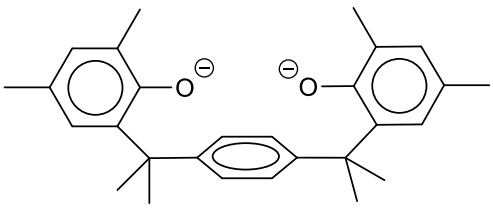

Figure 3.1 *p*Me$_2$O$_2$ ligand.

3.2 Novel Bis(phenoxide) Ligand

The *p*Me$_2$O$_2$ ligand was designed to form robust U(III) complexes that contain a reactive 'pocket' to facilitate the approach of small molecules towards the reducing U(III) centre. An important design consideration of the *p*Me$_2$O$_2$ ligand scaffold is the $C(CH_3)_2$ linkers; potentially reactive functional groups are avoided to mitigate undesired side reactions that can be brought about by the existence of such functionalities in the ligand scaffold. For example, previous work from our laboratory reported

that the silyl groups in UCp*($N^{TMS}N^{TMS}_2$)Cl underwent migration upon reaction with CO (**Scheme 1.1**).[3] Furthermore, Meyer *et al.* showed how [((^{Ad,Me}ArO)$_3$mes)U] underwent redox isomerisation at one of the methylene bridges upon reduction with KC_8 or Na metal at room temperature.[4]

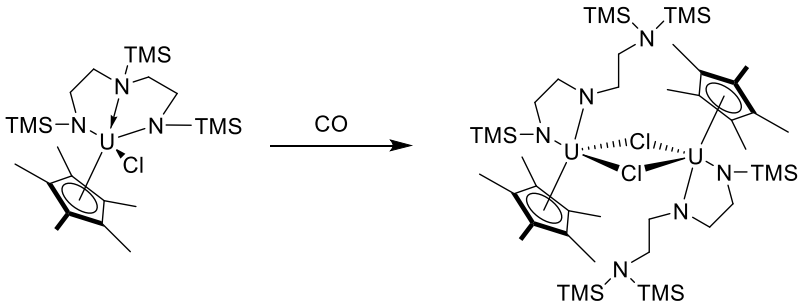

Scheme 1.1 Silyl group migration triggered by CO.

The central arene group is another key aspect of the ligand. Beyond simply providing steric bulk, the arene is centrally situated to promote stabilisation of low-valent uranium centres *via* δ backbonding. Inspiration was taken from [((^{Ad,Me}ArO)$_3$mes)U] which features a central chelating mesitylene ring which is able to form δ-backbonding interactions with uranium.[5] Such interactions have enabled the isolation of a U(II) complex and the electrocatalytic reduction of water as shown in the first chapter.[5]

Previous work in the group by Dr Alistair Frey led to the development of *p*$Me_2O_2H_2$ (**3.1**) *via* modification of a procedure reported in the patent literature.[6,7] α,α,α′,α′-Tetramethyl-1,4-benzenedimethanol undergoes an acid catalysed condensation reaction with 2,4-dimethylphenol (excess, as solvent) to give crude **3.1** (**Scheme 3.2**). Recrystallization from Et_2O gave **3.1** as white crystals in 40-50% overall yield, with analytical purity confirmed by elemental analysis. ^{1}H and ^{13}C{^{1}H} NMR spectroscopic data show 2-fold symmetry, indicating that in solution the phenol rings freely rotate around the $C(CH_3)_2$ units linking them and the central arene ring.

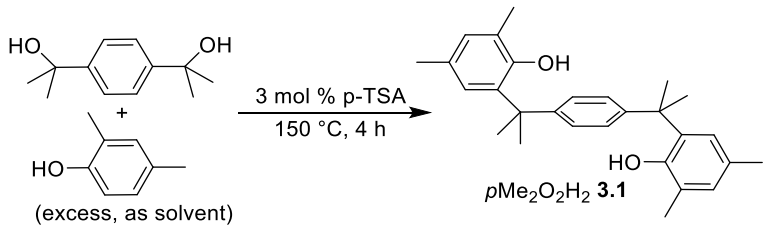

Scheme 3.2 Synthesis of **3.1**.

The solid-state molecular structure of **3.1** was determined by X-ray diffraction and is shown in **Figure 3.2**.[7] The phenol rings adopt an anti-conformation with respect to the central arene, and the quaternary sp^3 carbon (C9) linking the phenol and arene rings is tetrahedral (C6–C9–C12 angle of 109.05(10)°), consistent with a lack of strain. The central arene C–C distances are the same within error as those observed in the solid-state structure of p-xylene (**3.1**, average 1.3930 Å; p-xylene, average 1.392 Å), and the central arene displays a negligible amount of ring torsion (**3.1**, ±0.15°; p-xylene, ±0.10°).[8] The two phenol rings are related *via* a crystallographic inversion centre, and the angle between the planes of the central arene and each phenol ring is 81.51°.

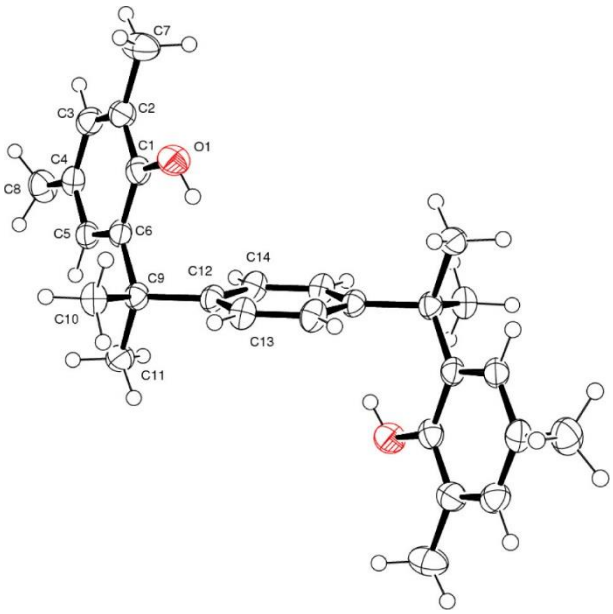

Figure 3.2 Molecular structure of **3.1**. Hydrogen atoms omitted for clarity and thermal ellipsoids are given at 50% probability. Selected structural parameters (Å, deg): C12–C13 = 1.390(17), C12–C14 = 1.3933(18), C6–C9–C12 = 109.05(10), C1–O1 = 1.3843(15).

Compound **3.1** is readily deprotonated by 2 equivalents of KH in DME to give the dipotassium salt [(*p*$Me_2O_2K_2$)$(DME)_n$] (**3.2**) as a fractional solvate (n = 1.5-2) in 85-95% yield. The crude material thus obtained returned elemental analyses which were slightly high in C and H; however, it was successfully used in subsequent salt metathesis reactions without further purification. Compound **3.2** is sufficiently soluble in d_5-pyridine to allow the degree of DME solvation in individual samples to be determined by ^{1}H NMR spectroscopy; these solutions were too dilute to allow acquisition of $^{13}C\{^1H\}$ NMR spectroscopic data.

3.3 Mixed-Ligand Uranium(III) Complex

Dipotassium salt **3.2** reacts with 1 equivalent of [U(Cp*)I_2(THF)$_n$] (prepared *in situ* in THF) to give, after workup, the mononuclear U(III) complex [U(Cp*)(*p*Me_2O_2)] **3.3** as dark green-black crystal plates in yields of 60-75% (**Scheme 3.3**).[7]

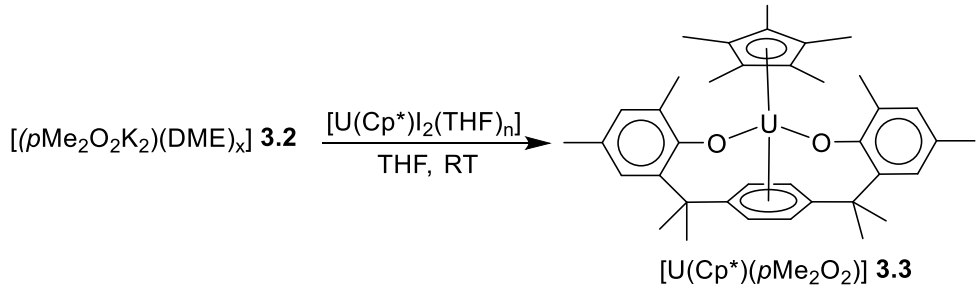

Scheme 3.3 Synthesis of **3.3**.

Complex **3.3** is soluble in hydrocarbons and ethers, and single crystals suitable for X-ray crystallography were obtained by recrystallization from pentane at -50 °C. The asymmetric unit contains two crystallographically independent molecules of **3.3** (**Figure 3.3**) featuring the bisaryloxide ligand in a syn conformation,[7] allowing both aryloxide oxygens to chelate to the U centre with an average U–O distance of 2.179 Å, which is within the range observed for other U(III) aryloxides (2.155-2.338 Å).[9] The Cp* ring assumes the usual η^5-binding mode (average Ct(Cp*)–U = 2.487 Å), while the central arene ring is planar (maximum deviation from C6 plane 0.038 Å) and is bound to the U centre *via* an η^6-arene interaction with an average U–C(arene) distance of 2.774 Å. This is similar to the U–C(arene) distance in the mesityl-anchored chelating U(III) complex [((^{tBu2}ArO)$_3$mes)U], (average 2.73 Å)[10] and somewhat shorter than those in other U(III) complexes featuring arene substituents on the ortho position of the aryloxide (*e.g.*, (2,6-Ph_2-4-Me-C_6H_3-O)$_3$U, 2.853 Å; (2,6-Ph_2-4-Me-C_6H_3-O)$_3$U(THF), 2.964 Å)[11] and discrete arenes (*e.g.*, (C_6Me_6)U($AlCl_4$)$_3$, 2.93 Å;[12] (C_6Me_6)U(BH_4)$_3$, 2.93 Å).[13] The central arene C–C distances in **3.3** (average 1.411 Å) are slightly longer than those observed in **3.1** (average 1.393 Å). Interestingly, the metal centre bears no coordinated Lewis base (*i.e.*, THF), unlike, for example, the mixed-sandwich complexes [U(η^8-C^8H^6{$SiMe_3$-1,4}$_2$)(η^5-C_5Me_4R)(THF)] (R = Me, Et, iPr, tBu).[14]

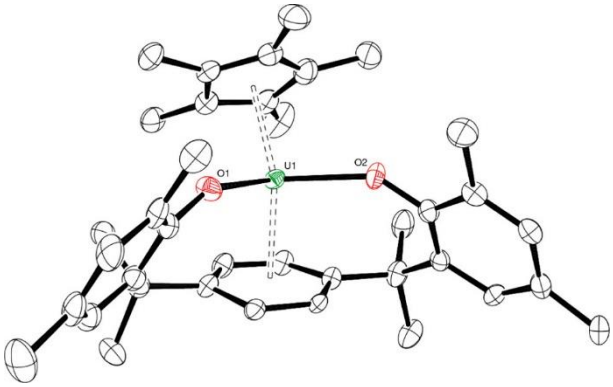

Figure 3.3 ORTEP diagram for the molecular structure of compound **3.3**. One crystallographically independent molecule is shown with 50% probability thermal ellipsoids, and H atoms are omitted for clarity. Selected structural parameters (Å, deg): average U–O = 2.179, average U–C(arene) = 2.774, average Ct(arene)–U = 2.388, average Ct(Cp*)–U = 2.487, average O1–U–O2 = 117.9.

The ^{1}H NMR spectrum of paramagnetic **3.3** contains resonances over the range 18.3 to -13.5 ppm (C_6D_6). Both the CH_3 groups of the bridging arms and the central arene protons appear as two distinct sets of resonances due to the reduced symmetry imposed by a rigid aryloxide and Cp* coordination environment.

3.4 Carbon Dioxide Activation

The reductive activation of $^{13}CO_2$ by **3.3** was investigated in solution (**Scheme 3.4**). An excess (*ca* 2 equiv) of $^{13}CO_2$ was added to a solution of **3.3** in $C_6D_5CD_3$ at -78 °C using a Töepler pump. When the sample was warmed to ambient temperature, the colour changed from black to orange, and the ^{1}H NMR spectrum showed the presence of two products (**3.4** and **3.5**). In addition to excess $^{13}CO_2$ and free ^{13}CO (arising from the reductive disproportionation of $^{13}CO_2$ to form the carbonate complex **3.4**), three paramagnetically shifted resonances were observed in the $^{13}C\{^{1}H\}$ NMR spectrum of the reaction mixture. A singlet at -101 ppm was assigned to the bridging $^{13}CO_3$ in **3.4**, and two mutually coupled doublets appeared at -130 and -199 ppm; all three resonances remained unchanged in the ^{1}H-coupled spectrum. The observed coupling in the latter is consistent with coupling between two proximal, inequivalent ^{13}C atoms (J_{CC} = 70 Hz), thus pointing towards the formation of an oxalate complex resulting from the reductive coupling of $^{13}CO_2$.

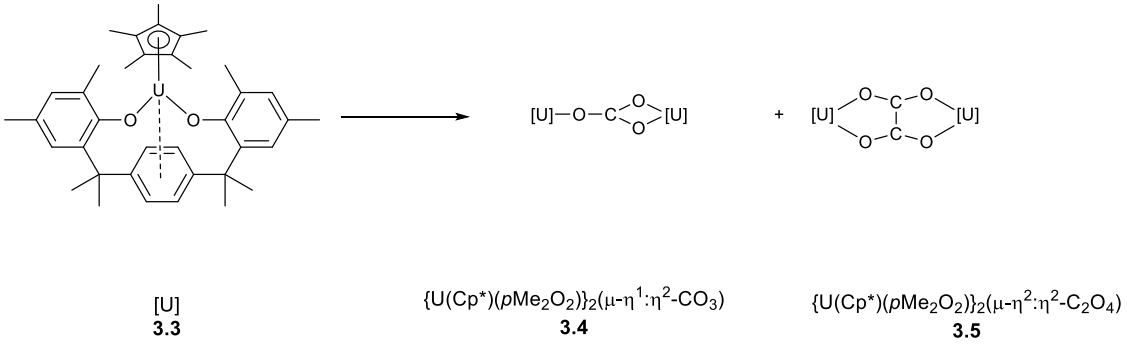

Scheme 3.4 Synthesis of **3.4** and **3.5** from **3.3** and CO_2.

The bridging carbonate complex{U(Cp*)(pMe$_2$O$_2$)}$_2$(μ-η^1:η^2-CO$_3$) **3.4** was identified by X-ray diffraction studies which were carried out by Dr Alistair Frey.[15] The solid-state molecular structure of **3.4** is shown in **Figure 3.4** and reveals a dinuclear structure with a μ-η^1:η^2-bound carbonate bridging two uranium centers. The central CO_3 unit is disordered in the crystal, resulting in superposition of two η^1:η^2 bound carboxylate units with 50:50 occupancy. The resulting model required isotropic refinement for the central carbonate (which has a regular planar triangular structure), and as a result the bond lengths and angles within the central carbonate unit cannot be determined accurately. The η^1-U–O distance (2.162(11) Å) is shorter than the η^2-U–O distances (average 2.448 Å), a feature which was also observed in the mixed-sandwich U(IV) carbonate complex {U(η^8-C$_8$H$_6${Si^{i}Pr$_3$-1,4}$_2$)(η^5-C$_5$Me$_4$H)}$_2$(μ-η^1:η^2-CO$_3$) (η^1, 2.227(12) Å; η^2, average 2.422(10) Å).[16] Each U centre is chelated by a pair of bisaryloxide oxygens (average U–O = 2.175 Å), with the central U–arene interaction (average U–C(arene) = 3.124 Å) significantly weaker than that observed in **3.3**, possibly due to the larger number of O donors and greater steric congestion in **3.4**. This weak U–arene interaction is consistent with a pair of U(IV) centres each binding to a neutral, unreduced central arene. The complex is twisted around the central carbonate unit to minimize steric interaction between opposite bisaryloxides (torsion angle as measured between opposite arene centroids Ct1(arene) – U1–U2–Ct2(arene) = 67.95°).

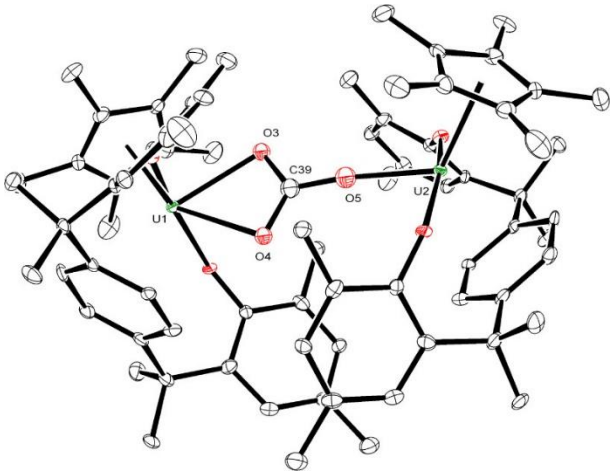

Figure 3.4 ORTEP diagram for molecular structure of compound **3.4**, with 50% probability thermal ellipsoids shown. Solvent masking was employed to remove a highly disordered C_6H_6 from the refinement. Selected structural parameters (Å, deg): average U–O(aryloxide) = 2.175, η^1-U2–O5 2.162(11), average η^2-U–O = 2.448, average U–C(arene) = 3.124, Ct(arene) – U = 2.7902(3), Ct(Cp*)–U = 2.4958(3), O1–U1–O2 = 161.6(3).

The torsion observed in the solid-state structure of **3.4** persists in solution. At 0 °C the ^{1}H NMR spectrum of **3.4** ($C_6D_5CD_3$) consists of eight CH resonances, eight CH_3 resonances, and one resonance for the two freely rotating Cp* ligands paramagnetically shifted between 33.0 and -67.1 ppm. Above 10 °C the aryloxide resonances exhibited varying degrees of coalescence in addition to the changes in chemical shift expected for a paramagnet, but there was no resolution to a discrete, higher symmetry species even at 100 °C.

Fractional crystallization from benzene and then diethyl ether produced yellow crystals of the bridging oxalate complex **3.5** suitable for single-crystal X-ray diffraction. The molecular structure is shown in **Figure 3.5** and shows a η^2:η^2 bridging oxalate unit in which the two carbons are inequivalent (the two Cp* ligands are effectively cis to one another) and hence consistent with ^{13}C{^{1}H} NMR data. Of note is the O1–C1–C2–O2 torsion angle of 22.2(12)°, which is not seen in the molecular structures of [{U(η^8-C_8H_6{$SiMe_3$-1,4}$_2$)(η^5-$C_5Me_4{}^i$Pr)}$_2$(μ-η^2:η^2-C_2O_4)][14] and [((^{nP,Me}ArO)$_3$tacn)U]U}$_2$(μ-η^2:η^2-C_2O_4),[17] possibly due to the steric hindrance around the uranium centre. The U–O(oxalate) and oxalate C–C and C–O bonds are, however, consistent with those found in the latter U(IV) oxalate complexes. The average arene centroid to uranium distance of 2.828 Å in **3.5** is again indicative of a weak interaction between the uranium centre and the central arene ring.

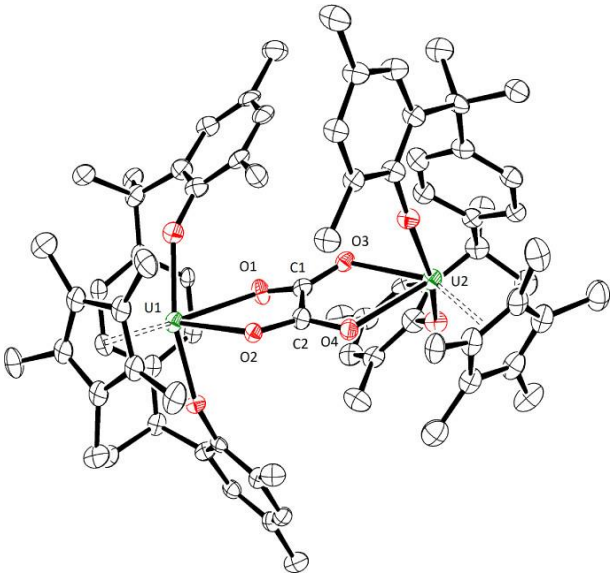

Figure 3.5 ORTEP diagram for molecular structure of compound **3.5**, with 50% probability thermal ellipsoids shown. Selected structural parameters (Å, deg): C1–C2 = 1.531(12), O1–C1–C2–O2 torsion angle = −22.2(12), average U–O(aryloxide) = 2.147, average Ct(Cp*)–U = 2.5030, average Ct(arene)–U = 2.828, average O–U–O (aryloxide) = 160.6, Ct(Cp*)–U–Ct(arene) = 120.184(14).

To gain further insight into the distribution of products (**3.4** and **3.5)** formed from **3.3** and $^{13}CO_2$, the reaction was repeated but the reaction mixture was allowed to stir at -78 °C for 2 days followed by slow warming to room temperature over 1 day. This furnished a mixture of **3.4** and **3.5** in a ratio of 30:70, as judged by the relative integration of the Cp* resonances in the ^{1}H NMR spectrum of the crude reaction mixture. When addition of $^{13}CO_2$ to **3.3** at -78 °C was followed by rapid equilibration to room temperature, the ratio of **3.4** to **3.5** was found to be 83:17. The above observations suggest that the formation of **3.4** competes with the formation of **3.5** and the two pathways can be manipulated.

3.5 Electrochemistry

To investigate the redox behaviour of the bis(aryloxide)/Cp* complexes and enable comparison with similar U(III) and U(IV) systems, voltammetric data for **3.3-3.5** were obtained in [$^{n}Bu_4N$][$B(C_6F_5)_4$]/THF.[18] Cyclic voltammetry was also carried out on the U(IV) derivative , UCp*(pMe_2O_2)I **3.6** by Dr Alexander Kilpatrick to gain insight into the nature of the processes seen in **3.3**.[7,19] UCp*(pMe_2O_2)I **3.6** was synthesised by Dr Alistair Frey. Tabulated electrochemical data can be found in the experimental section. The cyclic voltammogram of **3.3** is quite complex and displays

several processes, as shown in **Figure 3.6**. Four quasi-reversible processes were observed at -2.56, -2.18, -1.71, and +0.13 V *vs* $FeCp_2^{+/0}$. In addition, the CV of **3.3** shows a minor oxidation feature at *ca* -1 V *vs* $FeCp_2^{+/0}$.

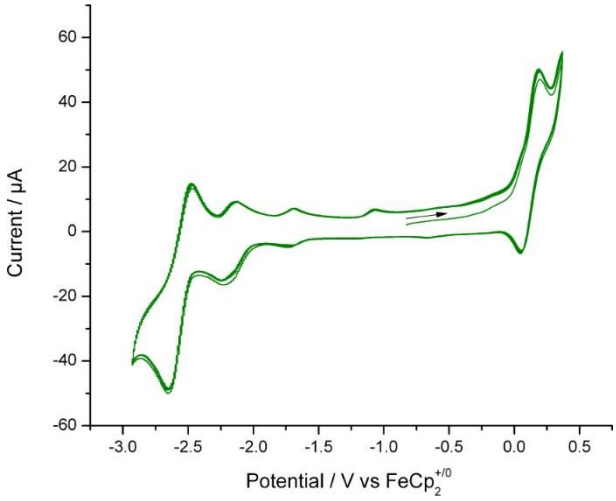

Figure 3.6 Overlaid CV scans (10 cycles) for **3.3** in THF/0.05 M [^{n}Bu$_4$N][B(C$_6$F$_5$)$_4$] (scan rate 100 mV s^{-1}).

Complex **3.6** shows an irreversible reduction wave at -2.19 V *vs* $FeCp_2^{+/0}$ (**Figure 3.7**), which is in excellent agreement with the quasi-reversible process at -2.18 V *vs* $FeCp_2^{+/0}$ seen in **3.3** and is assigned to the U^{IV}/U^{III} couple in this system. This value is similar to other U^{IV}/U^{III} redox couples found in other U(III) systems studied by us and others and is consistent with a strongly reducing metal centre.[14,20,21] Further supporting this assignment is the observation of a single quasi-reversible reduction process at -2.19 V *vs* $FeCp_2^{+/0}$ in the dinuclear U(IV) complex **3.4** (**Figure 3.8**).

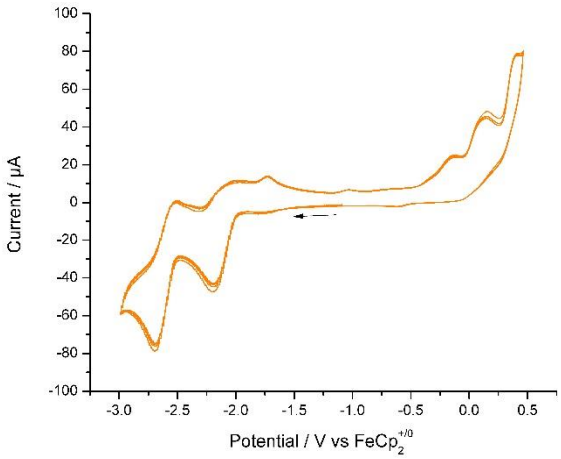

Figure 3.7 Overlaid CV scans (10 cycles) for **3.6** in 0.05 M [^{n}NBu$_4$][B(C$_6$F$_5$)$_4$] / THF, scan rate 100 mV s^{-1}.

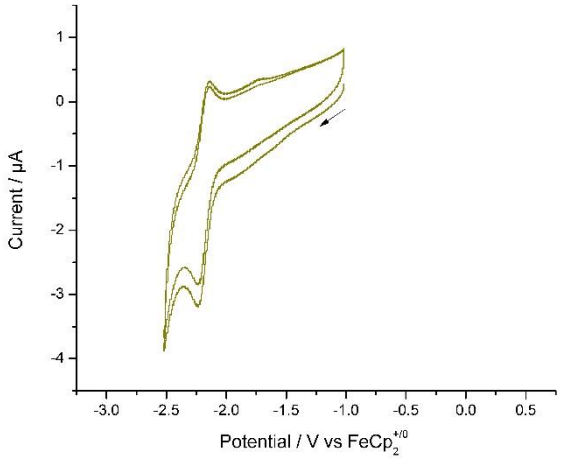

Figure 3.8 Overlaid CV scans (2 cycles) for **3.4** in THF / 0.05 M [^{n}NBu$_4$][B(C$_6$F$_5$)$_4$], scan rate 100 mV s^{-1}.

Upon scanning to more negative potentials, **3.3** and **3.6** showed a quasi-reversible process observed at -2.56 and -2.59 V *vs* FeCp$_2^{+/0}$ respectively. This process lies at an extremely negative potential and may be attributable to a ligand-based reduction; however, the free ligand **3.2** did not show a cathodic process within this potential region (**Figure 3.9**). Another possibility is a U^{III}/U^{II} reduction process, and Meyer and co-workers have recently reported a trivalent uranium monoarene complex derived from the chelating tris(aryloxide)arene ligand [((^{Ad,Me}ArO)$_3$mes)U], which shows a nearly reversible and chemically accessible reduction at -2.495 V *vs* FeCp$_2^{+/0}$.[5]

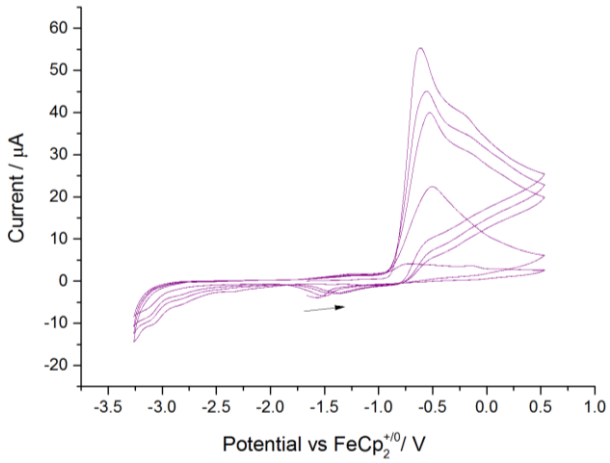

Figure 3.9 Overlaid CV scans (5 cycles) for **3.2** in THF / 0.05 M [^{n}NBu$_4$][B(C$_6$F$_5$)$_4$], scan rate 100 mV s^{-1}. Voltammetric data was collected by Dr Alexander Kilpatrick.

When **3.4** was studied in 0.1 M [^{n}Bu$_4$N][PF$_6$]/THF, the first U^{IV} to U^{III} reduction event occurred at -2.25 V *vs* FeCp$_2^{+/0}$ (**Figure 3.10**). For comparison reduction processes in the carbonate-bridged complexes

based on the [U(η^8-C^8H^6{SiMe^3-1,4}$_2$)(η^5-C_5Me_4R)] (R = Et, iPr, tBu) mixed-sandwich ligand system were observed between -2.11 and -2.17 V *vs* $FeCp_2^{+/0}$ in 0.1 M [^{n}Bu$_4$N][PF_6]/THF.[14]

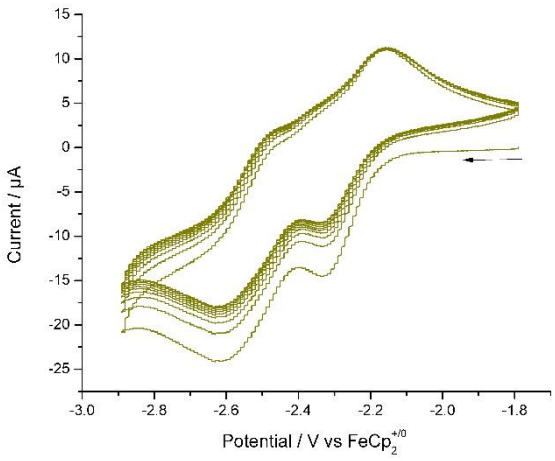

Figure 3.10 Overlaid CV scans (2 cycles) for **3.4** in THF / 0.1 M [^{n}NBu$_4$][PF_6], scan rate 100 mV s^{-1}.

The electrochemistry of **3.5** was studied in 0.05 M [^{n}Bu$_4$N][$B(C_6F_5)_4$]/THF and showed two quasi-reversible events at -2.24 and -2.56 V *vs* $FeCp_2^{+/0}$ (**Figure 3.11**). These processes are assigned to the $[U^{IV}–U^{IV}]/[U^{IV}–U^{III}]^-$ and $[U^{IV}–U^{III}]–/[U^{III}–U^{III}]^{2-}$ couples on the basis of reasonable agreement with corresponding processes observed in **3.3**, **3.4**, and **3.6** and in [U(η^8-C_8H_6{SiMe$_3$-1,4}$_2$)(η^5-$C_5Me_4{}^iPr$)]$_2$(μ-η^2:η^2-C_2O_4).[14] Peak current ratios (i_{pc}/i_{pa}) for these processes of 1.32 and 1.72, respectively, indicate that the species generated on the cathodic scan are not completely oxidized back on the return anodic scan. The $\Delta E_{1/2}^{I\text{-}II}$ value of 320 mV is indicative that a mixed-valance state is stable on the electrochemical timescale. Two minor anodic processes were observed at -520 and -1007 mV, which not assigned with any certainty.

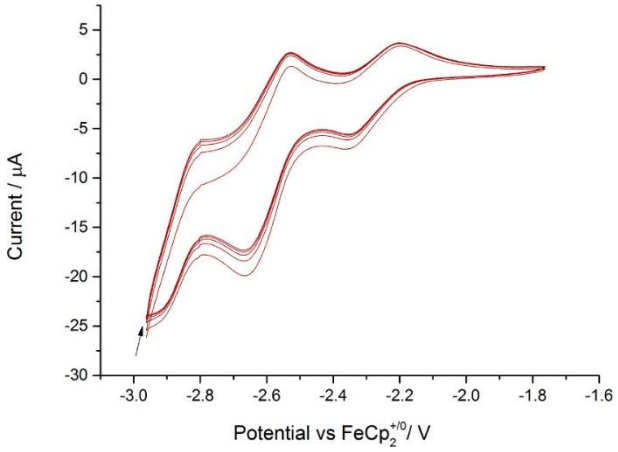

Figure 3.11 Overlaid CV scans (5 cycles) for 5 in THF/0.05 M [^{n}Bu4N][B(C6F5)4] (scan rate 100 mV s^{-1}).

3.3 Conclusions

The combination of the soft pentamethylcyclopentadienyl ligand and a hard, chelating aryloxide ligand affords the U(III) complex [U(Cp*)(*p*Me_2O_2)] **3.3**, whose U^{IV}/U^{III} redox couple is essentially identical with that of the mixed-sandwich complexes of the type U(η^8-C_8H_6{SiR_3-1,4}$_2$)(η-C_5Me_4R') (where R = Me or ^{i}Pr and R' = H, Me, Et, ^{i}Pr and ^{t}Bu).[14] The work presented here demonstrates that the new ligand (*p*Me_2O_2)$^{2-}$ in [U(Cp*)(*p*Me_2O_2)] can significantly alter the reactivity toward CO_2. The new bidentate ligand presented can be synthesized cleanly, in moderate yield and provides an alternative system to the COT- and pentalene-based mixed sandwiches already established in actinide chemistry. Using this ligand, a U(III) complex has been used to reductively disproportionate and reductively couple CO_2 to give the uranium carbonate and oxalate complexes (**3.4** and **3.5**), respectively. Studies have shown that the reactivity toward CO_2 can be controlled via temperature with the formation of **3.4** favoured at higher temperatures while **3.5** is favoured at lower temperatures. Electrochemical studies have shown that **3.3** has a U^{IV}/U^{III} redox couple of -2.18 V *vs* $FeCp_2^{+/0}$, indicating that this ligand supports a highly reducing metal centre and can thus promote reductive chemistry. Aspects of this reactivity towards other substrates other than CO_2 are addressed in the next chapter.

3.4 Experimental Details for Chapter Three

Synthesis of *p*$Me_2O_2H_2$ 3.1

α,α,α',α'-tetramethyl-1,4-benzenedimethanol (10 g, 50 mmol) was added over 4 h to a stirred solution of 2,4-dimethylphenol (45 g) containing *p*-tolylsulfonic acid (0.30g, 1.5 mmol, 3 mol%) at 150 °C. Na_2CO_3 (0.60 g, 5 mmol) was added to neutralise the catalyst and the mixture stirred for another 40 min. Excess 2,4-dimethylphenol was distilled off under vacuum and the solid, beige coloured reside stirred in Et_2O (100 mL) overnight. The solid was washed with Et_2O (3 x 10 mL), cold toluene (10 mL) and 40-60 petroleum ether (10 mL). The white solid was extracted with hot toluene (100 mL), filtered hot and stored at -45 °C to yield **3.1** as a white powder (11.8 g, 47%).

^{1}H NMR (399.5 MHz, d_1-chloroform, 303 K): δ_H 7.36 (s, 4H, Ar-H), 7.18 (s, 2H, Ar-H), 6.95 (s, 2H, Ar-H), 4.28 (s, 2H, OH), 2.39 (s, 6H, CH_3), 2.18 (s, 6H, CH_3), 1.73 (s, 12H, $C(CH_3)_2$).

^{13}C{^{1}H} NMR (100.5 MHz, d_1-chloroform, 303 K): δ_C 149.9 (Ar-C), 147.3 (Ar-C), 134.6 (Ar-C), 130.4 (Ar-C-H), 129.1 (Ar-C), 127.1 (Ar-CH), 126.2 (Ar-C), 124.9 (Ar-CH), 41.7 ($\underline{C}(CH)_3$), 30.0 ($C(\underline{C}H)_3$), 21.2 (Ar-CH_3), 16.4 ppm (Ar-CH_3).

Analysis calculated (found) for $C_{28}H_{34}O_2$: % C 83.54 (83.26), H, 8.51 (8.49).

MS (EI): *m*/*z* 953 (M^+).

Synthesis of *p*$Me_2O_2K_2(DME)_x$ 3.2

A solution of **3.1** (2.66 g, 6.62 mmol) in DME (40 mL) was added dropwise over 1 h to a stirred suspension of KH (0.533 g, 13.3 mmol) in DME (60 mL). After 18 h the reaction mixture was cooled to -30 °C for 1.5 h, filtered through a P3 frit, and the solids thus obtained dried in vacuo for 2.5 h to give the product as a white powder (3.95 g, 95%).

^{1}H NMR (399.5 MHz, d_5-pyridine, 303 K): δ_H 7.43 (s, 4H, Ar-H), 7.42 (s, 2H, Ar-H), 7.11 (s, 2H, Ar-H), 3.51 (s, 6.7H, DME CH, 6.6H, DME CH_2), 3.29 (s, 9.9H, DME CH_3), 2.54 (s, 6H, Ar-CH3), 2.33 (s, 6H, Ar-CH_3) 1.90 (s, 12H, $C(CH_3)_2$).

Unable to obtain ^{13}C NMR spectrum due to low solubility.

Analysis calculated (found) for $C_{28}H_{32}O_2K_2.1.65(C_4H_{10}O_2)$: % C 66.2 (69.2), H, 7.79 (8.19).

Synthesis of *p*$Me_2O_2K_2(Et_2O)_{0.05}$ 3.2a

An alternative preparation of **3.2** was developed to avoid filtration due to the difficulty in filtering the thick suspension that **3.2** forms in DME. Et_2O was used in place of DME due to its lower boiling point, meaning the removal of solvent is easier.

A solution of **3.1** (2.66 g, 6.62 mmol) in Et_2O (40 mL) was added dropwise over 1 h to a stirred suspension of KH (0.533 g, 13.3 mmol) in Et_2O (60 mL). After 18 h the reaction mixture was pumped to dryness *in vacuo* at 60 °C overnight.

^1H NMR (399.5 MHz, d_5-pyridine, 303 K): δ_H 7.43 (s, 4H, Ar-H), 7.42 (s, 2H, Ar-H), 7.11 (s, 2H, Ar-H), 3.37 (q, 0.24H, Et_2O CH_2), 2.54 (s, 6H, Ar-CH3), 2.33 (s, 6H, Ar-CH_3) 1.90 (s, 12H, $C(CH_3)_2$), 1.15 (t, 0.26H, Et_2O CH_3).

Unable to obtain ^{13}C NMR spectrum due to low solubility.

UCp*(*p*Me_2O_2) 3.3

[$UCp^*I_2(THF)_n$] was prepared by adding THF (30 mL) to KCp* (0.696 g, 4.00 mmol) and UI_3 (2.474 g, 4.00 mmol) with overnight stirring followed by filtration with toluene. To a -45°C THF solution (20 mL) of [$UCp^*I_2(THF)_n$] was added *p*$Me_2O_2K_2(DME)_{4.7}$ (3.07 g, 3.40 mmol) in THF (60 mL) over 2 h. The brown reaction mixture was left to warm to room temperature and stir overnight. The reaction mixture was stripped to dryness, extracted in pentane (150 mL), filtered through Celite® on a P4 frit and reduced to 100 mL. Slow cooling to -50 °C gave **3.3** as ink black crystals which were rinsed with cold pentane (3 x 5 mL) and dried *in vacuo* (1.55 g, 59%).

^1H NMR (399.5 MHz, d_6-benzene ,303 K): δ_H 18.54 (s, 2H, Ar-H), 10.13 (s, 2H, Ar-H), 9.07 (s, 2H, Ar-H), 4.53 (s, 6H, CH_3), 4.18 (s, 6H, CH_3), 0.86 (s, 6H, CH_3), -2.28 (s, 6H, CH_3), -3.92 (s, 15H, Cp*), -13.64 (s, 2H, Ar-H).

Synthesis of [{ UCp*(*p*Me$_2$O$_2$)}$_2$CO$_3$] 3.4 and [{ UCp*(*p*Me$_2$O$_2$)}$_2$C$_2$O$_4$] 3.5

A 50 mL J. Young ampoule was charged with UCp*pMe$_2$O$_2$ (300 mg, 0.385 mmol) and toluene (3 mL). The solution was cooled to -78 °C and degassed, and 4 equiv of CO_2 gas was added. A colour change from black to orange was observed shortly after the addition of CO_2. The reaction was stirred at -78 °C for 2 days and then at room temperature for 1 day. Volatiles were removed *in vacuo,* benzene (5 mL) was added and the suspension was heated at almost reflux and slowly cooled to ambient temperature overnight to afford **3.4** as a microcrystalline red solid. The latter was collected by filtration, and washed with benzene (3 x 3 mL), and the washings combined with the original filtrate. This solution was then concentrated to *ca* 3 mL and allowed to stand at room temperature overnight, depositing a further, small amount of [{UCp*(pMe$_2$O$_2$)}$_2$CO$_3$] which was filtered off. Finally, the filtrate from this second crystallisation was pumped to dryness, dissolved in Et_2O (3 mL), and stored at -35 °C to give small yellow crystals of **3.5** (32 mg, 10%).

3.4

^{1}H NMR (399.5 MHz, d_8-toluene, 273 K): δ_H 32.89 (s, 6 H, CH_3), 29.69 (s, 6H, CH_3), 28.81 (s, 6H, CH_3), 27.22 (s, 2H, CH), 19.01 (s, 2H, CH), 17.57 (s, 2H, CH), 14.81 (s, 6H, CH_3), 13.76 (s, 2H, CH), 10.64 (s, 6H, CH_3), 5.22 (s, 6H, CH_3), 0.15 (s, 6H, CH_3), −3.94 (s, 6H, CH_3), −10.65 (s, 30H, Cp*), −51.26 (s, 2H, CH), −61.22 (s, 2H, CH), −63.30 (s, 2H, CH), −67.11 (s, 2H, CH).

3.5

^{1}H NMR (399.5 MHz, d_6-benzene, 303 K): δ_H 39.34 (s, 12 H, CH_3), 31.67 (s, 4 H, Ar-H), 25.45 (s, 4 H, Ar-H), 22.68 (s, 12 H, CH_3), 14.82 (s, 12 H, CH_3), −3.77 (s, 12 H, CH_3), −7.62 (s, 30 H, Cp*), −53.91 (s, 4 H, Ar-H), −62.33 (s, 4 H, Ar-H).

Analysis calculated (found) for $C_{78}H_{94}O_8U_2$: % C 57.28 (57.00), H, 5.79 (6.02).

Cyclic Voltammetry Data

Table S4. Electrochemical parameters for **3.3** in 0.05 M [^{n}NBu$_4$][B(C$_6$F$_5$)$_4$] / THF.

	Process I	**Process II**	**Process III**	**Process IV**	**Process V**
E_{pa} / V vs $FeCp_2^{+/0}$	-2.466	-2.134	-1.686	-1.069	_
E_{pc} / V vs $FeCp_2^{+/0}$	-2.654	-2.242	-1.731	_	-0.652
$E_{1/2}$ / V vs $FeCp_2^{+/0}$	-2.560	-2.188	-1.709	_	_
ΔE_{pp} / mV	188	108	45	_	_
i_{pa} / µA	33.33	4.65	2.17	2.67	_
i_{pc} / µA	36.32	11.54	2.7	_	-2.10
i_{pa}/i_{pc}	1.09	2.48	1.24	_	_

$\Delta E_{pp} = | E_{pc} - E_{pa} |$

Table S5. Electrochemical parameters for **3.4** in 0.05 M [^{n}NBu$_4$][B(C$_6$F$_5$)$_4$] / THF.

	Process I
E_{pa} / V vs $FeCp_2^{+/0}$	-2.139
E_{pc} / V vs $FeCp_2^{+/0}$	-2.237
$E_{1/2}$ / V vs $FeCp_2^{+/0}$	-2.188
ΔE_{pp} / mV	98
i_{pa} / µA	1.70
i_{pc} / µA	2.13
i_{pa}/i_{pc}	1.33

$\Delta E_{pp} = | E_{pc} - E_{pa} |$

Table S6. Electrochemical parameters for **3.4** in 0.1 M [^{n}NBu$_4$][PF$_6$] / THF.

	Process I	**Process II**
E_{pa} / V vs $FeCp_2^{+/0}$	-2.447	-2.105
E_{pc} / V vs $FeCp_2^{+/0}$	-2.637	-2.384
$E_{1/2}$ / V vs $FeCp_2^{+/0}$	-2.542	-2.245
ΔE_{pp} / mV	190	279
i_{pa} / µA	19.07	13.03
i_{pc} / µA	19.08	17.96
i_{pa}/i_{pc}	1.00	1.38

$\Delta E_{pp} = | E_{pc} - E_{pa} |$

Table S7. Electrochemical parameters for **3.5** in 0.05 M $[^nNBu_4][(B(C_6F_5)_4]$ / THF.

	Process I	**Process II**	**Process III**	**Process IV**
E_{pa} / V vs $FeCp_2^{+/0}$	-2.493	-2.166	-0.520	-1.007
E_{pc} / V vs $FeCp_2^{+/0}$	-2.634	-2.322	–	–
$E_{1/2}$ / V vs $FeCp_2^{+/0}$	-2.564	-2.244	–	–
ΔE_{pp} / mV	141	156	–	–
i_{pa} / µA	9.56	3.21	1.07	3.34
i_{pc} / µA	12.66	5.53	–	–
i_{pa}/i_{pc}	1.32	1.72	–	–

$\Delta E_{pp} = | E_{pc} - E_{pa} |$

Table S8. Electrochemical parameters for **3.6** in 0.05 M $[^nNBu_4][B(C_6F_5)_4]$ / THF.

	Process I	**Process II**	**Process III**	**Process IV**	**Process V**	**Process VI**	**Process VII**	**Process VIII**
E_{pa} / V vs $FeCp_2^{+/0}$	-2.490	–	-1.725	-1.024	–	-0.122	0.150	0.409
E_{pc} / V vs $FeCp_2^{+/0}$	-2.692	-2.189	-1.777	–	-0.621	–	–	–
$E_{1/2}$ / V vs $FeCp_2^{+/0}$	-2.591	–	-1.751	–	–	–	–	–
ΔE_{pp} / mV	202	–	52	–	–	–	–	–
i_{pa} / µA	26.85	–	3.61	1.53	–	16.93	22.0	35.04
i_{pc} / µA	47.18	39.8	3.33	–	1.67	–	–	–
i_{pa}/i_{pc}	1.76	–	0.92	–	–	–	–	–

$\Delta E_{pp} = | E_{pc} - E_{pa} |$

Scans towards the positive region of the potential window of complex **3.6** revealed a series of irreversible oxidation waves at -0.12, 0.15, and 0.42 V vs $FeCp_2^{+/0}$ which may be attributed to loss of electrons from the coordinated phenoxide groups the central arene ring in the (bp) ligand, or possibly the U^{IV}/U^{V} couple. Survey scans of **3.3** to more positive potentials showed a single process at +11 V vs $FeCp_2^{+/0}$ showed electrochemically reversible behavior ($i_{pa}/i_{pc} \approx 1$)

3.5 References for Chapter Three

1 M. del Mar Conejo, J. S. Parry, E. Carmona, M. Schultz, J. G. Brennann, S. M. Beshouri, R. A. Andersen, R. D. Rogers, S. Coles and M. B. Hursthouse, *Chem. – Eur. J.*, 1999, **5**, 3000–3009.

2 S. M. Mansell, N. Kaltsoyannis and P. L. Arnold, *J. Am. Chem. Soc.*, 2011, **133**, 9036–9051.

3 J. Higgins, PhD thesis, University of Sussex, 2014.

4 H. S. La Pierre, H. Kameo, D. P. Halter, F. W. Heinemann and K. Meyer, *Angew. Chem. Int. Ed.*, 2014, **53**, 7154–7157.

5 H. S. La Pierre, A. Scheurer, F. W. Heinemann, W. Hieringer and K. Meyer, *Angew. Chem. Int. Ed.*, 2014, **53**, 7158–7162.

6 US3778409 A, 1973.

7 C. J. Inman, A. S. P. Frey, A. F. R. Kilpatrick, F. G. N. Cloke and S. M. Roe, *Organometallics*, 2017, **36**, 4539–4545.

8 H. van Koningsveld, A. J. van den Berg, J. C. Jansen and R. de Goede, *Acta Crystallogr. B*, 1986, **42**, 491–497.

9 I. Castro-Rodriguez, H. Nakai, P. Gantzel, L. N. Zakharov, A. L. Rheingold and K. Meyer, *J. Am. Chem. Soc.*, 2003, **125**, 15734–15735.

10 S. C. Bart, F. W. Heinemann, C. Anthon, C. Hauser and K. Meyer, *Inorg. Chem.*, 2009, **48**, 9419–26.

11 S. M. Franke, B. L. Tran, F. W. Heinemann, W. Hieringer, D. J. Mindiola and K. Meyer, *Inorg. Chem.*, 2013, **52**, 10552–10558.

12 F. A. Cotton and W. Schwotzer, *Organometallics*, 1987, **6**, 1275–1280.

13 D. Baudry, E. Bulot, P. Charpin, M. Ephritikhine, M. Lance, M. Nierlich and J. Vigner, *J. Organomet. Chem.*, 1989, **371**, 155–162.

14 N. Tsoureas, L. Castro, A. F. R. Kilpatrick, F. G. N. Cloke and L. Maron, *Chem. Sci.*, 2014, **5**, 3777–3788.

15 *The structure presented in figure 3.4 was obtained from a benzene solution from the reaction of 3.3 with scCO2 performed by Dr Alistair Frey and published (C. J. Inman, A. S. P. Frey, A. F. R. Kilpatrick, F. G. N. Cloke and S. M. Roe, Organometallics, 2017, 36, 4539–4545) The structure was also obtained from the reaction between 3.3 and CO2 in solution by the author. The data collected revealved exactly the same structureal motif and metric parameters.*

16 O. T. Summerscales, A. S. P. Frey, F. G. N. Cloke and P. B. Hitchcock, *Chem. Commun.*, 2009, 198–200.

17 A.-C. Schmidt, F. W. Heinemann, C. E. Kefalidis, L. Maron, P. W. Roesky and K. Meyer, *Chem. – Eur. J.*, 2014, **20**, 13501–13506.

18 *Dr Alexander Kilpatrick carried out the electrochemical studies on 3.3, 3.4 and UCp*(pMe2O2)I.*

19 *Compound 3.6 was synthesised by Dr Alistair Frey in an attempt to prepare 3.3 using DME as solvent instead of THF using equimolar amounts of 3.2 and [UCp*I2(DME)n], produced in situ from UI3 and KCp* in DME, resulted in the formation of the uranium(IV) iodo complex, 3.6, in 29% yield following work up.*

20 M. J. Monreal, R. J. Wright, D. E. Morris, B. L. Scott, J. T. Golden, P. P. Power and J. L. Kiplinger, *Organometallics*, 2013, **32**, 1423–1434.

21 C. Clappe, D. Leveugle, D. Hauchard and G. Durand, *J. Electroanal. Chem.*, 1998, **448**, 95–103.

4 Chapter Four: Reactivity of UCp*(*p*Me$_2$O$_2$) With Other Small Molecules

4.1 Introduction

As discussed in chapter three, the U(III) complex, UCp*(*p*Me$_2$O$_2$) **3.3**, reductively activates CO_2 to give the bimetallic U(IV) oxalate and carboxylate complexes. Reactivity towards CO_2 is assumed to proceed *via* a [U^{IV}]-CO_2-[U^{IV}] intermediate, though such a species eluded observation or isolation due to its transient nature. To circumvent this, CS_2 was used as a model for CO_2 to gain some insight into the reactivity of **3.3** towards CO_2 as it is known U(III) complexes can form the CS_2 analogue, [U^{IV}]-CS_2-[U^{IV}], as discussed in chapter one.

In the same light, these investigations were expanded to include other substrates – *i.e.* carbon suboxide and azobenzene– to further probe the reactivity of **3.3**.

4.2 Carbon Disulphide

4.2.1 Synthesis and Characterisation of [{UCp*(*p*Me$_2$O$_2$)}$_2${μ-η^2(C,S):η^2(S,S)-CS$_2$}] 4.1

Treatment of a C_6D_6 solution of **3.3** (0.13 M in 0.5 mL) with 1 equivalent of neat CS_2 at room temperature gave a dark brown solution. Subsequent work-up and cooling to -35 °C produced a dark brown solid in 28% crystalline yield (99% spectroscopic yield), which was identified as [{UCp*(*p*Me$_2$O$_2$)}$_2${μ-η^2(C,S):η^2(S,S)-CS$_2$}] **4.1** spectroscopically and analytically (**Scheme 4.1**). During the synthesis of **4.1**, it was found that a second product (**4.2**) was formed. To avoid the formation of this side-product, a high concentration of **3.3** relative to CS_2 was employed. ^{1}H NMR spectroscopy suggests **4.1** contains two uranium environments. The $^{13}CS_2$ analogue, **4.1**^{13C}, was also synthesised, though unfortunately the $^{13}CS_2$ ligand peak was not observed over a 2000 ppm window in the ^{13}C NMR spectrum.

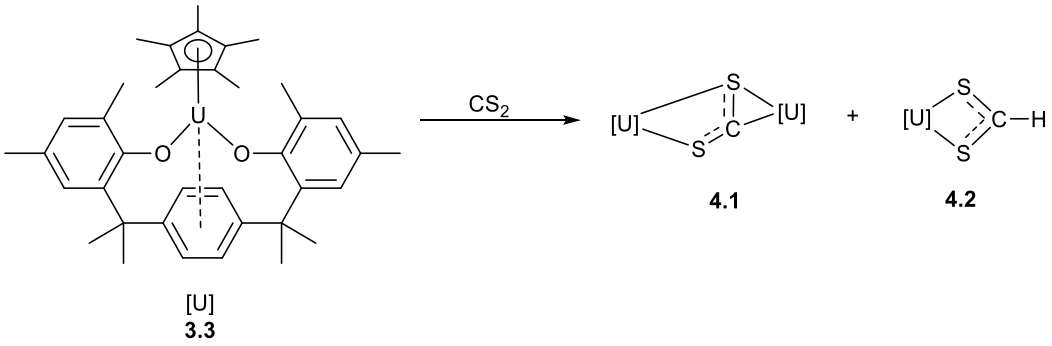

Scheme 4.1 Synthesis of **4.1** and **4.2** from **3.3**.

The bimetallic structure of **4.1** was confirmed by single crystal X-ray diffraction studies and is shown below in **Figure 4.1**, together with selected bond lengths and angles. The central CS_2 core is asymmetric and features C–S bonds (C1–S1 = 1.715(12) and C1–S2 = 1.736(11) Å) substantially lengthened in comparison to free CS_2 (C–S = 1.560(3) Å)[1]. Furthermore, the S1–C1–S2 angle of 116.3(6)° is 63.7 degrees less than free CS_2. These structural data are similar to those reported for other bimetallic U(IV) CS_2^{2-} complexes reported by Andersen *et* al. and Mazzanti *et al.*,[2,3] though there are key structural differences between these complexes and **4.1**. For example, in $[\{U(Cp^{Me})_3\}_2(\mu\text{-}\eta^1(S):\eta^2(C,S')\text{-}CS_2)]$ **4A** and $[\{U(OSi(OtBu)_3)_3\}_2\text{-}\{\mu\text{-}\eta_2(C,S):\eta_2(S,S)\text{-}CS_2\}]$ **4B**, the S–C–S angles are larger (**4A** = 143.8(11) and **4B** = 131.6(8) Å) and there is a greater difference between the two C–S bond distances in these complexes (**4A**: C–S = 1.831(19) and 1.464(19), **4B**: C–S = 1.747(13) and 1.594(11) Å, respectively)[2,3] indicating an unequal distribution of electron density in the CS_2^{2-} ligand. Also, the binding mode of CS_2 in **4.1** is $\mu\text{-}\eta^2(C,S):\eta^2(S,S)\text{-}CS_2$, which is identical to **4B** though slightly different to **4A** which binds in a $\mu\text{-}\eta^1(S):\eta^2(C,S)\text{-}CS_2$ fashion.

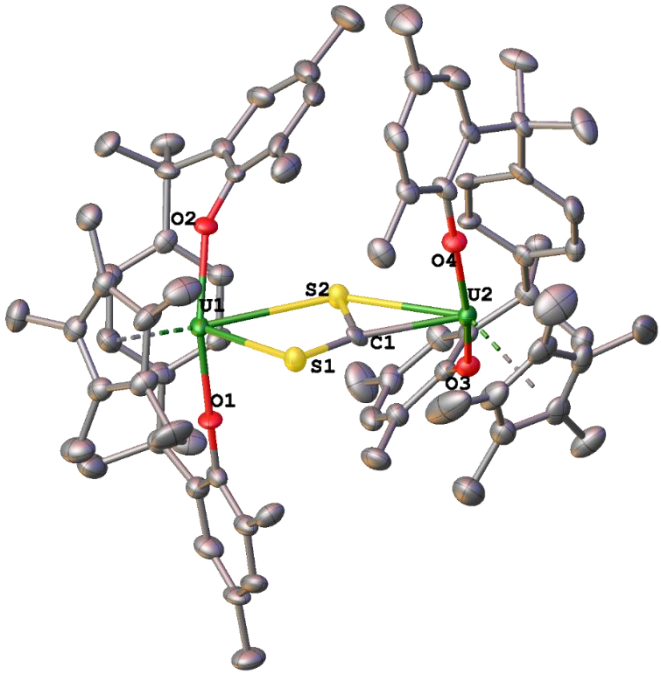

Figure 4.1 Molecular structure of **4.1**. Hydrogen atoms and toluene molecule removed for clarity. Thermal ellipsoids are given at 50% probability. Selected structural parameters (Å, °): C1–S1 = 1.715(12), C1–S1 = 1.737(11), S1–C1–S2 = 116.2(6), U1–S1 = 2.890(3), U1–S2 = 3.0672(17), U2–C1 = 2.409(11), U2–S2 = 2.9935(18), U1–O1 = 2.138(4), U1–O2 = 2.150(4), U2–O3 = 2.166(5), U2–O4 = 2.133(4), U1–Ct(Cp*) = 2.4973(2), U2–Ct(Cp*) = 2.5117(2), U1–Ct(arene) = 2.9647(3), U2–Ct(arene) = 2.8974(2), Ct(Cp*)–U1–Ct(arene) = 118.966(8), Ct(Cp*)–U2–Ct(arene) = 120.729(8), O1–U1–O2 = 158.53(18), O3–U2–O4 = 160.41(18).

The most obvious difference in structural parameters between **3.3** and **4.1** is the increase in the U–Ct(arene) distance from 2.382(6) Å to 2.8974(2) Å in **4.1** which could be due to the increased steric congestion around the uranium centre due to the bridging CS_2 unit and the smaller ionic radii of the formally U(IV) centres in **4.1**. In agreement with this observation, is the increase in the U–Ct(Cp*) distance in **4.1** compared to **3.3**, as well as an increase in the bite angle of the *p*Me_2O_2 ligand (**3.3**: 117.8.3, **4.1**: 158.53(18)°) and a decrease in the [Ct(Cp*)–U–Ct(arene)] angle, (**3.3**: 134.6(2), **4.1**: 118.996(8)°).

The reactivity of **3.3** towards CS_2 is similar to $U(Cp^{Me})_3$ and $U(OSi(OtBu)_3)_3$ in that all of the products of these reactions contain two U(IV) centres and a CS_2^{2-} core. In contrast to this, the U(III) complex, [($(^{Ad,Me}ArO)_3N$)U(DME)] **4C**, displays different reactivity towards CS_2, with its reactivity more similar

to U(III) CO_2 chemistry.[4] As outlined in **Scheme 1.5**, this complex reacts with CS_2 to form the tetrathiooxalate complex [{**4C**}$_2$(μ-η^2(S,S′):η^2(S′′,S′′′)-C_2S_4)] as the major product (80%) along with the trithiocarbonate-bridged complex [{**4C**}$_2$(μ-η^2(S,S′):η^2(S,S″)-CS_3] as the minor product (20%). [{**4C**}$_2$(μ-η^2(S,S′):η^2(S,S″)-CS_3] forms *via* a [{**4C**}$_2$(μ-S)] intermediate with concomitant loss of CS. The observation that the tris-aryloxide scaffold of **4C** can influence reactivity towards CS_2 and result in the loss of CS, given the relative instability of CS compared with CO ($\Delta_f H^0_{298\ K}$ = -110.5 and 276.5 kJ mol^{-1} respectively) is remarkable.[5,6] This is in stark contrast to **4.1**, **4A** and **4B** which do not induce formation of CS upon reaction with CS_2.

Further reactivity towards CS_2 was not observed despite heating a sample of **4.1** with five equivalents of CS_2 at 60 °C for three days. To investigate how the "soft" U–S and U–C bonds react with more nucleophilic substrates, two equivalents of N_2O were added to a solution of **4.1**, in the hope of synthesising a dithiocarbonate complex. Unfortunately, no reaction was observed by ^{1}H NMR spectroscopy.

4.2.2 Synthesis and Characterisation of [{UCp*(*p*Me$_2$O$_2$)}{η^2(S,S')-CS$_2$H] 4.2

The reaction between a solution of **3.3** and a solution of CS_2 with both reactants in more dilute toluene results in the formation of the dithioformate complex, **4.2** (**Scheme 4.1**). The addition of a 0.033 M CS_2 (1 equivalent) toluene solution to a 0.016 M toluene solution of **3.3** at -78 °C gives **4.1** and **4.2** in a ratio of 32:68 (*via* relative integration of Cp* peak in ^{1}H NMR spectrum). The ratio of these products does not show much variation with temperature as shown by carrying out the reaction at 25 °C and 45 °C. ^{1}H NMR spectroscopic data indicated that **4.2** contains a single "UCp*(*p*Me$_2$O$_2$)" environment with sharp signals over a window spanning from 43 ppm to -148 ppm. Upon use of $^{13}CS_2$, a doublet at -304 ppm ($^1J_{CH}$ = 180 Hz) is observed in the ^{13}C NMR spectrum as well as a doublet at -89 ppm ($^1J_{CH}$ = 180 Hz) in the ^{1}H NMR spectrum (**Figure 4.2**, left and right, respectively). When $^{12}CS_2$ is used, a singlet is observed at -89 ppm instead. This coupling constant is similar to the $^1J_{CH}$ value for the carbon adjacent to sulphur in thiophene (185 Hz)[7]. These NMR data provide strong evidence for the formation of a dithioformate moiety (S_2CH) though the proton source is unclear.

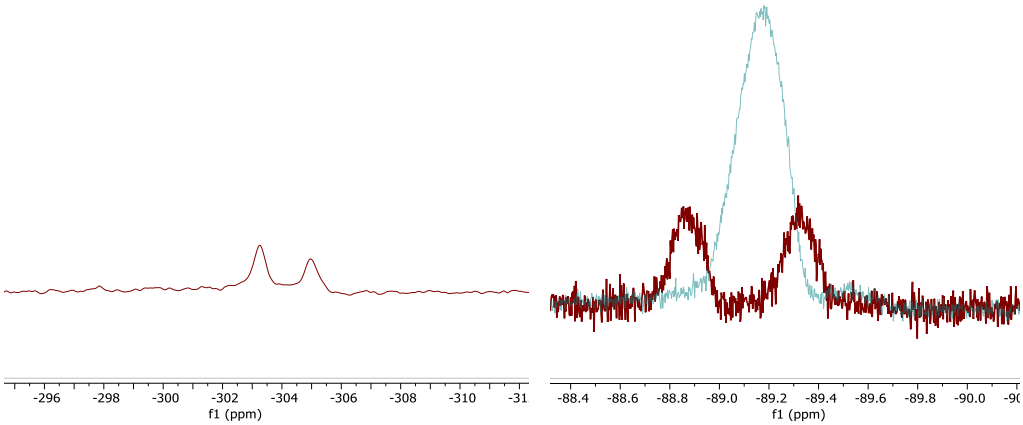

Figure 4.2 ^{13}C NMR spectrum of **4.2^{13C}** (left) and overlaid ^{1}H NMR spectra of the S_2CH peak of **4.2^{13C}** (red, doublet) and **4.2** (green, singlet) (right).

Unfortunately, the synthesis of analytically pure **4.2** proved challenging due to the persistent formation of **4.1** as an undesired side-product, between 5-40% in reactions employing the same conditions, highlighting the capricious nature of this chemistry. The formation of unknown side-products was also observed under these conditions.

The molecular structure of **4.2** is shown below in **Figure 4.3** and is consistent with the crude ^{1}H NMR data suggesting the presence of a species containing the Cp*(*p*Me_2O_2) ligand environment with a dithioformate ligand.

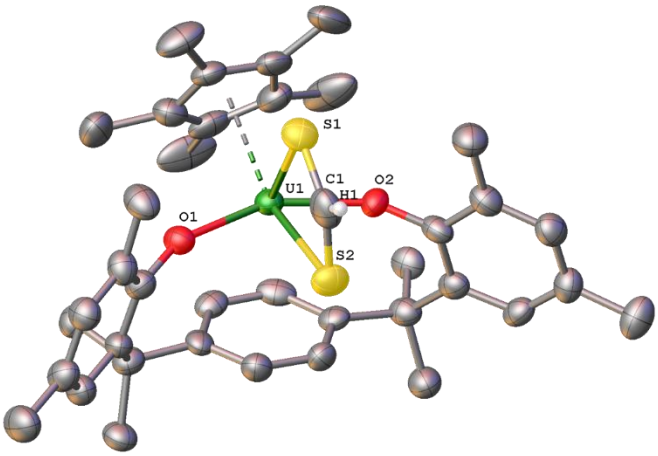

Figure 4.3 Molecular structure of **4.2**. All Hydrogen atoms except one on dithioformate removed for clarity. Thermal ellipsoids are given at 50% probability. Selected structural parameters (Å, °): C1–S1 = 1.666(11), C1–S2 = 1.629(12), S1–C1–S2 = 126.6(7), U1–S1 = 2.870(2), U1–S2 = 2.998(2), U–Ct(Cp*) = 2.5383(2), U1–O1 = 2.145(5), U1–O2 = 2.161(5), U–Ct(arene) = 2.8863(2), Ct(arene) –U–Ct(Cp*) = 121.698(8), O1 –U–O2 = 155.7(2).

The molecular structure of **4.2** reveals the formation of a monometallic CS_2H complex that features an S–C–S angle of 126.6(7)° that is bound to uranium in an η^2(S,S') fashion. The C–S bond lengths (C1–S1 = 1.666(11) Å and C1–S2 = 1.629(12) Å) lie between that of the C–S bond of free CS_2 (1.54(3) Å) and those found in the CS_2 moiety of **4.1**.[8] H1 was not found in the difference map but the metrical parameters of the S_2CH ligand are markedly similar to metal complexes containing a η^2(S,S')-S_2CR unit (where R = H or *p*-tolyl) (cis-[Ir(H)$_2$(η^2-S_2CH)(PCy_3)$_2$]: C–S = 1.657(3) and 1.671(3), S–C–S = 116.01(16)°. [W(η^2-($S_2CC_6H_4$Me-4)}(CO)$_2$(η-C_5H_5)]: C–S = 1.702(9) and 1.689(9) Å, S–C–S = 125.3(7)°)[9,10].

In comparison to **4.1**, the C–S bonds of **4.2** are shorter (C1–S1 = 1.666(11) Å and C1–S2 = 1.629(12) Å) and consistent with a CS_2 unit that has been activated to a lesser extent. The S–C–S angle of **4.2** is 10 degrees larger than **4.1**, further suggesting CS_2 has been activated to a lesser extent. Also, the U–S bonds of both complexes are similar. The U–Ct(Cp*) distance of **4.2** (2.5383(2) Å) is greater than in **4.1** (U1–Ct(Cp*) = 2.4973(2) and U2–Ct(Cp*): 2.5117(2) Å) by 0.041 and 0.0267 Å, respectively.

Complex **4.2** does not react with **3.3** though it is reactive towards CO (see below) and CO_2 albeit more slowly than **4.1** as judged by NMR-scale reactions between CO_2 and solutions containing **4.1** and **4.2**.

4.2.3 Reactivity of [{UCp*(*p*Me$_2$O$_2$)}$_2${μ-η^2(C,S):η^2(S,S)-CS_2] 4.1 Towards CO_2

With complex **4.1** in hand, its reactivity towards CO_2 was investigated. A d_8-toluene solution of **4.1** was reacted with one molar equivalent of $^{13}CO_2$ at -78 °C administered precisely *via* a Toepler pump and then immediately warmed to room temperature. ^{1}H NMR spectroscopic analysis of the crude reaction mixture revealed the consumption of **4.1** along with the formation of two new [Cp*pMe$_2$O$_2$] environments and 0.2 equivalents of the uranium carbonate species **3.4**. The ^{13}C NMR spectrum features a peak at -323 ppm which likely corresponds to the incorporation of ^{13}C into a uranium species. After 24 h, the peaks initially observed in the ^{1}H NMR spectrum had reduced by *ca* 95% and a new set of peaks which precluded assignment had formed. The ^{13}C NMR spectrum after 24 h does not contain any new peaks, although when **4.1^{13C}** is used, a peak at -330 ppm is observed, suggesting that the final

product contains a ^{13}C atom originating from **4.1^{13C}**. Unfortunately, due to time constraints it was not possible to purify samples for elemental analysis and fully assignable ^{1}H NMR spectra.

From the reaction mixture containing the final product, single crystals suitable for X-ray diffraction studies were obtained. The molecular structure of [{UCp*(*p*Me$_2$O$_2$)}$_2${μ-η^2(S,O):η^2(S,O')-CO$_2$S] **4.3** (**Figure 4.4**) contains two tetravalent uranium centres bridged by CO_2S^{2-} in a μ-η^2(S,O):η^2(S,O') fashion. Similar to the CO$_2$S ligand in **4.3** are the metrics of [{**4C**}$_2$(μ-η^1(O):η^2(O',S)-CO$_2$S)] (C–S = 1.742(5), C–O = 1.283(5) and 1.262(5) Å, though unlike **4.3** this complex features a different bonding mode and a planar CO$_2$S unit. As a result of this bonding mode, the U–S bonds are shorter than in complex **4.3** (U–S: 2.892(1) Å). The C–S distance of 1.761(9) Å is similar the monoanionic alkyl thiocarbonate complexes [CpFe(CO)$_2$SCO$_2$Et] and [*fac*-(CO)$_3$(dppe)MnSC(O)OCH$_3$] (C–S = 1.748(3) and 1.729(10) Å, respectively).[11,12] The two C–O bonds (1.284(11) and C1–O2: 1.257(11) Å) are characteristic of double bonds and the bridging CO$_2$S ligand is not flat across the U–U plane as shown in **Figure 4.5**, an indication that there is delocalisation of electron density along O–C–O and not C–S. U–Ct(Cp*), U–Ct(Cp*), U–O(Ar) bond lengths are consistent with other U(IV) complexes reported in this chapter.

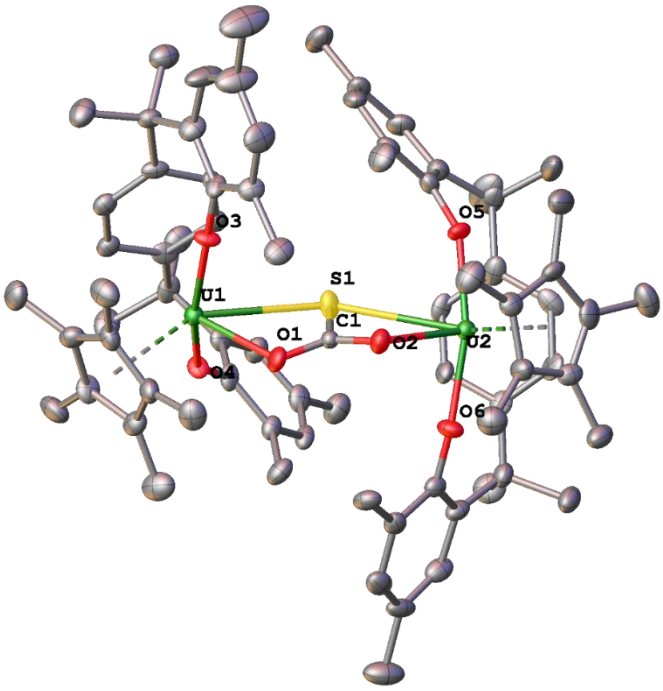

Figure 4.4 Molecular structure of **4.3**. Hydrogen atoms omitted for clarity. Thermal ellipsoids are given at 50% probability. Selected structural parameters (Å, °): C1–S1 = 1.761(9), C1–O1 = 1.284(11), C1–O2 = 1.257(11), U1–O1 = 2.343(7), U1–S1 = 3.031(2), U2–O2 = 2.376(7), U2–S1 = 3.068(2), U1–O3 = 2.128(6), U1–O4 = 2.159(6), U2–O5 = 2.137(6), U2–O6 = 2.151(6), U1–Ct(Cp*) = 2.5269(3), U2–Ct(Cp*) = 2.5118(3), U1–Ct(arene) = 2.9003(3), U2–Ct(arene) = 2.8158(3), Ct(Cp*)–U1–Ct(arene) = 120.959(10), Ct(Cp*)–U2–Ct(arene) = 121.140(11), O3–U1–O4 = 157.2(2), O5–U2–O6 = 160.8(3).

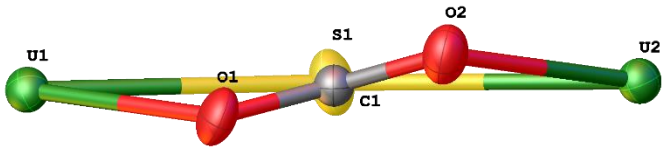

Figure 4.5 View across the U–U plane and CO_2S bridging ligand.

Computational studies by Maron *et al.* provided mechanistic insight into the reactivity of $UCOT^{TMS2}Cp^*$ with CO_2 (**Figure 4.6**).[13] Calculations of this complex revealed two main reaction pathways that led to the formation of a carbonate product. Pathway M1 involves the reductive disproportionation of CO_2 that leads to a μ-oxo-bridged species that then undergoes a CO_2 insertion

reaction to give the carbonate species. The other pathway, M2, features a bimetallic six-membered ring intermediate that loses CO_2 to give the carbonate product.

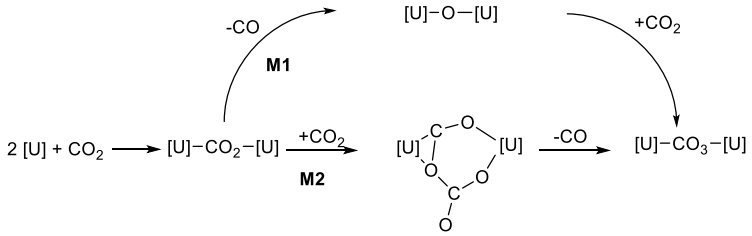

Figure 4.6 Mechanism for the activation of CO_2 to give diuranium carbonate. [U] refers to $UCOT^{TMS2}Cp^*$.

4.2.4 Reactivity of 4.1 Towards CO

It was envisaged that the 'soft' interactions between uranium and the CS_2 ligand in **4.1** would lead to interesting reactivity towards the 'harder' carbon monoxide due to the oxophilicity of uranium. Compound **4.1^{13C}** was prepared *in-situ* as a C_6D_6 solution and then one equivalent of ^{13}CO added with a Toepler pump. Analysis of the ^1H NMR spectrum taken after 24 h shows that >97% of **4.1** has been consumed and new products had formed. ^{13}C NMR spectroscopy shows two major peaks (643 and -244 ppm) and two minor peaks (-139 and -254 ppm). NMR spectroscopic data of the reaction mixture after 3 d exhibited significant changes. The ^1H NMR spectrum displays a reduction of some peaks and increase of others, suggesting the reaction proceeds though an intermediate. In agreement with this, the ^{13}C NMR spectrum shows the decrease of peaks at 643 and -244 ppm and the increase in intensity of peaks at -139 and -245 ppm. Unfortunately, due to time constraints it was not possible to purify samples for elemental analysis and fully assignable ^1H NMR spectra.

Single crystals suitable for X-ray diffraction studies were grown from a saturated benzene solution and the resulting molecular structure of [{UCp*(*p*Me$_2$O$_2$)}$_2${μ-η^2(S,O):η^2(C,S)-OSCCS] **4.4** is shown below in **Figure 4.7**.

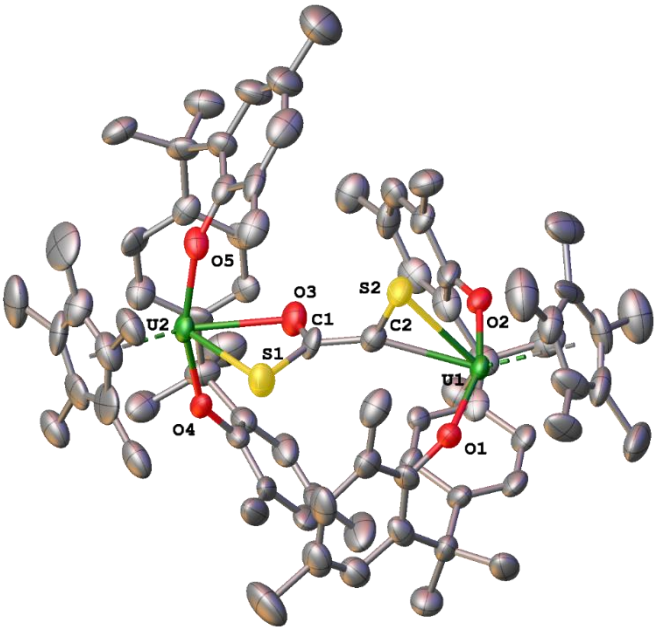

Figure 4.7 Molecular structure of **4.4**. Hydrogens, residual benzene atoms and three disordered Me groups on the Cp* ligands removed for clarity. Thermal ellipsoids are given at 50% probability. Selected structural parameters (Å, °): C1–C2 = 1.45(3), C1–O3 = 1.28(2), C1–S1 = 1.707(14), C2–S2 = 1.635(18), O3–C1–S1 = 120.5(14), C1–C2–S2 = 125.1(13), S2–C2–U1 = 82.2(7), U1–C2 = 2.469(17), U1–S2 = 2.771(5), U2–O3 = 2.469(13), U1–O1 = 2.134(9), U1–O2 = 2.156(11), U2–O4 = 2.160(12), U2–O5 = 2.133(12), U1–Ct(Cp*) = 2.522(10), U2–Ct(Cp*) = 2.519(8), U1–Ct(arene) = 2.748(7), U2–Ct(arene) = 2.839(6).

Complex **4.4** formed as the result of CO insertion into a C–S bond of **4.1**. The bimetallic complex is bridged by a thiocarboxylate-thiocarbene ligand which features a uranium-thienyl interaction perpendicular to the thiocarboxylate arm. The bond length values in this thiocarboxylate-thiocarbene moiety lie between those expected for single and double-bonds, suggesting delocalisation of electron density.[14] The uranium-based metrical parameters (distances: U–Ct(Cp*),U–O(Aryloxide). Angles: Ct(Arene)–U–Ct(Cp*) and Ct(Ar)–U–O(Ar)) are similar to **4.1**, **4.2** and **4.3**.

Calculations on the reactivity of **4.1** towards CO proved to be challenging so the model U(III) system in **Figure 4.8** is used. DFT studies by Maron *et al.* showed that the pathway to the final product could not be located due to the complexity of the reaction. The pathway to a potential intermediate is shown in **Figure 4.8** and may plausibly represent the intermediate observed in the NMR spectroscopy experiments.

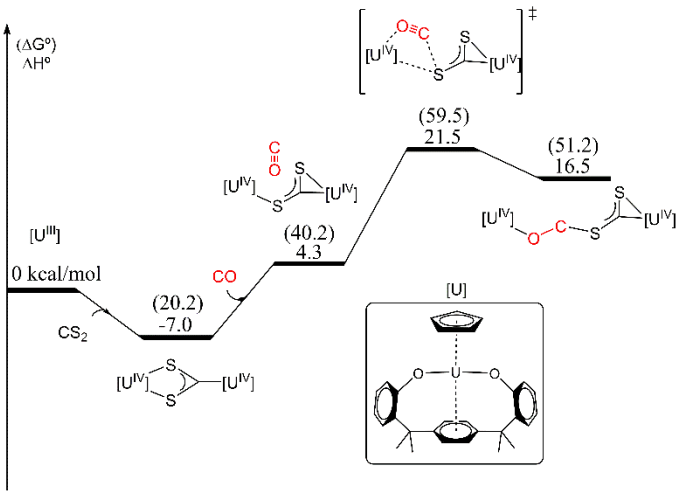

Figure 4.8 In complete computed free energy profile for the mechanism of CO reactivity with **4.1**.

Serendipitously, a small number of crystals of the compound with molecular structure shown below in **Figure 4.9** were grown from a reaction between **4.1** and CO which contained small amounts of **4.2**. The molecular structure shows a methyl group on the aryloxide arm that has been activated by a possible carbene-like intermediate because of CO insertion into a C–S bond. C1–C2, C2–C3, C3–C4 and C2–S2 are all consistent with single bonds as depicted more clearly in **Figure 4.10**. U–O(Ar), U–Ct(Cp*) and U–Ct(arene) bond lengths are similar to other U(IV) species reported in this chapter.

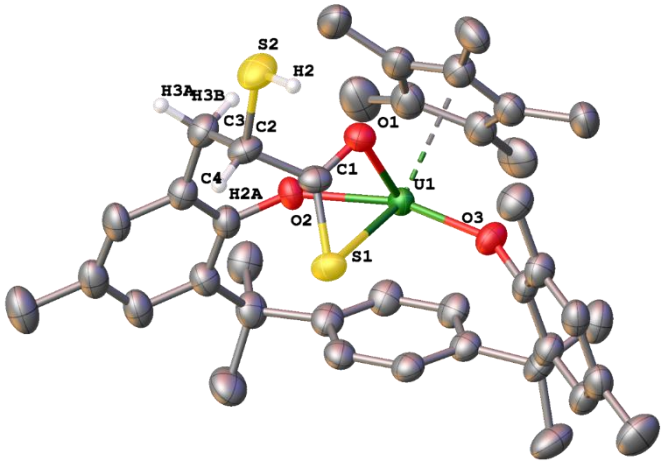

Figure 4.9 Molecular structure of **4.5**. All hydrogens bar four are removed for clarity. Thermal ellipsoids are given at 50% probability. Selected structural parameters (Å, °): C1–C2 = 1.511(14), C2–C3 = 1.586(14), C3–C4 = 1.504(14), C2–S2 = 1.825(10), C1–O1 = 1.275(12), C1–S1 = 1.690(9), U1–O1 = 2.369(7), U1–S1 = 2.987(3), U1–O2 = 2.173(6), U1–O3 = 2.135(6), U1–Ct(Cp*) = 2.4983(3), U1–Ct(arene) = 2.7864(3).

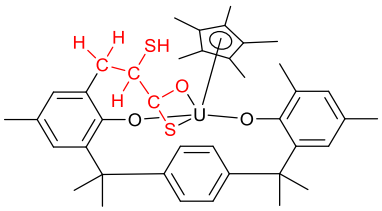

Figure 4.10 Diagram of **4.5**.

The mechanism of the formation of **4.5** is unclear. It is plausible that CO has inserted into the C–S bond of **4.2**, the product of which has attacked the usually inert methyl group on the aryloxide. Unfortunately, synthesis of **4.5** could not be scaled up in large enough quantities for further investigation.

4.3 Reactivity of 3.3 Towards Carbon suboxide

Carbon suboxide (C_3O_2) is an oxo-carbon belonging to the same series as CO_2. While the chemistry of CO_2 has been widely studied and documented,[15] the chemistry of C_3O_2 is much less developed.[16,17] Reactivity studies by Hillhouse *et al.* demonstrated how C_3O_2 can act as a source of CO and ketene (O=C=C:) towards phosphine-containing transition metal complexes. Reacting $WCl_2(PMePh_2)_4$ with C_3O_2 leads to the formation of $(CO)(PMePh_2)_2\{C,C':\eta^2\text{-}C(O)CPMePh_2\}$ which contains a phosphorus-ylide ligand as a result of ketene trapping.[18] Work by the same authors showed that C_3O_2 is also able to coordinate to Ni in an η^2 fashion similar to olefins. The reaction between $[(PPh_3)_2Ni(COD)]$ and C_3O_2 yielded $[(PPh_3)_2Ni(:\eta^2(C,C')\text{-}C_3O_2)]$.[19] Recent work from our laboratory showed that $[Ti_2(\mu{:}\eta^5, \eta^5\text{-}Pent^{TIPS2})_2]$ forms the mono C_3O_2 adduct, $[Ti_2(\mu{:}\eta^5, \eta^5\text{-}Pent^{TIPS2})_2(\eta^2\text{-}C_3O_2)]$, as the first step towards the C_3O_2 trimeric complex, $[Ti_2(\mu{:}\eta^5, \eta^5\text{-}Pent^{TIPS2})_2(\mu\text{-}C_9O_6)]$.[20] Given the dearth of C_3O_2 reactivity studies it is unsurprising that there have been no studies involving U(III) systems. Uranium(III) systems have mediated unique transformations of CO and CO_2 so it was envisaged that **3.3** would display equally exceptional reactivity towards C_3O_2.

C_3O_2 was prepared by a modified literature preparation which involves the dehydration of malonic acid with phosphorus pentoxide. Acetic acid is produced as side-product but can be easily removed *via*

passage of the gas mixture through a CaO scrubbing column. After this, CO_2 is easily removed from C_3O_2 under reduced pressure at -110 °C due to its higher vapour pressure. Carbon suboxide can then stored indefinitely at -78 °C.

Vacuum transfer of C_3O_2 to an ink-black d_8-toluene solution of **3.3** produced an instant colour change to brown-orange. The crude ^{1}H NMR could not be assigned and EI-MS was uninformative. Single crystals suitable for X-ray diffraction were grown from a saturated ^{i}Pr$_2$O solution that was allowed to evaporate slowly over two weeks. The molecular structure of [{UCp*(*p*Me$_2$O$_2$)}$_3${μ-η^1(O):η^2(C,O'): η^2(O'',O''')-C$_6$O$_4$] **4.6** is shown below. Unfortunately, due to an unforeseen issue with the cryostream, significant amounts of ice were deposited on the crystal and resulted in ice rings appearing on the diffraction data. Due to this, the dataset could not be refined below R_1 = 13.72%. The data provide confirmation of connectivity and allows discussion of bond lengths and bond angles with a degree of confidence. The molecular structure of **4.6** reveals a trimetallic uranium compound with a core composed of two units of C_3O_2 that have dimerised at the nucleophilic central and electrophilic terminal carbon atoms to form an C_4 moiety (**Figure 4.12**), possibly *via* a [2+2] cycloaddition mechanism. The C–C bonds (1.46643(4), 1.48745(5), 1.46081(4) and 1.47247(5) Å) in this unit are consistent with the ones found in the 1,2-diphenyl-3,4-bis(trimethylsilyl)-cyclobutadiene dianion (dilithium) (C–C: 1.462(4), 1.479(4), 1.488(4), 1.521(4) Å)[21].

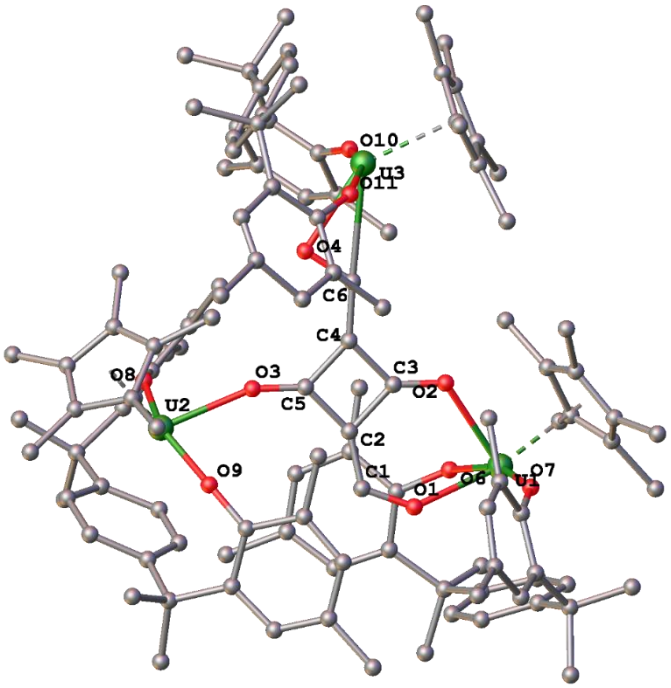

Figure 4.11 Molecular structure of **4.6**. Hydrogen atoms, residual $^{i}Pr_2O$ molecules, O4a atom and thermal ellipsoids not shown for clarity. Selected structural parameters (Å, °): C1–O1 = 1.28397(4), C1–C2 = 1.35065(6), C2–C3 = 1.46643(4), C3–O2 = 1.21786(3), C2–C3 = 1.46643(4), C3–C4 = 1.48745(5), C4–C5 = 1.46081(4), C5–C2 = 1.47247(5), C5–O3 = 1.22625(3), C4–C6 = 1.39496(6), C6–O4 = 1.31029(4), U1–O1 = 2.30752(5), U1–O2 = 2.44377(10), U2–O3 = 2.30922(6), U3–O4 = 2.45709(9), U3–C6 = 2.81579(13), U3–C6–O4 = 60.726(3), U1–Ct(Cp*) = 2.55752(6), U1–O6 = 2.14360(6), U1–O7 = 2.15876(6), U1–Ct(arene) = 3.05203(14), Ct(Cp*)–U1–Ct(arene) = 118.973(2), O6–U1–O7 = 159.8577(8), C37–O6–U1 = 141.5215(13), C17–O7–U1 = 149.3320(11), U2–Ct(Cp*) = 2.46456(8), U2–O8 = 2.12991(6), U2–O8 = 2.16691(6), U2–Ct(Arene) = 2.65274(10), Ct(Cp*)–U1–Ct(arene) = 128.313(2), O8–U2–O9 = 156.2484(8), C54–O8–U2 = 152.5539(11), C74–O9–U2 = 151.7276(12), U3–Ct(Cp*) = 2.51790(6), U3–O10 = 2.15704(6), U3–O11 = 2.15044(6), U–Ct(arene) = 2.74714(8), Ct(Cp*)–U3–Ct(arene) = 121.564(3), O10–U3–O11 = 160.3799(7), C92–O10–U3 = 153.6477(9), C117–O11–U3 = 154.5140(9).

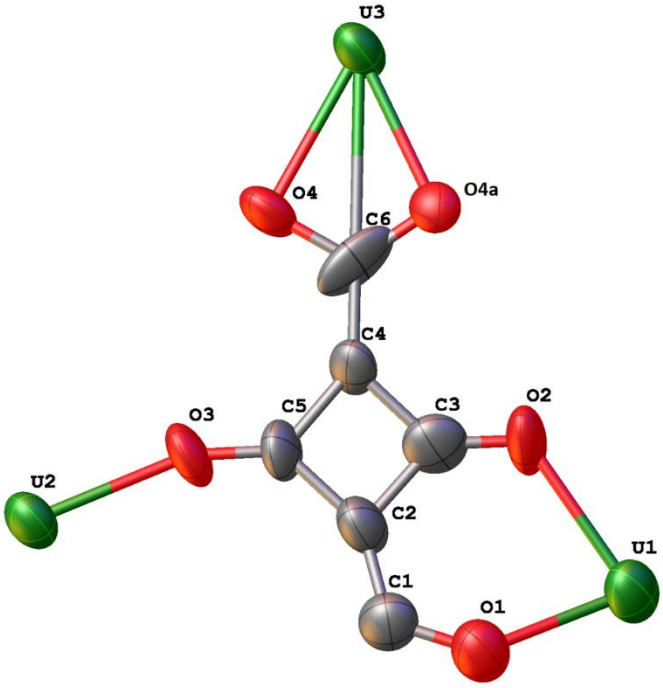

Figure 4.12 $C_6O_4U_3$ core of **4.6** from **Figure 4.11**. Atom O4a is shown.

The crystal structure contains two oxygen atoms (O4 and O4a) which may be disordered over two sites as shown in **Figure 4.12**, therefore it is reasonable to consider this may in fact be a carboxylate group that formed as a result of a reaction with an adventitious oxygen source. If the O4 atom is treated as disordered over two sites then the η^2 interaction between C6–O4 and U3 bears resemblance to the oxycarbene moieties in [Cp*$_2$Th(η^2(C,O)-COCH$_2$(CH$_3$)$_3$)Cl] **4D** (Th1–C1: 2.672(6) Å, Th–O: 2.37(2) Å, C1–O1: 1.18(3) Å Th1–C1–O1: 73(1)°)[22] and [Me$_2$Si(C$_5$Me$_4$)(NPh)Sc{η^2(C,O)-OCB(NDippCH)$_2$}(THF)] **4E** (Sc1–C1–O1: 69.48(12)°, C1–O1: 1.266(3) Å)[23]. The U1–C6–O4 angle in **4.6** (60.726(3)°) is more acute than in **4D** and **4E** while the C6–O4 distance (1.31029(4) Å) is slightly longer. The lengthened C–O distance may be due to greater carbene-like character as opposed to greater acyl-like character in **4D** and **4E**.

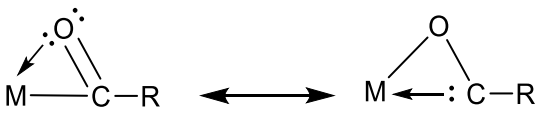

Scheme 4.2 Resonance structures highlighting the acyl and carbene like character of the MCOR moiety.

Interestingly, the three uranium centres of **4.6** have significantly different uranium-based metrical parameters, unlike **4.1**-**4.5** which feature less variation in the uranium-based parameters. U1 features the longest U–Cp* centroid distance (2.55752(6) Å), 0.09292 and 0.03962 Å longer than U2 and U3 (2.46456(8) and 2.51790(6) Å respectively)). U1 also has a much longer U–arene centroid distance (3.05203(14) Å), 0.3993 Å and 0.30549 Å longer than U2 and U3 (2.65274(10) and 2.74714(8) Å respectively)) which is closer in value to the U(IV) complex, **4.1** (U1–Ct(arene): 2.9647(3) Å). These parameters in U2 and U3 are closer to those in the U(III) complex **3.3** (**3.3**: U1–Ct(Cp*): 2.494(7), U1–Ct(arene): 2.382(6) Å respectively) than U1. These differences can be rationalised by the different groups ligated to the uranium centres. U1 features two O interactions with C_6O_4 while U2 features only one O bond and U3 is bonded to C–O.

The C4–C6 bond length (1.3946(6) Å) is reminiscent of a benzene C–C bond (1.38(1) Å)[24] while the C1–C2– bond length (1.35065(6) Å) is slightly shorter and more similar to ethylene (1.3305(10) Å).[25] The C5–O3 bond (1.22625(3) Å) is similar to a C–O double bond (1.230 Å).[26] The exact nature of the bonding situation in the central C_6O_4 moiety is unclear as many of the bond lengths lie in-between single and double bonds; (**Figure 4.13**) depicts a plausible structure given the bond lengths. Also of note is the flat nature of C_6O_4 core, possibly indicating a degree of aromaticity. Spectroscopic studies (IR, Raman, UV-vis/NIR) would provide vital evidence that would clarify this picture (**Figure 4.13**) and give some information as to the formal oxidation state of the uranium centres. Regrettably, it was not possible to synthesise large enough quantities of **4.6** for such spectroscopic studies due to significant amount of decomposition of the sample during crystallisation. Future studies will focus on fully characterising **4.6** and elucidating the reactivity of **3.3** towards C_3O_2.

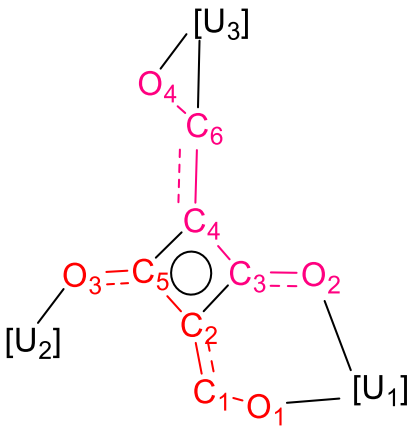

4.6

Figure 4.13 Diagram of **4.6**. Atom labels are from **Figure 4.11**.

4.4 Reactivity of 3.3 Towards Azobenzene

This chapter and the previous one have shown **3.3** is able to mediate the one electron reduction of several substrates, but multi-electron processes have yet to be realised with this system. Azobenzene is a substrate that can undergo multi-electron reduction upon reaction with uranium systems. Therefore, to explore the potential for **3.3** to mediate multi-electron processes, its reactivity towards azobenzene was investigated.

The four-electron reduction of azobenzene with uranium(III) complexes has been well documented. UCp^*_3, $[\{Cp^*_2U\}_2(\eta^6{:}\eta^6\text{-}C_6H_6)]$, $[Cp^*_2U][(\mu\text{-}Ph)_2BPh_2]$ have all been shown to effect the cleavage of azobenzene to give the uranium(VI) complex, $UCp^*_2(NPh)_2$.[27–29] The U(IV) complex, UCp*(PDI)(THF) (PDI = pyridine-(diamine) is also able to reductively cleave azobenzene to generate a uranium bis(imido) species,[30] $UCp^*(PDI)(NPh)_2$, in a four-electron reduction of azobenzene (**Scheme 4.3**), though in this case three electrons originate from the PDI ligand and one from uranium.

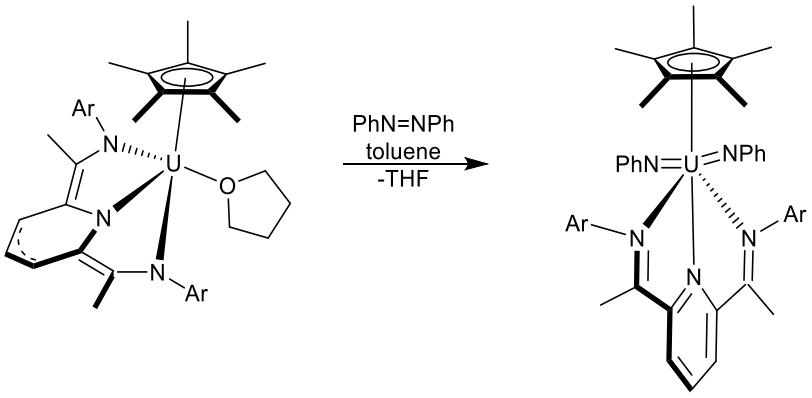

Scheme 4.3 Reaction between UCp*(PDI)(THF) and PhNNPh to form UCp*(PDI)$(NPh)_2$.

Another pathway for the activation of azobenzene is the comproportionation of uranium(III) halide complexes. UCp*$_2$Cl(NaCl) and [U(κ^6-{($tBu_2ArO)_2Me_2$-cyclam})I] react with azobenzene to give U(VI) bis(imido) species (UCp*$_2$$(NPh)_2$ and [U(κ^6-{($tBu_2ArO)_2Me_2$-cyclam})$(NPh)_2$] respectively) and U(IV) bis(halide) (UCp*$_2Cl_2$ and [U(κ^6-{($tBu_2ArO)_2Me_2$-cyclam})I][I] respectively. These reactions are proposed to go through a U(V) intermediate as shown in **Scheme 4.4**.

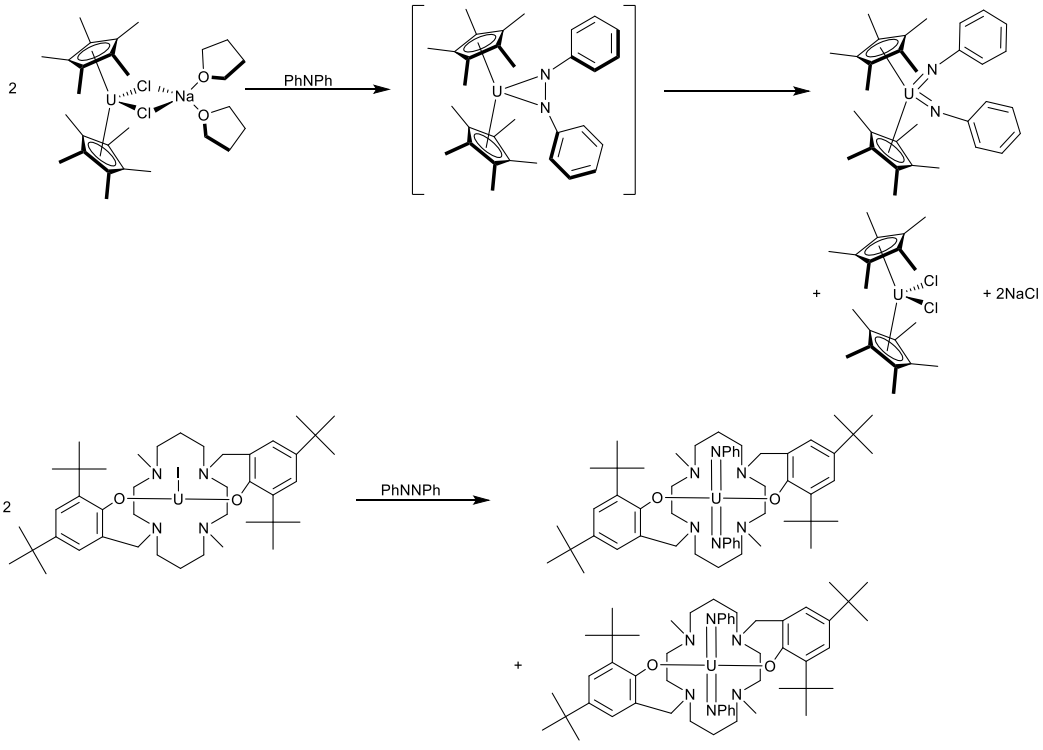

Scheme 4.4 Reactivity of UCp*$_2$Cl(NaCl) and [U(κ^6-{($tBu_2ArO)_2Me_2$-cyclam})I] towards PhNNPh.

Bart *et al.* showed how the formally U(III) complex featuring the redox-active 2,2'-bipyridine ligand, UTp^{Me2}_2(2,2'-bpy), is able to effect the two-electron reduction of azobenzene to $(PhN\text{-}NPh)^{2-}$,[31] with one electron provided by the uranium centre and the other by the 2,2'-bipyridine radical anion ligand.

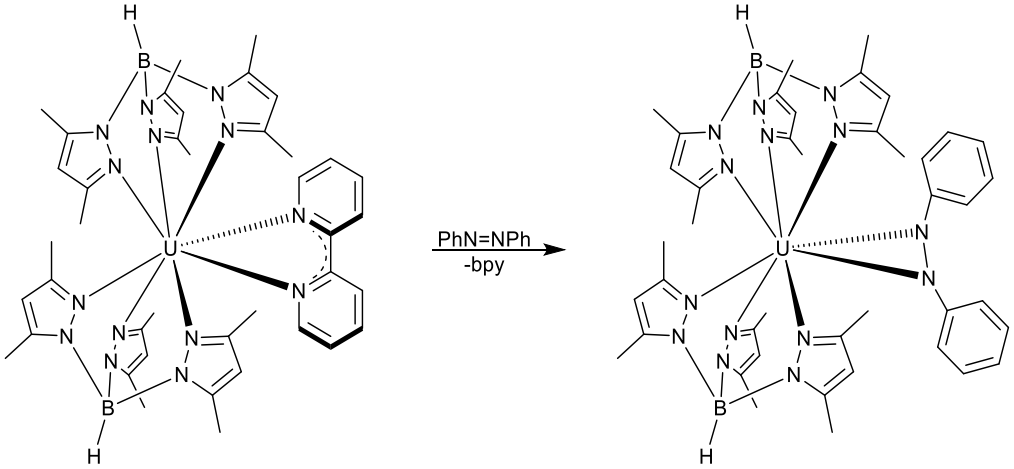

Scheme 4.5 Synthesis of UTp^{Me2}_2(PhN-NPh)

The one-electron reduction of azobenzene to the azobenzene radical has been well documented in lanthanide chemistry,[32–34] yet in uranium chemistry there has only been one report. The U(III) complex, [{$(SiMe_2NPh)_3$-tacn}U], is able to mediate the one-electron reduction of azobenzene to give the radical azobenzene complex, [{$(SiMe_2NPh)_3$-tacn}U(μ^2(N,N')-$N_2Ph_2^{\cdot}$)] **4F** (**Scheme 4.6**).[35]

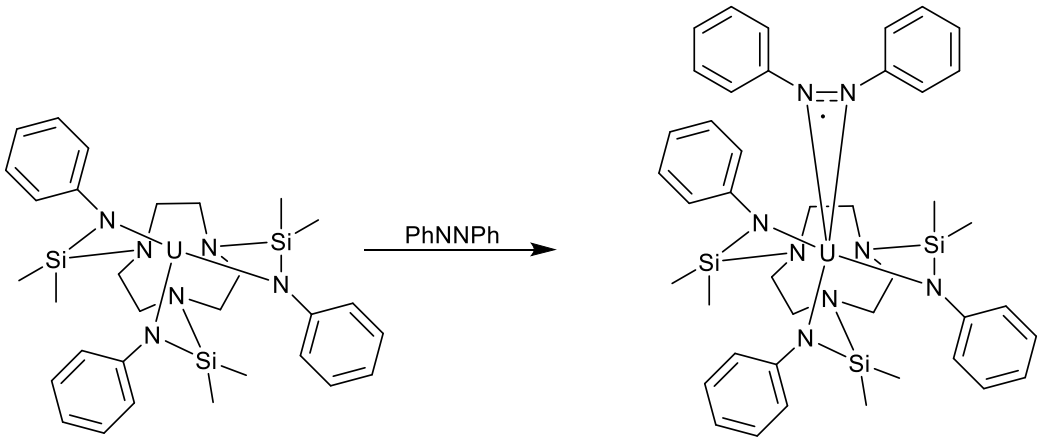

Scheme 4.6 Synthesis of , [{$(SiMe_2NPh)_3$-tacn}U(μ^2(N,N')-$N_2Ph_2^{\cdot}$)].

Addition of one equivalent of azobenzene to a C_6D_6 solution of **3.3** resulted in a colour change to dark maroon. Recrystallisation from pentane gave dark maroon crystals of [{UCp*(*p*Me_2O_2)}{μ^2(N,N')-

$N_2Ph_2^{\cdot}$}] **4.7** (**Scheme 4.7**). This formulation is consistent with combustion analysis and ^{1}H NMR spectroscopic data.

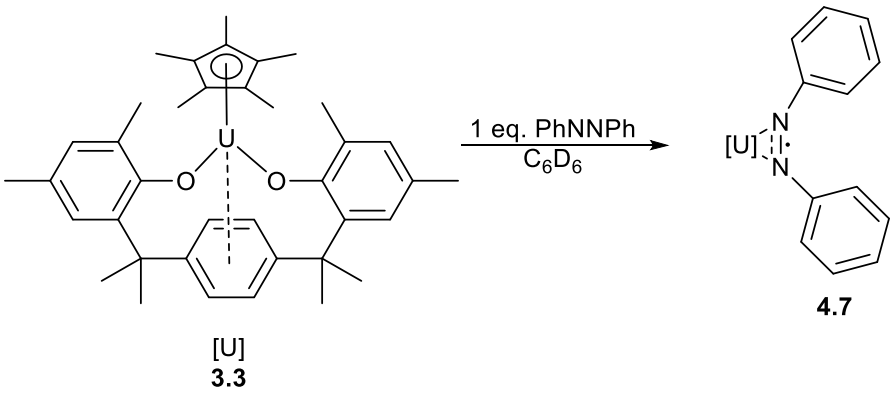

Scheme 4.7 Reaction between **3.3** and PhNNPh to form **4.7.**

The molecular structure of **4.7** is shown below in **Figure 4.14** with selected structural parameters. The complex is monometallic with a (N,N')-N_2Ph_2 interaction. Strong evidence for the radical nature of the azobenzene ligand is the N1–N2 bond length (1.337(8) Å) which has a value between that of the N=N bond of azobenzene (1.251 Å)[36] and the N-N bond of hydrazine (av. 1.45 Å)[37]. This value is also similar to reported values for **4F** (1.353(4) Å)[35], [{SmCp*$_2$}{μ^2(N,N')-$N_2Ph_2^{\cdot}$}] (1.32(1) Å)[32], and [{SmTp$^{Me2}_2$}{μ^2(N,N')-$N_2Ph_2^{\cdot}$}] (1.332(12) Å)[33]. The C39–N2–N1–C45 torsion angle (28.0 (10)°) is further crystallographic evidence for the reduction of the N=N bond as torsion angles of this size would not be possible in the presence of a double bond (*cis*-azobenzene torsion angle: 8°)[38]. The U–N bond lengths (U1–N1: 2.311(5) and 2.365(5) Å) are slightly shorter than those found in **4F** (2.353(3) and 2.413(3) Å)[35], possibly due to the different ligand environments. Complex **4.7** features U–Ct(Cp*), U–O(Ar), U–Ct(arene), O–U–O, Ct(Cp*)–U–Ct(arene) parameters that are similar to other U(IV) complexes discussed in this chapter.

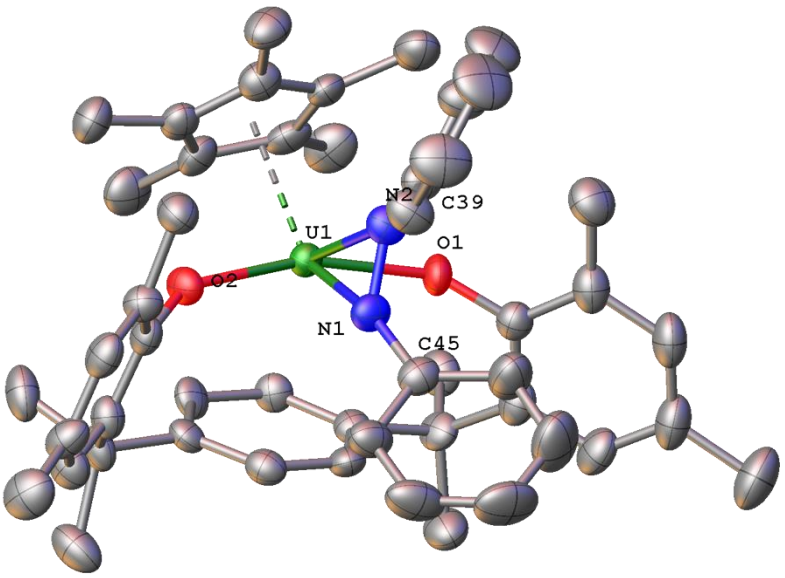

Figure 4.14 Molecular structure of **4.7**. Hydrogen atoms and other molecule of **4.7** in unit cell not shown for clarity. Thermal ellipsoids are given at 50% probability. Selected structural parameters (Å, °): N1–N2 = 1.337(8), C39–N2–N1–C45 = 28.0(10), U1–N1 = 2.311(5), U1–N2 = 2.365(5), N2–U1–N1 = 33.2(2), U1–Ct(Cp*) = 2.5504(2), U1–O2 = 2.171(4), U1–O1 = 2.186(4), U1–Ct(arene) = 2.8416(2), Ct(arene)–U1–Ct(Cp*) = 121.957(8).

The samarium azobenzene complex, [{SmCp*$_2$}{μ^2(N,N')-$N_2Ph_2^{\cdot}$}], has been shown to react with CO to form [{SmCp*$_2$}{μ-η^4-(C,O)-(PhN)OCCO(NPh)}] therefore it was envisaged that **4.7** would display similar behaviour.[32]

Further reactivity studies of **4.7** with CO, CO_2 and H_2 were unfruitful, possibly due to the stability of the U–N bonds and sterically encumbered nature of the uranium centre.

The reactivity of **3.3** towards PhNNPh is comparable to **4F** in that it also mediates the one-electron reduction of azobenzene. This contrasts with uranium complexes that feature redox-active ligands, which as a result, are able to mediate the multi-electron activation of azobenzene.

4.5 Conclusions

In summary, this chapter has expanded on the small molecule reactivity studies of **3.3** to include CS_2, C_3O_2 and azobenzene. Reaction with CS_2 gave the bimetallic complex, **4.1**, which features a doubly reduced CS_2 moiety, and the monometallic **4.2** that contains a dithioformate ligand, the presence of which was confirmed *via* NMR spectroscopic studies with $^{13}CS_2$. These studies also showed that the

relative quantities of **4.1** and **4.2** formed is concentration dependant. Compound **4.1** was then reacted with CO_2 to give the thiocarbonate product **4.3**. Compound **4.1** was also reacted with CO which gave the thiocarbonate-thiocarbene linked complex, **4.4**. During these studies compound **4.5** was also isolated, which had undergone ligand activation at a methyl position on the *p*Me_2O_2 ligand, highlighting the reactive nature of these reaction intermediates.

Complex **4.6** was isolated from the reaction of C_3O_2 and **3.3**. The molecular structure of this complex shows that C_3O_2 has been trimerized with three uranium centres. X-ray diffraction studies reveal that the three uranium centres have significantly different environments. Future studies will focus on elucidating the electronic structure of this complex.

The one-electron reduction of azobenzene with **3.3** was also discussed. Complex **3.3** reacts quantitatively to give **4.7**. The molecular structure is consistent with a mono-reduced azobenzene ligand.

4.6 Experimental for Chapter Four

Synthesis of [{ UCp*(*p*Me$_2$O$_2$)}$_2$CS$_2$] 4.1

A J. Young NMR tube was charged with UCp**p*Me$_2$O$_2$ (50 mg, 0.0643 mmol) and C_6D_6 (0.5 mL). To this was added neat CS_2 (4 µl, 0.066 mmol), and upon addition an instant colour change from black to dark brown was observed. Volatiles were removed and the resulting residues taken up in Et_2O (3 mL), toluene (0.7 mL) was added dropwise with heating until the residues had dissolved. This was followed by filtration and then storage at -35 °C for 3 days to yield the title compound as brown crystals (15 mg, 28%).

^{1}H NMR (399.5 MHz, d_6-benzene, 303 K): δ_H 55.84 (s, 6H, CH_3), 48.52 (s, 6H, CH_3), 37.47 (s, 2H, Ar-H), 37.15 (s, 2H, Ar-H), 36.56 (s, 2H, Ar-H), 33.71 (s, 2H, Ar-H), 24.85 (s, 2H, Ar-H), 22.55 (s, 2H, Ar-H), 16.38 (s, 6H, CH_3), 16.27 (s, 6H, CH_3), 15.44 (s, 6H, CH_3), 15.29 (s, 2H, Ar-H), 14.34 (s, 6H, CH_3), -3.58 (s, 6H, CH_3), -3.68 (s, 6H, CH_3), -5.71 (s, 2H, Ar-H), -6.83 (s, 15H, Cp*), -11.12 (s, 15H, Cp*), -45.74 (s, 2H, Ar-H), -55.77 (s, 2H, Ar-H), -57.44 (s, 2H, Ar-H), -58.00 (s, 2H, Ar-H).

Analysis calculated (found) for $C_{77}H_{94}O_4S_2U_2$: % C 57.18 (56.98), H, 5.97 (6.05).

Synthesis of [{UCp*(*p*Me$_2$O$_2$)}{η^2(S,S')-CS$_2$H] 4.2

A toluene solution of CS_2 (1.5 µl in 2 mL) was added to a toluene solution of **3.3** (30 mg in 3 mL) at -78 °C and stirred for 10 minutes. An instant colour change from dark purple to brown was observed. Volatiles were removed *in vacuo* and crystals of **4.2** suitable for X-ray diffraction studies were grown from a saturated heptane solution that was left to evaporate slowly over 2 d. Despite several attempts with various solvent systems and crystallisation methods, **4.2** could not be completely purified from concomitant **4.1** and unidentified products. It was also observed that the yields of **4.2** relative to **4.1** varied widely over several repeat reactions employing the same reaction conditions. These rations varied from 99:1 to 32:68 (using Cp* peak of both compounds as a reference).

^{1}H NMR (399.5 MHz, d_6-benzene, 303 K): δ_H 42.87(s, 2H, Ar–H), 31.69 (s, 2H, Ar–H), 30.72 (s, 6H, CH_3), 27.58 (s, 6H, CH_3), 14.54(s, 2H, Ar-H), 10.55 (s, 6H, CH_3), -0.94 (s, 6H, CH_3),-1.61 (s, 2H, Ar-H), -3.88 (s, 15H, Cp*), -89.13 (s, 1H, CS_2H).

Synthesis of [{UCp*(*p*Me$_2$O$_2$)}$_2${μ-η^2(S,O):η^2(S,O')-^{13}CO$_2$S] 4.3

A J. Young NMR tube was charged with **3.3** (50 mg, 0.0643 mmol) and C_6D_6 (0.5 mL). To this was added neat $^{13}CS_2$ (4 μl, 0.066 mmol) to give **4.1^{13C}** in quantitative spectroscopic yield. Two equivalents of $^{13}CO_2$ was administered to this solution accurately using a Toepler pump. The reaction mixture was reduced by half and left to stand overnight to precipitate concomitant **3.4** as red blocks. The mother liquor was evacuated to dryness, taken up in $^{i}Pr_2O$ (0.5 mL), filtered and stored at -35 °C to deposit brown crystals of **4.3**. The amount of material was not enough for ^{1}H NMR studies or elemental analysis and the crude NMR could not be assigned.

Synthesis of [{UCp*(*p*Me$_2$O$_2$)}$_2${μ-η^2(S,O):η^2(C,S)-OS^{13}C^{13}CS] 4.4

A J. Young NMR tube was charged with **3.3** (50 mg, 0.0643 mmol) and C_6D_6 (0.5 mL). To this was added neat $^{13}CS_2$ (4 μl, 0.066 mmol) to give **4.1^{13C}** in quantitative spectroscopic yield. Two equivalents of ^{13}CO were administered to this solution accurately using a Toepler pump. The reaction mixture was filtered and left to evaporate overnight to yield crystals of **4.4**. The amount of material was not enough for ^{1}H NMR studies or elemental analysis and the crude NMR could not be assigned with confidence.

Synthesis of 4.5

A J. Young NMR tube was charged with **3.3** (30 mg, 0.0643 mmol) and C_6D_6 (0.5 mL). To this was added neat CS_2 (4 μl, 0.066 mmol) to give **4.1** and **4.2** in a 87:13 ratio. Three equivalents of ^{13}CO were administered to this solution accurately using a Toepler pump. After 3 d the solution mixture was evacuated to dryness and single crystals were grown from a saturated solution of TBME (0.6 mL). The crystalline material deposited was not enough to carry out ^{1}H NMR experiments.

Synthesis of [{UCp*(*p*Me$_2$O$_2$)}$_3${μ-η^1(O):η^2(C,O'): η^2(O'',O''')-C$_6$O$_4$] 4.6

C_3O_2 (*ca*1 equivalent) was transferred to a toluene solution of **3.3** (80 mg in 0.8 mL) on a high-vacuum line at -78 °C. A colour change from dark purple to brown was observed. Volatiles were removed at -78 °C for 10 minutes then -15 °C for one hour. After this point the resulting sticky matrix was allowed to warm to room temperature while under vacuum. The brown solids were taken up in $^{i}Pr_2O$ (4 mL), filtered, and left to evaporate slowly over 14 d at room temperature. A small amount of single crystals suitable for X-ray diffraction studies were deposited. From this batch of single crystals was the structure of **4.6** obtained. Unfortunately, during this time significant amounts of product had also decomposed as indicated by the deposition of amorphous black solids. The amount of crystalline material was not enough for ^{1}H NMR studies. Despite several attempts with various solvent systems and crystallisation methods, it was not possible to produce crystalline material of **4.6**.

Synthesis of [{ UCp*(*p*Me$_2$O$_2$)}PhNNPh] 4.6

To an ampoule charged with UCp*pMe$_2$O$_2$ (325 mg, 0.411 mmol) and PhNNPh (75 mg, 0.412 mmol) was added C_6H_6 (4 mL), a colour change from black to dark maroon was observed. The reaction mixture was stirred for 2 hours and then pumped to dryness. Pentane (15 mL) was added, the residues extracted, filtered and then stored at -35 °C for 2 days to yield large black crystals of **4.6** (182 mg, 52%).

^{1}H NMR (399.5 MHz, d_6-benzene, 303 K): δ_H 71.11 (s, 6zH), 61.53 (s, 2H), 37.98 (s, 2H), 31.51 (s, 6H), 24.49 (s, 2H), 15.76 (s, 6H), -2.75 (s, 6H), -3.27 (s, 1H) , -5.18 (s, 15H), -54.49 (s, 2H), -56.05 (s, 2H), -114.41 (s, 2H), -134.45 (s, 2H), -216.26 (s, 2H), -245.32 (s, 1H).

Analysis calculated (found) for $C_{50}H_{57}N_2O_2U_2$: % C 63.62 (63.77), H, 6.43 (6.41), N, 2.82 (2.91).

4.7 References for Chapter Four

1 N. C. Baenziger and W. L. Duax, *J. Chem. Phys.*, 1968, **48**, 2974–2981.
2 V. Mougel, C. Camp, J. Pécaut, C. Copéret, L. Maron, C. E. Kefalidis and M. Mazzanti, *Angew. Chem. Int. Ed.*, 2012, **51**, 12280–12284.
3 J. G. Brennan, R. A. Andersen and A. Zalkin, *Inorg. Chem.*, 1986, **25**, 1756–1760.
4 O. P. Lam, L. Castro, B. Kosog, F. W. Heinemann, L. Maron and K. Meyer, *Inorg. Chem.*, 2012, **51**, 781–783.
5 J. H. D. Eland and J. Berkowitz, *J. Chem. Phys.*, 1979, **70**, 5151–5156.
6 J. D. Cox, D. D. Wagman and V. A. Medvedev, *CODATA Key Values for Thermodynamics*, Hemisphere, New York, 1989.
7 Thiophene C-H Coupling Constants, https://www.chem.wisc.edu/areas/reich/nmr/10-cdata-05-jch.htm, (accessed 5 June 2018).
8 P. C. Cross and L. O. Brockway, *J. Chem. Phys.*, 1935, **3**, 821.
9 H. V. Nanishankar, S. Dutta, M. Nethaji and B. R. Jagirdar, *Inorg. Chem.*, 2005, **44**, 6203–6210.
10 D. S. Gill, M. Green, K. Marsden, I. Moore, A. G. Orpen, F. G. A. Stone, I. D. Williams and P. Woodward, *J. Chem. Soc. Dalton Trans.*, 1984, 1343–1347.
11 M. El-khateeb, K. J. Asali and A. Lataifeh, *Polyhedron*, 2003, **22**, 3105–3108.
12 D. J. Darensbourg, W.-Z. Lee, A. L. Phelps and E. Guidry, *Organometallics*, 2003, **22**, 5585–5588.
13 N. Tsoureas, L. Castro, A. F. R. Kilpatrick, F. G. N. Cloke and L. Maron, *Chem. Sci.*, 2014, **5**, 3777–3788.
14 T. L. Cottrell, *The Strengths of Chemical Bonds*, Butterworths Scientific Publications, 1958.
15 J. Artz, T. E. Müller, K. Thenert, J. Kleinekorte, R. Meys, A. Sternberg, A. Bardow and W. Leitner, *Chem. Rev.*, 2018, **118**, 434–504.
16 G. Paiaro and L. Pandolfo, *Comments Inorg. Chem.*, 1991, **12**, 213–235.
17 L. H. Reyerson and K. Kobe, *Chem. Rev.*, 1930, **7**, 479–492.
18 A. K. List, G. L. Hillhouse and A. L. Rheingold, *Organometallics*, 1989, **8**, 2010–2016.
19 A. K. List, M. R. Smith and G. L. Hillhouse, *Organometallics*, 1991, **10**, 361–362.
20 N. Tsoureas, J. C. Green, F. G. N. Cloke, H. Puschmann, S. M. Roe and G. Tizzard, *Chem. Sci.*, DOI:10.1039/C8SC01127C.
21 A. Sekiguchi, T. Matsuo and M. Tanaka, *Organometallics*, 2002, **21**, 1072–1076.
22 P. J. Fagan, J. M. Manriquez, T. J. Marks, V. W. Day, S. H. Vollmer and C. S. Day, *J. Am. Chem. Soc.*, 1980, **102**, 5393–5396.
23 B. Wang, X. Kang, M. Nishiura, Y. Luo and Z. Hou, *Chem. Sci.*, 2015, **7**, 803–809.
24 L. Pauling, *The Nature of the Chemical Bond and the Structure of Molecules and Crystals: An Introduction to Modern Structural Chemistry*, Cornell University Press, 1960.
25 N. C. Craig, P. Groner and D. C. McKean, *J. Phys. Chem. A*, 2006, **110**, 7461–7469.
26 H. Feilchenfeld, *J. Phys. Chem.*, 1959, **63**, 1346–1346.
27 W. J. Evans, G. W. Nyce and J. W. Ziller, *Angew. Chem. Int. Ed.*, **39**, 240–242.
28 W. J. Evans, S. A. Kozimor, J. W. Ziller and N. Kaltsoyannis, *J. Am. Chem. Soc.*, 2004, **126**, 14533–14547.
29 W. J. Evans, S. A. Kozimor and J. W. Ziller, *Chem. Commun.*, 2005, 4681–4683.
30 D. P. Cladis, J. J. Kiernicki, P. E. Fanwick and S. C. Bart, *Chem. Commun.*, 2013, **49**, 4169–71.
31 S. J. Kraft, Ph.D., Purdue University, 2012.
32 L. R. Chamberlain and R. J. Doedens, *J. Am. Chem. Soc.*
33 J. Takats, X. W. Zhang, V. W. Day and T. A. Eberspacher, *Organometallics*, 1993, **12**, 4286–4288.
34 C. A. P. Goodwin, N. F. Chilton, G. F. Vettese, E. Moreno Pineda, I. F. Crowe, J. W. Ziller, R. E. P. Winpenny, W. J. Evans and D. P. Mills, *Inorg. Chem.*, 2016, **55**, 10057–10067.
35 M. A. Antunes, J. T. Coutinho, I. C. Santos, J. Marçalo, M. Almeida, J. J. Baldoví, L. C. J. Pereira, A. Gaita-Ariño and E. Coronado, *Chem. – Eur. J.*, 2015, **21**, 17817–17826.

36 C. J. Brown, *Acta Crystallogr.*, **21**, 146–152.
37 G. L. Miessler and D. A. Tarr, *Inorganic Chemistry*, Pearson Education, 2004.
38 A. Mostad and C. Romming, *Acta Chem Sc*, 1971, 3561–3568.

5 Chapter Five: Thorium-*p*Me_2O_2 Coordination Chemistry Including a Reduced Th(*p*Me_2O_2)$_2$ Species With a δ-Bonding Arene-Interaction

5.1 Introduction

Stabilisation of highly reactive, low-valent species through metal-arene interactions is a well understood concept within transition metal chemistry.[1] This bonding motif has also found application in actinide chemistry, in that recent advances in low-valent uranium chemistry have been facilitated by these stabilising metal-arene interactions. For example, the U(II) complex, [K(2.2.2-crypt)][((^{Ad,Me}ArO)$_3$mes)U],[2] features a central mesitylene anchor capable of δ-symmetry interactions with uranium. Furthermore, a covalent δ-bonding arene interaction in the complex, ((^{Ad,Me}ArO)$_3$mes)U, was found to be an essential component to the complex's ability to electrocatalytically split water.[3] Although these examples highlight the progress that has been made in low-valent uranium chemistry, our understanding of thorium chemistry is vastly underdeveloped by comparison. Thorium-arene interactions have been reported far less despite potentially supporting low-valent thorium systems that have unique electronic configurations and reactivity. The nine Th(III) complexes published to date all contain derivatives of the carbocyclic ligands, Cp or COT, as they contain orbitals of suitable symmetry and energy that are able to stabilise a $6d_{z2}^1$ configuration.[4–10]

It was envisaged that the carbocyclic C_6 ring of *p*Me_2O_2 would be able to support low-valent species in a similar manner to the aforementioned Cp and COT systems. Gambarotta *et al.* showed that it was possible to synthesise the reduced thorium-arene species, [η^5-{1,3-[(η^5-2-C_4H_3N)$(CH_3)_2$C]$_2C_6H_4$}ThK-(μ-Cl)$_3$][Li(DME)$_3$] **5A**, which contains a primarily ligand-based π-symmetry SOMO.[11] The arene in this complex is puckered, possibly because of the *meta* configuration of the pyrrolide 'arms' of this ligand therefore it was hoped that the *para* configuration of *p*Me_2O_2 would allow a more planar thorium-arene interaction and a δ-bonding interaction in a reduced species. *p*Me_2O_2 was also chosen due to the favourable Th–O bonds it would form in a thorium complex.

The synthesis of stable and isolable Th(III) complexes has historically proved to be a highly challenging endeavour; one that has yet to reach the same levels of success as analogous uranium(III) complexes.

For example, $ThCOT^{TIPS2}Cp^*X$ (X = Cl or I) displayed an irreversible one-electron reduction in cyclic voltammetry studies at *ca* -3.3 V *vs* $FeCp_2^{0/+}$, thus suggesting potential access to a Th(III) complex, however, attempts to chemically reduce these species resulted in the formation of $ThCOT^{TIPS2}{}_2$ and Th(0),[12] presumably due to disproportionation of a short-lived Th(III) complex.

It was hypothesised that the pMe$_2$O$_2$ scaffold could be used as an alternative to the venerable bis-Cp^R (where R = Me$_5$, 1,3-^{t}Bu *etc*) framework which has been widely utilised in thorium coordination chemistry,[13] with this framework supporting a range of ligands including hydrides,[14] alkyls and fluorides.[14,15] It was expected that the overall rigidity of pMe$_2$O$_2$ and its stabilising central arene ring, would provide a platform to investigate the coordination chemistry of thorium as well as grant access to thorium-arene interactions.

This chapter describes the entry of this ligand into thorium chemistry and investigations into the synthesis of homoleptic and heteroleptic Th(IV) and Th(III) complexes. Also reported in this chapter are the first examples of Th^{IV}/Th^{III} redox couple values.

5.2 Synthesis and Characterisation of Th(pMe$_2$O$_2$)$_2$ 5.1 and [K(2.2.2-cryptand)][Th(pMe$_2$O$_2$)$_2$] 5.2

The homoleptic complex, Th(pMe$_2$O$_2$)$_2$, was targeted as a pre-cursor to a reduced thorium species as it avoids the use of other ligands and therefore enables investigations into its viability to support low-valent thorium systems without relying on other ligands that may hinder the formation of a low-valent complex.

5.2.1 Th(pMe$_2$O$_2$)$_2$

ThBr$_4$THF$_4$ reacts with two equivalents of pMe$_2$O$_2$K$_2$ (**Scheme 5.1**) to give, after workup, the Th(IV) complex Th(pMe$_2$O$_2$)$_2$ **5.1** as white powder in excellent yield and high purity by ^{1}H and ^{13}C{^{1}H} NMR spectroscopy. The arene ring protons of **5.1** appear as two doublets ($^3J_{HH}$ = 8.14 Hz) in the ^{1}H NMR spectrum, consistent with coupling between two aromatic protons. The parent ion for **5.1** is observed in the EI-MS experiment with the expected isotope pattern. Elemental analysis is consistent with **5.1**.(Toluene)$_{0.7}$ following recrystallisation from toluene/Et$_2$O.

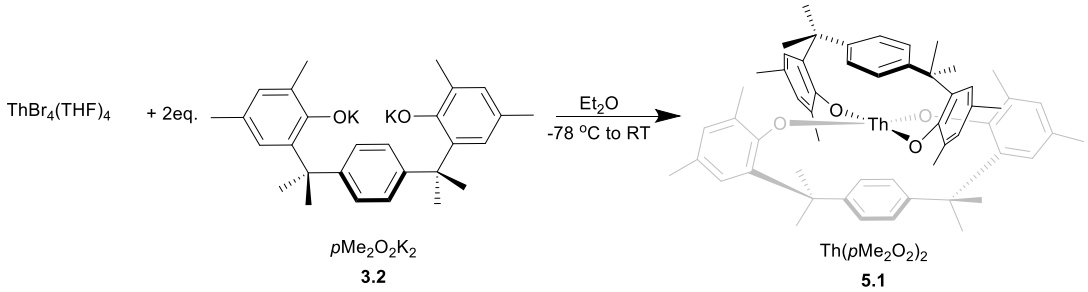

Scheme 5.1 Synthesis of **5.1**.

The molecular structure of **5.1** was determined using single crystal X-ray diffraction (**Figure 5.1**) by Dr Alistair Frey.[16] Complex **5.1** features thorium in a pseudo-octahedral geometry with four aryloxide and two η^6-arene interactions. The Th1–O1 and Th1–O2 bond lengths of 2.228(3) and 2.231(3) Å are slightly longer than other thorium aryloxide complexes reported in the literature (2.16(1) – 2.211(9) Å).[17–19] The Th-Cent(arene) distance of 2.88397(12) Å is indicative of a weak η^6-interaction unlike the two Th-arene contacts in [(trans-calix[2]benzene[2]pyrrolide)Th(C≡CSiMe$_3$)$_2$NiPCy$_3$] which are much stronger interactions (Th–Cent(arene)$_{avg}$ = 2.665 Å).[20]

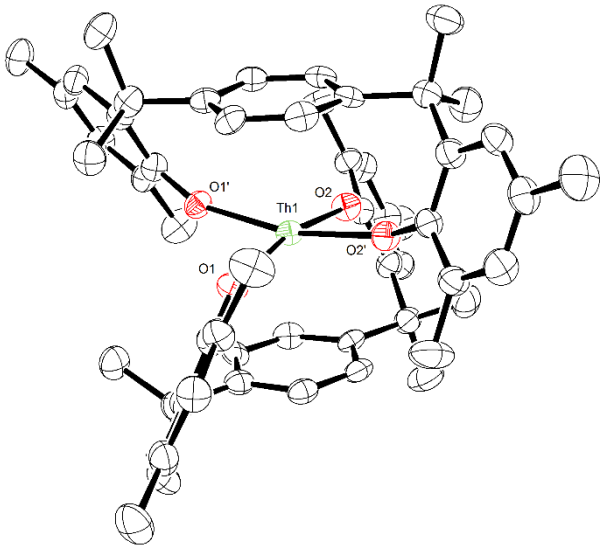

Figure 5.1 ORTEP diagram for the molecular structure of compound **5.1**. Structure with 50% thermal ellipsoids is shown, hydrogens omitted for clarity. Selected structural parameters (Å, deg): Th1–O1 = 2.228(3), Th1–O2 = 2.231(3) O1–Th1–O2 = 165.94(11), Th1–O1–C1 = 159.1(3), Th1–O2–C26 = 156.0(3), Th–Cent(arene) = 2.88397(12) and C–C (central arene ring)$_{avg}$ = 1.397.

5.2.2 [K(2.2.2-cryptand)][Th(*p*Me$_2$O$_2$)$_2$]

The quasi-reversible reduction in the voltammogram of **5.1** at -2.90 V *vs* $FeCp_2^{+/0}$ suggested that the reduction product could be chemically accessible (**Figure 5.2**). The i_{pa}/i_{pc} value of 0.62 points towards a quasi-reversible process that under-goes decomposition after the anodic scan. [^{n}NBu$_4$][BPh$_4$] was chosen as an electrolyte due to higher current responses and increased stability of analyte compared to [^{n}NBu$_4$][B(C$_6$F$_5$)$_4$], see section 5.2.3 for more detail.

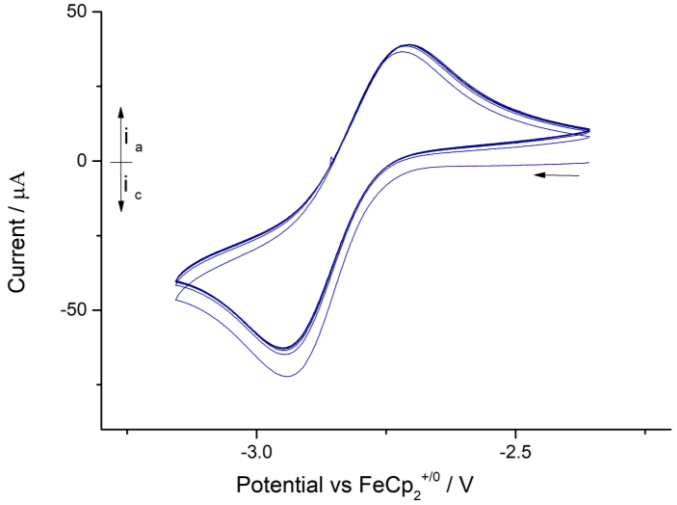

Figure 5.2 Overlaid CV scans (6 cycles) for 0.005 M **5.1** in 0.05 M [^{n}NBu$_4$][BPh$_4$] / THF, scan rate 100 mV s^{-1}.

Indeed, addition of K/Hg to a THF solution of **5.1** and 2.2.2-cryptand led to a rapid colour change from colourless to deep red. ^{1}H NMR spectroscopy indicated the consumption of **5.1** and the formation of a new paramagnetic species with broad peaks that precluded assignment. Elemental analysis is consistent with [K(2.2.2-cryptand)][Th(*p*Me$_2$O$_2$)$_2$] **5.2**. The Evans method shows that this new paramagnetic species (**5.2**) has a μ_B value of 1.80,[21] consistent with a species containing one unpaired electron with little spin-orbit coupling (spin-only value is 1.73 μ_B).

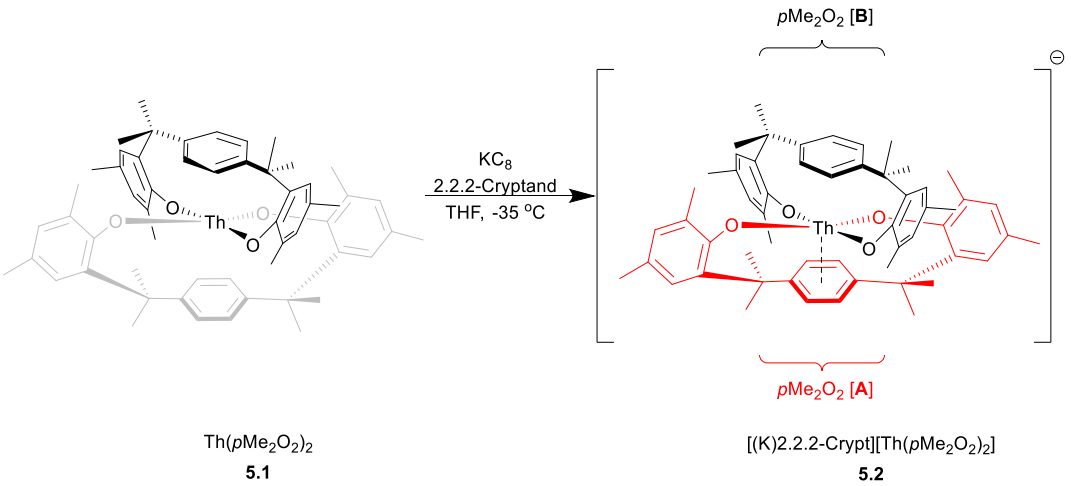

Scheme 5.2 Synthesis of **5.2**. Counter cation, [K(2.2.2-cryptand)], not shown for clarity. The notation pMe$_2$O$_2$[**A**] and pMe$_2$O$_2$[**A**] is used to differentiate the two pMe$_2$O$_2$ ligands of **5.2** and is used herein. Also, this notation is unrelated to the shorthand, **5A**.

To gain insight into the electronic structure of **5.2**, UV/vis-NIR spectra were recorded (**Figure 5.3**). A single broad absorbance was observed at 810 nm (ε = 68 M^{-1} cm^{-1}) which is far less intense than other Th(III) complexes (ThCp*$_3$: λ_{max} = 539 nm (ε = 9500 M^{-1} cm^{-1})[9], ThCp$^{TMS2}_3$: λ_{max} = 654 nm (ε = 5100 M^{-1} cm^{-1})[22]). It is unclear whether this absorbance is an f–f transition or a ligand-based transfer.

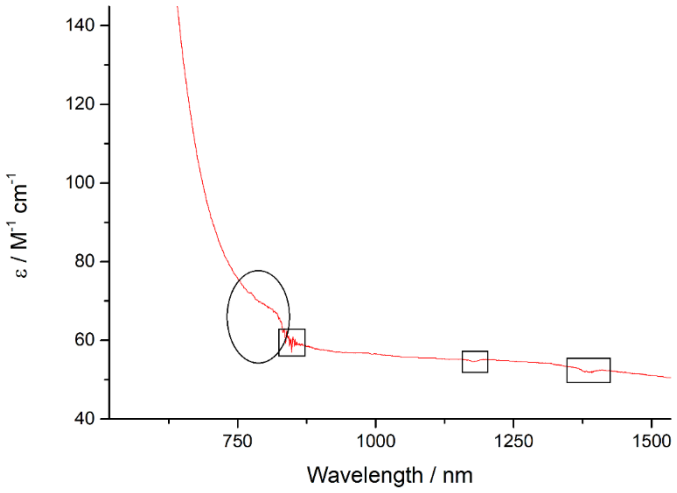

Figure 5.3 UV-vis/NIR spectrum of a 10 mM THF solution of **5.2**. Absorbance highlighted with a black circle and artefacts highlighted in black boxes.

To gain insight into the molecular structure of **5.2**, X-ray diffraction studies were carried out. Gratifyingly, single crystals suitable for X-ray diffraction studies were obtained by the drop-wise addition of DME to an Et$_2$O suspension of **5.2** (**Figure 5.4**). Owing to its highly symmetrical nature,

the thorium atom of **5.2** is disordered over two sites. This was overcome by splitting the thorium atom over two sites with occupancies of 0.6359 and 0.3641. Most strikingly, the molecular structure of **5.2** features a significantly contracted Th1–Cent(*p*Me$_2$O$_2$[**A**]) distance of 2.5109(16) Å, 0.373 Å shorter than in **5.1** and 0.145 Å less than the average value found in compound **5A**.[20] Arene bonding in *p*Me$_2$O$_2$[**A**] is only slightly perturbed as judged by the minimal distortion from planarity.

The geometrical parameters of **5.2** show that the *p*Me$_2$O$_2$ ligands are coordinated to thorium very differently. *p*Me$_2$O$_2$[**A**] features a shorter Th–Cent(arene) contact, shorter Th–O bonds, and a less acute ligand bite angle in comparison to *p*Me$_2$O$_2$[**B**]. These structural differences are due to the strong metal-arene interaction between thorium and *p*Me$_2$O$_2$[**A**], which result in the contraction of metrical parameters. Numerous structural parameters of **5.1** lie between the values found in *p*Me$_2$O$_2$[**A**] and *p*Me$_2$O$_2$[**B**]; this is the case for the Th–O bond lengths and some angles (O–Th–O and Th–O–C) (**Table 5.1**).

Table 5.1 Selected parameters for **5.1** and the *p*Me$_2$O$_2$[**A**] and *p*Me$_2$O$_2$[**B**] ligands in **5.2**.

	5.1	*p*Me$_2$O$_2$[**A**]	*p*Me$_2$O$_2$[**B**]
Th–O (Å)	2.228(3), 2.231(3)	2.229(3), 2.208(3)	2.313(3), 2.289(3)
O–Th–O (deg)	165.94(11)	174.65(2)	141.81(2)
Th–O–C (deg)	159.1(3), 156.0(3)	149.0(2), 145.9(3)	166.6(2), 170.9(2)

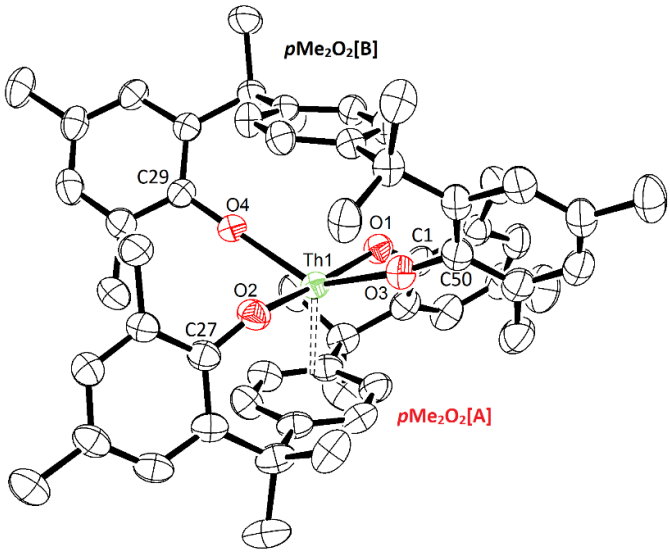

Figure 5.4 ORTEP diagram for the molecular structure of **5.2**. 50% thermal ellipsoids shown with [(K)2.2.2-crypt], hydrogens and an Et_2O molecule removed for clarity. Th2 atom not shown. Notation to differentiate the two pMe$_2$O$_2$ ligands of **5.2** is shown. Selected structural parameters (Å, deg): Th1–O1 = 2.229(3), Th1–O2 = 2.208(3), Th1–O3 = 2.313(3), Th1–O4 = 2.289(3), O1–Th1–O2 = 174.65(2), O3–Th1–O4 = 141.81(2), Th1–O1–C1 = 149.0(2), Th1–O2–C27 = 145.9(3), Th1–O3–C50 = 166.6(2), Th1–O4–C29 = 170.9(2), Th1–Cent(central arene of pMe$_2$O$_2$[**A**]) = 2.5109(16), Th1–Cent(central arene of pMe$_2$O$_2$[**B**]) = 3.4344(15), C–C(central arene of pMe$_2$O$_2$[**A**])$_{avg}$ = 1.404.

The X-band EPR spectrum of polycrystalline **5.2** shows a single broad resonance with a g-value of 1.964 (**Figure 5.5**) at 290 K that was successfully modelled.[23] The observation of a signal at 290 K rules out the possibility of a 5f-based electron as it is expected a signal will only be observed at low-temperature.[24] The g-value of 1.964 is very similar to that of [η^5-{1,3-[(η^5-2-C_4H_3N)$(CH_3)_2$C]$_2C_6H_4$}ThK-(μ-Cl)$_3$][Li(DME)$_3$] **5A** (2.0012 at 273 K) and [((^{Ad,Me}ArO)$_3$mes)U=O(THF)] (1.997 at 94 K) which both contain arene-based radicals.[11,25] The formally Th(III) complex, ThCp$_3^{TMS2}$ has a g-value of 1.910, significantly less than that of **5.2**.[22] It is unclear why there is a second signal in the EPR spectrum of polycrystalline **5.2**.

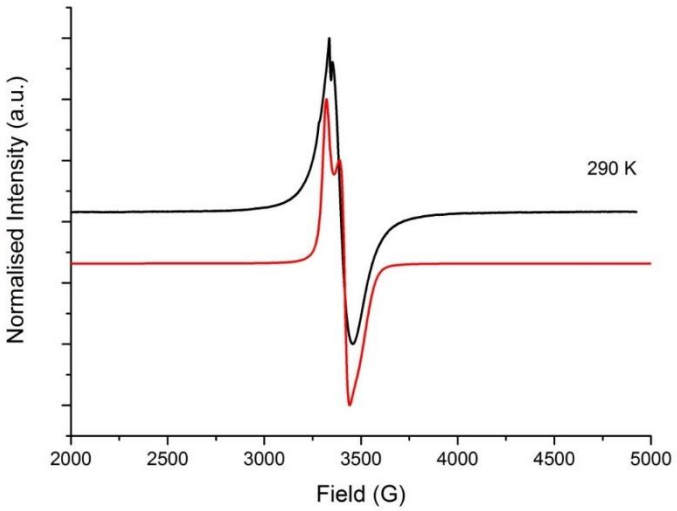

Figure 5.5 X-band EPR spectrum of polycrystalline powder **5.2** at 290 K. Experimental (black) and simulated (red).

The X-band EPR spectrum of **5.2** in 1-MeTHF displays an axial signal with three principal g-values from 290 to 5 K (**Figure 5.6** and **Table 5.2**).

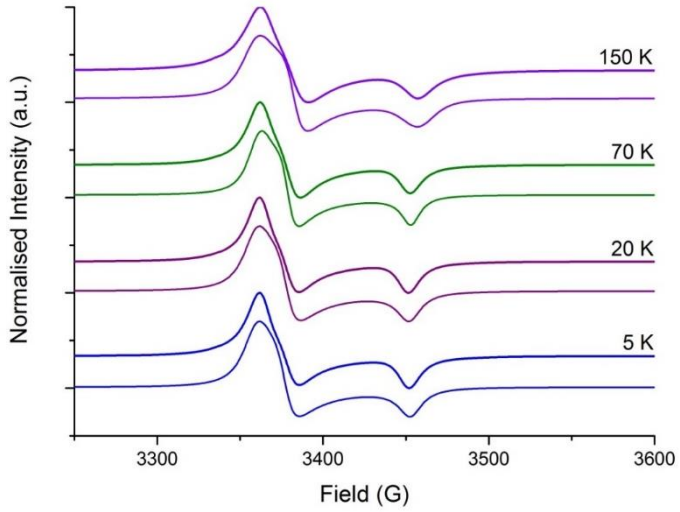

Figure 5.6 X-band EPR spectrum of **5.2** in 1-MeTHF at different temperatures. Experimental (top) and simulated (bottom).

Table 5.2 g-values from the X-band EPR spectrum of **5.2** in 1-MeTHF at several temperatures.

Temperature	g_x	g_y	g_z
290 K	2.020	1.962	1.920
150 K	1.997	1.984	1.941
70 K	1.997	1.986	1.943
20 K	1.997	1.9865	1.943
5 K	1.997	1.987	1.943

To elucidate the electronic structure of **5.2**, density functional calculations were performed by Professor Jennifer Green using the ADF program suite (BP86/TZP). The optimized geometries of **5.1** and **5.2** were in good agreement with the X-ray structures and for **5.2** reproduced the shorter Th-arene distance and the increase in O–Th–O bite angle for ligand [**A**]. A view of the calculated geometry of **5.2** is shown in **Figure 5.7** which indicates the Cartesian axes used in the calculation. The four-fold orientation of the coordinating O atoms lifts the degeneracy of the Th d(±2) and f(±2) orbitals. With our axis choice the O atoms lie on the bisectors of the x and y axes and interact strongly with the Th $6d_{xy}$ orbital, whereas the Th $6d_{x2-y2}$ and $5f_{z(x2-y2)}$ are non-bonding with respect to any O σ-donation. The coordinating arene is not aligned with the x and y axes.

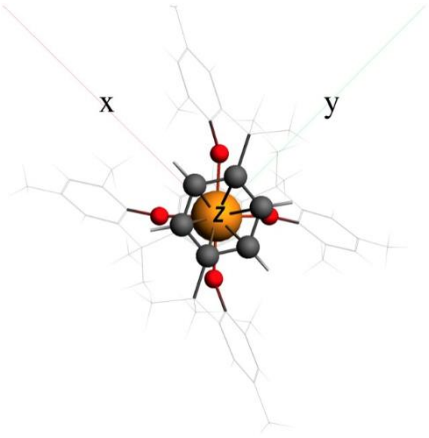

Figure 5.7 Calculated structure of **5.2** indicating orientation of axes.

The unpaired electron of **5.2** occupies an orbital responsible for the covalent binding of the arene ring to thorium and consequently the short associated distance found experimentally. As shown in **Figure**

5.8 it takes the anticipated form of a δ bond. The calculated composition of the arene ring closest to thorium is 73% C 2p, 13% Th 5f $_{z\,(x2-y2)}$ and 6% Th $6d_{x2-y2}$. The orientation of the arene discussed above ensures that all six C atoms of the arene ring are involved in the bonding hence there is no apparent distortion of the ring from planarity. An indication of the strength of the thorium-arene interaction is given by the difference in energy of the SOMO and an unoccupied δ orbital on the uncoordinated arene ring of ligand [**B**]. The SOMO is 0.96 eV more stable.

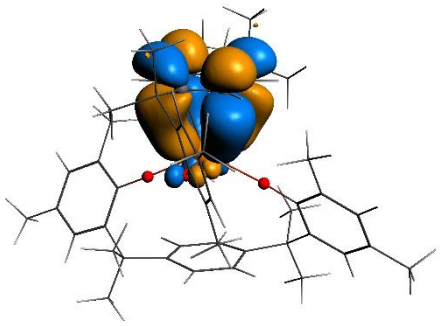

Figure 5.8 SOMO of **5.2**.

The g-values of **5.2** were calculated in order to establish whether the calculated electronic structure was consistent with the EPR measurements. For the calculations, which used full spin-orbit coupling, the structure was simplified by replacing the methyl groups with H atoms (**5.2^{H}**). The principal g values were calculated as 1.81, 1.95 and 1.97, the pattern of two larger than the third being consistent with that found experimentally.

The electronic structure of the thorium-arene interaction is different to that of [η^5-{1,3-[(η^5-2-C_4H_3N)$(CH_3)_2C]_2C_6H_4$}ThK-(μ-Cl)$_3$] (**Figure 5.9**), which was used as a simplified model for **5A** in electronic structure calculations.[11] These studies showed that the SOMO is purely π-character and Mulliken population analysis indicated that the spin density is concentrated on the distorted carbon atom above the plane of the arene ring (69.8%). Compound **5.2** features a similar amount of spin density located on the arene ring although the ring in **5.2** features much less distortion and a SOMO with δ character. This difference in electronic structure is probably due to the meta arrangement of the pyrrolide arms which pushes the carbon atom out of the plane due to increased steric repulsion in

comparison to the para configuration of **5.2**. The thorium atom in this system contains 13.4% of the electron spin density in this system, similar to that calculated for **5.2.**

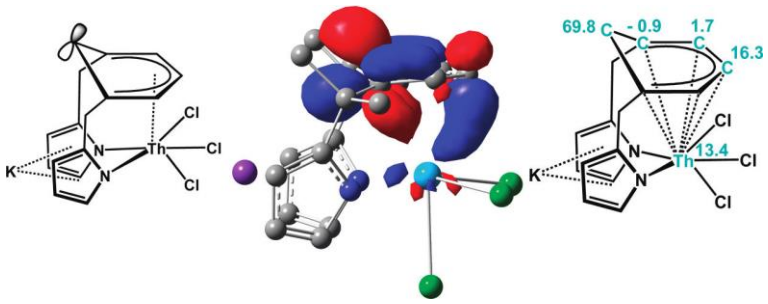

Figure 5.9 α-HOMO and Atomic Spin Density Distribution Values (%) for the Simplified Model of Complex **5A**. Image from reference[11].

The voltammogram of **5.2** (**Figure 5.10**, **Figure 5.11** and **Figure 5.12**) shows a quasi-reversible oxidation at -2.90 V *vs* $FeCp_2^{+/0}$, which is in agreement with the voltammogram of **5.1**. Interestingly, a quasi-reversible process is also observed at -3.4 V *vs* $FeCp_2^{+/0}$, which alludes to the possibility of accessing even lower formal oxidation states of thorium supported by this ligand. These two processes (-2.90 and -3.4 V *vs* $FeCp_2^{+/0}$) are also present when voltammograms are scanned anodically.

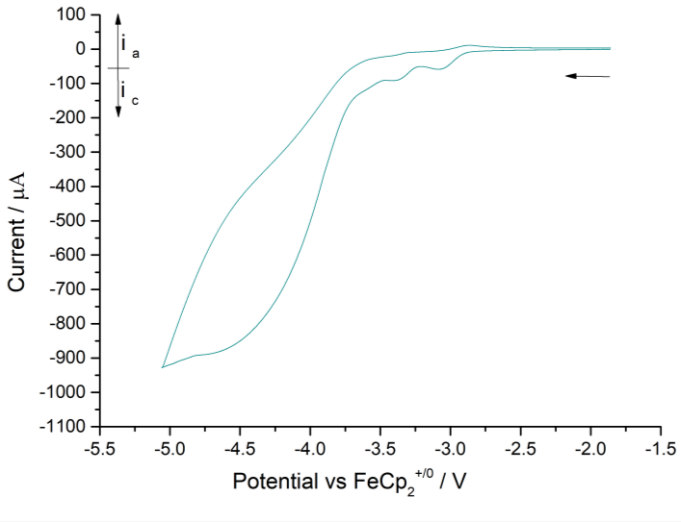

Figure 5.10 CV scan for 0.005 M **5.2** in 0.05 M [^{n}NBu$_4$][BPh$_4$] / THF, scan rate 100 mV s^{-1}.

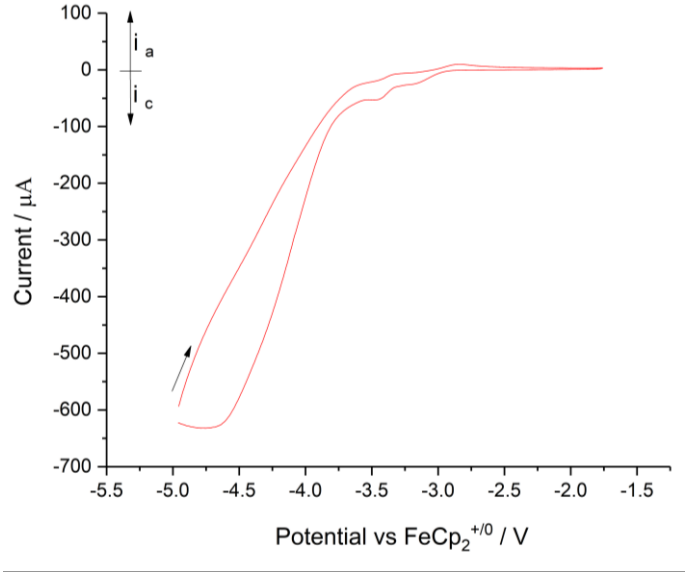

Figure 5.11 CV scan for 0.005 M **5.2** in 0.05 M [^{n}NBu$_4$][BPh$_4$] / THF, scan rate 200 mV s^{-1}.

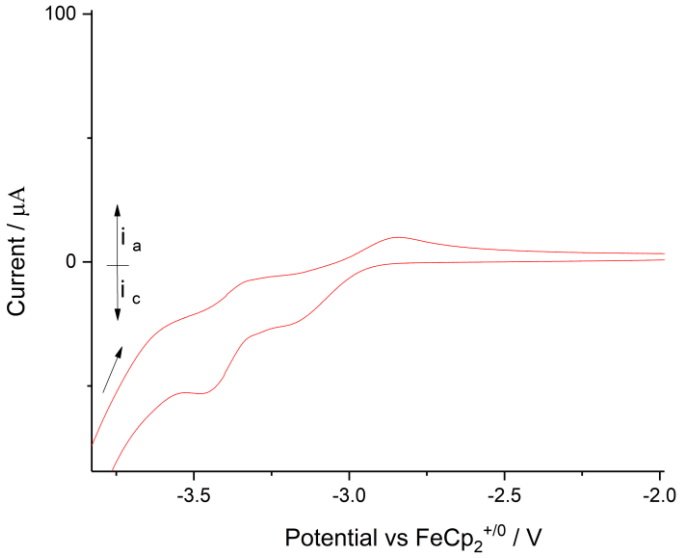

Figure 5.12 Zoomed in view of voltammogram in **Figure 5.11**.

5.2.3 Cyclic Voltammetry Studies on the Th^{IV}/Th^{III} Redox Couple

There is a paucity of electrochemical studies on known Th(III) complexes, therefore several Th(III) complexes were synthesised and studied using cycling voltammetry to enable comparisons with the electrochemical behaviour of **5.1** and **5.2**. These studies will also enable the comparison of different ligand systems and how they influence the Th^{IV}/Th^{III} reduction potential. Values often referenced for the estimated Th^{IV}/Th^{III} redox couple (-3.0 and -3.7 V *vs* SHE) date back to the 1970s and 1980s and are based on atomic spectroscopy and theoretical calculations,[26,27] but not voltammetry. In the absence of $E_{1/2}$ values for the Th^{IV}/Th^{III} redox couple, such potentials have been indirectly estimated by the

reaction of Th(III) complexes with substrates of known $E_{1/2}$ values.[28] This method offers an indirect way to gauge the minimum of this value but its obvious limitations such as steric properties of the substrates, are a hindering factor.

The lack of thorium electrochemistry studies is partly due to the rarity of thorium complexes in the +3 oxidation state and the incompatibility with common electrolytes such as [^{n}Bu$_4$N][PF$_6$]. For instance, we have previously observed that the Th^{IV} complex ThCOT^{TIPS2}Cp*Cl displays an irreversible reduction wave at -3.33 V *vs* $FeCp_2^{+/0}$ in [^{n}Bu$_4$N][PF$_6$] / THF but decomposes over several cycles.[12] Our group has had success using the more inert electrolyte, [^{n}Bu$_4$N][B(C$_6$F$_5$)$_4$],[29,30] with U(III) complexes which are stable on the electrochemical timescale over many cycles. Unfortunately, this was not the case when this electrolyte was used to study such processes with various Th(IV) complexes (**Figure 5.13** and **Figure 5.14**) and therefore a different electrolyte was sought.

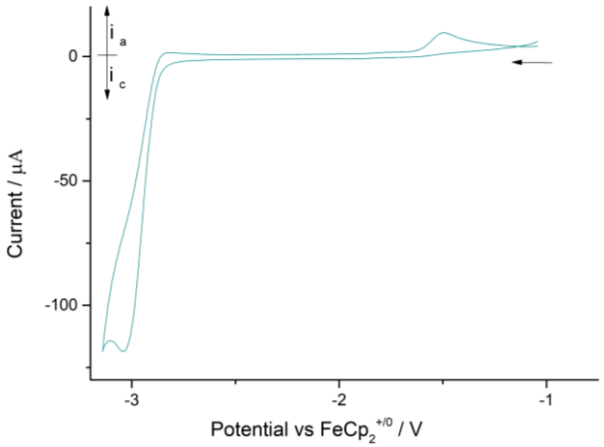

Figure 5.13 CV scan for 0.005 M ThCp$^{TMS2}_3$Cl in 0.05 M [^{n}Bu$_4$N][B(C$_6$F$_5$)$_4$] / THF, scan rate 200 mV s^{-1}.

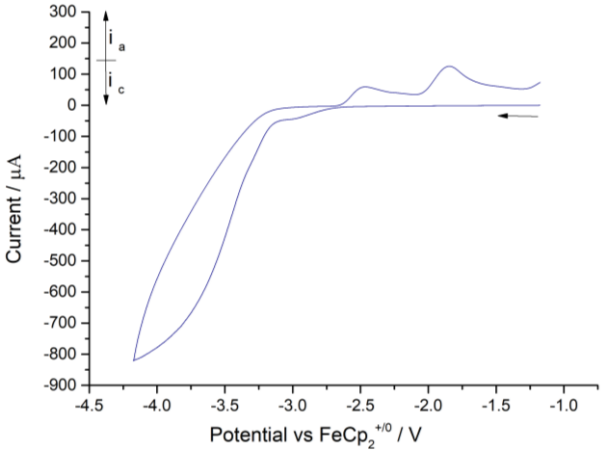

Figure 5.14 CV scan for 0.005 M $ThCOT^{TBDMS2}{}_2$ in 0.05 M [^{n}Bu$_4$N][B(C$_6$F$_5$)$_4$] / THF, scan rate 200 mV s^{-1}.

Due to the fluorophilic nature of thorium we postulated that an electrolyte devoid of fluorides had to be used to increase current response and stability of the analyte. Arnold *et al.* have reported the use of [^{n}Bu$_4$N][BPh$_4$] to successfully study electrochemical processes in uranium compounds.[31,32] We decided to test the viability of [^{n}Bu$_4$N][BPh$_4$] as an electrolyte and to our delight it proved highly compatible; for example a sample of $ThCp^{TMS2}{}_3$ in 0.05 M [^{n}Bu$_4$N][BPh$_4$] / THF was stable over a 24 hour period. Therefore, we decided to use this electrolyte in the investigation of the Th^{IV}/Th^{III} redox couple using CV. Gratifyingly, it allowed us to study a range of Th(IV) compounds that are precursors to known Th(III) complexes as well as an authentic Th(III) complex (**Figure 5.15**). Tables of electrochemical parameters are given in the experimental section of this chapter.

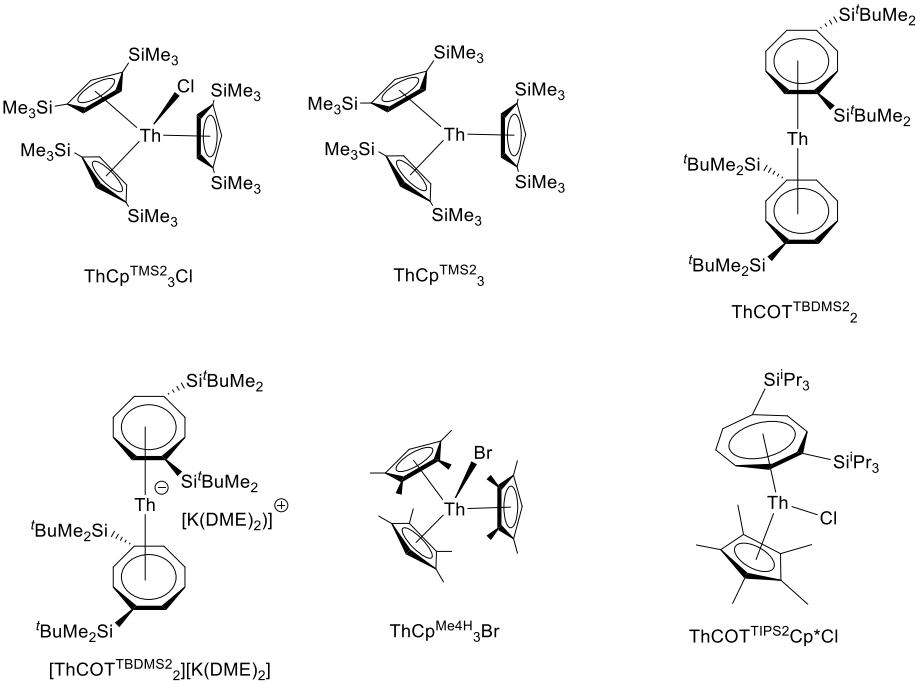

Figure 5.15 Thorium compounds included in this electrochemical study.

Table 5.3 summarizes the results obtained from CV for the compounds depicted in **Figure 5.15**. As can be seen they all display processes between -2.92 and -3.29 V *vs* $FeCp_2^{+/0}$ which we assign to the Th^{IV}/Th^{III} redox couple and are indicative of strongly reducing metal centres.[28]

Table 5.3: Thorium compounds and their Th^{IV}/Th^{III} redox couples.

Compound	**Th^{IV}/Th^{III} redox couple *vs* $FeCp_2^{+/0}$ / V**
$ThCp^{TMS2}{}_3Cl$ [4]	-2.92
$ThCp^{TMS2}{}_3$ [4]	-2.95
$ThCOT^{TBDMS2}{}_2$ [5]	-3.21
$[ThCOT^{TBDMS2}{}_2][K(DME)_2]$[5]	n/a
$ThCp^{Me4H}{}_3Br$ [7]	-3.23
$ThCOT^{TIPS2}Cp^*Cl$ [12]	-3.29

ca 0.005 M analyte in 0.05 M [^{n}Bu$_4$N][BPh$_4$] / THF.

For example, the cyclic voltammogram of $ThCp^{TMS2}{}_3Cl$ (**Figure 5.16**, right) features a process at -2.92 V *vs* $FeCp_2^{+/0}$ which is in excellent agreement with voltammograms obtained for $ThCp^{TMS2}{}_3$ (**Figure 5.16**, left and **Figure 5.17**) which display a process at -2.95 V *vs* $FeCp_2^{+/0}$. The voltammogram of $ThCp^{TMS2}{}_3$ in **Figure 5.17** also features a process at a very negative potential (*ca* -3.3 V *vs* $FeCp_2^{+/0}$) with a very small current response. Electrochemical studies on [2.2.2-Cryptand][$ThCp^{TMS2}{}_3$] would provide further information which may verify this assignment as a Th^{III}/Th^{II} redox process.[33] These two compounds also feature a process at *ca* -1.4 V *vs* $FeCp_2^{+/0}$ (**Figure 5.17**) which we attribute to a ligand based process. $ThCp^{TMS2}{}_3$ also features an irreversible reduction at -2.2 V *vs* $FeCp_2^{+/0}$ which is only observed when scanning oxidatively. Linear dependence of i_{pa} versus $\nu_{1/2}$ (**Figure 5.18**) for the Th^{IV}/Th^{III} redox couple in the voltammogram of $ThCp_3{}^{TMS2}Cl$ indicates the process is diffusion controlled and the observed increase in ΔE_{pp} with increasing ν is consistent with quasi-reversible electron-transfer kinetics (Table S4, experimental section).

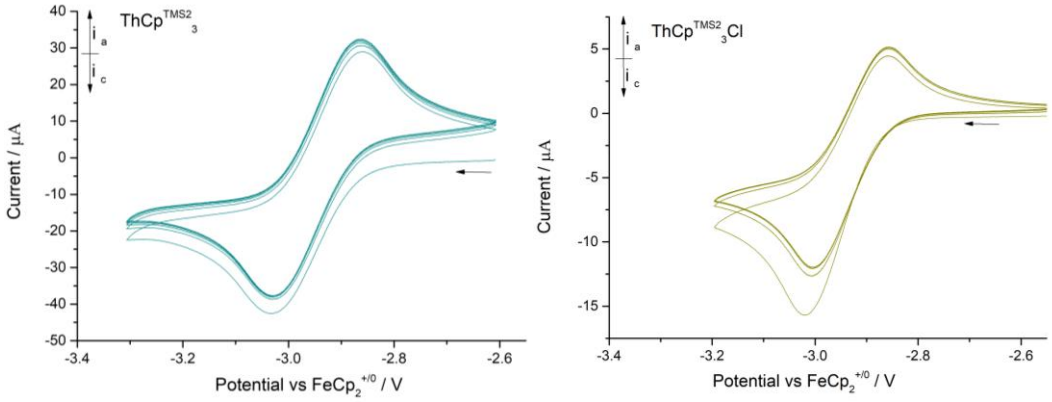

Figure 5.16 Overlaid CV scans for $ThCp^{TMS2}{}_3$ (6 cycles, 7 mM) (left) and $ThCp^{TMS2}{}_3Cl$ (5 cycles, 3 mM) (right) in 0.05 M [^{n}Bu$_4$N][BPh$_4$] / THF, scan rate 100 mV s^{-1}. $ThCp^{TMS2}{}_3$ $|i_{pa}/i_{pc}|$ = 0.90, $ThCp^{TMS2}{}_3Cl$ $|i_{pa}/i_{pc}|$ = 0.80.

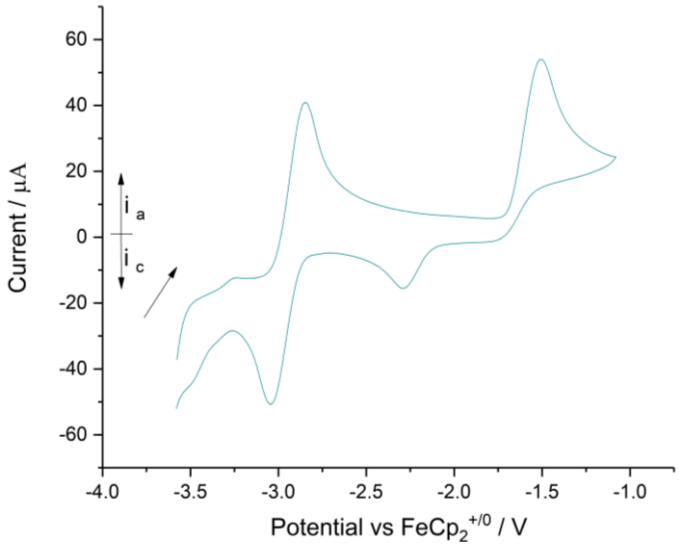

Figure 5.17 CV scan for $ThCp^{TMS2}{}_3$ in 0.05 M [^{n}Bu$_4$N][BPh$_4$] / THF, scan rate 200 mV s^{-1}.

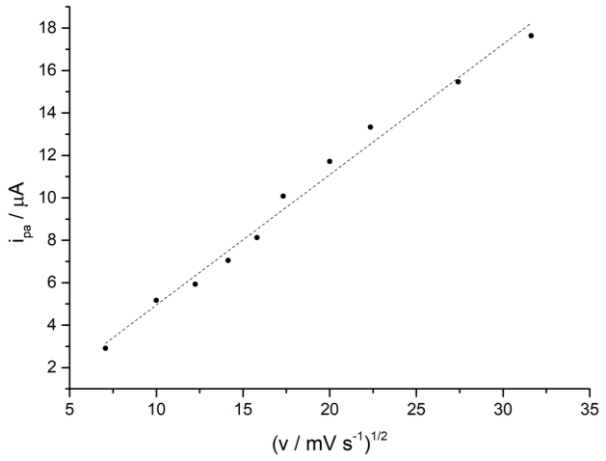

Figure 5.18 Plot of i_{pa} versus $v^{1/2}$ for the Th^{III}/Th^{IV} process in the CV of $ThCp^{TMS2}{}_3Cl$. R^2 = 0.9881.

In comparison to $ThCp^{Me4H}{}_3Br$ (**Table 5.3**), $ThCp^{TMS2}{}_3Cl$ is easier to reduce as expected for a less electron rich cyclopentadienyl ligand. Such an effect has been observed in the La(III) complexes ($LaCp^{tBu2}{}_3$ $E_{1/2}$ = -3.1 V *vs* $FeCp_2{}^{+/0}$, $LaCp^{TMS2}{}_3$ $E_{1/2}$ = -2.8 V *vs* $FeCp_2{}^{+/0}$).[34,35] In more detail, cathodic scans of $ThCp^{Me4H}{}_3Br$ in the same solvent and electrolyte system revealed a quasi-reversible process at -3.23 V *vs* $FeCp_2{}^{+/0}$ (**Figure 5.19**), this process has a very small anodic current response (i_{pa}/i_{pc} = 0.14) indicating that the electrochemically generated species on the anodic wave is unstable. This complex also displays three irreversible oxidation processes which we are unable to assign with any certainty.

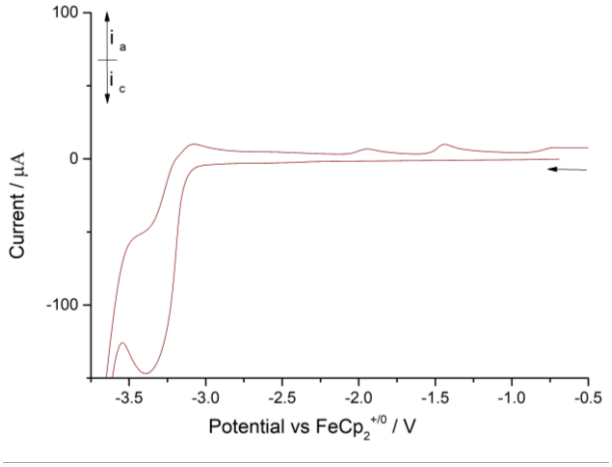

Figure 5.19 CV scan for $ThCp^{Me4H}{}_3Br$ in 0.05 M [^{n}Bu$_4$N][BPh$_4$] / THF, scan rate 100 mV s^{-1}.

In the case of $ThCOT^{TBDMS2}{}_2$ its CV features a quasi-reversible process at -3.21 V *vs* $FeCp_2{}^{+/0}$ (**Figure 5.20**). Further ligand-based processes at -0.88 and 0.72 V *vs* $FeCp_2{}^{+/0}$ were also observed.

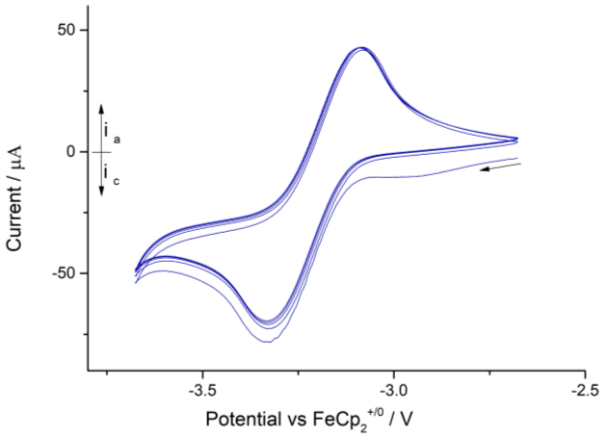

Figure 5.20 Overlaid CV scans (5 cycles) for $ThCOT^{TBDMS2}{}_2$ in 0.05 M [^{n}Bu$_4$N][BPh$_4$] / THF, scan rate 100 mV s^{-1}.

Unfortunately, we were unable to study the redox behavior of [$ThCOT^{TBDMS2}{}_2$][K(DME)$_2$] by CV due to rapid decomposition of the analyte evidenced by an immediate change of colour from dark green to pale yellow with significant amounts of precipitate (**Figure 5.21**).

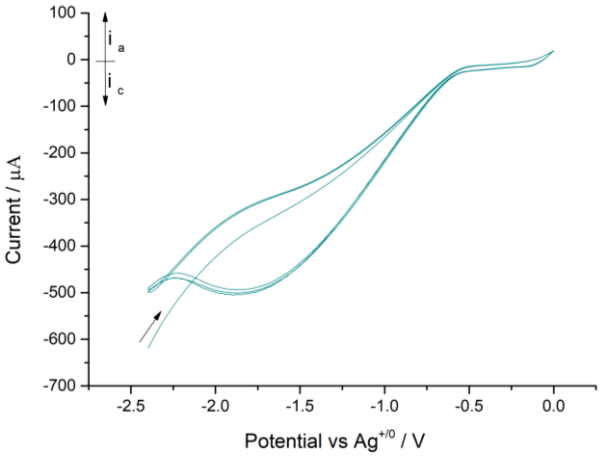

Figure 5.21 Overlaid CV scans (3 cycles) for [$ThCOT^{TBDMS2}{}_2$][K(DME)$_2$] in 0.05 M [^{n}Bu$_4$N][BPh$_4$] / THF, scan rate 200 mV s^{-1}.

$ThCOT^{TIPS2}$Cp*Cl displays a quasi-reversible process at -3.29 V *vs* $FeCp_2^{+/0}$ that has a decreasing current response over several cycles, (**Figure 5.22**) and is in good agreement with the irreversible reduction we previously reported for this compound.[12] $ThCOT^{TIPS2}$Cp*Cl exhibits an irreversible process at -1.49 V *vs* $FeCp_2^{+/0}$ which we assign as a ligand-based process.

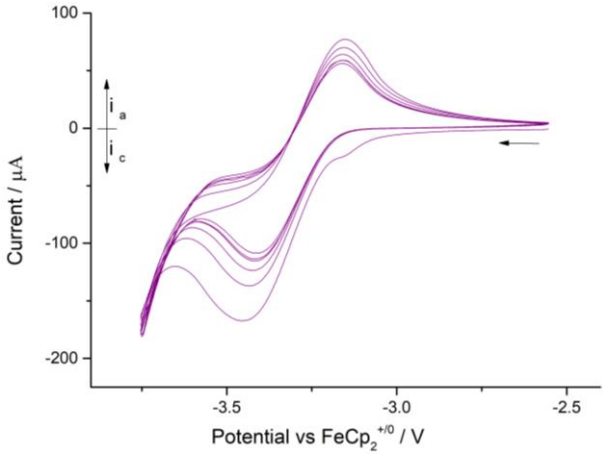

Figure 5.22 Overlaid CV scans (6 cycles) for ThCOT^{TIPS2}Cp*Cl in 0.05 M [^{n}Bu$_4$N][BPh4] / THF, scan rate 200 mV s^{-1}.

The Th^{IV}/Th^{III} redox couples studied range from -2.92 to -3.29 V *vs* FeCp$_2^{+/0}$ and are indicative of extremely reducing metal centres which are well placed to activate substrates. Compounds **5.1** and **5.2** also feature an extremely negative reduction process (-2.90 V *vs* FeCp$_2^{+/0}$) which is comparable to the Th^{IV}/Th^{III} redox couple of ThCp$_3^{TMS2}$ (-2.92 V *vs* FeCp$_2^{+/0}$). These two compounds also display a process at *ca* -3.3 V *vs* FeCp$_2^{+/0}$ which is similar to the possible Th^{III}/Th^{II} process observed in the voltammogram of ThCp$_3^{TMS2}$.

5.3 Thorium- *p*Me$_2$O$_2$ Coordination Chemistry

5.3.1 Attempts Towards ThCp*(*p*Me$_2$O$_2$)

The previous section showed that it was possible to synthesise a thorium-*p*Me$_2$O$_2$ complex (**5.2**) that features an extremely reducing formally Th(III) centre. Inspired by this result and the synthesis of UCp*(*p*Me$_2$O$_2$) **3.3**, the analogous thorium complex, ThCp*(*p*Me$_2$O$_2$), was targeted.

There are several plausible synthetic routes to synthesise ThCp*(*p*Me$_2$O$_2$), starting from ThCp*(*p*Me$_2$O$_2$)X (X = Cl, Br or I) prior to reduction. Two sensible retrosynthetic procedures to synthesise ThCp*(*p*Me$_2$O$_2$)X are outlined in **Scheme 5.3**, the first of which, a) (**Scheme 5.3**), will be discussed in the following section.

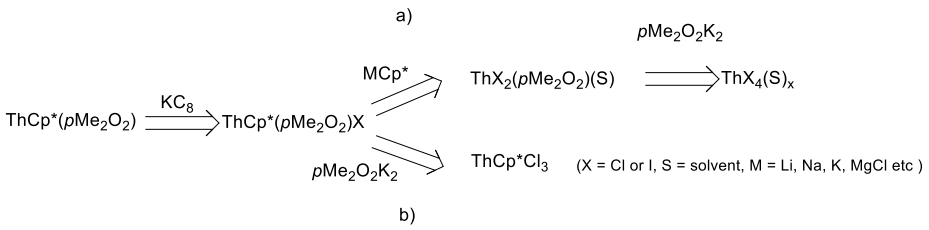

Scheme 5.3 Retrosynthesis of ThCp*(pMe$_2$O$_2$).

5.3.2 Synthesis, Characterisation, and Reactivity of ThI$_2$(pMe$_2$O$_2$)(THF) 5.3

A complex of the formula ThI$_2$(pMe$_2$O$_2$) would be an ideal precursor to ThCp*(pMe$_2$O$_2$)X for two reasons. Firstly, it is free of coordinating ethereal solvent, which are prone to activation by strongly Lewis-acidic thorium centres.[36] Secondly, iodide ligands are a superior leaving group to chlorides and more amenable to reduction. Unfortunately, it proved not possible to synthesise ThI$_2$(pMe$_2$O$_2$) as reactions between ThI$_4$ and one equivalent of pMe$_2$O$_2$K$_2$ in toluene produced **5.1**. The use of a coordinating solvent, either as a bulk solvent or as an adduct on thorium tetraiodide, was found to be essential in supressing the formation of **5.1**, as it stabilises adducts such as ThI$_2$(pMe$_2$O$_2$)(THF) and prevents their rearrangement to **5.1**.

Thus, ThI$_4$(THF)$_4$ was chosen as a suitable thorium halide precursor. Regrettably, the sample of ThI$_4$(THF)$_4$ had decomposed to ThI$_3$(OBuI)(THF)$_3$, as determined *via* ^{1}H NMR spectroscopy.[36] Despite this, reaction with pMe$_2$O$_2$K$_2$ in C$_6$H$_6$ at 85 °C yielded ThI$_2$(pMe$_2$O$_2$)(THF) (**5.3**), with small amounts of the side product Th(pMe$_2$O$_2$)$_2$. To produce **5.3** quantitatively, it was found that 1.2 equivalents of ThI$_3$(OBuI)(THF)$_3$ were required. This slight excess ensures that the formation of **5.1** is supressed *via* a ligand rearrangement to form exclusively **5.3**. This result was confirmed in the independent reaction of ThI$_3$(OBuI)(THF)$_3$ and Th(pMe$_2$O$_2$)$_2$, which produced **5.3** in approximately 20% yield.

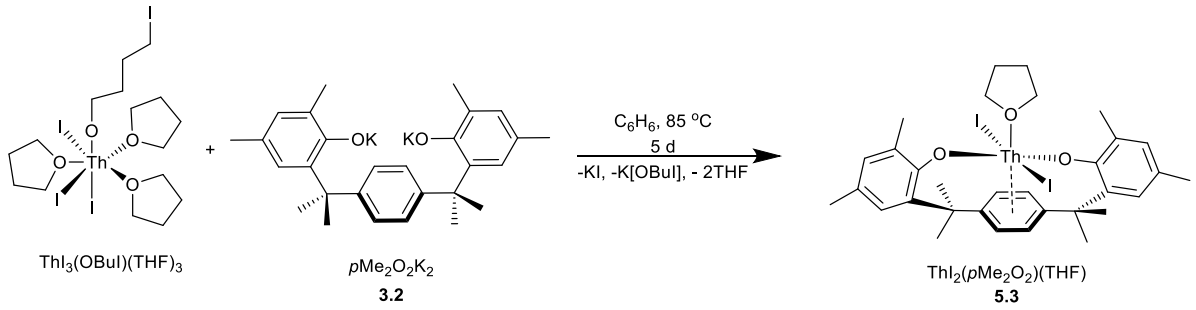

Figure 5.23 Synthesis of **5.3**.

The synthesis of **5.3** is easily scalable and after work-up, 3.2 g of the title compound could be isolated routinely as an off-white solid. NMR spectroscopic analysis (^{1}H and ^{13}C{^{1}H}) revealed the expected product. Elemental analysis was consistent with the proposed formulation. Unfortunately, **5.3** could not be observed by mass spectrometry (EI).

Single crystals of **5.3** suitable for X-ray diffraction studies were grown from a saturated solution of THF at -35 °C. Analysis of XRD data revealed **5.3** crystallised in the $P2_1/c$ space group with two independent molecules in the unit cell. The two independent molecules have similar metric parameters therefore the parameters for one of the molecules will be discussed.

The Th–$O_{aryloxide}$ bond lengths (2.141(6) and 2.127(5) Å) are ordinary and comparable to other thorium aryloxide complexes reported in literature (2.16 – 2.21 Å)[17,18,37], as are the Th–I bonds (**5.3**: 3.1205(7) and 3.1376(7) Å, selected literature: 3.155 – 3.165 Å)[36] while the Th–O(THF) bond is shorter in comparison to similar moieties found in the literature (**5.3**: 2.149(7) Å, selected literature: 2.474 - 2.549 Å[36,38]). More interestingly, **5.3** features a thorium-arene interaction as indicated by the centroid distance of 2.7177(3) Å, similar to other neutral complexes featuring a thorium-arene interaction (2.665 – 2.815(3) Å).[20,39]

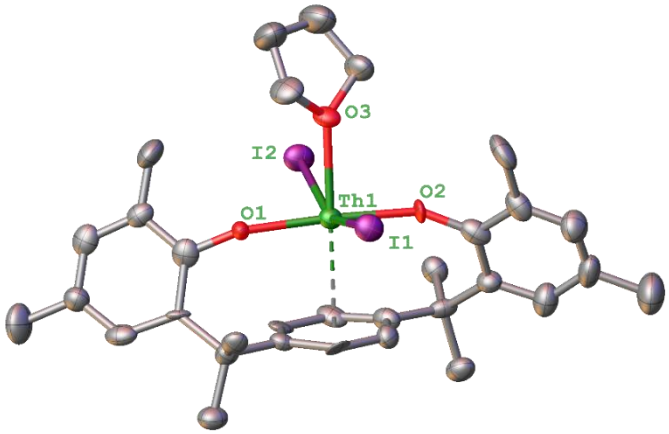

Figure 5.24 Molecular structure of **5.3**. Thorium, green; iodide, purple; oxygen, red; carbon, grey. Hydrogens and other molecule in the unit cell omitted for clarity and thermal ellipsoids given at 50% probability. Selected structural parameters (Å, deg): Th1–O1 = 2.141(6), Th1–O2 distance = 2.127(5), Th1–O3 distance = 2.419(7), Th1–I1 distance = 3.1205(7), Th1 to I2 distance = 3.1376(7), Th–Ct(arene) 2.7177(3).

With **5.3** in hand, reactivity towards Cp* transfer agents was explored. Compound **5.3** and one equivalent of MCp* (M = Li, Na, K or MgCl) were stirred in a benzene solution at room temperature. After 24 h, crude ^{1}H NMR spectroscopic data revealed the presence of unreacted **5.3**, small amounts of Th(*p*Me$_2$O$_2$)$_2$ and Cp*H. Using THF as the solvent had no effect on reactivity nor did alterations in temperature and stoichiometry of the reaction.

Upon heating to 85 °C and addition of excess MCp* (M = Li, Na, K, MgCl), complete consumption of **5.3** was observed with formation of Th(*p*Me$_2$O$_2$)$_2$ and peaks corresponding to a new species *via* ^{1}H NMR spectroscopy. EI-MS of crude reaction mixtures also confirmed the presence of a new species with an *m*/*z* value corresponding to the formulation ThCp*(*p*Me$_2$O$_2$)I. Unfortunately, isolation of this species *via* fractional crystallisation was unsuccessful, probably due to other by-products present in the crude reaction mixture.

During these endeavours the molecular structure of ThCp*(*p*Me$_2$O$_2$)(OBuCp*) was obtained from a reaction of **5.3** with KCp* in THF (**Figure 5.25**). Though the data was of poor quality, it was sufficient

to confirm connectivity. Isolation of bulk material was unfortunately not possible and thus no other spectroscopic or analytical data are available.

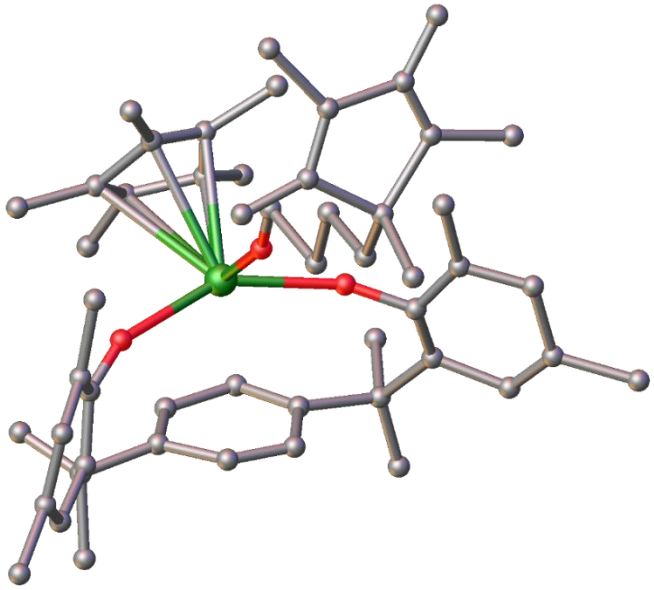

Figure 5.25 Molecular structure of ThCp*(*p*Me$_2$O$_2$)(OBuCp*). Th, green; oxygen, red; carbon, grey. Hydrogens omitted for clarity. Ellipsoids not shown due to poor quality of data.

There are two conceivable pathways for the formation of ThCp*(*p*Me$_2$O$_2$)(OBuCp*) (**Scheme 5.4**). One possible pathway involves the complex ThCp*(*p*Me$_2$O$_2$)(OBuI), formed by the activation of THF by ThCp*(*p*Me$_2$O$_2$)I, which then undergoes a salt metathesis reaction with KCp*. An alternative pathway is the sterically-induced reduction of THF mediated by ThCp*$_2$(*p*Me$_2$O$_2$) to generate the complex ThCp*(*p*Me$_2$O$_2$)(OBuCp*). Sterically induced reduction has been documented with bulky tris-cyclopentadienyl lanthanide and uranium compounds.[40,41] As both of these pathways involve the activation of THF, substitution for other coordinating solvents may assist efforts towards the synthesis of ThCp*(*p*Me$_2$O$_2$)I.

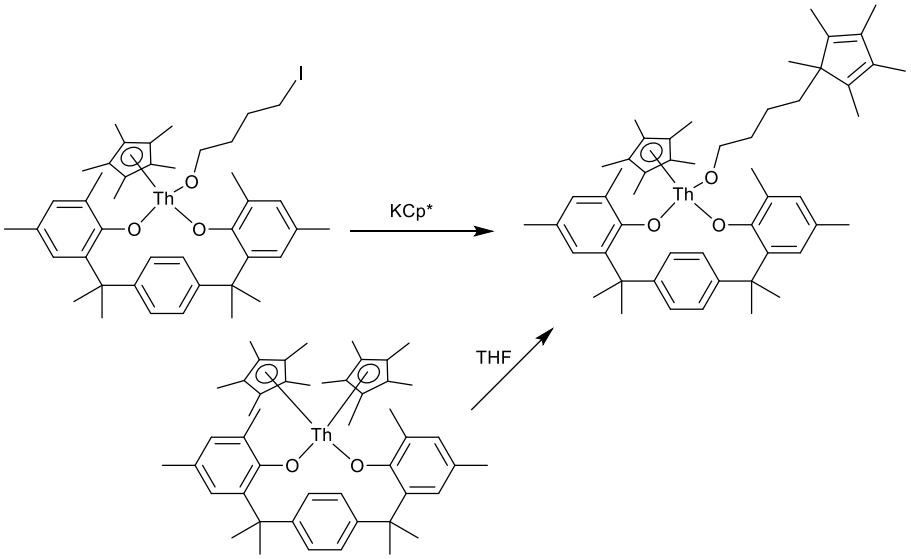

Scheme 5.4 Plausible pathways for the formation of ThCp*(*p*Me$_2$O$_2$)(OBuCp*).

In thorium chemistry, DME is often used in place of THF as a solvent in order to avoid activation of the latter.[38,42] With this in mind, a solution of **5.3** was stirred in thoroughly dried and degassed DME at room temperature overnight. ^{1}H NMR spectroscopy revealed the formation of a new species consistent with the formulation ThI$_2$(*p*Me$_2$O$_2$)(DME), plus 0.17 equivalents of *p*Me$_2$O$_2$H$_2$. It remains unclear as to why *p*Me$_2$O$_2$H$_2$ forms in such significant amounts. Unfortunately again, it was not possible to separate and purify ThI$_2$(*p*Me$_2$O$_2$)(DME) due to its similar solubility with *p*Me$_2$O$_2$H$_2$.

As further attempts to replace THF with DME yielded intractable mixtures, our attention was instead turned to Et$_2$O, to replace the coordinating THF. Compound **5.3** was stirred in Et$_2$O for 24 hours, evacuated to dryness and then the procedure repeated a further two times. ^{1}H NMR spectroscopy indicated the formation of a new species consistent with the formulation, ThI$_2$(*p*Me$_2$O$_2$)(Et$_2$O) **5.4**, although 0.6 equivalents of unreacted **5.3** were still present. Unfortunately, attempts to remove residual **5.3** through fractional crystallisation were in vain due to the large amount of co-crystallised **5.3** present as these two compounds have similar solubilities.

Despite this, the molecular structure of ThI$_2$(*p*Me$_2$O$_2$)(Et$_2$O) was obtained from X-ray suitable crystals grown from a saturated Et$_2$O solution at room temperature (**Figure 5.26**). Structural parameters are similar to **5.3**. As it was not possible to synthesis **5.4** cleanly, further reactivity studies involving Cp* transfer agents were not carried out.

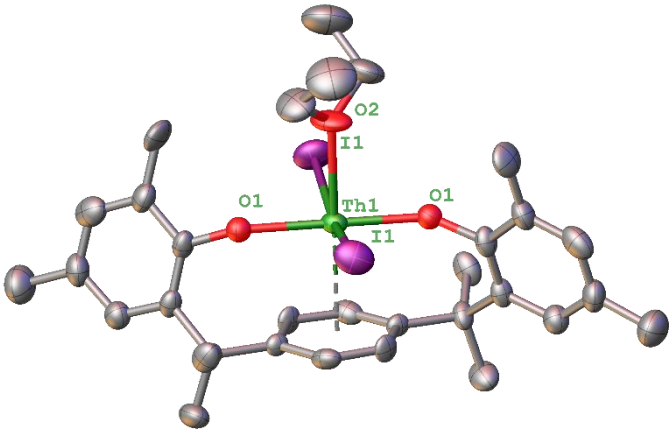

Figure 5.26 Molecular structure of **5.4**. Thorium, green; iodide, purple; oxygen, red; carbon, grey. Hydrogens omitted for clarity and thermal ellipsoids given at 50% probability. Selected structural parameters (Å, deg): Th1–I1 = 3.1249(9), Th–O1 = 2.145(9), Th–O2 = 2.460(14), Th–Ct(arene) = 2.7063(4).

5.3.3 Synthesis, Characterisation, and Reactivity of $ThI_2(pMe_2O_2)ITMe$

In continual efforts to synthesise an appropriate precursor to $ThCp^*(pMe_2O_2)I$, a ligand with stronger donor properties and lacking oxygen atoms was targeted, as this may provide cleaner reactivity towards Cp* transfer agents. NHC ligands have found applications in a variety of research areas due to their electron-rich and strong σ-donating nature, in contrast to classical ligands such as phosphines.[43] NHC complexes of thorium are rare by comparison and only a handful have been reported, all of which feature a tethered NHC unit incorporated into anionic ligands.[44–49]

$Th(L)_4$ (L = $[OCMe_2CH_2(1\text{-}C\{NCHCHN^iPr\})]$) (**Figure 5.27**, left) contains four alkoxy-tethered NHC ligands that coordinate around the thorium metal in a square-antiprismatic fashion. Th–C bond lengths range from 2.852(6) Å to 2.884(5) Å.[44] In 2016, Arnold *et al*. synthesised the bis(NHC)borate complex, $Th(Bc^{Mes})_2I_2$ (**Figure 5.27**, right)[45] with Th–$C_{carbene}$ bond lengths ranging from 2.623(6) to 2.634(6) Å.

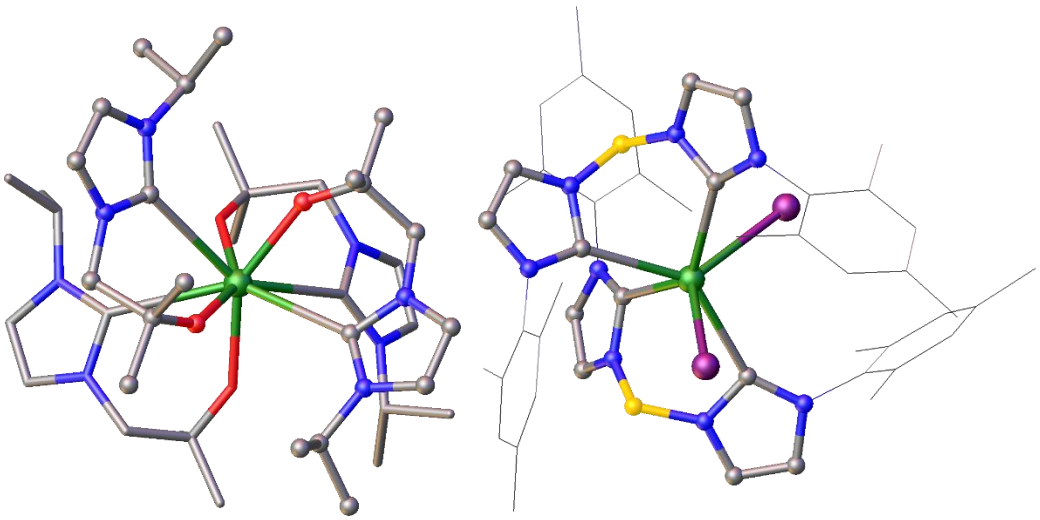

Figure 5.27 Molecular structures of $Th(L)_4$ (left) and $Th(Bc^{Mes})_2I_2$ (right). Thorium, green; iodide, purple; oxygen, red; nitrogen, blue; boron, yellow; carbon, grey. Thermal ellipsoids, hydrogens and parts of molecular structures deemphasised for clarity. Molecular structures are from references [44,45].

ITMe was chosen for its small size and strongly σ-donating ability in order to substitute the THF ligand in **5.3**. Reaction of **5.3** with ITMe resulted in the formation of a white suspension (**Scheme 5.5**) that *via* NMR spectroscopy was consistent with the formulation $ThI_2(pMe_2O_2)$(ITMe) **5.5**. A distinctive $^{13}C_{carbene}$ shift of 210.2 ppm was observed, in agreement with other Th-NHC complexes.[44,45] The molecular ion peak of **5.5** was not observed *via* mass spectrometry analysis. Elemental analysis results were consistently low in carbon. This has been previously been observed in other organothorium complexes.

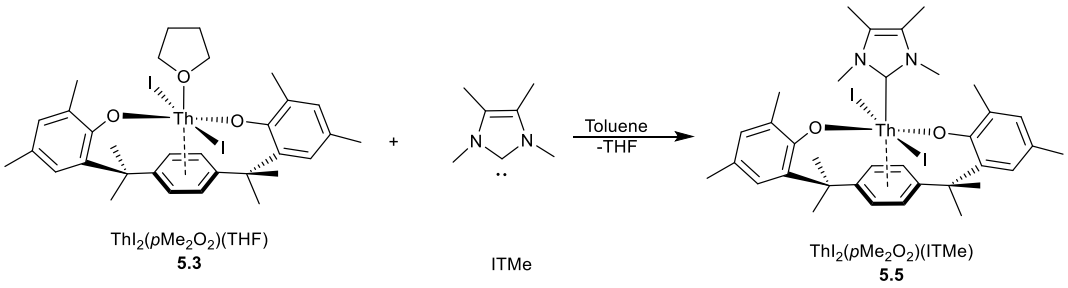

Scheme 5.5 Synthesis of $ThI_2(pMe_2O_2)$(ITMe) **5.5**.

Colourless crystals of **5.5** were obtained by Mr Ryan Brown from a concentrated solution of toluene with the molecular structure shown below in **Figure 5.28**.[50] Unsurprisingly, there are similarities

between the structure of **5.5** and **5.3** and **5.4** as shown by similar Th–O, Th–I and Th–Ct(arene) distances. The Th–C1 distance of 2.625(9) is similar to the Th–C(NHC) distances in $Th(Bc^{Mes})_2I_2$ (2.623(6) to 2.634(6) Å)[45] and shorter than the distances in $Th([OCMe_2CH_2(1\text{-}C\{NCHCHN^iPr\})])_4$ (2.852(6) Å to 2.884(5) Å)[44].

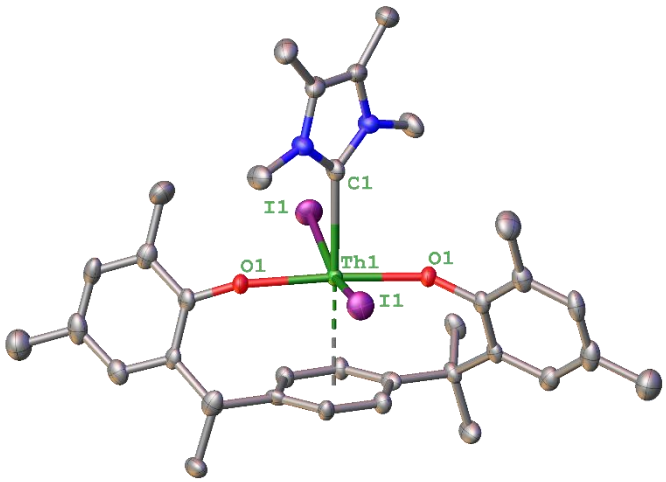

Figure 5.28 Molecular structure of **5.5**. Thorium, green; iodine, purple; oxygen, red; nitrogen, blue; carbon, grey. Hydrogen atoms omitted for clarity and thermal ellipsoids given at 50% probability. Selected structural parameters (Å): Th1–I1 = 3.31307(4), Th–O1 = 2.172(4), Th–Ct(arene) = 2.7548(3) and Th–C1 = 2.625(9).

Unfortunately, **5.5** displayed reactivity towards Cp* transfer agents akin to **5.3**. Large amounts of Cp*H and unreacted **5.5** were observed in the ^{1}H NMR spectrum of the crude reaction mixture. Reactivity of **5.3** and **5.5** towards MCp* suggest the iodide ligands may hinder the formation of $ThCp^*(pMe_2O_2)I$, possibly due to undesired solvent activation pathways. Therefore, synthesis of a chloride and THF-free analogue of **5.3** was pursued. It was anticipated that chloride ligands may alleviate solvent activation issues due to the increased Lewis-acidity of the chloride ligands in comparison to the iodide ligands. Also, coordinating DME as opposed to THF may also mitigate solvent activation due to its non-cyclic nature.

$ThCl_4(DME)_2$ was reacted with $pMe_2O_2K_2$ in DME (**Scheme 5.6**) to give $ThCl_2(pMe_2O_2)(DME)$ **5.6** as the major product. The ^{1}H spectrum of the crude reaction mixture revealed that the target complex and 0.25 equivalents of $pMe_2O_2H_2$ and 0.13 equivalents of $Th(pMe_2O_2)_2$ are present. Despite several

attempts, purification of **5.6** proved non-trivial therefore $^{13}C\{^{1}H\}$ NMR spectroscopy and elemental analysis were not attempted.

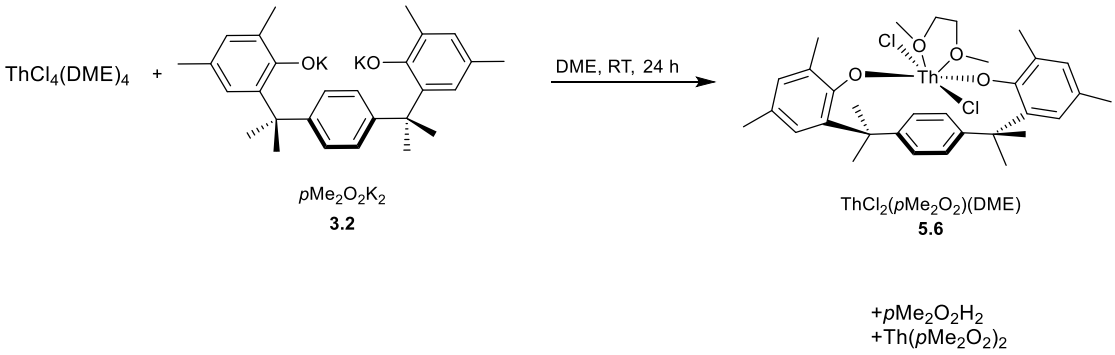

Scheme 5.6 Synthesis of $ThCl_2(pMe_2O_2)(DME)$ **5.6**.

Single crystals of **5.6** were grown from a saturated benzene solution at room temperature. The Th–Cl bond lengths (2.7334(6) and 2.7293(6) Å) are longer that in $ThCl_4(DME)_2$ (2.675(1) – 2.697(1) Å)[42], while the Th–O_{DME} bond lengths (2.579(5) and 2.578(6) Å) are similar to that in $ThCl_4(DME)_2$ (2.567(3) – 2.616(3) Å)[42]. The Th–Ct(arene) distance of 2.954(3) Å is remarkably longer than in **5.3** (2.707 Å) and **5.5** (2.7548(3) Å).

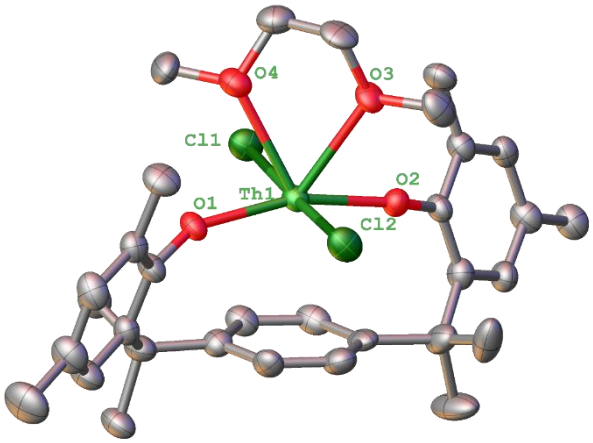

Figure 5.29 Molecular structure of **5.6**. Thorium, light green; chloride, dark green; oxygen, red; carbon, grey. Hydrogens and residual solvent molecules omitted for clarity and thermal ellipsoids given at 50% probability. Selected structural parameters (Å): Th1–Cl1 = 2.7334(6), Th1–Cl2 = 2.7293(6), Th1–O1 = 2.177(6), Th1–O2 = 2.175(6), Th1–O3 = 2.579(5), Th1–O4 = 2.578(6), Th–Ct(arene) = 2.954(3).

5.3.4 Attempted synthesis of ThCp*(*p*Me_2O_2)Cl from ThCp*Cl_3

As outlined in **Scheme 5.3**, another potential route towards ThCp*(*p*Me_2O_2)Cl involves ThCp*Cl_3. Our group has previously used ThCp*Cl_3 as a precursor in the synthesis of ThCp*COT^{TIPS2}Cl so it was proposed that this methodology could be applied to ThCp*(*p*Me_2O_2)Cl.[12]

A THF slurry of *p*$Me_2O_2K_2$ was added to a -40 °C THF solution of ThCp*Cl_3 over the course of 30 minutes. The reaction mixture was left to stir overnight, after which time an aliquot was taken and analysed by ^{1}H NMR spectroscopy and EI-MS. ^{1}H NMR spectroscopy revealed significant amounts of *p*$Me_2O_2H_2$ and Th(*p*Me_2O_2)$_2$ and small amounts of unassignable peaks. Due to the high quantities of undesired side products, isolation of the new products was not pursued. Instead, toluene was used in place of THF, but again this gave similar results. One possibility would be to use lithium, sodium or even thallium salts of *p*$Me_2O_2^{2-}$ as transfer agents, as potassium salts potentially interfere with salt metathesis reactions due to their nucleophilicity. Unfortunately, due to time constraints this was not carried out.

5.3.5 Synthesis and Characterisation of Th(*p*Me_2O_2)N''$_2$ 5.7

The *p*Me_2O_2 ligand scaffold is an ideal candidate to investigate thorium coordination chemistry and arene interactions due to the proximity of the central arene ring to thorium. Silyl-amide ligands such as (N'' = (N($SiMe_3$)$_2$) are commonly used in inorganic chemistry as they increase the solubility of complexes in hydrocarbon solvents, impart crystallinity and increase volatility to aid purification *via* sublimation. Moreover, the ^{29}Si nucleus provides a useful 'handle' for NMR spectroscopy.

The synthesis of **5.7** was achieved by the reaction of **5.3** and two equivalents of KN'' in C_6H_6 at room temperature. ^{1}H, ^{13}C{^{1}H} and ^{29}Si{^{1}H} NMR spectroscopy indicated **5.7** is C_{2v}-symmetric in solution. The expected parent ion was observed in EI mode mass spectrometry with the expected isotope envelope. Unfortunately, crystalline samples of **5.7** returned values low for %C. This has previously been observed for other silicon rich f-element compounds.[51]

Single crystals of **5.7** suitable for X-ray diffraction studies were grown from a TBME/hexane solution at -35 °C, the molecular structure of which is shown below in **Figure 5.30**. The thorium metal centre is in a pseudo-tetrahedral geometry. Complex **5.7** features a Th–Ct(arene) distance of 2.91891(18) Å, *ca* 0.2 Å longer compared to **5.3** (2.7177(3) Å) and **5.7** (2.7548(3) Å).

The Th–N bond distance of 2.326(4) Å is slightly longer than that in ThN''$_3$Cl (2.2923(17) Å),[52] possibly caused by the increased steric bulk of the *p*Me$_2$O$_2$ ligand. In **5.7** the Th–O bond length (2.207(3) Å) is slightly longer than **5.3** and **5.5**. The O–Th–O angle of 162.45(19)° is more acute than in **5.3** (176°(average)).

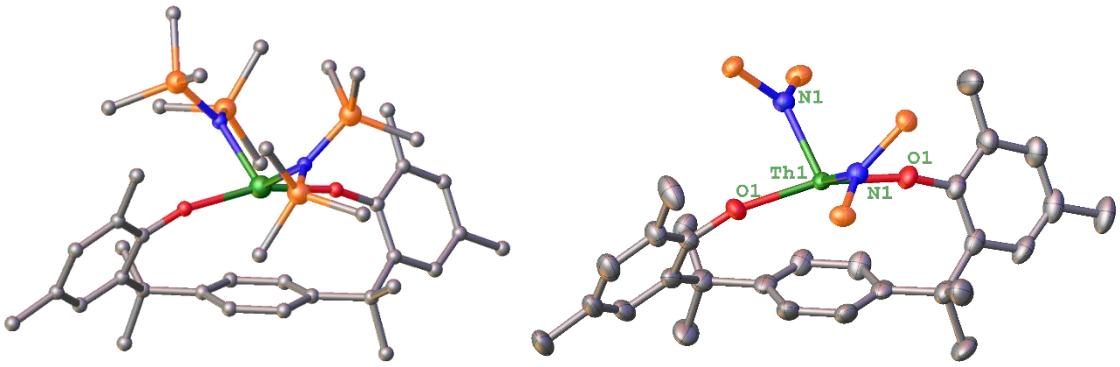

Figure 5.30 Grown molecular structure of **5.7** shown, image on left drawn as ball and stick model with no labels for clarity. Methyl groups of the N'' are omitted for clarity on the image on the right. Thermal ellipsoids are given at 50% probability. Thorium, green; oxygen, red; nitrogen, blue; silicon, orange; oxygen, red; carbon, grey. Hydrogens omitted for clarity. Selected structural parameters (Å, °): Th1–O1 = 2.207(3), Th1–N1 = 2.326(4), Th–Ct(arene) = 2.91891(18), O1–Th1–O1 = 162.45(19), N1–Th–N1 = 118.80(19).

Compound **5.7** was reacted with TMSCl with the aim of synthesising the base-free dichloride complex ThCl$_2$(*p*Me$_2$O$_2$). Unfortunately, ^{1}H NMR spectroscopic data indicated no reaction had occurred between a C$_6$D$_6$ solution of **5.7** and one equivalent of TMSCl, even when heated to 85 °C overnight.

5.3.6 Synthesis and characterisation of Th(*p*Me$_2$O$_2$)Bz$_2$ 5.8

Organothorium complexes have been earmarked for potential use in organic synthesis and catalysis. For example, thorium-alkyl complexes in particular are used as catalysts for the polymerisation of cyclic esters.[53–55]

Benzyl complexes of thorium are easily prepared by salt metathesis from KBz (potassium benzyl) and an appropriate thorium halide complex such as $ThCp_2^{2tBu}Cl_2$, as shown by Ren *et al*..[56] A benzene slurry of **5.3** and two equivalents of KBz was vigorously stirred for 24 h to yield Th(*p*Me$_2$O$_2$)Bz$_2$ (**5.8**). ^{1}H and ^{13}C{^{1}H} NMR spectroscopy indicated **5.8** is both Bz ligands and all four protons in the central arene are ring equivalent. Unfortunately, the molecular ion of **5.8** was not observed in EI-MS. Elemental analysis results consistently returned low values for carbon despite the samples being pure by ^{1}H NMR spectroscopy. Single crystals of **5.8** suitable for X-ray diffraction studies were grown from a TBME (tert-butyl methyl ether) solution layered with hexane, the molecular structure of which is shown below in **Figure 5.31**.

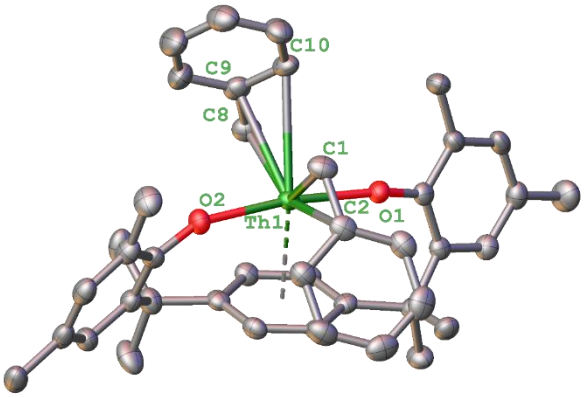

Figure 5.31 Molecular structure of **5.8**. Thorium, green; oxygen, red; carbon, grey. Hydrogens omitted for clarity. 50% thermal ellipsoids shown. Selected structural parameters (Å, °): Th1–C1 = 2.544(4), Th1–C8 = 2.547(5), Th1–O1 = 2.194(3), Th1–O2 = 2.190(3), Th1–Ct(arene) = 2.75971(16), Th1–C1 = 2.544(4), Th1–C2 = 2.960(4), Th1–C8 = 2.547(5), Th1–C9 = 2.840(4), Th1–C10 = 3.024(4), C1–Th–C8 = 123.72(15), Th1–C1–C2 = 91.1(3), Th1–C8–C9 = 86.1(3), O1–Th1–O = 171.86(11).

The two benzyl ligands in **5.8** are coordinated in a η^3 and η^2 fashion and the Th1–C1–C2 and Th1–C8–C9 angles of 91.1(3)° and 86.1(3)° are more acute than in $ThCp_2^{2tBu}Bz_2$ (129.3(2) and 134.6(2) Å)[56], due to the *p*Me$_2$O$_2$ scaffold of **5.8**. Th1–C1 and Th1–C8 distances of 2.544(4) and 2.547(8) Å are comparable to $ThCp_2^{2tBu}Bz_2$.[56] Complex **5.8** features a Th1–Ct(arene) distance of 2.75971(16) Å, similar to **5.3** and **5.5**, yet shorter than **6.3**.

With complex **5.8** in hand, reactivity towards small molecules was investigated in collaboration with Mr Ryan Brown. A C_6D_6 solution of **5.8** was exposed to 1 bar of H_2.[57] After 12 h, a peak at 17.98 ppm

was observed in the ^{1}H NMR spectrum, possibly suggesting the formation of a hydride complex.[18,58] The formation of toluene and the consumption of **5.8** was observed after 3 d. Unfortunately, the hydride species was also consumed after 3 d. Formation of a hydride species is assumed to form *via* a sigma-bond metathesis pathway.

Attempts to optimise reaction conditions and increase the yield of the hydride species failed. Further addition of more H_2 and leaving the reaction mixture to stir for a longer period of time resulted in the formation of significant amounts of **5.1** and toluene. In an attempt to access the transient hydride compound *via* another synthetic route, **5.3** was reacted with KH d_8-THF. As can be seen in **Figure 5.32**, the highlighted section of the downfield section of the ^{1}H NMR spectrum is complex. Unfortunately, **5.1** was again the major product (> 90%).

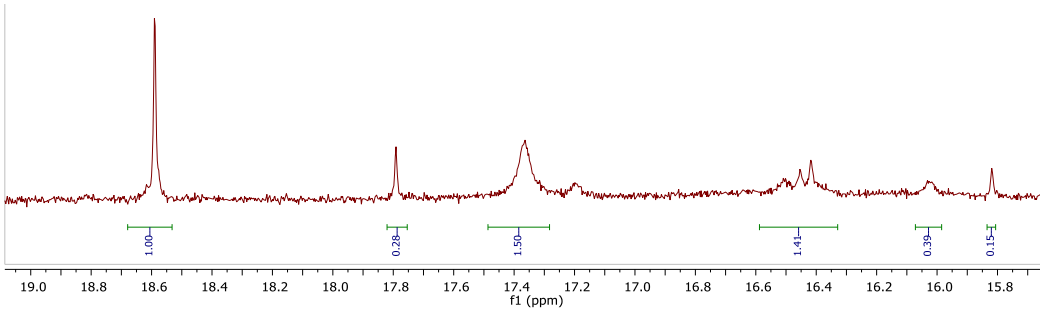

Figure 5.32 ^{1}H NMR spectrum of reaction between **5.3** and excess KH in d_8-THF.

Exposure of **5.7** to $^{13}CO_2$ resulted in the formation of a significant amount of Th(pMe$_2$O$_2$)$_2$ plus a new species, as observed by ^{1}H NMR spectroscopy. The ^{13}C{^{1}H} NMR spectrum displayed a peak at 167.23 ppm, consistent with a thorium benzyl-carboxylate species.[12] Only the parent ion peak for Th(pMe$_2$O$_2$)$_2$ was present in the EI-MS data. Unfortunately, it was not possible to isolate any new complexes *via* crystallisation.

5.4 Conclusions

In section 5.2 the synthesis and characterisation of homoleptic **5.1** was described which was subsequently reduced to **5.2**. Compound **5.2** features a δ bonding SOMO involving the thorium metal centre and the adjacent arene ring as indicated by EPR and DFT studies. Voltammograms of **5.1** and **5.2** show that both complexes feature a process at *ca* -2.90 V *vs* $FeCp_2^{+/0}$. In section 5.2.3 The first

measured values for the Th^{IV}/Th^{III} redox couple in organometallic complexes using cyclic voltammetry was reported. These studies indicate the thorium centre is highly reducing and that reduction potentials range from -2.92 to -3.29 V *vs* $FeCp_2^{+/0}$ and to the best of our knowledge this is the first example of such an investigation using CV.

In section 5.3 the synthesis and characterisation of six new thorium-*p*Me_2O_2 compounds was described. These complexes were characterised by NMR spectroscopy, single crystal XRD studies and in some cases EA and EI-MS. Unfortunately, attempted synthesis of ThCp*(*p*Me_2O_2)X (X = Cl or I) or precursors towards ThCp*(*p*Me_2O_2) were unsuccessful.

Experimental Details for Chapter Five

Synthesis of Th(*p*Me_2O_2)$_2$ 5.1

Et_2O (30 mL) was added to a mixture $ThBr_4(THF)_4$ (1.566 g, 1.86 mmol) and *p*$Me_2O_2K_2$ (1.809 g, 3.73 mmol) in a Schlenk flask. The mixture was allowed to warm to room temperature and stirred for 20 h. The solvent was removed *in vacuo* and the product extracted in toluene (3 x 25 mL) and filtered over Celite®. The solvent was removed to yield **1** as a white powder (1.64 g, 85%).

^{1}H NMR (399.5 MHz, d_6-benzene/drop of d_8-THF, 303 K): δ_H 7.82 (d, J_{HH} = 7.82 Hz, 4H, Ar-H), 7.46 (d, J_{HH} = 7.45 Hz, 4H, Ar-H), 7.12 (s, 4H, Ar-H), 6.99 (s, 4H, Ar-H), 2.32 (s, 12H, Ar-CH_3), 2.16 (s, 12H, Ar-CH_3), 1.61 (s, 12H, C-CH_3), 1.42 (s, 12H, C-CH_3).

^{13}C{^{1}H} NMR (125.7 MHz, d_6-benzene, 303 K): δ_C 159.9 (Ar C), 149.3 (Ar C), 134.0 (Ar C), 130.1 (Ar C), 129.6 (Ar C), 127.5 (Ar C-H), 126.6 ((Ar C), 124.4 (Ar C-H), 41.4 ($\underline{C}(CH_3)_2$), 32.2 (Ar-CH_3), 27.7 (Ar-CH_3), 20.9 (C($\underline{C}H_3)_2$), 18.0 (C($\underline{C}H_3)_2$).

Analysis calculated (found) for $C_{56}H_{64}O_4Th.(Toluene)_{0.7}$: % C 66.64 (66.56), H, 6.39 (6.48).

Synthesis of [K(2.2.2-cryptand)][Th(*p*Me_2O_2)$_2$] 5.2

To an ampoule containing **1** (100 mg, 0.0967 mmol), 2.2.2-cryptand (36.5 mg, 0.0969 mmol) and a glass-coated stirrer bar was added THF (1 mL). K/Hg (0.4% K, 1.233 g, 0.114 mmol, 1.17 eq.) was added and the mixture stirred for 1 hour upon which time a red solution had formed. The solution was filtered and dried *in vacuo*. Et_2O (0.7 mL) was added to the residues followed by THF (7 drops). This was followed by immediate deposition of large red crystals which were washed with toluene (3 x 3 mL) and Et_2O and dried. The compound was recrystallised a further three times in a similar manner.

Unable to assign ^{1}H NMR spectroscopic data due to the paramagnetic nature of the complex.

Analysis calculated (found) for $C_{74}H_{100}KN_2O_{10}Th$: % C 61.350 (60.899), H, 6.957 (6.790), N, 1.934 (1.742).

Synthesis of $ThI_2(pMe_2O_2)THF$ 5.3

An ampoule was charged with $ThI_3(OBuI)(THF)_3$ (4.066 g, 3.96 mmol), $pMe_2O_2K_2(Et_2O)_{0.207}$ (1.594 g, 3.23 mmol), benzene (30 mL) and heated at 75 °C for 3 days. The crude reaction mixture was extracted with hot toluene (4 x 30 mL), filtered through Celite®, followed by removal of all volatiles to yield the title compound as an off-white powder (3.117 g, 98.5%). Single crystals suitable for X-ray diffraction were grown from a saturated THF solution at -35 °C.

^{1}H NMR (399.5 MHz, d_6-benzene, 303 K): δ_H 7.60 (s, 4H, Ar-H), 7.06 (s, 2H, Ar-H), 6.93 (s, 2H, Ar-H), 4.28 (s, 4H, THF-H), 2.44 (s, 6H, Ar-Me), 2.31 (s, 6H, Ar-Me), 1.48 (s, 12H, $C(C\underline{H}_3)_2$), 1.26 (s, 4H, THF-H).

^{13}C {^{1}H} NMR (125.7 MHz, d_6-benzene, 303 K): δ_C 158.16 (Ar-C), 153.11 (Ar-C), 133.27 (Ar-C), 131.82 (Ar-CH), 130.92 (Ar-CH), 129.39 (Ar-C), 127.87, 127.41 (Ar-C), 124.44 (Ar-CH), 75.18 (THF-CH_2), 42.11($\underline{C}(CH_3)_2$, 30.53 (CH_3), 24.66 (THF-CH_2) , 21.29 (CH_3), 18.88 (CH_3).

EI-MS: Molecular ion not observed, only $Th(pMe_2O_2)_2$ was observed in the mass spectrum.

Analysis calculated (found) for $C_{32}H_{40}I_2O_3Th$: % C 40.10 (40.25), H, 4.21 (4.29).

Attempted synthesis of $ThI_2(pMe_2O_2)Et_2O$ 5.4

An ampoule was charged with **5.3** (300 mg, 0.306 mmol, Et_2O (50 mL) and stirred for 24 h. The resulting white suspension was evacuated to dryness and this procedure repeated a further two times. The white suspension was extracted in Et_2O (20 mL), filtered and stored at -35 °C. The molecular structure of **5.4** was obtained form this batch of crystals though unfortunately ^{1}H NMR analysis revealed the presence of *ca* 1.5 equivalents of **5.1**.

^{1}H NMR (399.5 MHz, d_6-benzene, 303 K): δ_H 7.57 (s, 2H, Ar–H), 7.13 (s, 4H, Ar–H), 6.83 (s, 2H, Ar–H), 4.23 (s, 4H, Et_2O), 2.55 (s, 6H, Ar–CH_3), 2.27 (s, 6H, Ar–CH_3), 1.52 (s, 12H, $C(CH_3)_2$), 1.02 (s, 6H).

Synthesis of ThI_2(*p*Me_2O_2)ITMe 5.5

ThI_2(*p*Me_2O_2)THF (308 mg, 314 mmol), ITMe (41 mg, 0.333 mmol) and toluene (30 mL) were added to an ampoule and stirred for 1 h after which time the crude reaction mixture was filtered and pumped to dryness. The reaction mixture was washed with pentane (3 x 1 mL) and dried for 1 h under vacuum. Crystals were obtained from a saturated toluene solution.

^{1}H NMR (399.5 MHz, d_6-benzene, 303 K): δ_H 7.74 (s, 4H, Ar-H), 6.98 (s, 2H, Ar-H), 3.76 (s, 6H, IT-CH_3), 2.55 (s, 6H, Ar-CH_3), 2.37 (s, 6H, Ar-CH_3), 1.65 (s, 12H, $C(CH_3)_2$), 1.11 (s, 6H, IT-CH_3).

^{13}C {^{1}H} NMR (125.7 MHz, d_6-benzene, 303 K): δ_C 210.24 (carbene), 158.49, 152.26, 133.97, 131.56, 130.97, 129.09, 127.64, 124.97, 124.52, 42.25, 38.34, 30.79, 21.29, 18.62, 8.08.

Elemental analysis results consistently returned low carbon values.

Synthesis of $ThCl_2$(*p*Me_2O_2)DME 5.6

An ampoule was charged with $ThCl_4(DME)_4$ (0.325 mg, 0.443 mmol), *p*$Me_2O_2K_2(Et_2O)_{0.207}$ (0.242 g, 0.489 mmol), DME (30 mL) and stirred for 3 days. The crude reaction mixture was extracted with benzene (4 x 30 mL), filtered through Celite®, followed by removal of all volatiles to yield the title compound as an off-white powder.

^{1}H NMR (399.5 MHz, d_6-benzene, 303 K): δ_H 7.60 (s, 4H, Ar-H), 7.06 (s, 2H, Ar-H), 6.93 (s, 2H, Ar-H), 4.28 (s, 4H, THF-H), 2.44 (s, 6H, Ar-Me), 2.31 (s, 6H, Ar-Me), 1.48 (s, 12H, $C(C\underline{H}_3)_2$), 1.26 (s, 4H, THF-H).

Synthesis of $ThI_2(pMe_2O_2)N''_2$ 5.7

$ThI_2(pMe_2O_2)THF(toluene)_{0.227}$ (300 mg, 0.306 mmol), KN'' (122 mg, 0.613 mmol) and toluene (10 mL) were added to an ampoule and stirred overnight. The reaction mixture was pumped to dryness, extracted with hexane (30 mL), filtered and dried *in vacuo* to give an off-white oil. The oil was triturated with TMS (5 mL) and pumped to dryness to give an off-white powder (137 mg, 47%).

^{1}H NMR (499.9 MHz, d_8-toluene, 303 K): δ_H 7.37 (s, 4H, Ar-H), 7.16 (s, 2H,Ar-H), 6.92 (s, 2H, Ar-H), 2.45 (s, 6H, Ar-CH_3), 2.28 (s, 6H, Ar-CH_3), 1.53 (s, 12H, $C(CH_3)_2$), 0.33 (s, 36H, Si-CH_3).

$^{13}C\{^1H\}$ NMR (125.7 MHz, d_8-toluene, 303 K): δ_C 160.28 (Ar-C), 135.77 (Ar-C), 131.27 (Ar-CH),128.22 (Ar-CH), 125.46 (Ar-CH), 42.17 (CH_3), 31.75 (CH_3), 5.64 (CH_3), 3.04 (CH_3). Several peaks are covered by solvent.

$^{29}Si\{^1H\}$ NMR (79.4 MHz, d_8-toluene, 303 K): δ_{Si} -9.38.

MS (EI)+: *m*/*z* 402 (M+).

Several batches of this compound were sent for combustion analysis and all results returned low carbon values, consistent with thorium carbide formation.

Synthesis of $ThI_2(pMe_2O_2)Bz_2$ 5.8

$ThI_2(pMe_2O_2)THF(toluene)_{0.227}$ (300 mg, 0.306 mmol), benzyl potassium (80.7 mg, 0.621 mmol) and toluene (8 mL) were added to an ampoule and stirred vigorously overnight by which time a yellow solution with white precipitate had formed. The crude reaction mixture was filtered and evacuated to dryness. The resulting yellow residue was extracted in TBME (5 mL), filtered to remove white solids, reduced to 1 mL and layered with hexane (3 mL). 3 d later large yellow crystals were deposited, the mother liquor was removed and the material washed with hexane (1 mL) to give the title compound (103 mg, 41%).

^{1}H NMR (499.9 MHz, d_6-benzene, 303 K): δ_H 7.14 (s, 2H, H-ArO), 7.07 (t, 4H, H_{para}-Ar(Bz)), 7.00 (s, 4H, H-Ar(central)), 6.93 (s, 2H, H-ArO), 6.83 (d, 4H, H_{ortho}-Ar(Bz)), 6.67 (t, 2H, H_{meta}-Ar(Bz)), 2.34 (s, 6H, CH_3-ArO), 2.32 (s, 6H, CH_3-ArO), 2.03 (s, 4H, C<u>H</u>$_2$Bz), 1.33 (s, 12H, C(CH_3)$_2$).

^{13}C {^{1}H} NMR (125.7 MHz, d_6-benzene, 303 K): δ_C 158.44(Ar C), 152.84 (Ar C), 149.41 (Ar C), 133.57 (Ar C), 131.65 (Ar CH/CH_3), 130.97 (Ar CH/CH_3), 128.87 (Ar CH/CH_3), 128.24 (Ar C) 127.27 (Ar C), 125.28 (Ar CH/CH_3), 124.26 (Ar CH/CH_3), 121.00 (Ar CH/CH_3), 75.54 (CH_2-Ar), 42.08 (<u>C</u>(CH_3)$_2$) , 30.77 (CH_3), 21.23 (CH_3), 18.25 (CH_3).

EI-MS: molecular ion peak not seen due to thermal instability.

Anal. Calcd for $C_{42}H_{46}O_2Th$: C, 61.907; H, 5.690. Found: C, 58.489; H, 5.711. This is an average from two samples (each ran twice) which were independently synthesized and spectroscopically pure prior to sample submission. The results obtained don't agree with spectroscopic evidence. We postulate low value for C content is due to thorium carbide formation as seen in other carbon rich thorium complexes.[5]

Cyclic Voltammetry Studies

$ThCp^{TMS2}{}_3Cl$,[4] $ThCp^{TMS2}$,[4] $ThCOT^{TBDMS2}{}_2$[5] and $ThCp^{Me4H}{}_3Br$[7] were prepared using standard literature procedures. Samples of [$ThCOT^{TBDMS2}{}_2$][$K(DME)_2$][1] and $ThCOT^{TIPS2}Cp^*Cl$[12] have been previously synthesised in our group.

Table S1 Electrochemical parameters for $ThCp^{TMS2}{}_3Cl$ in 0.05 M $[^nBu_4N][B(C_6F_5)_4]$ / THF, scan rate 200 mV s^{-1}.

	Process I	**Process II**
E_{pa} / V vs $FeCp_2^{+/0}$	-	-1.52
E_{pc} / V vs $FeCp_2^{+/0}$	-3.04	-
$E_{1/2}$ / V vs $FeCp_2^{+/0}$	-	-
ΔE_{pp} / mV	-	-
i_{pa} / µA	-	8
i_{pc} / µA	110	-
$\lvert i_{pa}/i_{pc} \rvert$	-	-

$\Delta E_{pp} = \lvert E_{pc} - E_{pa} \rvert$

Table S2 Electrochemical parameters for $ThCOT^{TBDMS2}{}_2$ in 0.05 M $[^nBu_4N][B(C_6F_5)_4]$ / THF, scan rate 200 mV s^{-1}

	Process I	**Process II**	**Process III**
E_{pa} / V vs $FeCp_2^{+/0}$	-	-2.47	-1.85
E_{pc} / V vs $FeCp_2^{+/0}$	-2.954	-	-
$E_{1/2}$ / V vs $FeCp_2^{+/0}$	-	-	-
ΔE_{pp} / mV	-	-	-
i_{pa} / µA	-	63	91
i_{pc} / µA	42	-	-
$\lvert i_{pa}/i_{pc} \rvert$	-	-	-

$\Delta E_{pp} = \lvert E_{pc} - E_{pa} \rvert$

Table S3 Electrochemical parameters for $ThCp^{TMS2}{}_3Cl$ in THF / 0.05 M [^{n}Bu$_4$][BPh$_4$].

	Process I	**Process II**
E_{pa} / V vs $FeCp_2^{+/0}$	-2.85	-1.41
E_{pc} / V vs $FeCp_2^{+/0}$	-3.00	-
$E_{1/2}$ / V vs $FeCp_2^{+/0}$	-2.92	-
ΔE_{pp} / mV	150	-
i_{pa} / µA	8	5
i_{pc} / µA	9	-
$\lvert i_{pa}/i_{pc} \rvert$	0.80	-

$\Delta E_{pp} = \lvert E_{pc} - E_{pa} \rvert$

Table S4 Table of parameters for variable scan rate studies of process I in $ThCp^{TMS2}{}_3Cl$.

v / mV s^{-1}	**E_{pa}**	**i_{pa}**	**E_{pc}**	**i_{pc}**	$\lvert i_{pa}/i_{pc} \rvert$	**v$^{1/2}$**	**ΔE_{pp}**
50	-2285	3	-2403	-8	0.343	7.071	-118
100	-2285	5	-2413	-10	0.495	10.000	-128
150	-2258	6	-2411	-12	0.492	12.247	-153
200	-2265	7	-2424	-13	0.528	14.142	-159
250	-2259	8	-2433	-16	0.519	15.811	-174
300	-2249	10	-2425	-15	0.670	17.321	-176
400	-2245	12	-2432	-17	0.692	20.000	-187
500	-2235	13	-2441	-19	0.718	22.361	-206
752	-2228	15	-2455	-20	0.757	27.423	-227
1000	-2237	18	-2469	-24	0.747	31.623	-232

Table S5: Electrochemical parameters for $ThCp^{TMS2}{}_3$ in THF / 0.05 M [^{n}Bu$_4$N][BPh4].

	Process I	**Process II**
E_{pa} / V vs $FeCp_2^{+/0}$	-2.86	-1.45
E_{pc} / V vs $FeCp_2^{+/0}$	-3.03	-
$E_{1/2}$ / V vs $FeCp_2^{+/0}$	-2.95	-
ΔE_{pp} / mV	170	-
i_{pa} / µA	27	41
i_{pc} / µA	30	-
$\lvert i_{pa}/i_{pc} \rvert$	0.90	-

$\Delta E_{pp} = \lvert E_{pc} - E_{pa} \rvert$

Large broad cathodic current response more negative than process I was observed in survey scans of $ThCp^{TMS2}{}_3$, we postulate this is due to decomposition of $ThCp^{TMS2}{}_3$ to Th(0) and Th(IV) species.

Table S6 Electrochemical parameters for $ThCOT^{TBDMS2}{}_2$ in THF / 0.05 M [^{n}Bu$_4$][BPh$_4$].

	Process I	**Process II**	**Process III**	**Process IV**
E_{pa} / V vs $FeCp_2^{+/0}$	-3.06	-2.20	-0.88	0.724
E_{pc} / V vs $FeCp_2^{+/0}$	-3.35	-		
$E_{1/2}$ / V vs $FeCp_2^{+/0}$	-3.21	-		
ΔE_{pp} / mV	290	-		
i_{pa} / µA	61	18	4	3
i_{pc} / µA	62	-		
$\lvert i_{pa}/i_{pc} \rvert$	0.98	-		

$\Delta E_{pp} = \lvert E_{pc} - E_{pa} \rvert$

Table S7 Electrochemical parameters for $ThCp^{Me4H}{}_3Br$ in THF / 0.05 M [^{n}Bu$_4$][BPh$_4$].

	Process I	**Process II**	**Process III**	**Process IV**
E_{pa} / V vs $FeCp_2^{+/0}$	-3.16	-1.95	-1.44	-0.60
E_{pc} / V vs $FeCp_2^{+/0}$	-3.35	-	-	-
$E_{1/2}$ / V vs $FeCp_2^{+/0}$	-3.23	-	-	-
ΔE_{pp} / mV	190	-	-	-
i_{pa} / µA	20	1.1	2	1.4
i_{pc} / µA	146	-	-	-
/ i_{pa}/i_{pc} /	0.14	-	-	-

$\Delta E_{pp} = | E_{pc} - E_{pa} |$

Table S8 Electrochemical parameters for $ThCOT^{TIPS2}Cp^*Cl$ in THF / 0.05 M [^{n}Bu$_4$N][BPh4].

	Process I	**Process II**
E_{pa} / V vs $FeCp_2^{+/0}$	-3.16	-1.49
E_{pc} / V vs $FeCp_2^{+/0}$	-3.42	-
$E_{1/2}$ / V vs $FeCp_2^{+/0}$	-3.29	-
ΔE_{pp} / mV	260	-
i_{pa} / µA	108	15
i_{pc} / µA	138	-
$\| i_{pa}/i_{pc} \|$	0.79	-

$\Delta E_{pp} = | E_{pc} - E_{pa} |$

5.5 References for Chapter Five

1 P. E. Kündig, Ed., *Transition Metal Arene π-Complexes in Organic Synthesis and Catalysis*, Springer-Verlag, Berlin Heidelberg, 2004.
2 H. S. La Pierre, A. Scheurer, F. W. Heinemann, W. Hieringer and K. Meyer, *Angew. Chem. Int. Ed.*, 2014, **53**, 7158–62.
3 D. P. Halter, F. W. Heinemann, J. Bachmann and K. Meyer, *Nature*, 2016, **530**, 317–321.
4 P. C. Blake, M. F. Lappert, J. L. Atwood and H. Zhang, *J. Chem. Soc. Chem. Commun.*, 1986, 1148–1149.
5 J. S. Parry, Cloke, S. J. Coles and M. B. Hursthouse, *J. Am. Chem. Soc.*, 1999, **121**, 6867–6871.
6 J. R. Walensky, R. L. Martin, J. W. Ziller and W. J. Evans, *Inorg. Chem.*, 2010, **49**, 10007–10012.
7 N. A. Siladke, C. L. Webster, J. R. Walensky, M. K. Takase, J. W. Ziller, D. J. Grant, L. Gagliardi and W. J. Evans, *Organometallics*, 2013, **32**, 6522–6531.
8 A. Formanuik, A.-M. Ariciu, F. Ortu, R. Beekmeyer, A. Kerridge, F. Tuna, E. J. L. McInnes and D. P. Mills, *Nat. Chem.*, 2017, **9**, 578.
9 R. R. Langeslay, G. P. Chen, C. J. Windorff, A. K. Chan, J. W. Ziller, F. Furche and W. J. Evans, *J. Am. Chem. Soc.*, 2017, **139**, 3387–3398.
10 A. B. Altman, A. C. Brown, G. Rao, T. D. Lohrey, R. D. Britt, L. Maron, S. G. Minasian, D. K. Shuh and J. Arnold, *Chem. Sci.*, DOI:10.1039/C8SC01260A.
11 I. Korobkov, B. Vidjayacoumar, S. I. Gorelsky, P. Billone and S. Gambarotta, *Organometallics*, 2010, **29**, 692–702.
12 Z. E. Button, J. A. Higgins, M. Suvova, F. G. N. Cloke and S. M. Roe, *Dalton Trans.*, 2014, 1–10.
13 M. Sharma and M. S. Eisen, in *Organometallic and Coordination Chemistry of the Actinides*, ed. T. E. Albrecht-Schmitt, Springer Berlin Heidelberg, 2008, pp. 1–85.
14 P. J. Fagan, J. M. Manriquez, E. A. Maatta, A. M. Seyam and T. J. Marks, *J. Am. Chem. Soc.*, 1981, **103**, 6650–6667.
15 B. D. Kagan, A. G. Lichtscheidl, K. A. Erickson, M. J. Monreal, B. L. Scott, A. T. Nelson and J. L. Kiplinger, *Eur. J. Inorg. Chem.*, 2018, **2018**, 1247–1253.
16 The molecular structure of **5.1** was obtained by Dr Alistar Frey and Mr Arnaud Jaoul. The author obtained EA, ^{1}H NMR and EI-MS data.
17 I. Korobkov, S. Gambarotta and G. P. A. Yap, *Angew. Chem. Int. Ed.*, 2003, **42**, 4958–4961.
18 R. J. Butcher, D. L. Clark, S. K. Grumbine, B. L. Scott and J. G. Watkin, *Organometallics*, 1996, **15**, 1488–1496.
19 I. Korobkov, A. Arunachalampillai and S. Gambarotta, *Organometallics*, 2004, **23**, 6248–6252.
20 M. Suvova, K. T. P. O'Brien, J. H. Farnaby, J. B. Love, N. Kaltsoyannis and P. L. Arnold, *Organometallics*, 2017, **36**, 4669–4681.
21 J. Evans, *J. Chem. Soc. Resumed*, 1959, 2003–2005.
22 P. C. Blake, N. M. Edelstein, P. B. Hitchcock, W. K. Kot, M. F. Lappert, G. V. Shalimoff and S. Tian, *J. Organomet. Chem.*, 2001, **636**, 124–129.
23 EPR mesaurements and simulations were carried out by Dr Floriana Tuna.
24 D. Gourier, D. Caurant, T. Arliguie and M. Ephritikhine, *J. Am. Chem. Soc.*, 1998, **120**, 6084–6092.
25 D. P. Halter, F. W. Heinemann, L. Maron and K. Meyer, *Nat. Chem.*, 2018, **10**, 259–267.
26 L. J. Nugent, R. D. Baybarz, J. L. Burnett and J. L. Ryan, *J. Phys. Chem.*, 1973, **77**, 1528–1539.
27 S. G. Bratsch and J. J. Lagowski, *J. Phys. Chem.*, 1986, **90**, 307–312.
28 A. Formanuik, F. Ortu, J. Liu, L. E. Nodaraki, F. Tuna, A. Kerridge and D. P. Mills, *Chem. – Eur. J.*, 2017, **23**, 2290–2293.
29 N. Tsoureas, L. Castro, A. F. R. Kilpatrick, F. G. N. Cloke and L. Maron, *Chem. Sci.*, 2014, **5**, 3777–3788.
30 C. J. Inman, A. S. P. Frey, A. F. R. Kilpatrick, F. G. N. Cloke and S. M. Roe, *Organometallics*, 2017, **36**, 4539–4545.

31 J. A. L. Wells, M. L. Seymour, M. Suvova and P. L. Arnold, *Dalton Trans.*, 2016, **45**, 16026–16032.
32 J. A. Hlina, J. R. Pankhurst, N. Kaltsoyannis and P. L. Arnold, *J. Am. Chem. Soc.*, 2016, **138**, 3333–3345.
33 R. R. Langeslay, M. E. Fieser, J. W. Ziller, F. Furche and W. J. Evans, *Chem. Sci.*, 2014, **6**, 517–521.
34 M. C. Cassani, D. J. Duncalf and M. F. Lappert, *J. Am. Chem. Soc.*, 1998, **120**, 12958–12959.
35 M. C. Cassani, M. F. Lappert and F. Laschi, *Chem. Commun.*, 1997, **0**, 1563–1564.
36 N. E. Travia, M. J. Monreal, B. L. Scott and J. L. Kiplinger, *Dalton Trans.*, 2012, **41**, 14514–23.
37 I. Korobkov, A. Arunachalampillai and S. Gambarotta, *Organometallics*, 2004, **23**, 6248–6252.
38 J. M. Berg, D. L. Clark, J. C. Huffman, D. E. Morris, A. P. Sattelberger, W. E. Streib, W. G. V. D. Sluys and J. G. Watkin, *J. Am. Chem. Soc.*, 1992, **114**, 10811–10821.
39 J. McKinven, G. S. Nichol and P. L. Arnold, *Dalton Trans.*, 2014, **43**, 17416–17421.
40 W. J. Evans, *J. Organomet. Chem.*, 2002, **647**, 2–11.
41 N. A. Siladke, J. W. Ziller and W. J. Evans, *Z. Für Anorg. Allg. Chem.*, 2010, **636**, 2347–2351.
42 T. Cantat, B. L. Scott and J. L. Kiplinger, *Chem. Commun.*, 2010, **46**, 919–921.
43 M. N. Hopkinson, C. Richter, M. Schedler and F. Glorius, *Nature*, 2014, **510**, 485–496.
44 P. L. Arnold, T. Cadenbach, I. H. Marr, A. A. Fyfe, N. L. Bell, R. Bellabarba, R. P. Tooze and J. B. Love, *Dalton Trans.*, 2014, **43**, 14346–14358.
45 M. E. Garner, S. Hohloch, L. Maron and J. Arnold, *Organometallics*, 2016, **35**, 2915–2922.
46 M. E. Garner, S. Hohloch, L. Maron and J. Arnold, *Angew. Chem.*, 2016, **128**, 13993–13996.
47 M. E. Garner and J. Arnold, *Organometallics*, 2017, **36**, 4511–4514.
48 M. E. Garner, B. F. Parker, S. Hohloch, R. G. Bergman and J. Arnold, *J. Am. Chem. Soc.*, 2017, **139**, 12935–12938.
49 M. E. Garner, T. D. Lohrey, S. Hohloch and J. Arnold, *J. Organomet. Chem.*, 2018, **857**, 10–15.
50 Compound **5.5** was synthesised by Mr Ryan K Brown with the supervision of the author. The author also obtained X-ray diffraction data of this compound and solved the structure.
51 C. A. P. Goodwin, N. F. Chilton, L. S. Natrajan, M.-E. Boulon, J. W. Ziller, W. J. Evans and D. P. Mills, *Inorg. Chem.*, 2017, **56**, 5959–5970.
52 D. E. Smiles, G. Wu, N. Kaltsoyannis and T. W. Hayton, *Chem. Sci.*, 2015, **6**, 3891–3899.
53 E. Barnea and M. S. Eisen, *Coord. Chem. Rev.*, 2006, **250**, 855–899.
54 T. Andrea and M. S. Eisen, *Chem. Soc. Rev.*, 2008, **37**, 550–567.
55 E. Barnea, D. Moradove, J.-C. Berthet, M. Ephritikhine and M. S. Eisen, *Organometallics*, 2006, **25**, 320–322.
56 W. Ren, N. Zhao, L. Chen and G. Zi, *Inorg. Chem. Commun.*, 2013, **30**, 26–28.
57 Reactivity studies of **5.8** towards H_2 were carried out by the author and Mr Ryan K Brown.
58 C. M. Fendrick, L. D. Schertz, W. Victor and T. J. Marks, *Organometallics*, 1988, **7**, 1828–1838.

Appendix One: Experimental Details

A1.1 General procedures and techniques

All manipulations were carried out in an MBraun glovebox under N_2 or Ar (O_2 and H_2O < 1 ppm) or by using standard Schlenk techniques under Ar (BOC Pureshield) passed through a column containing BASF R3-11(G) catalyst and activated molecular sieves (4 Å). All glassware was dried at 160 °C overnight before use. Celite® was pre-dried in a 270 °C oven and flame dried under dynamic vacuum (<2 x 10^{-2} mbar) or heated at 180 °C overnight under dynamic vacuum (< 10 x 10^{-1} mbar) and stored in an Ar-filled glovebox before use. Filter cannulas were made using Whatman® 25 mm glass microfibre filters and were pre-dried at 160 °C.

A1.2 Purification of solvents

Solvents were pre-dried over sodium wire. Toluene, benzene, DME, TBME, $^{i}Pr_2O$ and THF were dried over molten K for a minimum of 3 days and distilled under an N_2 atmosphere and stored over activated molecular sieves (with the exception of toluene and benzene which were stored over a potassium mirror). Pentane and Et_2O were dried over NaK for a minimum of 3 days, distilled under an N_2 atmosphere and stored in a Young ampoule over a potassium mirror. Methylcyclohexane and $SiMe_4$ was dried over NaK, distilled under Ar and stored over activated molecular sieves (4 Å) in a Ar-filled glovebox. Deuterated solvents were degassed by three freeze-pump-thaw cycles, dried by refluxing over K for 3 days, vacuum distilled and stored in a glovebox.

A1.3 Preparation of reagents

The following reagents were prepared according to the literature procedures: K_2Pent^{TIPS2},[1] UI_3,[2] KTp^{Me2},[3], $ThCl_4(DME)_4$,[4] KCp* (synthesised by deprotonating HCp* with KN^{TMS2}).[5]

K_2COT^{TMS2}, K_2COT^{TIPS2}, PhNNPh, K/Hg, $ThI_3OBuI(THF)_3$, ITMe, KBz, KH CS_2, $[^{n}Bu_4N][B(C_6F_5)_4]$, NaCp*, MgClCp* and LiCp* were kindly donated. $^{13}CS_2$ was purchased without purification and used. The following chemicals were purified following their purchase: ^{n}Buli (filtered over Celite then titrated), KN^{TMS2} (recrystallized from toluene), K and Na metal (washed with pentane and oxide layer

removed in glove box), 2.2.2-cryptand (dried overnight *in vacuo*) , COT (stored in the dark over 4 Å molecular sieves and degassed before use) and [^{n}Bu$_4$N][BPh$_4$] (dried overnight *in vacuo*). Isotopically enriched gases (^{13}CO, ^{13}CO$_2$) were supplied by Cambridge Isotope Laboratories Inc., and used without further purification. Cylinders of ^{12}CO$_2$ (100.00%) and H$_2$ (99.999%) were supplied by BOC gases and used as supplied. ^{13}CS$_2$

A1.4 Instrumentation

A1.4.1 NMR spectroscopy

NMR spectra were either recorded on a Varian VNMRS 400 spectrometer operating at 399.49 MHz (^{1}H), 128.17 MHz (^{11}B) 79.35 MHz (^{29}Si) and 100.45 MHz (^{13}C) or on a Varian VNMRS 500 MHz spectrometer operating at 499.91 MHz (^{1}H) and 125.72 MHz (^{13}C). The spectra were referenced internally to the residual protic solvent or the signals of the solvent (^{13}C). ^{29}Si NMR spectra were referenced externally to SiMe$_4$ and ^{11}B referenced externally to BF$_3$.Et$_2$O. All spectra were recorded at 303 K unless stated otherwise.

A1.4.2 Mass spectrometry

EI-MS mass spectra were recorded on a VG-Autospec Fisions (electron ionisation at 70 eV) instrument at the University of Sussex.

A1.4.2 Cyclic voltammetry

Cyclic voltammetry studies were performed in an Ar glovebox using a BASi-Epsilon potentiostat under computer control. IR drop was compensated using the feedback method. CV experiments were performed using the three electrode method with glassy carbon disk (7.0 mm^2) as the working electrode, Pt wire as the counter electrode and Ag wire as the pseudoreference electrode. Sample solutions were prepared by dissolving the appropriate supporting electrolyte in 2 mL of solvent followed by addition of the analyte to give a concentration of *ca* 5mM. The reported half potentials are referenced to FeCp$_2^{+/0}$ redox couple, which was measured by adding ferrocene (*ca* 1mg) to the sample solution.

A1.4.3 Elemental analysis

Elemental analyses were performed at the School of Chemistry at University of Bristol or Mr Stephen Boyer of London Metropolitan University.

A1.4.4 X-ray crystallography

Data sets were collected on an Agilent Gemini Ultra diffractometer with an Enhance source (Mo Kα or Cu Kα) equipped with an Eos CCD area detector and an Oxford Cryosystems low-temperature device (173 K), operating in ω scanning mode with ψ and ω scans to fill the Ewald sphere. The program used for control, integration, and absorption correction was CrysalisPro.[6] The crystals were mounted on glass fibers or MiTiGen loops with vacuum oil. All solutions and refinements were performed using the OLEX2 package.[7] The author solved all of the datasets apart from where it is mentioned in the text. The author also received assistance from Dr N. Tsoureas (disorder in **4.1**, **4.4**) and Dr M.S Roe (thorium atom disorder in **5.2**). All non-hydrogen atoms were refined using anisotropic thermal parameters, and hydrogens were added using a riding model. Single-crystal XRD data for **3.4** were collected by the UK National Crystallographic Service (NCS) at the University of Southampton[8] on a Rigaku FR-E+ Ultra High Flux diffractometer (Mo Kα) equipped with VariMax VHF optics and a Saturn 724+ CCD area detector. The data were collected at 100 or 150 K using an Oxford Cryostreams Cobra low-temperature device. An empirical absorption correction was carried out using the MULTI-SCAN program. Data collected by the NCS were processed using CrysAlisPro, and unit cell data parameters were refined against all data.

A1.4.5 EPR spectroscopy

EPR spectroscopy was carried out by Dr F. Tuna and Ms. L.E. Nodaraki with the assistance of Dr F. Ortu at the EPSRC National UK EPR Facility and Service at the University of Manchester. X-band EPR measurements were performed using a Bruker E580 ELEXSYS spectrometer and simulated with the XSophe suite.[9]

A1.4.6 IR spectroscopy

IR spectra were recorded using a Mettler-Toledo ReactIR system featuring an IR probe inside a gas-tight cell attached to a Toepler pump. IR spectra were also recorded on a Perkin-Elmer 1600 Fourier Transform spectrometer. Samples were prepared in a glove box as a thin film between NaCl plates.

A1.5 Computational Details

Unrestricted density functional calculations were carried out using the ADF program suite version 2016.107.[10] The Slater-type orbital (STO) basis sets were of triple-ζ quality augmented with a one polarization function (ADF basis TZP). Core electrons were frozen (C, O 1s; Th 4f) in our model of the electronic configuration for each atom. The local density approximation (LDA) by Vosko, Wilk and Nusair (VWN)[11] was used together with the exchange correlation corrections of Becke and Perdew (BP86).[12,13] Scalar relativistic corrections were made using ZORA. Optimized geometries were ascertained as local mimima *via* frequency calculations. The g-tensor and the nuclear magnetic dipole hyperfine interaction (A-tensor) were calculated using a spin-orbit coupled spin unrestricted relativistic ZORA calculation.[14,15]

References for Appendix One

1 F. G. N. Cloke, M. C. Kuchta, R. M. Harker, P. B. Hitchcock and J. S. Parry, *Organometallics*, 2000, **19**, 5795–5798.

2 G. K. B. Clentsmith, F. G. N. Cloke, M. D. Francis, J. R. Hanks, P. B. Hitchcock and J. F. Nixon, *J. Organomet. Chem.*, 2008, **693**, 2287–2292.

3 S. Trofimenko, *J. Am. Chem. Soc.*, 1966, **88**, 1842–1844.

4 T. Cantat, B. L. Scott and J. L. Kiplinger, *Chem. Commun.*, 2010, **46**, 919–921.

5 W. J. Evans, S. A. Kozimor, J. W. Ziller, A. A. Fagin and M. N. Bochkarev, *Inorg. Chem.*, 2005, **44**, 3993–4000.

6 Agilent Technologies, *CrysalisPro 11713632*.

7 O. V. Dolomanov, L. J. Bourhis, R. J. Gildea, J. A. K. Howard and H. Puschmann, *J. Appl. Crystallogr.*, 2009, **42**, 339 –341.

8 S. J. Coles and P. A. Gale, *Chem. Sci.*, 2012, **3**, 683–689.

9 G. R. Hanson, K. E. Gates, C. J. Noble, M. Griffin, A. Mitchell and S. Benson, *J. Inorg. Biochem.*, 2004, **98**, 903–916.

10 ADF2016, SCM, Theoretical Chemistry, Vrije Universiteit, Amsterdam, The Netherlands, http://www.scm.com.

11 S. H. Vosko, L. Wilk, M. Nusair, *Can. J. Phys.* **1980**, *58*, 1200.

12 A. D. Becke, *Phys. Rev. A, Gen. Phys.* **1988**, *38*, 3098.

13 J. P. Perdew, *Phys. Rev. B,* 1986, **33**, 8822–8824.

14 E. van Lenthe, A. van der Avoird and P.E.S. Wormer, Journal of Chemical Physics 107, 2488 (1997)

15 E. van Lenthe, A. van der Avoird and P.E.S. Wormer, Journal of Chemical Physics 108, 4783 (1998)

Appendix Two: Crystallographic Information

Identification code	$UTp^{Me2}COT^{TMS2}$ (**2.1**) (CJI1066)	$UTp^{Me2}Pent^{Tips2}Cl$ (**2.5**) CJI219	*p*$Me_2O_2H_2$ (**3.1**)
Empirical formula	$C_{29}H_{46}BN_6Si_2U$	$C_{41}H_{61}BClN_6Si_2U$	$C_{17}H_{20}O$
Formula weight	783.74	978.42	240.33
Temperature/K	173(2)	173(2)	173
Crystal system	orthorhombic	triclinic	monoclinic
Space group	Pbca	P-1	I2/c
a/Å	10.5992(4)	10.4912(3)	12.2074(3)
b/Å	24.6462(10)	13.6484(5)	10.8875(3)
c/Å	25.4849(8)	18.6544(7)	21.4159(7)
α/°	90	71.230(4)	90
β/°	90	75.911(3)	93.108(3)
γ/°	90	72.842(3)	90
Volume/$Å^3$	6657.4(4)	2383.71(17)	2842.17(14)
Z	8	2	8
$\rho_{calc}g/cm^3$	1.564	1.363	1.123
μ/mm^{-1}	4.976	10.822	0.519
F(000)	3096.0	982.0	1040.0
Crystal size/mm^3	? × ? × ?	0.3 × 0.1 × 0.05	0.42 × 0.38 × 0.1
Radiation	MoKα (λ = 0.71073)	CuKα (λ = 1.54184)	CuKα (λ = 1.54184)
2Θ range for data collection/°	6.476 to 54.966	7.04 to 143.182	8.27 to 144.294
Index ranges	$-13 \le h \le 13, -31 \le k \le 32, -33 \le l \le 32$	$-12 \le h \le 12, -15 \le k \le 16, -22 \le l \le 21$	$-14 \le h \le 9, -13 \le k \le 13, -25 \le l \le 26$
Reflections collected	31520	17909	8919
Independent reflections	7472 [R_{int} = 0.1238, R_{sigma} = 0.1486]	9089 [R_{int} = 0.0523, R_{sigma} = 0.0688]	2755 [R_{int} = 0.0322, R_{sigma} = 0.0284]
Data/restraints/parameters	7472/516/395	9089/0/485	2755/84/184
Goodness-of-fit on F^2	1.196	0.780	1.064
Final R indexes [I>=2σ (I)]	R_1 = 0.0892, wR_2 = 0.2311	R_1 = 0.0363, wR_2 = 0.1021	R_1 = 0.0457, wR_2 = 0.1305
Final R indexes [all data]	R_1 = 0.1474, wR_2 = 0.2564	R_1 = 0.0422, wR_2 = 0.1062	R_1 = 0.0483, wR_2 = 0.1339
Largest diff. peak/hole / e $Å^{-3}$	1.80/-1.69	1.16/-1.90	0.22/-0.21

Identification code	UCp*(*p*Me$_2$O$_2$) (**3.3**)	[{ UCp*(*p*Me$_2$O$_2$)}$_2$CO$_3$] (**3.4**)	[{ UCp*(*p*Me$_2$O$_2$)}$_2$C$_2$O$_4$](**3.5**)
Empirical formula	$C_{38}H_{47}O_2U$	$C_{38.5}H_{47}O_{3.5}U$	$C_{78}H_{94}O_8U_2$
Formula weight	773.78	803.79	1635.59
Temperature/K	173(2)	173	100.15
Crystal system	orthorhombic	tetragonal	triclinic
Space group	$P2_12_12_1$	P-4	P-1
a/Å	16.74311(19)	16.7904(4)	12.2345(7)
b/Å	17.08611(18)	16.7904(4)	14.6878(10)
c/Å	25.4469(3)	12.4156(5)	20.2521(14)
α/°	90	90	68.893(6)
β/°	90	90	89.659(5)
γ/°	90	90	76.512(5)
Volume/Å^3	7279.71(14)	3500.2(2)	3289.2(4)
Z	8	4	2
ρ_{calc}g/cm^3	1.412	1.525	1.651
μ/mm^{-1}	12.754	13.320	4.975
F(000)	3064.0	1592.0	1620.0
Crystal size/mm^3	? × ? × ?	0.46 × 0.21 × 0.16	0.08 × 0.07 × 0.06
Radiation	CuKα (λ = 1.54184)	CuKα (λ = 1.54184)	MoKα (λ = 0.71075)
2Θ range for data collection/°	7.392 to 138.254	5.264 to 144.034	4.358 to 54.994
Index ranges	-13 ≤ h ≤ 20, -18 ≤ k ≤ 20, -30 ≤ l ≤ 30	-18 ≤ h ≤ 20, -16 ≤ k ≤ 20, -11 ≤ l ≤ 14	-15 ≤ h ≤ 15, -19 ≤ k ≤ 18, -26 ≤ l ≤ 26
Reflections collected	52545	11255	42086
Independent reflections	13500 [R_{int} = 0.0606, R_{sigma} = 0.0544]	6469 [R_{int} = 0.0501, R_{sigma} = 0.0666]	15081 [R_{int} = 0.1136, R_{sigma} = 0.1641]
Data/restraints/parameters	13500/0/765	6469/10/399	15081/6/819
Goodness-of-fit on F^2	1.061	1.057	0.978
Final R indexes [I>=2σ (I)]	R_1 = 0.0497, wR_2 = 0.1353	R_1 = 0.0360, wR_2 = 0.0927	R_1 = 0.0677, wR_2 = 0.1237
Final R indexes [all data]	R_1 = 0.0575, wR_2 = 0.1428	R_1 = 0.0370, wR_2 = 0.0937	R_1 = 0.1392, wR_2 = 0.1477
Largest diff. peak/hole / e Å^{-3}	2.71/-1.74	1.53/-2.27	2.35/-2.11

Identification code	[{ UCp*(*p*Me$_2$O$_2$)}$_2$CS$_2$] (**4.1**) CJI279	[{UCp*(*p*Me$_2$O$_2$)}$_2$CS$_2$H] (**4.1**) CJI482-2	[{UCp*(*p*Me$_2$O$_2$)}$_2$OSCCS] **4.4** CJI578
Empirical formula	$C_{84}H_{94}O_4S_2U_2$	$C_{39}H_{47}O_2S_2U$	$C_{87}H_{97}O_5S_2U_2$
Formula weight	1707.87	849.91	1762.82
Temperature/K	173.15	173	173(2)
Crystal system	orthorhombic	monoclinic	triclinic
Space group	Pbca	$P2_1/c$	P-1
a/Å	14.4443(2)	9.3301(3)	13.0928(8)
b/Å	28.7119(5)	20.7632(5)	13.8896(8)
c/Å	35.2879(5)	18.4239(5)	22.3563(10)
α/°	90	90	103.164(4)
β/°	90	103.075(3)	97.641(5)
γ/°	90	90	100.935(5)
Volume/Å^3	14634.7(4)	3476.60(17)	3820.3(4)
Z	8	4	2
ρ_{calc}g/cm^3	1.5502	1.624	1.532
μ/mm^{-1}	13.273	14.507	12.740
F(000)	6707.7	1684.0	1750.0
Crystal size/mm^3	0.2 × 0.2 × 0.08	0.1 × 0.1 × 0.001	0.070 × 0.050 × 0.020
Radiation	Cu Kα (λ = 1.54184)	CuKα (λ = 1.54184)	CuKα (λ = 1.54184)
2Θ range for data collection/°	7.3 to 143.16	8.518 to 143.36	8.522 to 134.158
Index ranges	-17 ≤ h ≤ 13, -34 ≤ k ≤ 35, -43 ≤ l ≤ 40	-10 ≤ h ≤ 11, -24 ≤ k ≤ 25, -22 ≤ l ≤ 19	-15 ≤ h ≤ 15, -15 ≤ k ≤ 16, -17 ≤ l ≤ 26
Reflections collected	36136	19486	22622
Independent reflections	14006 [R_{int} = 0.0634, R_{sigma} = 0.0663]	6709 [R_{int} = 0.0437, R_{sigma} = 0.0450]	13469 [R_{int} = 0.0921, R_{sigma} = 0.1209]
Data/restraints/parameters	14006/0/855	6709/456/410	13469/16/867
Goodness-of-fit on F^2	1.040	1.158	1.026
Final R indexes [I>=2σ (I)]	R_1 = 0.0488, wR_2 = 0.1203	R_1 = 0.0451, wR_2 = 0.1327	R_1 = 0.0814, wR_2 = 0.2086
Final R indexes [all data]	R_1 = 0.0604, wR_2 = 0.1307	R_1 = 0.0514, wR_2 = 0.1449	R_1 = 0.1092, wR_2 = 0.2383
Largest diff. peak/hole / e Å^{-3}	1.73/-2.20	2.08/-1.76	4.14/-2.17

Identification code	**4.5** CJI315	**4.6** CJI533	**4.7** CJI323-1
Empirical formula	$C_{78}H_{94}O_5S_2U_2$	$C_{124}H_{144}O_{12}U_3$	$C_{50}H_{57}N_2O_2U$
Formula weight	1651.71	2540.47	956.00
Temperature/K	173(2)	173(2)	173(2)
Crystal system	monoclinic	triclinic	monoclinic
Space group	$P2_1/c$	P-1	$P2_1/c$
a/Å	13.8556(3)	15.6902(4)	10.0517(3)
b/Å	12.3174(3)	16.3604(5)	21.2380(5)
c/Å	22.8357(6)	27.0111(8)	39.8748(9)
α/°	90	93.873(2)	90
β/°	93.285(2)	101.068(2)	90
γ/°	90	110.285(3)	90
Volume/Å^3	3890.83(16)	6314.6(3)	8512.4(4)
Z	3	3	8
ρ_{calc}g/cm^3	2.115	2.004	1.492
μ/mm^{-1}	18.700	16.670	11.041
F(000)	2454.0	3780.0	3832.0
Crystal size/mm^3	0.12 × 0.07 × 0.05	0.4 × 0.2 × 0.01	0.2 × 0.2 × 0.05
Radiation	CuKα (λ = 1.54184)	CuKα (λ = 1.54184)	CuKα (λ = 1.54184)
2Θ range for data collection/°	7.756 to 143.014	3.368 to 135.63	7.846 to 143.92
Index ranges	$-12 \le h \le 16$, $-15 \le k \le 12$, $-28 \le l \le 26$	$-17 \le h \le 18$, $-19 \le k \le 19$, $-32 \le l \le 31$	$-12 \le h \le 11$, $-26 \le k \le 25$, $-49 \le l \le 34$
Reflections collected	21579	95460	63582
Independent reflections	7448 [R_{int} = 0.0688, R_{sigma} = 0.0656]	21932 [R_{int} = 0.1232, R_{sigma} = 0.0819]	16427 [R_{int} = 0.0787, R_{sigma} = 0.0605]
Data/restraints/parameters	7448/579/428	21932/0/1444	16427/0/1017
Goodness-of-fit on F^2	1.309	1.873	0.956
Final R indexes [I>=2σ (I)]	R_1 = 0.0614, wR_2 = 0.1649	R_1 = 0.1373, wR_2 = 0.3193	R_1 = 0.0482, wR_2 = 0.1276
Final R indexes [all data]	R_1 = 0.0754, wR_2 = 0.1781	R_1 = 0.1555, wR_2 = 0.3369	R_1 = 0.0578, wR_2 = 0.1397
Largest diff. peak/hole / e Å^{-3}	3.73/-2.40	7.44/-2.05	2.92/-1.74

Identification code	**5.1** AJ64_1	[K(2.2.2-cryptand)][Th(pMe2O2)2] **5.2** CJI443	$ThI_2(pMe_2O_2)(THF)$ **5.3** CJI376-2
Empirical formula	$C_{56}H_{64}O_4Th$	$C_{77}H_{107}KN_2O_{11}Th$	$C_{32}H_{40}I_2O_3Th$
Formula weight	1033.11	1507.78	958.48
Temperature/K	173(2)	173(2)	173
Crystal system	monoclinic	monoclinic	monoclinic
Space group	C2/c	P21/c	$P2_1/c$
a/Å	24.0498(11)	20.3425(5)	31.6217(6)
b/Å	13.1618(5)	14.7794(4)	9.5305(2)
c/Å	18.2697(8)	24.5893(6)	32.7296(7)
α/°	90	90	90
β/°	103.520(4)	97.437(3)	112.737(3)
γ/°	90	90	90
Volume/$Å^3$	5622.8(4)	7330.6(3)	9097.1(4)
Z	4	4	8
$\rho_{calc}g/cm^3$	1.220	1.366	1.400
μ/mm^{-1}	8.842	7.535	21.388
F(000)	2088.0	3120.0	3616.0
Crystal size/mm^3	0.200 × 0.050 × 0.050	0.15 × 0.08 × 0.01	0.3 × 0.05 × 0.03
Radiation	CuKα (λ = 1.54184)	CuKα (λ = 1.54184)	CuKα (λ = 1.54184)
2Θ range for data collection/°	7.562 to 134.14	6.994 to 142.804	7.564 to 134.16
Index ranges	-28 ≤ h ≤ 25, -15 ≤ k ≤ 12, -21 ≤ l ≤ 20	-22 ≤ h ≤ 24, -11 ≤ k ≤ 17, -29 ≤ l ≤ 30	-19 ≤ h ≤ 14, -17 ≤ k ≤ 12, -23 ≤ l ≤ 32
Reflections collected	8550	28986	15933
Independent reflections	4962 [R_{int} = 0.0336, R_{sigma} = 0.0541]	13909 [Rint = 0.0374, Rsigma = 0.0520]	15933 [R_{int} = 0.0725, R_{sigma} = 0.0897]
Data/restraints/parameters	4962/0/284	13909/0/866	15933/0/695
Goodness-of-fit on F^2	0.653	0.999	0.987
Final R indexes [I>=2σ (I)]	R_1 = 0.0310, wR_2 = 0.0845	R1 = 0.0391, wR2 = 0.0971	R_1 = 0.0645, wR_2 = 0.1588
Final R indexes [all data]	R_1 = 0.0352, wR_2 = 0.0893	R1 = 0.0520, wR2 = 0.1048	R_1 = 0.0820, wR_2 = 0.1685
Largest diff. peak/hole / e $Å^{-3}$	1.33/-1.28	0.74/-1.04	4.15/-2.46

Identification code	$ThI_2(pMe_2O_2)(Et_2O)$ **5.4** CJI446	$ThI_2(pMe_2O_2)(ITMe)$ **5.5** RKB122	$ThCl_2(pMe_2O_2)(DME)$ **5.6** CJI530
Empirical formula	$C_{16.5}H_{22}IOTh_{0.5}$	$C_{35}H_{44}I_2N_2O_2Th$	$C_{32}H_{42}ClO_4Th$
Formula weight	479.26	1010.56	792.28
Temperature/K	173(2)	173(2)	173
Crystal system	monoclinic	monoclinic	triclinic
Space group	C2/c	C2/c	P-1
a/Å	14.7150(5)	12.7205(5)	10.8745(6)
b/Å	10.8193(3)	13.3241(5)	14.2643(9)
c/Å	21.2433(5)	21.2968(7)	15.4791(9)
α/°	90	90	80.535(5)
β/°	96.713(3)	89.990(3)	84.420(5)
γ/°	90	90	78.696(5)
Volume/$Å^3$	3358.86(17)	3609.6(2)	2317.2(2)
Z	8	5	4
$\rho_{calc}g/cm^3$	1.895	2.324	1.473
μ/mm^{-1}	28.939	33.734	11.758
F(000)	1816.0	2400.0	1032.0
Crystal size/mm^3	? × ? × ?	0.15 × 0.1 × 0.05	0.5 × 0.2 × 0.007
Radiation	CuKα (λ = 1.54184)	CuKα (λ = 1.54184)	CuKα (λ = 1.54184)
2Θ range for data collection/°	8.382 to 142.084	8.304 to 142.464	7.968 to 143.188
Index ranges	$-17 \le h \le 17, -11 \le k \le 13, -25 \le l \le 22$	$-14 \le h \le 15, -15 \le k \le 16, -25 \le l \le 25$	$-13 \le h \le 12, -16 \le k \le 17, -18 \le l \le 19$
Reflections collected	10023	5917	17188
Independent reflections	3211 [R_{int} = 0.0668, R_{sigma} = 0.0500]	3402 [R_{int} = 0.0557, R_{sigma} = 0.0593]	8805 [R_{int} = 0.0938, R_{sigma} = 0.0968]
Data/restraints/parameters	3211/0/173	3402/12/197	8805/0/524
Goodness-of-fit on F^2	1.989	1.033	1.049
Final R indexes [I>=2σ (I)]	R_1 = 0.0691, wR_2 = 0.2167	R_1 = 0.0399, wR_2 = 0.0992	R_1 = 0.0588, wR_2 = 0.1496
Final R indexes [all data]	R_1 = 0.0759, wR_2 = 0.2360	R_1 = 0.0427, wR_2 = 0.1023	R_1 = 0.0648, wR_2 = 0.1630
Largest diff. peak/hole / e $Å^{-3}$	7.18/-6.27	1.27/-2.72	2.79/-3.03

Identification code	Th(*p*Me$_2$O$_2$)N''$_2$ **5.7** CJI427	Th(*p*Me$_2$O$_2$)Bz$_2$ **5.8** CJI428-2
Empirical formula	$C_{40}H_{68}N_2O_2Si_4Th$	$C_{42}H_{46}O_2Th$
Formula weight	953.36	814.83
Temperature/K	173(2)	173
Crystal system	monoclinic	monoclinic
Space group	I2/a	$P2_1/n$
a/Å	11.99936(18)	13.7202(2)
b/Å	16.8590(3)	17.2826(3)
c/Å	22.6661(4)	15.3571(3)
α/°	90	90
β/°	103.0469(15)	106.166(2)
γ/°	90	90
Volume/Å^3	4466.92(12)	3497.50(11)
Z	4	4
ρ_{calc}g/cm^3	1.418	1.547
μ/mm^{-1}	12.042	14.000
F(000)	1936.0	1616.0
Crystal size/mm^3	0.3 × 0.05 × 0.01	0.2 × 0.05 × 0.01
Radiation	Cu Kα (λ = 1.54184)	Cu Kα (λ = 1.54184)
2Θ range for data collection/°	6.596 to 142.454	7.652 to 142.438
Index ranges	$-14 \le h \le 13$, $-20 \le k \le 19$, $-27 \le l \le 26$	$-16 \le h \le 15$, $-20 \le k \le 13$, $-17 \le l \le 18$
Reflections collected	8574	12334
Independent reflections	4259 [R_{int} = 0.0459, R_{sigma} = 0.0523]	6644 [R_{int} = 0.0276, R_{sigma} = 0.0396]
Data/restraints/parameters	4259/0/232	6644/0/414
Goodness-of-fit on F^2	1.061	1.042
Final R indexes [I>=2σ (I)]	R_1 = 0.0318, wR_2 = 0.0813	R_1 = 0.0284, wR_2 = 0.0696
Final R indexes [all data]	R_1 = 0.0358, wR_2 = 0.0844	R_1 = 0.0338, wR_2 = 0.0735